SOLUBILITY STUDIES OF CARBON DIOXIDE IN NOVEL HYBRID SOLVENTS USING A NEW STATIC SYNTHETIC APPARATUS

By

Mojgan Ebrahiminejadhasanabadi

(MSc in Chemical Engineering, Isfahan University of Technology)

Submitted in fulfilment of the academic requirements for the degree of Doctor of Philosophy in Engineering to the School of Engineering, Discipline of Chemical Engineering,

University of KwaZulu-Natal, Durban.

November 2019

Supervisor: Dr. Wayne Michael Nelson

Co-supervisors: Prof. Paramespri Naidoo, Prof. Amir H. Mohammadi and Prof. Deresh Ramjugernath

PREFACE

The investigation or study presented in this thesis entitled "solubility studies of carbon dioxide in novel hybrid solvents using a new static synthetic apparatus" was undertaken at the University of KwaZulu-Natal in the School of Engineering, Howard College Campus, Durban, South Africa. The duration of the study was from February 2016 to November 2019. The study was supervised by Dr. Wayne Michael Nelson.

This thesis has been submitted as the fully requirement for the award of the Doctor of Philosophy (PhD) degree in Chemical Engineering. The study presented in this thesis is my original work, unless otherwise stated.

The thesis has not previously been submitted for degree or examination at any other tertiary institute or university.

As the candidate's supervisor, I, Dr. Wayne Michael Nelson, agree to the submission of this thesis.

_____   _____

Dr. Wayne Michael Nelson   Date

As the candidate's co-supervisor, I, Prof. Paramespri Naidoo, agree to the submission of this thesis.

_____   _____

Prof. Paramsepri Naidoo   Date

DECLARATION 1 - PLAGIARISM

I, Mojgan Ebrahiminejadhasanabadi, student number 216072591 declare that:

The reported research project is my original research work.

   i.   This thesis has not been submitted for any degree or examination at any other university before.

   ii.   All the data such as pictures, graphs or any other information presented in this dissertation, has been acknowledged as being sourced from other persons, except in a case where is my original work.

   iii. All the graphs, tables or text copied and pasted from the Internet, has been acknowledged, and the referenced source in this thesis is presented in detail in the References section.

   iv.   All the other persons' writing in this thesis has been referenced and acknowledged.

   a.   Their words have been re-written but the general information attributed to them has been referenced.

   b.   Where their exact words have been used, then their writing has been placed in italics and inside quotation marks and referenced.

Signed:

_____   _____

Mojgan Ebrahiminejadhasanabadi   Date

DECLARATION 2 - PUBLICATIONS

DETAILS OF CONTRIBUTION TO PUBLICATIONS that form part and/or include research presented in this thesis (include publications in preparation, submitted, *in press* and published and give details of the contributions of each author to the experimental work and writing of each publication) .

Publication 1: Mojgan Ebrahiminejadhasanabadi, Wayne Michael Nelson, Paramespri Naidoo, Amir H. Mohammadi, Deresh Ramjugernath "Experimental measurement of carbon dioxide solubility in 1-methylpyrrolidin-2-one (NMP) + 1-butyl-3-methyl-1H-imidazol-3-ium tetrafluoroborate (bmim[BF$_4$]) mixtures using a new static-synthetic cell", Fluid Phase Equilibria 477 (2018) 62-77.

Publication 2: "Experimental measurement of carbon dioxide solubility in, and densities, viscosities and evaporation rates of , 2-aminoethanol (MEA) + 1-methylpyrrolidin-2-one (NMP)/water + ionic liquids mixtures", (in preparation).

Publication 3: "Experimental measurement of carbon dioxide solubility in, and densities, viscosities and evaporation rates of , 2-(2-aminoethoxy)ethanol (DGA) + 1-methylpyrrolidin-2-one (NMP)/water + ionic liquids mixtures", (in preparation).

Publication 4: "Modelling of acid Gas solubility in alkanolamine aqueous solution using Kent-Eisenberg and Deshmukh–Mather models", (in preparation).

Signed:

_____   _____

Mojgan Ebrahiminejadhasanabadi   Date

ACKNOWLEDGMENTS

I would like to thank my dear God for granting me the grace and strength to complete this thesis.

First and foremost, I would like to express my sincere appreciation to my supervisors, Dr. W. M. Nelson, Prof. P. Naidoo and Prof. D. Ramjugernath for their tremendous support and encouragement throughout this project.

I would like to thank my supervisor Dr. W. M. Nelson for his assistance in the design and development of the experimental apparatus and procedure.

Most importantly, I would like to express my deepest thanks to Prof. Amir H. Mohammadi who accepted my application and gave me the opportunity to join the Thermodynamic Research Unit. He has been an essential part of my studies at University of KwaZulu-Natal.

Thanks are also due to the workshop staff: Mr. D. Padayachee, Mr. S. Deeraj and Mr. G. Addieah, and the laboratory technician, Mr. A. Khanyile, for their assistance, support and collaboration.

A special thanks to my friends: Eva, Leticia, Marcin, Mehdi, Samira and Simon, for their invaluable inspiration and support.

Finally, my heartfelt thanks go to my family for their wonderful support throughout my life.

ABSTRACT

The use of alkanolamine solutions in removing acidic gases from natural gas is common in the industry, but such technologies have disadvantages which include amongst others, solvent loss, corrosion and high heat consumption. This study aimed to provide a comprehensive theoretical and experimental investigation of selected fluorinated ionic liquids (ILs) and their use as additives to amine solutions for CO_2 absorption, hereby attempting to reduce the disadvantages of amine technology. Solubility measurements of CO_2 in five hybrid solvents, viz. (n-methyl-2-pyrrolidone (NMP) + 1-butyl-3-methylimidazolium tetrafluoroborate (bmim[BF_4]), monoethanolamine (MEA) / diglycolamine (DGA) + water + 1-butyl-3-methylimidazolium trifluoromethanesulfonate (bmim[OTF]), MEA/DGA + NMP + 1-butyl-3-methylimidazolium bis(trifluoromethanesulfonyl)imide (bmim[TF_2N]), were conducted using a new static-synthetic apparatus, designed and commissioned for this project. Additionally, viscosity, density, sound velocity and evaporation rate for the solvents were measured.

Overall, replacing the entire water present in the aqueous amine solvents with NMP increased the CO_2 solubility, except at low pressures depending on the concentration of amine. Although the addition of IL into the aqueous amine solvents or the water-free NMP-containing amine solvents decreased the CO_2 solubility, all the studied hybrid solvents could achieve the maximum loading of CO_2 allowed in the industrial amine processes. The addition of IL into the amine solutions decreased the volatile part of the solvent and, in most cases, decelerated the evaporation rate of solvent, while the loss of ILs was almost zero. However, the addition of IL into the amine solvents increased viscosity.

The theoretical development of a new thermodynamic approach to predict the aqueous amine + ILs + acidic gases systems was performed. The consistency between modelled results and reliable data reported in the literature demonstrated the validity of the proposed method. The present model was limited to predict gas loading at very low pressures depending on the temperature and initial concentration of amine.

This study can be continued in many aspects. It is recommended to investigate the potential of physical solvents to reduce the energy consumption and corrosion rate of amine processes. Additionally, the solubility of H_2S and hydrocarbons in the solvents studied in this work can be further investigated as a continuation of this project.

Contents

LIST OF FIGURES

LIST OF TABLES

NOMENCLATURE

Symbols

a	Peng-Robinson equation of state parameter
a_{CO_2}	CO_2 solubility
a_{H_2O}	Water activity
A	Debye–Hückel proportionality factor
A^*	Peng-Robinson equation of state parameter
b	Peng-Robinson equation of state parameter
B	Debye–Hückel equation parameter
B^*	Peng-Robinson equation of state parameter
c	Sound velocity
c'	Molarity concentration
f	Fugacity
H	Henry's constant
I	Ionic strength
k_i	Equilibrium ratio for species i
$\bar{k}$	Binary interaction coefficient for the mixing rule
K	Equilibrium constant
K'	Apparent equilibrium constant
l_i	Mole fraction of species i in liquid or gas phase
m	Molality concentration
M_i	Molar mass of species i
n	Number of moles
n_{CO_2}	Moles of carbon dioxide transferred into the equilibrium cell
n_{gas}	Total moles in vapour phase
n_L	Mole fraction of the mixture presented in the liquid phase
n_{liquid}	Total moles in liquid phase
$n_{solvent}$	Moles of solvent within the equilibrium cell
n_t	Total moles of gas and solvent within the equilibrium cell
n_V	Mole fraction of the mixture presented in the liquid phase
$n_{CO_2}^L$	Moles of CO_2 in the liquid phase
$n_{CO_2}^V$	Moles of CO_2 in the gas phases
N_p	Number of data points
P	Pressure

P_{CO_2}	Partial pressure of CO_2
P_{eq}	Pressure of the equilibrium cell at the equilibrium condition
P_1	Pressure of the gas reservoir before gas loading
P_2	Pressure of the gas reservoir after gas loading
$P_{solvent}^v$	Vapour pressure of the solvent
R	Gas constant
T	Temperature
T_{eq}	Temperature of the equilibrium cell at the equilibrium condition
T_1	Temperature of the gas reservoir before gas loading
T_2	Temperature of the gas reservoir after gas loading
u_c	Combined uncertainty
u_i	Standard uncertainty
U_c	Expanded combined uncertainty
v	Molar volume
V	Volume
V_{cell}	Volume of the equilibrium cell
V_{GR}	Volume of the gas reservoir
V^E	Excess molar volumes
x	Liquid phase mole fraction
y	Vapour phase mole fraction
z_i	Total mole fraction of species i
z_i'	Electrical charge of species i
Z	Compressibility factors

Greek letters

α	Coefficients of thermal expansions
α^E	Excess coefficients of thermal expansion
β	Binary interaction parameter for Debye–Hückel equation
γ_i	Activity coefficient for species i
δ	Peng-Robinson equation of state parameter
η	Viscosity
ρ	Density
$\rho_{g,EOS}$	Molar density of the gas phase
ϕ_i	Fugacity coefficient for species i
ω	Acentric factor

φi	Volumetric fraction
$\Delta\eta$	Deviations of viscosity

Subscripts

c	Critical state
cal	Calculated value
$cell$	Equilibrium cell
exp	Experimental value
GR	Gas reservoir
i	Component identification
j	Component identification
L	Liquid phase
t	Total
V	Vapour phase
π	Liquid (L) or vapour phase (V)

Superscripts

m	Molality based
t	Total
V	Vapour phase
π	Liquid (L) or vapour phase (V)
0	Standard state of water

Abbreviations

AAD	Absolute average deviation
AARD	Average absolute relative deviation
ACGIH	American Conference of Governmental Industrial Hygienists
AMP	Amino methyl propanol
ATC	Automatic temperature compensation
Bmim[BF$_4$]	1-butyl-3-methyl-1H-imidazol-3-ium tetrafluoroborate
Bmim[OTF]	1-butyl-3-methylimidazolium trifluoromethanesulfonate
Bmim[TF$_2$N]	1-butyl-3-methylimidazolium bis(trifluoromethanesulfonyl)imide
BSP	British Standard Pipe
BU1 Thiol	Butane-1-thiol

BV	Ball valve
C1	Gas cylinder
DC	Brush DC motor
DEA	Diethanolamine
DG	Depth gauge
DGA	Diglycolamine
DIPA	Di-isopropanol amine
EC	Equilibrium cell
EJ	Electronic jack
E-mercaptan	Ethyl mercaptan
GC	Gas Chromatography
GR	Gas reservoir
HSS	Heat stable salts
HX1 Thiol	Hexane-1-thiol
IC	Immersion circulator
ID	Internal diameter
IEA	International Energy Agency
ILs	Ionic liquids
LB	Liquid bath
MEA	2-aminoethanol
MDEA	Methyl diethanolamine
MSB	Magnetic suspension balance
M-mercaptan	Methyl mercaptan
NIST	National Institute of Standards and Technology
NMP	1-methylpyrrolidin-2-one
NOISH	National Institute for Occupational Safety and Health
NV	Needle valve
OD	Outer diameter
OSHA	Occupational Safety and Health Administration
PEL	Permissible Exposure Limit
PP	platinum resistance temperature probe
PR EoS	Peng Robinson equation of state
PR1 Thiol	Propane-1-thiol
PT	Pressure transmitter
R	Regulator
REL	Recommended exposure limit

RTILs	Room-Temperature Ionic Liquids
SCBA	Self-contained breathing apparatus
SS	Stainless steel
STEL	Short-term exposure limit
TEA	Triethanolamine
TGA	Thermogravimetric analyser
TLV	Threshold limit value
TP	Temperature probe
TR	Temperature regulation
TRU	Thermodynamics Research Unit
TSILs	Task-specific ionic liquids
TWA	Time weighted average
VFT	Vogel–Fulcher–Tammann
VLE	Vapour-liquid equilibrium
VP	Vacuum pump

1. INTRODUCTION

Fossil fuels supplied over 85% and 80% of world energy demand in 2008 and 2013, respectively. They have continued to dominate energy consumption patterns and account for the majority of increased energy demand to 2035, contributing 75% of global energy demand [1-3]. The International Energy Agency (IEA) predicts a 57% increase in energy demand from 2004 to 2030 [2, 4], which was updated in the New Policies Scenario[5], to 30% between 2017 and 2040. This is the equivalent to an additional demand the size of combined economies of China and India to today's global need [5]. The rise in global energy demand means an increase in consumption for all fuels including fossil fuels. For instance, the annual growth of natural gas demand is 1.9% [6], and the IEA predicts a rise in natural gas use of 45% by 2040 [5].

Natural gas is the most environmentally friendly fossil fuel compared to oil and coal. It is becoming one of the most significant and attractive sources of energy for future because it is the earth's cleanest burning hydrocarbon, and ample domestic reservoirs of natural gas are available [7, 8]. The composition of natural gas varies, as this depends on the type, depth, and location of the underground reservoirs, the porosity of the sedimentary deposits and the geology of the area. The gas produced from two wells in the same reservoir may also differ in composition. Natural gas consists primarily of methane (70 – 90 % of the total) with heavier hydrocarbons and impurities that need to be removed [6, 9, 10].

Natural gas contains several impurities, in particular, CO_2 and H_2S that form an acidic solution in the presence of water. These acidic gases need to be removed from raw natural gas because they are not only corrosive, resulting in technological problems in process equipment, transportation and distribution lines, but they also reduce the heating value of natural gas [7, 11-13]. In addition, when natural gas is cooled to a very low temperature, CO_2 can crystallize and block pipeline systems, leading to transportation breakdowns [9]. Moreover, H_2S is a toxic gas that generates sulfur dioxide (SO_2) during combustion. There is also an undeniable connection between CO_2 with global warming and climate change [7, 8, 10-14]. CO_2 is an important heat-trapping (greenhouse) gas which is released through human activities, such as burning fossil fuels and deforestation and, as well as natural processes. Direct measurements show rising atmospheric CO_2 concentrations which intensifies climate change [15].

Table 1-1 presents the composition of natural gas from different reservoirs compiled from various literature [9, 10, 16, 17].

1

Table 1-1: The composition[a] of natural gas reservoirs in various parts of the world [9, 10, 16, 17].

Components	Location of reservoir						
	Iran	Canada	Western Colorado	Miskar Field Tunisia	France	Pakistan	Saudi Arabia
CH_4	84.95	76.10	29.59	63.07	69	27.3	55.5
C_2H_6	5.43	6.51	0.54	3.3	3	0.7	18
C_3H_8	2.01	3.06	0.28	0.95	0.9	0.3	9.8
C_4H_{10}	0.94	1.97	0.21	0.54	0.5	0.3	4.5
C_5+	0.60	2.96	0.25	0.62	0.5	-	1.6
N_2	3.47	3.16	25.76	16.68	1.5	25.5	0.2
H_2S	0.69	3.26	0	0.09	15.3	-	1.5
CO_2	1.83	1.68	42.11	13.41	9.3	46.2	8.9
H_2O	0.06	1.3	1.3	1.3	-	-	-
COS ppm mole	3	-	-	-	-	-	-
Mercaptans (M-mercaptan, E-mercaptan, PR1Thiol, BU1 Thiol, HX1Thiol) ppm mole	245	-	-	-	-	-	-

[a]Data for Iran, Canada, Western Colorado and Miskar Field Tunisia are in mole percent basis; and data for France, Pakistan and Saudi Arabia are in a volume percent basis.

Although the purification process brings extra costs, the increase in demand for natural gas has resulted in the increasing use of gas reservoirs containing higher concentration of impurities. The composition of these natural gas reservoirs such as those in France, Pakistan and Western Colorado as shown in Table 1-1 along with the ones with less impurities, such as reservoirs in Netherland or Iran [7].

Due to the technological problems and environmental impacts of the emissions, there are strict regulations on CO_2 and H_2S concentrations and emissions to mitigate their impacts. Although the allowed quantities of common impurities may vary from pipeline to pipeline depending on the source and the system's design, natural gas pipeline specifications usually limit the CO_2 and H_2S content to less than 2% and 4 ppm, respectively. The standard specifications for common impurities allowed, in the United States of America, prior to the delivery of natural gas to pipelines, are given in Table 1-2 [9, 12].

Table 1-2: The allowable amounts of common impurities for the natural gas delivery to U.S.A. pipeline[9].

Component	U.S. pipe line specification
CO_2	< 2 mol %
H_2S	< 4 ppm
H_2O	< 0.1 g/m^3 (<120 ppm)
C_3+	950-1050 Btu/scf dew point -20 °C
Total inert (N_2, He, Ar, etc)	< 4 mol%

The use of absorption with alkanolamine solutions in removing impurities, such as H_2S and CO_2 is common in the industry, but amine technology has several disadvantages. These include amongst others, loss of solvent, corrosion and high heat consumption. It is necessary to periodically add pure solvent to the solution because of the loss of solvent during operation [7, 18-22]. On the other hand, ionic liquids (ILs) are nonvolatile (so-called 'green') and recyclable solvents [7, 18, 23-25]. Their immeasurable vapour pressure causes ILs not to contaminate gas stream and environment even in small amounts [26]. Fluorinated ILs have presented an appreciable capacity for absorbing H_2S and CO_2 [7, 18]. It can be predicted that the combination of ionic liquids, particularly fluorinated ones, with amine solutions is efficient in CO_2 and H_2S capture, and may be a boon for natural gas sweetening, avoiding the disadvantages of the current amine technology.

The aim of this study is to provide a comprehensive theoretical and experimental study of selected fluorinated ionic liquids and their use as an additive to aqueous amine solutions and free-water amine solutions for the absorption of CO_2.

The initial proposal of this PhD topic was to study H_2S systems, with phase equilibrium data measured for H_2S with new solvent blends and hybrid solvents. Due to many constraints and safety aspects when working with H_2S, as well as the time for the necessary facilities to be available, the aim and objectives were modified to focus on CO_2 with novel hybrid solvents.

The objectives include:
1. A literature review followed by a selection of suitable fluorinated ILs which could be added to current solvents to enhance the properties.
2. Commissioning of a new "static-synthetic" phase-equilibrium apparatus with a low-volume equilibrium cell capable of measuring gas solubility data for systems of hazardous and expensive chemicals.
3. Experimental measurements of CO_2 solubility in known systems followed by novel measurements.

4. Thermodynamic modelling of the measured CO_2 (and H_2S) + aqueous amine + ionic liquid systems.

Solubility experiments were performed for three test systems, viz. (NMP, hexane and bmim[BF_4]) and five new systems, viz. (NMP + bmim[BF_4], MEA/DGA + water + bmim[OTF] and MEA/DGA + NMP + bmim[TF_2N]). For the purpose of characterizing the solvents, experimental measurements also included the evaporation rate, viscosity, density, speed of sound and refractive indices at varying temperatures. The thermodynamic modeling for the CO_2/H_2S + aqueous amine + ionic liquid phase data included the development a new model approach using Kent-Eisenberg and Deshmukh–Mather models. The results from this study were compared to the solvent blends in literature. The findings and analyses from these investigations are presented in the document.

This thesis consists of seven Chapters. The second chapter of this work reviews the technologies used for H_2S and CO_2 capture from the petrochemical streams, with a particular emphasis on the amine process. The chapter also assesses ionic liquids, their properties and potential applications in separation processes, and solubility data available in the literature with reference to the CO_2 absorption using ionic liquids. The chapter also designates the importance of providing a more efficient route for acid gas removal and the probable advantages of coupling conventional absorption processes with ionic liquids.

The third chapter briefly reviews methods used to measure vapour-liquid equilibrium data. The chapter then presents a review of techniques used to measure the solubility of H_2S and CO_2 in hybrid solvents. The chapter also justifies the measurement method suited to this study. The fourth chapter features the static-synthetic setup designed, constructed and commissioned for systems containing gases, ionic liquids and amines. The equilibrium cell as the core of the apparatus has some novelty in the design to measure the liquid phase volume directly. The low-volume equilibrium cell suits the measurements of expensive and hazardous components. The fifth chapter describes the experimental method applied to obtain accurate solubility data.

The sixth chapter describes the thermodynamic models used in this study to predict the solubility of CO_2 and H_2S in chemical and/or physical solvents. An applicable method to model the solubility of acid gases in chemical solvents developed in this work is discussed in this chapter. The seventh chapter presents the results of the experimental measurements and thermodynamic modellings. The data on the solubility of CO_2 in three test systems, viz. (NMP, hexane and bmim[BF_4]) and five new systems, viz. (NMP + bmim[BF_4], MEA/DGA + water + bmim[OTF] and MEA/DGA + NMP + bmim[TF_2N]) are presented. The chapter also assesses the ability of the method developed in this study to model the solubility of acid gases in the aqueous amine solutions and their mixture with ILs.

2. PROJECT BACKGROUND

An overview of the technologies currently used for the removal of H_2S and CO_2 impurities from natural gas, with a particular emphasis on chemical absorption, are discussed in this chapter. The applications, advantages and limitations of these processes are also presented. An overview is provided on the properties of ionic liquids and their potential applications in petrochemical industries and in gas separation. Standard technologies and new technologies, using ionic liquids, are compared. Finally, the possibility of coupling current technologies with ionic liquids and the probable advantages is explained.

2.1 CO_2 and H_2S capture technologies

The available technologies used to purify a wide variety of petrochemical streams include absorption, adsorption, cryogenic condensation, membranes and hybrid separation processes [27]. The technologies have been developed throughout the years with the aim of optimizing capital and operating costs and complying with product specifications and environmental standards. The key parameters affecting the selection of an acid gas removal process are: 1) feed gas composition including acid gases, hydrocarbons and other contaminants, 2) feed gas pressure and flow rate, 3) ambient conditions, 4) the availability of existing equipment and process configuration, 5) required recovery efficiency, 6) concentration of sulphur species in the stack gas, 7) ease of operation, 8) the selectivity of acid gas removal required, 9) product quality, 10) environmental restrictions, either local or global, including air pollution regulations and disposal of byproducts considered hazardous chemicals, and 11) costs (capital and operating) [17, 28, 29].

Absorption is one of the most versatile processes for CO_2 and H_2S removal and sweetening of industrial gas streams, especially natural gas. At present, gas absorption processes represent approximately 70% of the techniques used for treating natural gas, where a gaseous phase is contacted with a liquid solvent in which CO_2 and/or H_2S are either physically or chemically dissolved [30, 31]. Absorption is usually carried out in a countercurrent tower (column), through which liquid descends and gas ascends, and equipped with trays or packing beds [31].

Absorption processes can be divided into three categories:
1) Physical absorption processes where the dissolved gas only interacts physically with the solvent. Solvents used in these processes are called physical solvents, such as chilled methanol, a mixture of dimethyl ethers of polyethylene glycol and propylene carbonate, used in the Rectisol, Selexol, and Fluor processes, respectively. These are non-reactive compounds with an affinity for acid gas that interact physically with the acid gases. These physical methods of absorption are

more efficient at high partial pressures of acid gas (approximately 50 psi or higher) [17, 18, 32-34].

2) Chemical absorption processes where the dissolved gas reacts chemically with the chemical solvent. Chemical solvents, such as monoethanolamine, methyldiethanolamine and potassium carbonate are the preferred solvents at low (partial) pressures, as deep H_2S and CO_2 removal (acid gas partial pressure of 10^0 psi or less in the product) is possible at a low feed pressure [17, 18, 32-34].

3) Physico-chemical absorption aims to combine the best qualities of chemical absorption (a high absorption potential) and physical absorption (a low regeneration energy requirement). Solvents used in these processes are called hybrid solvents such as Sulfinol (a mixture of sulfolane and an aqueous solution of either diisopropanolamine or methyldiethanolamine) [17, 31, 32].

Selection criteria for the solvent-based processes are presented in Figure 2-1. The guidelines in this figure have been approximated and applies to the simultaneous removal of H_2S and CO_2. This figure is for solvent-based processes only, thus, it excludes some commonly used processes, such as adsorption and membranes [17]. A process selection chart for CO_2 removal with no H_2S present, H_2S removal with no CO_2 present, and selective H_2S removal with CO_2 present can be found in Kidnay and Parrish (2006) [17].

The following criteria are useful when selecting an economically feasible solvent: 1) high gas solubility, 2) high solvent selectivity for acid gases when compared to other components of the gas phase such as heavy hydrocarbons, 3) low effects on product and environment, 4) low vapour pressure to prevent solvent loss, 5) high thermal and chemical stability, 6) low cost and high availability, 7) low heat requirements for solvent regeneration 8) non-corrosive and non-flammable behaviours, 9) low viscosity, and 10) low freezing point [9, 18]. Unfortunately, commercially employed solvents cannot meet all of these criteria. For instance, amine solutions have high heat requirements for solvent regeneration and high vapour pressure (at high temperatures required for the regeneration of chemical solvent) causing loss of solvent [18, 33]. The application of ionic liquids (ILs), these carefully constructed liquids, is often limited in the industry due to their high viscosity and high cost [23, 33, 35]. The need to refrigerate methanol and complexity of the process make the Rectisol process[1] the most expensive of such treatment methods. Therefore, its use is only justified where almost pure gas, containing <0.1 ppmv total sulfur, is desired as a product [36, 37]. In the Rectisol process, solvent loss is considerable due to

---

[1] In the Rectisol process, chilled methanol at a temperature of approximately −40 to −62°C absorbs the acid gases from the feed stream at relatively high pressure, usually 2.76 to 6.89 MPa *36. https://www.sciencedirect.com/topics/engineering/rectisol-process.*

high vapour pressure of methanol even at low temperatures [36]. Table 2-1 compares the physicochemical properties of some solvents used for acid gas removal [38, 39].

In general, among absorption solvents, chemical alkanolamine-based solvents are the most common for H_2S and CO_2 removal, because of their highly reactive nature and low cost [12, 31].
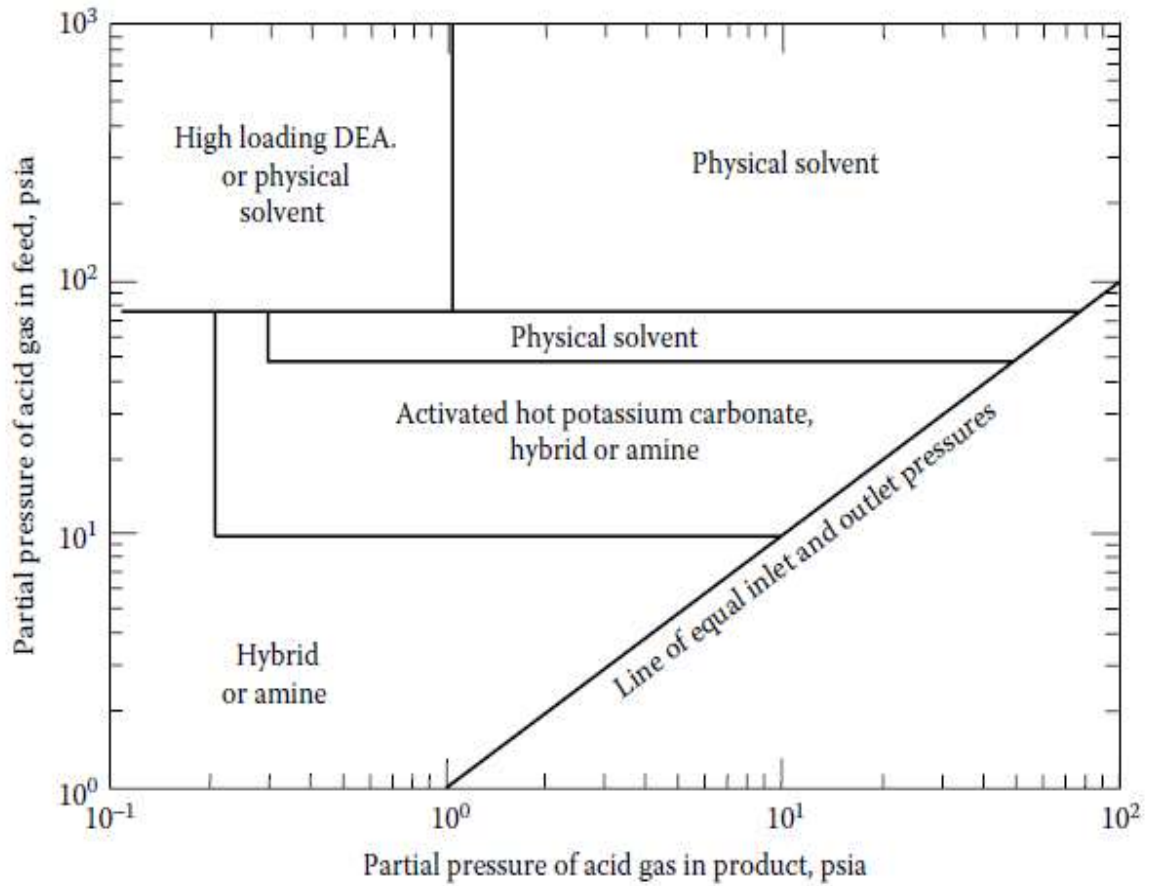
Figure 2-1: Process selection chart for simultaneous H_2S and CO_2 removal [17].

Table 2-1: Comparison of physicochemical properties of various solvents [36, 38-44].

Property	Amines	Ionic liquids	Fluor solvent[a]	Purisol solvent[b]	Selexol solvent[c]	Rectisol solvent[d]
Type of absorption	chemical	physical/ chemical	physical	physical	physical	physical
Molecular weight	60 to 250	70-800	102.089	99.133	280	32.042
Density (g/cm^3) at T=25 °C	0.65 to 1.20	0.80-2.10	1.195	1.027	1.03	0.7863
Viscosity (mPa.s)	<7 to 460 (25 for MEA at T=20 °C)	7-1800	2.47 at T=25 °C	1.65 at T=25 °C (2.94 to 1.112 (T= 0 to 54 °C))	5.8 at T=25 °C	0.544 at T=25 °C
Boiling Point (°C)	111 to 350	>250	241.6	202	275	64.7
Flash point (°C)			135 °C	90	>110	11
Melting Point (°C)	(-65) to 25	-100 to 113	−48.8 °C	-24	-28 °C	−97.6
Vapour Pressure (mmHg)	<0.001 -11 at T=25 °C	0.000001 at T=25 °C	0.023 at T=25 °C	0.4 at T=25 °C 0.237 at T=20 °C	0.00073 at T=25 °C	127 at T=25 °C
Water solubility	variable, amines with low molar mass are very soluble	variable	very soluble	completely miscible with water	soluble in water	miscible in water
Thermal stability	100-251°C	>500 °C		high thermal and chemical stability		
Tunability	NO	highly tunable	NO	NO	NO	NO
Solubility of H_2S/solubility of CO_2 (selectivity); volume based, at 25 C and 1 atm	1-13 variable	2-15 variable	3.2 NO	10.2 highly Selective for H_2S	8.92 YES	7.06[e] YES (only slightly less than Selexol)

[a] Propylene carbonate
[b] N-Methyl-2-pyrrolidone, NMP
[c] Dimethyl ether of polyethylene glycol
[d] Methanol
[e] Relative solubility of H_2S in methanol at −25 °C

2.1.1 Absorption of CO_2 and H_2S in alkanolamine solutions

 The use of aqueous alkanolamine solutions was first proposed by R.R. Bottoms in 1930, and it has been applied for CO_2 and H_2S removal from natural gas for over 80 years [45, 46]. Triethanolamine (TEA) was the first commercially available alkanolamine used in early gas treating plants. However, it has been replaced largely because of its undeniable disadvantages, such as low absorption capacity, slow reaction rate and relatively poor stability [45].

Alkanolamines are organic compounds with at least one amine group and a hydroxyl (or alcohol) group. The hydroxyl group is responsible for increasing the boiling point, improving the solubility of amines in water and decreasing vapour pressure. As a result, less solvent is lost from the absorber or stripper towers (columns). The amino group contributes to the basicity or alkalinity in the aqueous solution for the absorption process [9, 11, 45-47]. Generally, amines, depending on the number of alkyl groups attached to the nitrogen atom in the molecular structure, are classified as three types: primary, secondary and tertiary alkanolamines [17, 48, 49]. Primary amines are the most reactive, followed by secondary and tertiary amines [17]. Figure 2-2 presents the molecular structures of different types of amines.
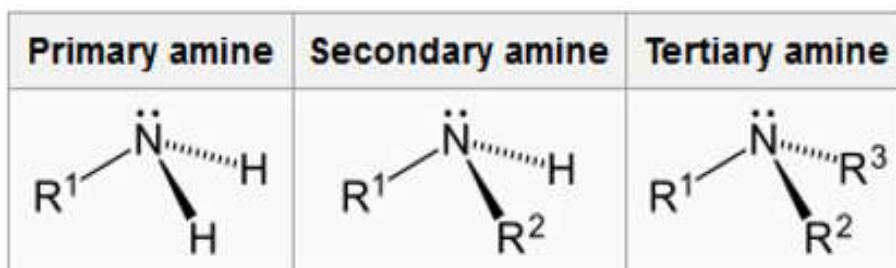
Figure 2-2: Molecular structure for three types of amines [48, 49].

Alkanolamines remove H_2S and CO_2 in a two-step process. Firstly the acid gas dissolves in the aqueous amine (physical absorption). The dissolved gas, which is a weak acid, then reacts with the weakly basic amines (chemical absorption) [17]. The alkanolamines typically employed in gas sweetening industries are monoethanolamine (MEA), diethanolamine (DEA), di-isopropanol amine (DIPA), methyl diethanolamine (MDEA) and Diglycolamine (DGA) [9, 31, 45].

MEA is a primary amine that has two replaceable hydrogen atoms. MEA is used in aqueous solutions in concentrations between 10 and 20 wt.% MEA. The most widely used aqueous concentration is 15 wt.% MEA which freezes at -4 °C. Corrosion problems limit the allowable acid gas loading, thus, the maximum is usually 0.3 to 0.35 mole/mole (moles acid gas per mole of amine) for carbon steel equipment. Although, acid gas loadings as high as 0.7 to 0.9 mole/mole have been applied using stainless steel equipment, with no corrosion problems [31, 45, 49, 50].

Aqueous MEA solutions are useful for deep removal of CO_2 when the feed gas is free from H_2S, deep removal of H_2S when the feed gas is free from CO_2, and deep removal of both H_2S and CO_2 when both components are present in the feed gas. Consequently, this process is not appropriate for the selective removal of either H_2S or CO_2 when both are present in the gas [31]. MEA is the most basic of the amines employed in acid treating and therefore the most reactive for acid gas capture and used in applications with low feed pressure requiring stringent outlet gas specifications or total removal of the acid gases [17, 51]. An aqueous MEA solution reacts with H_2S faster than CO_2 and is able to easily reduce the H_2S concentrations to less than 4 ppm in the treated gas [31]. This can be illustrated by considering the following reactions [52]:

$$H_2S \leftrightarrow H^+ + HS^- \tag{2-1}$$

$$H^+ + RNH_2 \leftrightarrow RNH_3^+ \tag{2-2}$$

$$HS^- \leftrightarrow H^+ + S^{2-} \tag{2-3}$$

$$H_2O \leftrightarrow H^+ + OH^- \tag{2-4}$$

The overall reaction of MEA with H_2S is [17, 31, 47, 52] :

$$RNH_2 + H_2S \leftrightarrow RNH_3^+ + HS^- \tag{2-5}$$

When the gas stream contains CO_2, it reacts with the MEA as a primary amine via two different mechanisms. In the first mechanism, the reaction of CO_2 with MEA produces a carbamate species. The CO_2 reacts with one amine molecule to produce the carbamate intermediate that reacts with a second amine molecule to form the carbamate species. The reactions (equation 2-8 is the overall reaction) are as following [17, 31, 33]:

$$CO_2 + RNH_2 \leftrightarrow RHN^+HCOO^- \tag{2-6}$$

$$RHN^+HCOO^- + RNH_2 \leftrightarrow RHNCOO^- + RNH_3^+ \tag{2-7}$$

$$CO_2 + 2RNH_2 \leftrightarrow RHNCOO^-(\text{carbamate}) + RNH_3^+ \tag{2-8}$$
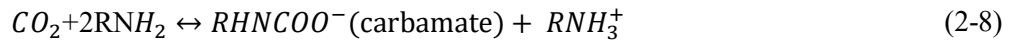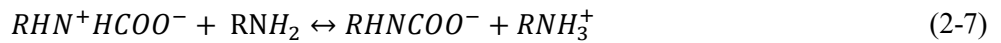
In the second mechanism for the reaction of CO_2 with amines, the amine reacts with CO_2 via hydrolysis as CO_2 hydrolyzes in water to form carbonic acid, followed by dissociation to bicarbonate and then carbonate. Finally, the amine reacts with the bicarbonate and proton by following equations [33, 53]:

$$CO_2 + H_2O \leftrightarrow H_2CO_3 (\text{carbonic acid}) \tag{2-9}$$

$$H_2CO_3 \leftrightarrow H^+ + HCO_3^- \ (\text{bicarbonate}) \tag{2-10}$$

$$HCO_3^- \leftrightarrow CO_3^{2-} + H^+ \ \ (\text{carbonate}) \tag{2-11}$$

$$H_2O \leftrightarrow H^+ + OH^- \tag{2-12}$$

$$H^+ + RNH_2 \leftrightarrow RNH_3^+ \tag{2-13}$$

$$HCO_3^- + RNH_2 \leftrightarrow RHNCOO^-(\text{carbamate}) + H_2O \tag{2-14}$$
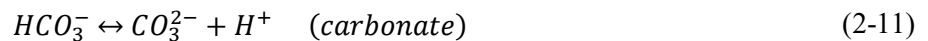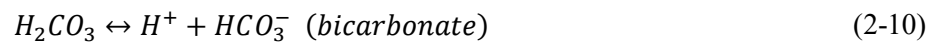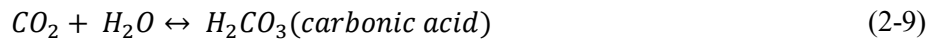
The above reactions are reversible. Forwards reactions illustrate the absorption process. This is an exothermic process that is faster and more efficient at low temperatures and high pressures.

On the other hand, reverse reactions are endothermic indicating regeneration process. Thus, the reactions are more efficient at high temperatures and low pressures [31, 33].

Although aqueous MEA is not considered as a particularly corrosive solution, its degradation products are extremely corrosive. This amine reacts irreversibly with sulfur compounds such as COS, CS_2, SO_2, SO_3, and oxygen. Heat stable salts (HSS) are the undesirable products of these reactions which cause corrosion and foaming in equipment and also decrease the absorption of H_2S [17, 31, 45, 47, 50]. Therefore, a special piece of equipment called reclaimer using compounds such as sodium carbonate or sodium hydroxide, is required to neutralize the HSS, clean the solution and avoid serious corrosion problems [17, 31]. If mercaptans are present in the feed gas, the aqueous MEA solution removes only a part of these impurities and priority is given to light mercaptans such as methyl-mercaptan [31]. High reactivity and low cost are the advantages of MEA [47].

DEA is a secondary amine and commonly used in aqueous solutions in concentrations between 25 and 35 wt.% DEA. A 25 wt.% DEA solution freezes at -6 ℃. The total acid gas loading for aqueous DEA is also limited to 0.3 to 0.35 mole/mole for carbon steel equipment. The loading can be as high as ~1 mole/mole when using stainless steel equipment. The degradation products of DEA are much less corrosive than those of MEA [31, 45, 49, 50]. DEA does not require reclaimer. This is one of its main advantage of DEA over the primary amines [31, 51]. DEA is less basic and reactive than MEA and has a reduced affinity for H_2S and CO_2, thus, it may not be able to produce pipeline gas specification for low-pressure feed streams, and it is used in medium to high-pressure treating. Compared with MEA, it has a lower vapour pressure leading to lower evaporation losses [17, 50, 51].

Similar to MEA solutions, aqueous DEA solutions generally do not display selectivity for H_2S or CO_2 and removes both of them, except under particular limited conditions. Therefore, this is not a suitable process for selective removal of H_2S or CO_2 when both are present in the feed gas [31].

Under special conditions, such as low pressure (~ 11 psig) and a short liquid residence time on the tray, of about 2 seconds, aqueous DEA is selective toward H_2S and a significant portion of the CO_2 remains in the product gas. If mercaptans are present in the feed gas, the DEA solution removes a portion of them according to their boiling points. Priority is given to light mercaptans [50].

The aqueous DEA reacts with H_2S faster than with CO_2. The overall reaction is:

$$R_2NH + H_2S \leftrightarrow R_2NH_2^+ + HS^- \tag{2-15}$$

When the feed gas contains CO_2, it reacts with the DEA (as a secondary amine-solution) via two different mechanisms, as with primary amines. As explained above for MEA, in the first mechanism, the reaction of CO_2 with DEA forms a carbamate species (R_2NCOO^-). In the second mechanism, the amine solution reacts with bicarbonate species and protons that are products of the reaction between CO_2 and H_2O. The overall reactions for the two mechanisms are similar to those of the primary amines [31, 33]. The heat of reaction for DEA with CO_2 is 653 BTU/lb CO_2, which is about 25% less than that for MEA (825 BTU/lb CO_2). The heat of reaction for DEA with H_2S is 511 BTU/lb H_2S, which is close to that for MEA (550 BTU/lb H_2S) [50]. The magnitude of the exothermic heat of reaction is important because the heat released in reaction and during absorption step must be added back in the regeneration step [17]. Therefore, energy consumption and reboiler duty for the regeneration of DEA are less than that of MEA.

MDEA is a tertiary amine and generally applied in aqueous solutions in concentrations between 20 and 50 wt.% MDEA. Due to considerably fewer corrosion problems compared to primary and secondary amines, the total acid gas loading for MDEA can be as high as 0.7 to 0.8 mole acid gas/mole amine for carbon steel equipment. Aqueous MDEA is considered as a selective solvent towards H_2S, with a stated removal efficiency of less than 4 parts-per-million level and lower, from a feed gas containing both CO_2 and H_2S [45, 49, 50]. In addition, the use of aqueous MDEA for bulk removal of CO_2 is interesting due to its low heat of reaction with this compound and the resulting energy saving at the regeneration step [31, 50]. Activated MDEA (through licensers) can be used to deeply remove both H_2S and CO_2. Based on the type of acid gas removal requirement, licensers add specific activated agents to the MDEA to change the selectivity of MDEA. Main licensers of MDEA-based processes are BASF, DOW, EE(P) and UOP [31].

Despite the fact that MDEA is more expensive than MEA and DEA, it has several advantages over primary and secondary amines which include lower vapour pressure or volatility, lower heats of reactions (600 BTU/lb CO_2 and 522 BTU/lb H_2S), higher resistance to degradation (reaction with sulfur compounds, such as CS_2, COS and SO_2) and fewer corrosion problems. The advantage of MDEA in comparison to other amines is its selectivity toward H_2S in the presence of CO_2 [31, 45, 50]. At high CO_2/H_2S ratios, most of the H_2S can be removed while a major portion of CO_2 remains in the gas stream. In addition, optimizing the design of the absorption column increases the selective absorption of H_2S, for instance by setting a liquid tray residence time between 1.5 - 3.0 seconds and/or by increasing the temperature in the column [50].

The selectivity of MDEA toward H_2S originates from the fact that tertiary amines do not have a hydrogen attached to the nitrogen so they cannot directly react with CO_2 or bicarbonate to form a carbamate. Consequently, CO_2 reacts with MDEA only via one mechanism, unlike primary and

secondary amines. Through this mechanism, MDEA reacts with protons that are products of the reaction between CO_2 and H_2O. Hence, MDEA is not able to react with CO_2 in the absence of water, and the dissolving of CO_2 in water is a necessary requirement for the reaction to occur [17, 33, 50].

The CO_2 reactions with MDEA are as follows:

$$CO_2 + H_2O \leftrightarrow H_2CO_3 (carbonic\ acid) \tag{2-16}$$

$$H_2CO_3 \leftrightarrow H^+ + HCO_3^- \ (bicarbonate) \tag{2-17}$$

$$HCO_3^- \leftrightarrow CO_3^{2-} + H^+ \quad (carbonate) \tag{2-18}$$

$$H_2O \leftrightarrow H^+ + OH^- \tag{2-19}$$

$$H^+ + R_3N \leftrightarrow R_3NH^+ \tag{2-20}$$
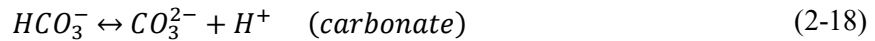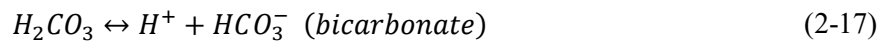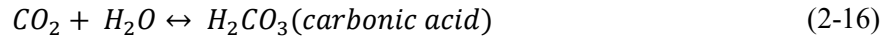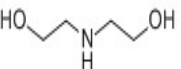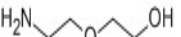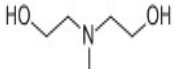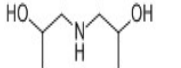
The reaction between H_2S and MDEA occurs immediately by the same proton transfer mechanism found in primary and secondary amines [17, 31, 50, 53].

DGA is a primary amine that shows high reactivity with acid gases. It is used in aqueous solutions in concentrations between 50 and 70 wt.% DGA. A high concentration of DGA in the solution is considered as a definite advantage over other amines since higher concentrations result in lower circulation rates and also in lower freezing points. Due to corrosion problems, the maximum acid gas loading should not be more than 0.35 moles acid gas per mole of amine. Aqueous DGA reacts with H_2S and CO_2 in the same manner as MEA; it is not selective toward H_2S or CO_2. Therefore, an absorption process using the aqueous DGA is not a suitable process for the selective removal of H_2S in the presence of CO_2. Similar to MEA, DGA reacts with sulfur compounds (COS and CS_2) resulting in undesirable and corrosive products, so a reclaimer is required to clean the solution. The high heat of reaction for both CO_2 (850 BTU/lb CO_2) and H_2S (674 BTU/lb H_2S) is another primary disadvantage of DGA [31, 50]. If mercaptans are present in the feed gas, the aqueous DGA solution removes a small part of these impurities, so the bulk of these contaminants remain in the output gas stream [17, 31].

In this discussion, only the main constituents of aqueous solutions used in industrial natural gas sweetening are considered. Table 2-2 summarizes some characteristics of commonly used amines for acid gas removal processes.

Table 2-2: Typical characteristics of commonly used amines [9, 31, 50, 54-57].

Amine	MEA	DEA	DGA	MDEA	DIPA[1]
Structure	H_2N–OH	HO–N–OH	H_2N–O–OH	HO–N–OH	HO–N–OH
Solution concentration wt.%	10 - 20	25 - 35	50 - 70	20 - 50	30 - 40
Acid gas loading, mole/mole (carbon steel)	0.3 - 0.35 (0.7 to 0.9 mole/mole in stainless steel equipment)	0.3 - 0.35 (~1 mole/mole in stainless steel equipment)	0.3 - 0.35	0.7 - 0.8	0.41-0.61
Ability to selectively absorb H_2S	NO	Some limited conditions	NO	YES	YES
Vapour pressure (mmHg)	0.500 at 303.14 K, 1.3914 at 313.15 K	0.0899 at 303.14 K, 0.3600 at 323.14 K	0.0276 at 303.2 K, 0.0719 at 313.2 K	0.0123 at 303.14 K, 0.0315 at 313.14 K	115.7199 at 303.14 K, 164.2035 at 313.76 K
Freezing point (°C)	10.3, -4 (15 wt. % solution)	28, -6 (25 wt. % solution)	-11, -35 (50 wt. % solution)	−21.00, -6 (25 wt. % solution)	44 °C
Heat of reaction CO_2 (BTU/lb CO_2)	825	653	850	600	-
Heat of reaction H_2S (BTU/lb H_2S)	550	511	674	522	-

[1] This secondary amine is not used by itself as a sweetening solvent but is part of the Sulfinol solvent formulation

The major advantages of the amine absorption processes are that it is a widely commercialized technology, the hydrocarbon loss is almost negligible, high reactivity with CO_2 and H_2S, and the significant ability for deep removal of the acid gas [18, 33]. However, the corrosive nature, high vapour pressure, loss of solvent, transfer of water into the gas stream during regeneration step and high-energy consumption are disadvantages to be addressed [7, 18-22].

Amines, especially MEA, are not very stable, and under process conditions some of the amines degrade, forming corrosive products, reducing process efficiency, increasing viscosity and producing excessive foaming [7, 18, 20]. Amine solutions cause corrosion problems in the units that limit the maximum acid gas loading in solvents. For instance, a carbon steel plant for gas sweetening using an MEA solution has a corrosion rate of about 1 mm per year [18]. To reduce these problems the use of corrosion inhibitors is suggested, but this has some problems, i.e., the solvent reacts with some of the corrosion inhibitors potentially causing erosion of the unit and an increase in foaming (as a result, the injection of antifoaming agents is required as well) [9].

The high vapour pressure of amine solutions leads to the release of amine and water into the gas phase during the desorption step [18, 20]. As a result, all the solvent cannot be transferred back to the absorber column and some solvent is lost in each cycle of the absorption process and must be replaced regularly [10, 18]. Moreover, the solvent loss results in environmental hazards [9, 10, 18, 58]. They can be partly reactive in the environment forming toxic materials, such as nitrosamines, nitramines, and amides. Most nitrosamines are carcinogenic causing cancers in a wide variety of animal species and in humans, even at low levels [18].

The amine processes have a high energy consumption, especially during the desorption step, to break the chemical bonds formed in the absorption step [7, 18, 19]. The cost of the regeneration step is estimated at around 70-80% of the total operating costs of the separation process [7, 59]. In addition, the regenerated solvent leaves the desorption column at its saturated temperature and is supposed to move through a pump [9]. Therefore, there is a possibility for cavitation if the temperature of the flow is not lowered.

All of these factors make the amine process costly for most applications. Consequently, to meet market demand an alternative solvent is required that possesses fewer drawbacks and lower costs than current solvents. This ideal solvent should have properties, such as low vapour pressure, high thermal and chemical stability, high absorption capacity, low corrosivity and low viscosity. To this end, the use of ILs as alternative absorbents for H_2S and CO_2 are discussed in the following section.

2.2 Ionic liquids (ILs)

Ionic liquids (ILs) are commonly defined as salts that are only composed of tunable ionic species including large organic cations and organic/inorganic anions, without any neutral molecules [18, 33, 37, 60]. They are liquids in their pure state near ambient conditions [19, 20, 30, 61, 62]. The bulky asymmetric structure of cation causes that ions of IL (cation and anion) do not pack very well, thus, it reduces the lattice energy[1] and bond force between ions [64]. The lattice energy is reflected in the melting points of ionic compounds. During melting, the ions obtain sufficient kinetic energy to overcome the potential energy of bonding, and they move away from each other. Therefore, as the lattice energy decreases, the ions need less energy to separate from each other, thus, the melting point decreases as well [26]. These principles result in ILs having melting points below 100 °C. In addition, most ILs have melting points around or below room temperature and are called Room-Temperature Ionic Liquids (RTILs) [18, 25, 26, 33, 37, 60, 64, 65]. Liquid organic salts, molten salts, fused salts and non-aqueous ionic liquids are other common names applied to describe ILs [26].

Low-melting ionic liquids are an exciting class of compounds being investigated for their applications in a variety of technologies such as solar cells, lubricants, biomass processing, heat transfer fluids, separation techniques, non-volatile electrolytes, mass spectrometry, electrochemical capacitors and gas capture [7, 18, 35, 37, 64, 66, 67]. This has become possible due to a large number of ILs that can be synthesized via different combinations of anions and cations [7, 18, 26, 60, 61, 64, 66]. It has been claimed that the theoretical number of potential ILs is to the order of 10^{18}. They may have the potential to overcome many of the problems that current techniques have [7, 18, 61]. Task-specific ionic liquids (TSILs) are resulted from the functionalization of ILs by tuning and designing the structures of both cations and anions according to special purposes [66]. As a consequence, the usage of TSILs or functional ILs can be highly efficient according to our requirements, with better control over the overall process [35, 67]. On the other hand, conventional ionic liquids are described as ILs that do not have an attached functional group [18].

ILs are composed of N-containing organic cations, with highly different sizes and shapes, such as quaternary ammonium, imidazolium or pyridinium ions combined with anions which basically have a more symmetrical shape and are smaller in size compared to their cations. There are a wide variety of anions that range from simple inorganic ions (such as halides) to more complicated

---

[1] Lattice energy is the energy released when one mole of an ionic compound is formed. This means when the individual ions of the compound come together to form the ionic lattice, they require less energy to stay together, thus they release it. when the ions are small the more energy is released, it results in more lattice energy and the stronger bond 63. Chang, R., *Chemistry (8th Edition)*. 8th ed. 2004.

organic species (such as bis[(trifluoromethyl)sulfonyl]imide) [65, 68]. The common cations and anions used in ILs synthesis are listed in Table A-1.

2.2.1 Ionic liquid properties

ILs have several unique and remarkable properties such as tuneable nature or structural designability, negligible vapour pressure (a significant vapour pressure is often observed at 300 – 400 ˚C above room temperature), wide liquidus range, high thermal and electrochemical stabilities up to high temperatures, wide range of polarities and excellent solvent properties for a range of polar or nonpolar and organic or inorganic compounds [7, 18, 23, 26, 30, 33, 34, 58, 65, 69, 70]. They are also assumed to be recyclable and reusable [19, 33, 67].

ILs are tuneable meaning that they can be designed or 'tailor-made' for a specific task and/or to achieve desirable physicochemical properties. This allows ILs to present a wide range of physicochemical properties including melting point, viscosity, absorption capacity (various selectivity and solubility for solute), water-miscibility, density, hydrophobicity, heat capacities, thermal decomposition temperatures, surface tension, toxicity and health issues, and corrosion. Since the physicochemical features of an ionic liquid are dependent on the nature and structure of its ions, they can be adjusted by attaching different chemical structures and branched alkyl groups, functionalizing ions, varying their chain lengths, and making an appropriate combination of anion and cation [7, 18, 33, 34, 37, 65, 71]. For instance, the substitution of a fluorinated anion group to an ionic liquid species, is shown to increase the solubility of the CO_2 and H_2S in ionic liquid [7, 18]. Similarly, creating an anion or cation that is more symmetric increases the melting point [60]. Therefore, it has been demonstrated that an ionic liquid can be conveniently manipulated to be suited for a specific purpose.

Although volatility is a common problem for organic solvents, ILs are considered non-volatile liquids. ILs have extremely low vapour pressure which means they demonstrate low volatility and flammability at room temperature. Hence, there is little or no concern for cross-contamination of the gas stream and pollution of the environment; this fact makes these particular chemicals referred to as "green" or "environmentally friendly" solvents. In addition, non-volatile nature decreases solvent loss, flammability danger and worker exposure [7, 20, 25, 30, 33, 37, 61, 72]. Regeneration of ILs is easy. For instance, a simple flash or mild distillation step can be applied to remove the solute from the solvent as reported by Pomelli et al. [25].

In general, most ILs are assumed to have high thermal stability at temperatures up to several hundred degrees centigrade (200 - 400 ˚C before noticeable thermal decomposition[1]). Thus, ILs exist as liquids over a wider temperature range than organic solvents. The thermal stability strongly depends on the structure of IL (especially on anion part), purity of IL and the moisture content of systems. For instance, the stability decreases as the anion hydrophilicity increases. On the other hand, it increases with increasing ion size [7, 25, 30, 33, 37, 58, 60, 71].

The toxicity of ILs has rarely been investigated, therefore, it is difficult to judge their toxicity based on scare knowledge provided in the literature. It is reported that the toxicity increases as the alkyl chain length increases. In addition, ILs with fluorine atom are more toxic. However, they do not contaminate the environment due to their extremely low vapour pressure, non-volatility, nonflammability and reusability [7, 33].

An attractive feature of ILs is their conductivity mostly ranging from 0.1 to 20 mS.cm^{-1}. Therefore, ILs can be utilized as both solvents and electrolytes in electrochemical reactions. Many factors have an effect on the conductivity, such as viscosity (inverse effect), density of liquid, ion size, anionic charge delocalization and water and chloride impurities [26, 35, 60].

Although the viscosities of ILs widely range from 10 to 10^4 mPa.s, most of them are relatively high in comparison to those of conventional solvents, typically ranging from 0.2 to 10 mPa.s. For instance, the measured viscosity of one of the most common ILs, bmim[BF$_4$], at 30 ˚C is 79.5 mPa.s. This is much higher than the viscosity of pure MEA (25 mPa.s) and about 40 times higher than that of the aqueous solution of 30 wt.% MEA at 30 ˚C (2 mPa.s). Additionally, ILs are several tens to hundreds times more viscous than water at room temperature [7, 33-35, 60]. The high viscosity of ILs is due to their high molecular weight and intermolecular interactions, such as hydrogen bonding and Van der Waals interactions that increase the energy required for molecular motions. Increasing the length of alkyl chains of ions, branching and increasing the functional groups in ions make the van der Waals interactions stronger [26, 33, 60]. Fluorination of anions decreases intermolecular interaction leading to less viscous ILs. The strong electronegative character of the CF$_3$ groups makes the negative charge distribute along the anion that reduces the interactions with the cations and hence the viscosity [33, 74]. Presence of water or other co-solvents decreases the viscosity while the presence of a chloride significantly increases the viscosity even in very low concentrations [26, 33, 66]. From an engineering aspect, the high

---

[1] Thermal decomposition, also called thermolysis, is a chemical reaction where a single substance breaks into two or more simple substances when heated. Thermal decomposition values of a substance are reported in terms of thermal decomposition temperature Td, as the substance fully decomposes into smaller substances or into its constituent atoms 73. Liu, W., et al., *The Physical Properties of Aqueous Solutions of the Ionic Liquid [BMIM][BF4]*. Journal of Solution Chemistry, 2006. **35**(10): p. 1337-1346.

viscosity of ILs is a significant disadvantage affecting stirring, mixing and pumping operations, and increasing related operating costs [35, 37, 60, 74]. This problem can be overcome by three methods: 1) combining convenient anion and cation, 2) diluting IL with a low viscous compound; and 3) increasing the operating temperature as much as possible [7, 33, 34, 66]. It is observed that increasing the temperature from 30 °C to 70 °C reduces the viscosity of bmim[BF$_4$] by a factor of 4.5 while a similar increase in temperature decreases the viscosity of aqueous 30% MEA solution by a factor of 2.7 [34].

2.2.2 Applications of ionic liquids as a solvent in separation processes

The application of ILs for gas removal has been studied and reported extensively due to the following reasons. Firstly, most ILs (conventional ILs) absorb gases via physical mechanism, therefore, energy consumption for the regeneration of solvent is less in comparison to processes with chemical absorption such as amine technology [7, 18, 23-25]. Secondly, due to the low vapour pressure of ILs, the loss of solvent during the process is not sensible, and all solvent can be regenerated and reused. This property causes ILs not to contaminate the passing gas stream and being emitted into the environment even in small amounts, unlike most common solvents. [18, 23, 25, 26, 33, 64, 66, 71, 72, 75]. Thirdly, ILs are reusable and recyclable affecting process cost. Huang et al. [67] investigated the gas absorption capacity of the ILs during four absorption/desorption cycles and indicated the complete reversibility of the ILs [67]. Guo et al. [19] studied the absorption capability of the ILs during six consecutive absorption cycles. They reported that ILs could be reused multiple times without any loss of absorption capacity, and reusing ILs has little effect on the acid gas solubility [19]. The fourth motivation is based on the high thermal and chemical stability of ILs which minimizes degradation of solvent at high temperatures and prevents it from reacting with impurities present in phases [23, 33, 65, 66, 75]. Finally, supercritical fluids such as CO$_2$ and compressed gases can be used to separate a wide variety of species from the IL solutions. It is possible to extract conventional organic liquids and water from ILs using low-pressure CO$_2$ [71].

The high viscosity and cost of ILs limit their applications in industrial separation processes. The design of less viscous ILs is still a challenge for many applications. Although the price of ILs is much higher than common solvents (common ILs are averagely four times more expensive than common amines), they do not decompose easily; therefore, their cost just increases the one-time investment. In addition, current studies on the synthesis of ILs address the viability and feasibility of its production with desirable properties such as reduced viscosity [18, 23, 33, 35].

2.2.3 Acid gas capture using ionic liquids

In recent years, a significant amount of experimental data on the solubility of acidic gases in numerous ILs in a wide variety of pressure and temperature has been reported [7, 18]. Such studies have shown that ILs have an affinity towards acidic gases such as H_2S and CO_2, hence encouraging researchers to investigate ILs with improved selectivity, solubility and lower viscosities. Table 2-3 presents a selection of data published for the solubility of CO_2 in ILs. In preliminary studies, ILs with imidazolium-based cations attracted a lot of attention due to their observed affinity towards CO_2 [7, 18]. As expected, the solubility of CO_2 in the ILs increases with a decrease in temperature and an increase in pressure. In addition, the choice of anion or cation affects the ability of the IL in absorbing such gases. The fluorination of the anion and in some cases the cation, and the addition of the fluoroalkyl group (-CF_3) to the anion are common ways to improve the absorption of CO_2 [7, 18]. Results show that as the number of –CF_3 groups increases in the anion, the solubility of CO_2 increases too because the affinity of CO_2 to the fluoroalkyl groups is well-known [7, 30].

Table 2-3 shows that the physical solubility of CO_2 in [$C_n$mim] cation-based ILs with the same cation follows the general trend of [NO_3] < [SCN] < [BF_4] < [TFES] ~ [PF_6] < [TFA] < [TfO] < [Tf_2N] < [FEP] < [FAP]. It seems that the presence of sulphur in the anion has a positive effect on the solubility of the gas. In addition, changing only the structure of cation affects the CO_2 solubility as well. For instance, the longer alkyl chain on the imidazolium-based cation mostly results in higher CO_2 solubility, as shown in Table 2-3 for [PF_6]/ [Tf_2N]/ [OTF]/ [AC]/ [TFA] anion-based ILs. The solubility of CO_2 in these ILs follows the general trend of C_2mim < C_4mim < C_6mim < C_8mim. The differences among the solubilities of CO_2 in these ILs increase with increasing pressure as reported by Kroon et al. [76] and Shin and Lee [77]. Overall, the results emphasize the tunability characteristic of ILs with the appropriate cation and anion combination.

Ionic liquids such as bmim[AC], emim[AC], bmim[PRO], bmim[ISB], bmim[TMA], bmim[LEV] and $bmim_2$[IDA] absorb CO_2 via chemical mechanisms. Thus, similar to other chemical absorbents, they present a high CO_2 solubility at low pressures. But as the pressure increases, the rate of increase in solubility decreases exponentially. For example, measured data by Carvalho et al. [78] shows that at pressures below 0.4 MPa and a temperature of 313 K, the solubility of CO_2 in bmim[AC] is higher than that in bmim[TFA], but the solubilities become more pronounced for bmim[TFA] at high pressures [78]. A similar trend is observed for emim[AC] and hmim[FAP] as chemical and physical absorbents, respectively. The solubility of CO_2 in hmim[FAP] is higher than in emim[AC] at the temperature of 298.2 K and pressures higher than 1.4 MPa, as reported by Yokozeki et al. [24].

The solubility of H_2S in many ILs is higher than that of CO_2 at the same conditions. Pomelli et al. [25] reported that the main reason for the considerable solubility/selectivity of H_2S is the development of common hydrogen bonding with the anion of the IL [25].

Table 2-3: CO_2 solubility data in ionic liquids.

Ionic liquid	T_{min} (°C)	T_{max} (°C)	P_{min} (MPa)	P_{max} (MPa)	Mole fraction (at 40 °C and 2 MPa)	Mole fraction[a] (at 25 °C and 2 MPa)	Ref.
emim[PF$_6$]	24.96	74.63	1.42	97.10	-	-	[79]
bmim[PF$_6$]	9.9	75.1	0.0097	73.50	0.22	0.286; 0.108[b]	[24, 80-86]
C$_6$mim[PF$_6$]	25	90.43	0.296	94.6	0.243	0.112[b]	[81, 87]
C$_8$mim[PF$_6$]	40	60	0.097	9.288	0.255		[80]
emim[BF$_4$]	25		0.251	0.875		0.077[b]	[81]
bmim[BF$_4$]	9.6	110	0.0102	67.62	0.2	0.277	[24, 76, 83, 88-90]
C$_6$mim[BF$_4$]	20	95	0.312	86.6	0.236	0.119[b]	[81, 91]
C$_8$mim[BF$_4$]	40	60	0.097	9.373	0.226		[80]
N-bupy[BF$_4$]	40	60	0.097	9.580	0.178		[80]
C$_6$mim[FAP]	25		0.0101	1.999		0.493	[24]
bmim[TFES]	25		0.0101	1.999		0.285	[24]
emim[EtSO$_4$]	40	60	0.097	9.461	0.114		[80]
emim[Ac]	24.95	75.05	0.01	2		0.428	[24, 92]
C$_4$mim[Ac]	25	80	0.0102	75.53	0.326	0.455	[24, 78]
emim[TFA]	25	75.02	0.01	2		0.282	[24, 92]
bmim[TFA]	20.28	90.03	0.979	62.47	0.249	0.301	[78]
bmim[NO$_3$]	40	60	0.097	9.2	0.143	0.182	[80, 89]
emim[Tf$_2$N]	25		0.213	0.903		0.39; 0.145[b]	[24, 81, 85]
bmim[Tf$_2$N]	24.39	71.36	0.6	31.72	0.358	0.43	[89, 93]
C$_6$mim[Tf$_2$N]	24.25	60	0.0091	122.4		0.437; 0.185[b]	[24, 81, 94]
(ETO)$_2$IM[Tf$_2$N]	29.8	90	2.15	31.24	0.3486		[88]
C$_2$mim[TfO]	30.7	71.4	0.8	37.8	0.27996		[77]
C$_4$mim[TfO]	30.7	71.4	0.85	37.5	0.33		[77, 89]
C$_6$mim[TfO]	30.7	71.4	1.25	36.30	0.341		[77]
C$_8$mim[TfO]	30.7	71.4	0.68	34	0.356		[77]
dmim[MP]	40	100	3.4	37.29	0.069		[88]
bmim[SCN]	19.2	111	1.05	37.31	0.149		[88]
hmim[FEP]	10.35	50.05	0.0297	1.799		0.444	[95]
ETT[FEP]	10.05	50.35	0.0048	1.799		0.424	[95]
bmpyrr[FEP]	10.35	50.15	0.0297	1.799		0.428	[95]
HEF	29.85	49.85	0.44	10.01	0.101		[96]
HEA	25	55	0.116	10.98	0.118	0.193	[70, 96]
HEL	25	55	0.156	10.09	0.071	0.140	[70, 96]

Ionic liquid	T_{min} (°C)	T_{max} (°C)	P_{min} (MPa)	P_{max} (MPa)	Mole fraction (at 40 °C and 2 MPa)	Mole fraction[a] (at 25 °C and 2 MPa)	Ref.
THEAA	29.85	49.85	1.03	10.12	0.072		[96]
THEAL	29.85	49.85	0.96	8.47	0.166		[96]
HEAF	29.85	49.85	0.66	8.52	0.063		[96]
HEAA	29.85	49.85	0.76	7.67	0.176		[96]
HEAL	29.85	49.85	1.24	8.50	0.093		[96]
BHEAA	25	55	0.125	1.515	0.121	0.141	[70]
HHEMEA	25	55	0.124	1.542	0.077	0.101	[70]
BHEAL	25	55	0.124	1.598	0.092	0.11	[70]
HHEMEL	25	55	0.154	1.562	0.078	0.101	[70]
bmim[PRO]	25		0.0103	1.999		0.393	[24]
bmim[ISB]	25		0.0102	1.999		0.403	[24]
bmim[TMA]	25		0.0101	2		0.431	[24]
TBP[FOR]	25		0.0100	1.999		0.348	[24]
bmim[LEV]	25		0.0101	1.999		0.460	[24]
bmim[SUC]	25		0.0100	1.999		0.232	[24]
$bmim_2[IDA]$	25		0.0101	1.999		0.395	[24]
bmim[IAAc]	25		0.0101	1.999		0.191	[24]

[a] mole fractions (mole CO_2/total mole) extrapolated from literature values
[b] mole fraction of CO_2 at 25 °C and 0.6 MPa

2.3 Hybrid solvents of ionic liquids and common physical or chemical solvents

Available absorption processes have a few disadvantages that limit the efficient and selective removal of acid gases from petrochemical streams. Conventional physical solvents have usually an undeniable affinity for heavy hydrocarbons that are a source of energy. These solvents absorb heavy hydrocarbons during sweetening processes, thus, there is a loss of hydrocarbons. Major problems with ILs limiting their commercial viability in the industry are their high viscosity and price. From an environmental perspective, ILs are green solvents, mostly because of nonvolatility and thermal stability, which are beneficial in addressing the disadvantages of conventional solvents [65, 66, 68, 97, 98].

Many existing technologies worldwide use amine solvents to remove acidic gases from feed streams. Replacing these units with new technologies is not economically practical. On the other hand, changing the composition of amine solutions slightly should not require considerable process and equipment modifications [98]. In such cases, hybrid solvents, containing amine solutions and new solvents, may be quite adequate for such purposes and increase the efficiency of the amine process considerably, though require some modifications to the process units.

Hybrid processes, such as the Sulfinol process[1], couple the properties of physical and chemical solvents in order to take advantage of favourable aspects of solvents, minimize their disadvantages, and bring much improvement in the gas absorption processes. Therefore, eco-friendly properties of ILs and low viscosity and low price of conventional solvents can be merged to provide a more efficient route for the acid gas capture [38, 99]. Even if the presence of IL in an aqueous amine solution displays some slight improvement in the absorption process, this slight improvement over long time can be considerable.

In recent years, the solubility of CO_2 in hybrid solvents of IL and aqueous amine solutions has attracted a lot of attention with promising results reported in the literature. Table B-1 summarizes the studies related to CO_2 removal using the combination of ILs and amines. The results show that ILs can reduce the corrosion of process equipment which is one of the main drawbacks of the amine technology [100]. Furthermore, the addition of the IL is helpful in reducing the energy consumption for solvent regeneration [97, 101-104], and increasing absorption rate [21, 22, 105-109]. Haghtalab and Shojaeian [97] demonstrated that the enthalpy of solution of CO_2 in a mixture of MDEA and bmim[acetate] is about half of the enthalpy of solution of CO_2 in H_2O + MDEA. It means that replacing the aqueous part of the amine solution by the IL reduces energy required for the regeneration of the solvent [97]. Despite the promising results reported in the literature, more rigorous and systematic analyses are required to anticipate the use of hybrid solvents for acid gas removal.

Although the solubility of CO_2 in mixtures of ILs with chemical solvents has been studied by many researchers, the reported data on CO_2 capture with physical hybrid solvents are rare. Shokouhi et al. [110] mixed three different amine-functionalized ILs with methanol and measured the CO_2 solubility and initial absorption rate at temperature of 303.15 K and pressures from 1 to 4 MPa [110]. Zhigang et al. [109] studied the CO_2 solubility in hybrid solvents of omim[TF$_2$N] and methanol. They indicated that addition of IL to methanol at the temperature of 313.2 K and pressures between 2 to 6 MPa increases the CO_2 absorption by approximately 3% to 70% (dependant on the pressure and composition of solvent) in comparison to the pure methanol. Additionally, the rate of increase in CO_2 solubility decreases as pressure increases [109]. Tian et al. [111] studied the physical properties of hybrid solvents of NMP and bmim[BF$_4$] with mass fractions of 0.1, 0.3 and 0.5 of NMP. They measured the CO_2 solubility and indicated that CO_2

---

[1] It is a mixture containing sulfolane (a physical solvent), water and either diisopropanolamine or methyldiethanolamine (two chemical solvents). The process requires low energy and has a high acid gas loading. But, heavy hydrocarbon loss during absorption is not deniable 88.　　Revelli, A.-L., F. Mutelet, and J.-N. Jaubert, *High Carbon Dioxide Solubilities in Imidazolium-Based Ionic Liquids and in Poly(ethylene glycol) Dimethyl Ether.* The Journal of Physical Chemistry B, 2010. **114**(40): p. 12908-12913.

solubility in terms of molality increases with decreasing mass fraction of IL. Reported data shows that the addition of NMP to bmim[BF$_4$], resulting in a mixture with a mass fraction of 0.1019 of NMP, reduces the viscosity of IL by 43% on average, while the solubility of CO_2 in mixture is very close to that in pure bmim[BF$_4$] [111]. To the best of our knowledge, no results on the absorption of H$_2$S using hybrid solvents of ILs and amines, and acid gas capture in a mixture of NMP and amine have been reported in the open literature.

From the literature review performed, the solubility of CO_2 in five physical/chemical hybrid solvents, namely (NMP + bmim[BF$_4$], MEA/DGA + water + bmim[OTF] and MEA/DGA + NMP + bmim[TF$_2$N]) was studied experimentally. In addition, some thermodynamic properties of new solvents including evaporation rate, viscosity, density, speed of sound and refractive index were measured.

3. EXPERIMENTAL METHODS FOR SOLUBILITY STUDIES

Although there are many modelling and theoretical approaches to determine thermodynamic phase behaviour and more specifically gas solubility in a solvent, experimental measurement of precise data is of significant importance. It is true that it is difficult and expensive to measure accurate data but it could also be costly for a company to estimate data using a thermodynamic model [112].

This chapter classifies the experimental methods used to measure vapour-liquid equilibrium. A literature review of reported techniques and apparatuses used to measure the solubility of H_2S in ionic liquids is presented[1]. An appropriate measurement method is justified for the proposed systems in this study.

3.1 Classification of methods for vapour-liquid equilibrium measurements

No single instrument or technique can measure VLE data for all kind of systems. Thus, a variety of techniques are employed for measuring VLE data. Each technique is applicable for systems with determined properties and in a specified range of temperature and pressure [113]. Considering isothermal solubility data, typical VLE apparatus consists of an equilibrium cell where the components are allowed to equilibrate at isothermal condition provided by utilizing an oil, air or water bath. It is very important to control and monitor the temperature of bath precisely. Pressure transducers and temperature sensors are employed to record system variables [114, 115].

There are different criteria to classify VLE experimental techniques. Firstly, considering the working regime in which equilibrium is reached, all the techniques are divided into static methods and dynamic methods. Secondly, depending on how the composition of the two coexisting phases is obtained in an equilibrium state, these can fall into two categories, synthetic methods and analytical methods [18, 112, 113]. These methods will be elaborated in the following sections.

Dynamic methods involve the circulation of one or both of the coexisting phases through the equilibrium cell to attain an equilibrium state. Recirculation of the phases aids in the agitation of the cell contents, thus, additional stirring is not used [112-115].

---

[1] As explained in Chapter 1, the initial proposal of this PhD thesis was to study H_2S systems. Therefore, the literature review to choose measurement method focused on equipment employed for H_2S solubility measurements. But, due to many constraints and safety aspects when working with H_2S, as well as the time for the necessary facilities to be available, the aim and objectives were modified to focus on CO_2 measurements. It is obvious that if the equipment is utilised for H_2S, it can be used for CO_2 as well.

In the static methods, the samples are loaded into the equilibrium cell (preliminary evacuated) at the isothermal condition and mixed to attain an equilibrium state. The phases do not leave the equilibrium cell during the experiment [112]. For the static type of design, various mixing mechanisms are used to hasten the mass transfer between phases and reduce the time required for the mixture to reach equilibrium. Such devices include an internal magnetic/mechanical stirring or an external rocking design [113, 114, 116]. Depending on the volume of the equilibrium cell which can be constant or variable, static apparatuses are divided into the constant volume cell apparatus and the variable volume cell apparatus. The change in the volume of the cell is possible by moving a piston or injecting a small amount of an immiscible liquid into the cell [112].

Analytical methods (direct sampling methods) enable the analysis of the equilibrium compositions of the coexisting phases either via directly from the cell (spectroscopic or gravimetric methods) or outside (chromatography, refractometry, titration or pressure drop) [112, 113, 117]. Therefore, this method does not need data reduction via thermodynamic models to determine the equilibrium compositions of the phases [117]. Gas chromatography is the most common technique to analyse samples [113, 114]. Analytical methods can be performed under isobaric conditions (T-x-y) or under isothermal conditions (P-x-y) [114].

In the analytical method, the sampling of the coexisting phases can present great difficulty, especially at low pressures. A considerable pressure drop and perturbation of the equilibrium state occur when withdrawing a large sample volume from the equilibrium cell [112, 115]. This problem can be avoided by the following mechanisms: utilizing a variable volume cell, blocking off a large sampling volume before the pressure drop, and taking small quantities of sample compared with the volume of the phases using capillaries, special valves (HPLC - valves or fast acting pneumatic valves) or syringe pumps [112].

Synthetic methods (indirect methods) can overcome the difficulties in sample analysis. But the overall composition of mixture injected to the cell must be known accurately since it is required in calculating the compositions of the coexisting phases through mass balances and the use of thermodynamic models [112, 113, 116]. It is therefore important to prepare and degas the solvent properly. No sampling is required, thus, the experimental procedure is relatively simple and no sampling facilities and expensive or complicated analytical devices are necessary [115]. However, the chosen thermodynamic model to perform material balance calculations may influence experimental results [117]. There are several synthetic methods using variable volume cell or constant volume cell, such as (i) direct measurement of bubble or dew points, (ii) simultaneous measurement of bubble and dew points, and (iii) total pressure measurements [113].

In some cases when the analytical method fails, the synthetic method is used. For example, when the two coexisting phases have similar density and phase separation is difficult, the synthetic method is preferred. In low-pressure systems, if the amount of vapour needed for the analysis is of the same order of magnitude as the total amount of the vapour phase in the equilibrium cell, removal of a sample disturbs clearly the equilibrium [112, 118]. Therefore, the synthetic method has preference over the analytical method.

The static-synthetic method shares some similarities with the static-analytical setups. The general description of the static apparatuses stated above is correct to both static-synthetic and static-analytical methods. To take advantage of both analytical and synthetic methods, a static apparatus then can combine both methods called combined static technique [113, 114, 116].

The equilibrium cell, the main part of the VLE apparatus, can be visual having high-pressure resistant windows, e.g. sapphire to allow observation of the phase behaviour, or non-visual mostly constructed from stainless steel [112]. Although earlier investigators used glass instruments to measure VLE because of their possibility for manufacturing into different shapes, recent researchers preferably use strong material such as stainless steel to construct their apparatus, mainly due to safety concerns [116].

3.2 Selection of a suitable experimental method for systems containing H_2S and ionic liquid

Accurate VLE measurements are required to design, optimize and upgrade of chemical processes. For instance, VLE measurements are applied in characterizing properties such as selectivity and capacity of solvents. Then, given the results, more efficient and productive industrial processes can be designed. In addition, experimental VLE data have a key role in developing thermodynamic predictive models. Therefore, choosing a reliable experimental apparatus based on variables, such as temperature, pressure and nature of components is an important step in obtaining accurate data.

In order to design equipment which is compatible with acidic gases (H_2S and CO_2) and amine solutions, and usable for ionic liquids which are expensive chemicals, it was necessary to review equipment used by previous researchers for such systems. It is obvious that if the equipment is utilised for H_2S, it can be used for CO_2 as well. Therefore, the literature review focused on equipment employed for H_2S solubility measurements. To the best of our knowledge, IL + amine + H_2S systems have not been investigated to date. Thus, reviewing the apparatus used for the IL + H_2S systems prompted the design of suitable equipment. Table 3-1 summarises some of the equipment designs employed by previous studies related to ILs + H_2S systems. The current price of ILs limits the size of the equilibrium cell. It is expensive to introduce a huge amount of IL to

the equilibrium cell. Thus, use of apparatuses similar to the ones presented by Jou and Mather (2007) [119, 120] and Heintz et al. (2009) [13-15] may not be economical due to the size of the equilibrium cell and the amount of solvent used. In the view of safety concerns, especially working with H_2S which is highly flammable, toxic and a potentially corrosive gas, it is better to use a gas reservoir and equilibrium cell with the lowest volume that can produce accurate and reliable phase equilibrium data. Shiflett et al. [121] used a Gravimetric Microbalance to measure the H_2S solubility in ILs, but H_2S reacted with a copper coil inside the apparatus and formed copper sulfide (a dark solid) [121]. Thus, it was proved that this equipment is not a proper choice for H_2S solubility measurements.

Although the Thermodynamics Research Unit (TRU) at the University of KwaZulu-Natal has a wide variety of phase equilibria equipment which has been developed over the years, most of them were based on the static-analytical method equipped with Gas Chromatography (GC). These could not be used for systems including solvents with a high boiling point such as ILs. Other analytical instruments such as NMR spectroscopy employed by Pomelli et al. [13] were not available in the research unit. Non-compatibility of gravimetric microbalance with H_2S made it an inappropriate instrument for H_2S measurement. Additionally, the literature survey revealed that the static-synthetic method is the most common technique used to measure the solubility of H_2S in ionic liquids. The volume of the apparatus and safety concerns, especially when working with H_2S, were prohibiting factors to use the available static-synthetic apparatus in the TRU labs.

Thus, it was decided to design and construct a new static-synthetic apparatus in this study. The review of static-synthetic apparatuses introduced in the literature, especially the ones employed by Kuan Huang et al. [122] and Jalili et al. [20], provided a good basis for the design.

Table 3-1: A review of VLE apparatus used for H_2S + IL systems.

Authors	Experimental method	Description of apparatus	Temperature (°C)	Pressure (MPa)
Jou and Mather (2007) [119, 120]	Dynamic analytic	• Equilibrium cell consisted of Jerguson liquid level gauge, and was mounted in an air bath equipped with a heater and a refrigeration system, the range of operation was -25 to 160 °C • Gas phase was circulated and bubbled through the liquid phase by using a magnetic pump. • Volume of gas reservoir was 50 cm^3 and the total volume of the apparatus was about 250 cm^3 • Titration method and chromatographic technique were used to analyse the liquid phase and measure water content respectively. • 80 ml solvent was introduced to the cell for each run	24.85–129.85	Up to 9.6
Pomelli et al. (2007) [25]	Static-analytical	• Medium-pressure NMR spectroscopy was used to measure solubility data	25	1.4
Heintz et al. (2009) [37, 123, 124]	Static-synthetic; Static analytical (for a mixture of gases)	• Mass spectrometer was used to monitor the gas phase composition when a mixture of gases was loaded into the ell. • Equilibrium cell was a 4-litre Zipper Clave agitated reactor with two sight-windows	27–227	0.6-30
Jalili et al. (2009) [20]	Static-synthetic	• Apparatus consisted mainly of a high-pressure equilibrium cell and a H_2S gas container. • Graduated side glass was used to measure the volume of the liquid phase • Magnetically driven mechanical stirrer was used to agitate the contents of equilibrium cell. • All wetted compartments of the apparatus were made of stainless steel 316. • 10 g solvent was introduced to the equilibrium cell for each run	30-70	up to 1

Authors	Experimental method	Description of apparatus	Temperature (˚C)	Pressure (MPa)
Bin Guo et al. (2010) [19]	Dynamic-analytic	• Gas phase was circulated and bubbled with a flow rate of 10 ml/min through the IL loaded in a glass vessel (about 5 g IL for each run) • Balance with an uncertainty of 0.0001 g was used to weigh the glass cell and to determine the mass of H_2S absorbed	30.05-90.05	Atmospheric pressure
Shiflett et al. (2010) [121]	Static-analytical	• Gravimetric microbalance (model: IGA 003, Hiden Isochema Ltd.) was used to measure the H_2S solubility in ILs.	24.85	Up to 0.75
Kuan Huang et al. (2012) [122]	Static-synthetic	• Apparatus consisted of two 316L stainless steel chambers used as equilibrium cell and gas reservoir whose volumes were 47.073 cm^3 and 121.025 cm^3 respectively. • Equilibrium cell was equipped with a magnetic stirrer • 3 to 5 g solvent was introduced to the equilibrium cell for each run	20-60	Up to 0.35

3.3 The static-synthetic method

In regard to the acquisition of gas solubility in solvents with a high boiling point and/or similar structure and chemical nature, static-synthetic techniques are the best choice since sampling and/or compositional analysis of components in mentioned circumstances is difficult [125]. Figure 3-1 shows a simple process flow diagram of a typical static-synthetic set-up. The operation of a typical static-synthetic apparatus involves preparing a mixture of known composition in an evacuated equilibrium cell which is placed in a liquid or air bath providing the isothermal condition. Then, gas is fed into the equilibrium cell from a gas reservoir. The content of the equilibrium cell is agitated by an external rocking or magnetic/ mechanical stirring until an equilibrium state is established between the liquid and vapour phases. At equilibrium, by recording temperature and pressure of the equilibrium cell and knowledge of overall compositions and volume of the equilibrium cell and liquid phase, one can deduce phase compositions via material balance and thermodynamic models. The entire phase envelope is determined by successive increases in pressure by loading more gas into the equilibrium cell and recording the P-T-x data. It is worth noting that the overall composition, equilibrium cell and gas reservoir volumes, and volume of the liquid phase are required in calculating the phase compositions. It is important to measure these with a high level of accuracy.

If the volume of the liquid phase is not directly measured and the initial mass and density of solvent loaded into the equilibrium cell are used to calculate the volume of the liquid phase, without considering the effect of dissolved gas on the mass and density of the liquid phase, these result in undeniable uncertainty especially at high pressures. On the other hand, available technologies such as laser to measure the height of the liquid phase and its volume in small scales are expensive. A sapphire tube was already available within the TRU. Thus, a new viewable equilibrium cell was designed. The new equilibrium cell was decided to have a depth gauge or ruler to directly measure the volume of the liquid phase within the equilibrium cell.

Moreover, material compatibility studies relevant to H_2S, ILs, amine solutions and NMP demonstrated that stainless steel (SS) 316L, sapphire glass and Teflon (PTFE) and Kalrez sealing media are suitable materials for construction of the equilibrium cell and other pieces of the apparatus. Additional factors, such as high tensile strength of sapphire glass and SS 316L and transparency of sapphire made them preferred material for the construction of the equilibrium cell.
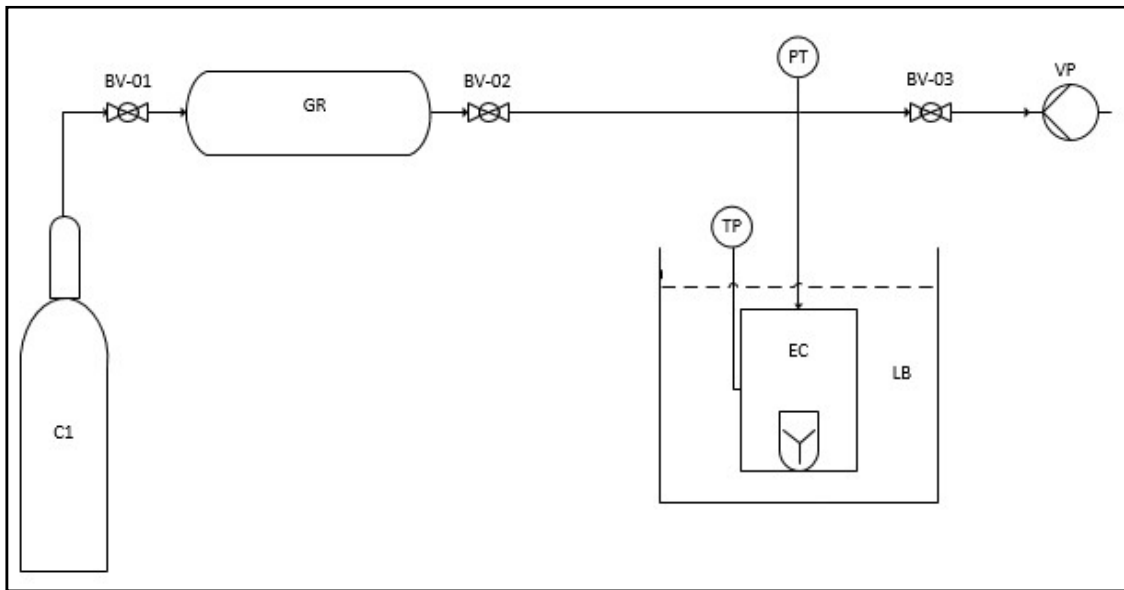
Figure 3-1: Schematic diagram of a typical static-synthetic apparatus, BV: ball valve, C1: Gas cylinder, EC: equilibrium cell, GR: gas reservoir, LB: liquid bath, PT: pressure transmitter, TP: temperature probe, VP: vacuum pump.

4. DESIGN OF A NEW STATIC-SYNTHETIC APPARATUS

The experimental setup designed, constructed and commissioned for systems containing IL, amines and acid gas is presented in this chapter. The designs featured along with some novelty in the method of measurement have been incorporated from the literature presented in Chapter 3. The unit was designed and commissioned in the Thermodynamics Research Unit, University of KwaZulu-Natal.

4.1 Equilibrium cell

The equilibrium cell is central to the apparatus into which the solvent and gas are injected and brought to the thermodynamic equilibrium state.

The equilibrium cell, shown in Photograph 4-1, mainly consists of a sapphire tube sealed with O-rings between weld-neck (tapered) and flat SS 316L flanges using four SS bolts. Photograph 4-2 shows the main parts of the equilibrium cell separately including the sapphire tube, flanges and O-rings. The sapphire tube was identical to those used in other experimental apparatuses developed within the TRU laboratories [125, 126].

The dimensions of the sapphire tube are: height of 70.0 mm, outer diameter (OD) of 35.6 mm and an internal diameter (ID) of 17.8 mm. The top flange is 16 mm in thickness and has three inlet/outlet ports. The bottom tapered flange has a thickness of 12.30 mm in the base and one inlet/outlet port. The inlet/outlet ports to the equilibrium cell are drilled wells within the flanges. They are sealed into the flanges via 1/8" SS Valco compression fittings. The bottom flange contains a single drain valve (1/8" SS 316 Swagelok ball valve; 40G series). The top flange contains a single loading valve (1/8" SS 316 Parker needle valve; 10V series). Each flange has in its interior a groove that houses an O-ring (24.5 mm OD and 3 mm thickness) which provides good sealing between the sapphire tube and the flanges. The thickness of the sapphire tube and flanges provide an increased safety factor.

Figure 4-1 displays a cross-sectional diagram of the equilibrium cell. The resultant cavity in the bottom flange increases the total capacity of the equilibrium cell (volume of 36.29 cm^3). Apart from increasing the total capacity of the equilibrium cell, the tapered flange provides a wider base improving agitation of the equilibrium cell contents. Secondly, the tapered flange allows for a notable displacement of the liquid level within the sapphire tube due to its low internal diameter. Thus, a change in the liquid level can be recorded more accurately and easily along the length of the sapphire tube.

During the design of the apparatus, uncertainty calculations were carried out to determine the approximate volumes of the equilibrium cell and gas reservoir. These were determined based on having an acceptable uncertainty compared to the data in the literature. In addition, the volumes were preferred to be minimum due to the chemical cost and safety factor. According to the uncertainty analysis, the desirable volume of the equilibrium cell should be approximately 50 cm^3. The method of uncertainty analysis and optimization procedure are explained in Appendix C.

Once the apparatus was constructed, the volume of the equilibrium cell was determined by metering a known amount of degassed water into the equilibrium cell via a high accuracy syringe pump (ISCO Teledyne; 100 DX; capacity ~ 100 cm^3) at 303.15 K. The equilibrium cell has a total interior volume of 36.29 cm^3. This includes the volumes of tubes between the equilibrium cell and three pieces connected to the equilibrium cell (pressure transducer, top and bottom valves), and excludes the volume of the stirrer and the internal dead volume of the ball valve (0.035 cm^3) connected to the bottom flange. The volume of equilibrium cell is close to the one with the volume of 47.073 cm^3 used by Kuan Huang et al. (2012) [122].

Photograph 4-1: Sapphire equilibrium cell with level gauge.

Photograph 4-2: Image of various sections of the equilibrium cell; [*top-left*] overhead view of the bottom flange of the equilibrium cell; [*top-right*] overhead view of the top flange of the equilibrium cell; [*down-left*] view of the sapphire tube; [*down -right*] view of the O-rings.
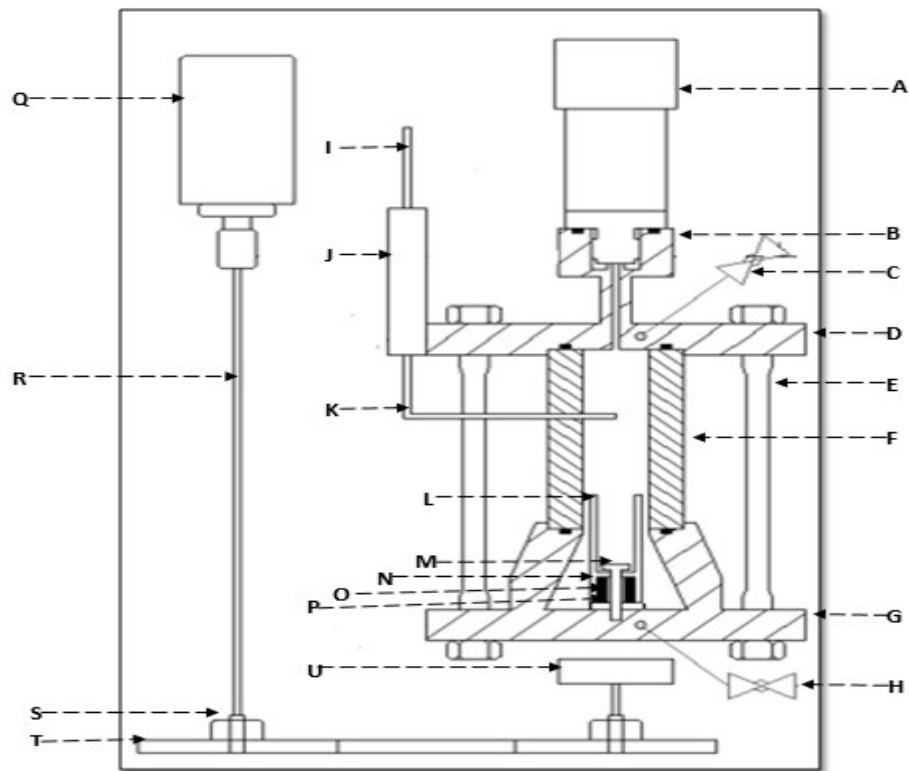
Figure 4-1: Cross-sectional diagram of the equilibrium cell with depth gauge and mixer (drawing not to scale): A- pressure transmitter; B- 1/4" British Standard Pipe (BSP) fitting; C- 1/8" SS 316 Parker needle valve for loading ; D- top flange; E- SS bolt; F-sapphire tube; G- bottom flange; H- 1/8" SS 316 Swagelok ball valve for drain; I- movable bar of the depth gauge; J- hollow rod of the depth gauge built into the top flange; K- flat pointer of the depth gauge surrounding sapphire tube; L- impellor blades; M- 3 mm half-threaded screw; N- SS 316L sheath; O- nickel-coated Neodymium ring magnet; P- Teflon washer; Q- brush DC motor; R- shaft connecting motor to gears; S- bush; T- gear; U- external rotating neodymium magnet. ■ indicates the grooves housing O-rings.

4.2 Depth gauge

A SS depth gauge, shown in Figure 4-1 and Photograph 4-3, was designed to allow for accurate measurement (± 0.4 mm) of the liquid level and to calculate the volume of the liquid phase within the equilibrium cell. It consists of a hollow thin rod built into the top flange, an adjustable bar moving through the hollow rod, and a flat pointer attached to the end of the bar and surrounding the sapphire tube. For each measurement, the pointer is adjusted to indicate the level of the liquid, and then the displacement of the bar on the top of the rod is measured by an electronic precision measuring gauge. The displacement of the bar on the top of the rod has a linear relationship with the volume of the liquid phase. The calibration procedure and method to increase the accuracy of the depth gauge are explained in Chapter 5.

Photograph 4-3: Depth gauge connected to the top flange of the equilibrium cell.

4.3 Mixing

In order to reach equilibrium faster, the contents of the equilibrium cell are agitated via an internal mixer. Suitable mixing of the internal contents of this equilibrium cell is particularly important due to the low internal diameter of the cell in relation to its total volume. The mixer (shown in Figure 4-1 and Photograph 4-4) consists of a nickel-coated neodymium ring magnet inserted into a SS 316L sheath containing two straight impeller blades. This stirrer rotates on a 3 mm half-threaded screw axle located in the centre of the bottom flange. A Teflon washer is used to reduce friction between screw axle, as well as the bottom of the stirrer and the surface of the bottom flange. A brush DC motor, driven by an adjustable DC power supply (MASTECH: HY3005D-3,

VA 131008667) and mounted at the top of the equilibrium cell housing, runs the mixer via magnetic coupling. In other words, torque is transferred from the axle of the brush DC motor through a shaft and three gears (made of Nylon-6) to an external rotating neodymium magnet located beneath the bottom flange. The magnetic coupling arrangement transfers torque from the external magnet to the mixer inside the equilibrium cell using a magnetic field. The DC power supply enables precise control of speed for the mixer. The mass transfer rate and the time needed to reach equilibrium depend strongly on the speed and size of the mixer and properties of the liquid solvent.

Photograph 4-4: Internal mechanical mixer housing a nickel-coated neodymium ring magnet.

4.4 Housing and framework for the equilibrium cell

The equilibrium cell was supported by a framework constructed in-house. Photograph 4-5 displays the equilibrium cell housing constructed of SS 316 L which is suspended from the top frame of the water bath using four bolts. It consists of a fixed support for the equilibrium cell in which the external rotating neodymium magnet is placed, two plates in the base in which three gears are embedded, two small plates in the top in which the brush DC motor is embedded, and four long solid rods that go through the plates. In addition, the support of the equilibrium cell is fixed on the plate using four short solid rods.
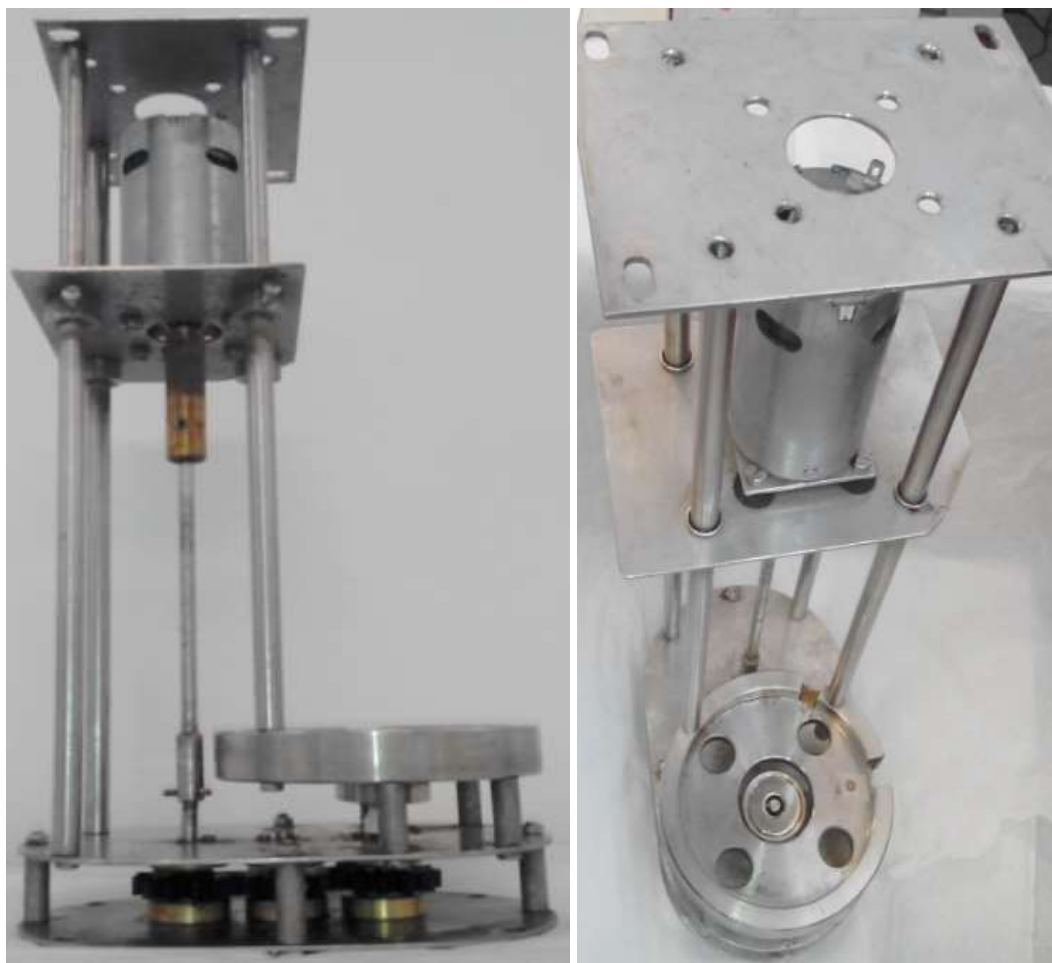
Photograph 4-5: Equilibrium cell housing; [left] front view; [right] overhead view.

4.5 Temperature and pressure sensors

Temperature and pressure measurements have critical importance in VLE measurements. Two 100 Ω Platinum Resistance (Pt-l00) probes (WIKA; 1/10 DIN) are used to measure the temperature of the equilibrium cell contents. The sensor has a 90-degree bend with a total length of 350 mm, a diameter of 3 mm and insertion length of 100 mm, and covered with SS 316L. The bend allows it to fit in the water bath. The tips of the Pt-100 probes are inserted into wells drilled into the top and bottom flanges of the equilibrium cell. It is important to ensure that the temperature sensors are as close to the equilibrium cell contents, to provide an accurate measurement of the equilibrium cell contents. An average temperature measurement taken using the top and bottom sensor readings is taken as the equilibrium cell temperature.

The pressure within the equilibrium cell is measured via a single pressure transmitter (WIKA; P-30; 4 MPa) with a manufacturer rated accuracy of 0.05% of the total span. The pressure transmitter is sealed via a nitrile rubber O-ring (18.72 mm ID and 2.02 mm thickness) into a 1/4" British Standard Pipe (BSP) fitting welded directly onto the top flange. In comparison to the traditional pressure transducer housing with a long curved tube, the BSP fitting with short tube

reduces the dead volume and the likelihood of formation of condensate (when volatile liquids are used) disturbing the performance of the transducer. The BSP fitting is maintained at the same temperature as the equilibrium cell by allowing it to be immersed in the water bath. In addition, this improves the accuracy of pressure measurement. The transmitter is rated for 4 MPa, thus, the pressure within the equilibrium cell should not be increased beyond its rating. The output signals of the pressure transducer and temperature sensors are relayed to a data acquisition unit (Agilent; 34972A). It is linked to a desktop computer allowing real-time pressure and temperature measurement and recording. Pressure and temperature measurement devices have to be calibrated to give the actual reading. Their calibration procedure is discussed in Chapter 5.

4.6 Gas reservoir

A gas reservoir was designed and commissioned to allow for accurate metering of a gaseous component into the equilibrium cell. After conducting an uncertainty analysis, it was found for the pressure and composition range of this work that a gas reservoir of roughly 3.5 times the capacity of the equilibrium cell would enable the lowest uncertainty in the overall composition of the contents in the equilibrium cell. The cylindrical gas reservoir was constructed of SS 316L with a height of 84 mm, OD of 60 mm, a wall thickness of 5 mm and a total working capacity of 137.09 cm^3. Figure 4-2 displays a drawing of the gas reservoir. All process connections were attached to a single inlet 1/4" port welded onto the top of the gas reservoir. A four-way union attached to this port allows for the location of a 1/4" BSP fitting and two ball valves (Swagelok; 1/8" and 1/4"; 40G series). The total working volume of gas reservoir includes the interior volume of its cylinder and volumes of tubes and fittings (according to Figure 4-2: 1/4" four-way union, 1/8" union Tee, BSP fitting and dead volume of 1/4" ball valve placed after the gas reservoir) between the gas reservoir and equilibrium cell. The volume of gas reservoir is close to the one with the volume of 121.025 cm^3 used by Kuan Huang et al. (2012) [122].

The temperature of gas within the gas reservoir is measured by a single Pt-100 probe. The sensor tip is inserted into a well drilled into the frame of the gas reservoir since the wall of the gas reservoir is not thick enough to drill a well for the temperature probe. The pressure within the gas reservoir is measured via a single pressure transmitter (WIKA; P-30; 2.5 MPa) with a manufacturer rated accuracy of 0.05% of the total span. The pressure transmitter is sealed via a nitrile rubber O-ring (18.72 mm ID and 2.02 mm thickness) into the 1/4" BSP fitting connected directly to the four-way union. The transmitter is rated for 2.5 MPa. Thus, the pressure within the gas reservoir should not be increased beyond its rating. The output signals of the pressure transducers and temperature sensor are relayed to a data acquisition unit (Agilent; 34972A). It is linked to a desktop computer allowing real-time pressure and temperature measurement and

recording. Pressure and temperature measurement devices have to be calibrated to give the actual reading. Their calibration procedures are discussed in Chapter 5.
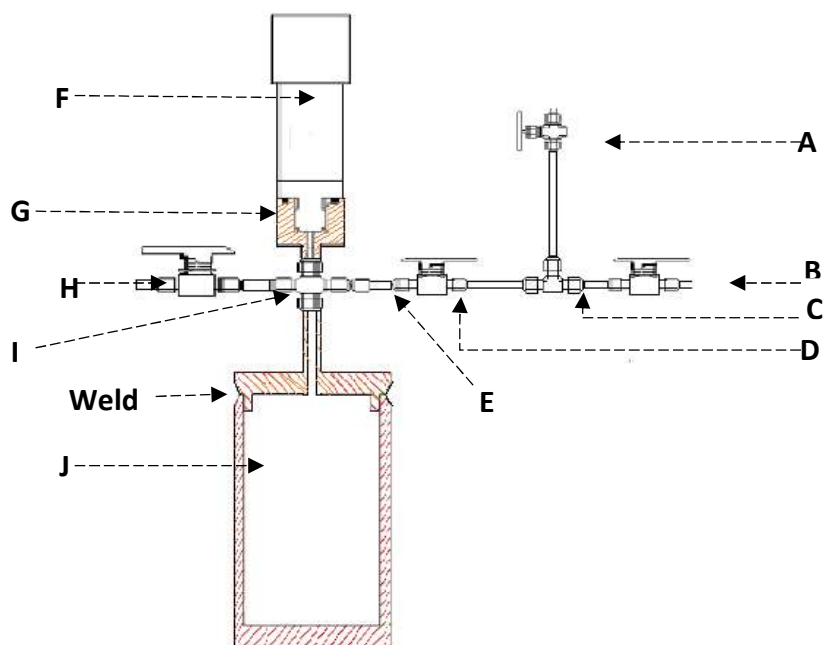
Figure 4-2: Cross-sectional diagram of the gas reservoir and associated fittings (drawing not to scale): A- 1/8" SS 316 Parker needle valve connected to the top flange of equilibrium cell; B- 1/8" SS 316 Swagelok ball valve; C- 1/8" SS 316 Swagelok union Tee; D- 1/8" SS 316 Swagelok ball valve ; E- SS 316 Swagelok 1/4" to 1/8" reducer; F- pressure transmitter; G- 1/4" British Standard Pipe (BSP) fitting; H- 1/4" SS 316 Swagelok ball valve ; I- 1/4" SS 316 Swagelok four-way union; J- gas reservoir cylinder. ■ indicates the groove housing o-ring.

4.7 Constant temperature baths

The temperature of the equilibrium cell is controlled by submerging the cell into a thermo-regulated 45 dm^3 SS bath containing water. The insulated bath contains two viewing glass windows enabling observation of the equilibrium cell. The temperature of the bath fluid is controlled by an immersion circulator (Grant; TX-150) and chiller (EK20, Type 002-4269).

The temperature of the gas reservoir is controlled by submerging the reservoir into a thermo-regulated 17 dm^3 SS bath containing water. The temperature of water is controlled using an immersion circulator (Grant; TX-150). The total working volume of the gas reservoir is not limited only to the interior volume of its cylinder. Thus, the cylinder, fittings and all the lines that contribute to the total working volume of the gas reservoir must be at the same temperature. Otherwise, the uncertainty of measured data will be considerable. To this aim, fittings and lines are also thermo-regulated by the fluid contained within the bath. The 1/8" line leading to Parker needle valve (connected to the top flange of the equilibrium cell) cannot be submerged into the fluid. It was regulated by pumping this fluid through silicone tubing located concentrically on the

outside of the 1/8" SS line. Thus, the total working volume of the gas reservoir is maintained at the same temperature.

4.8 Auxiliary equipment

The experimental equipment also consists of a two-stage vacuum pump (Edwards; RV3), chiller unit, electric jack, three DC power supplies and data acquisition unit. The whole apparatus is mounted on a trolley that is housed within an extraction fumehood to remove contaminated air quickly. The constant temperature bath of the equilibrium cell is the movable part of the set-up. The electronic car jack is used to raise the bath to submerge the equilibrium cell into the fluid and to lower the bath to expose the equilibrium cell. The vacuum pump is used for evacuation of the gas reservoir and the equilibrium cell.

If the equilibrium cell contents are loaded at low temperatures to 2.5 MPa (the rating of the pressure transducer of the gas reservoir) and then temperature is increased, the equilibrium cell can be used at pressures up to 4 MPa. The transmitter was removed, then the equilibrium cell was tested up to 10 MPa. All materials (316 L SS, Sapphire, PTFE, Kalrez and nitrile rubber) in contact with the chemicals are resistant to corrosion. It is very important since no contamination is vital for accurate VLE measurements. In addition, corrosion of the apparatus results in a gas leak that may cause death, fire and explosion hazards.

Gas-tight sealing of the SS 316L lines connected to the equilibrium cell, valves and all auxiliary equipment is accomplished with Swagelok, Valco and Parker compression fittings. The sealing system consists of the line, compression nut and both the back and front ferrules. Tightening of the nut compresses both the back and front ferrules against the line and the nut end, resulting in excellent gas-tight sealing. The back and front ferrule geometry provide excellent vibration fatigue resistance and tube support. "*Intermixing of different manufactures nuts, compression ports, and ferrules is foolish, as the critical interaction of precision parts is essential for reliability and safety; not to mention that manufacturers porting thread ends tend to vary slightly (thus, intermixing will permanently damage the thread)*" [113].

Photograph 4-7 and Figures 4-3 show a photograph taken in the laboratory and a process flow diagram of the static assembly set-up respectively. Chapter 5 focuses on the experimental technique applied for data measurement.

Photograph 4-7: Overview of the set-up.
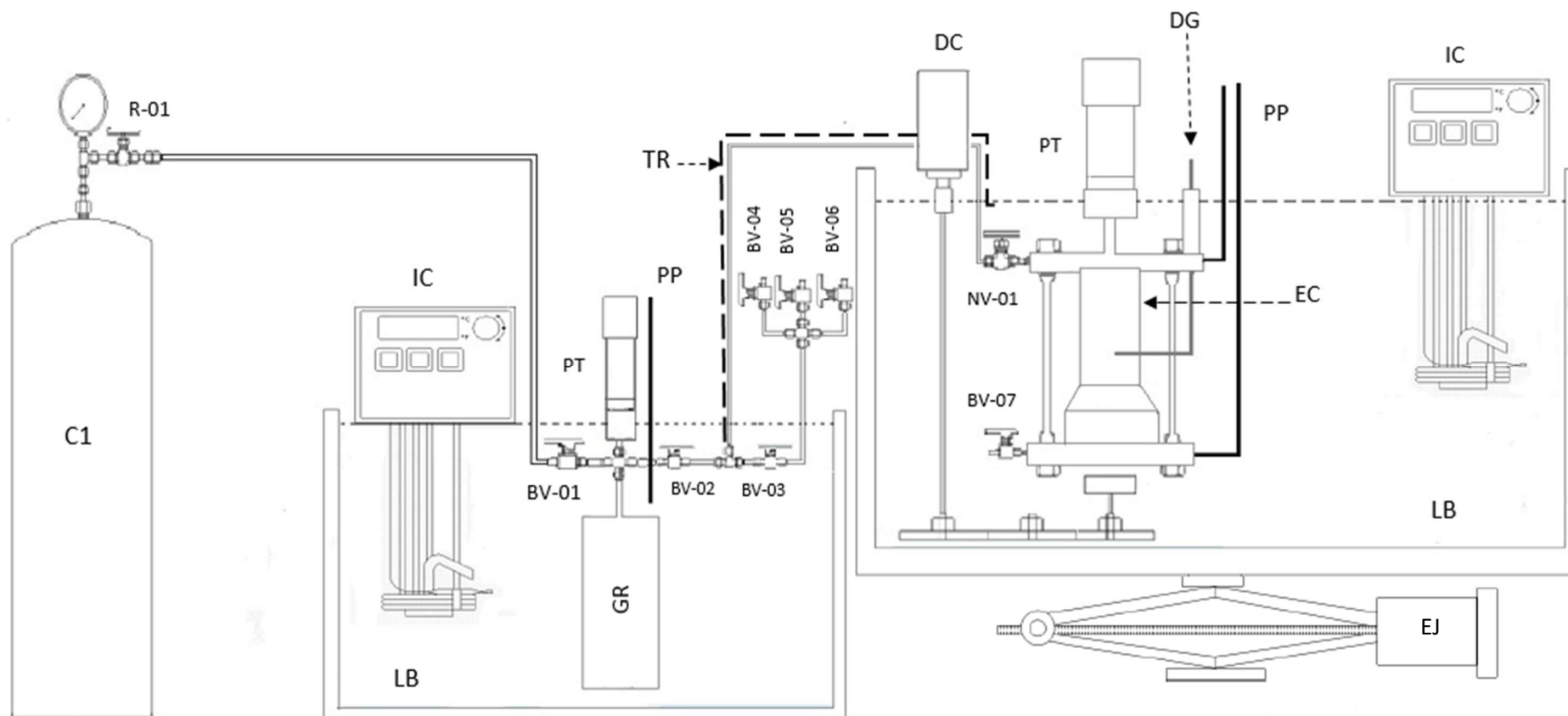
Figure 4-3: Schematic diagram of the "static synthetic" apparatus, BV: ball valve, C1: Gas cylinder, DC: brush DC motor, DG: depth gauge, EC: equilibrium cell, EJ: electronic jack, GR: gas reservoir, IC: immersion circulator, LB: liquid bath, NV: needle valve, PP: platinum resistance temperature probe, PT: pressure transmitter, R: regulator, TR: temperature regulation. BV-04, BV-05 and BV-06 are connected to vacuum pump, release cylinder and trap respectively.

4.9 Emergency procedures

Carbon dioxide as a gas is colourless, odourless, tasteless and non-flammable. Thus, it cannot be detected with the human senses. It is heavier than air (approximately 1.5 times) and it tends to be more highly concentrated in low lying areas and near the floor. The air naturally contains about 0.03 vol% CO_2 which is not hazardous to human health. But at higher concentrations, CO_2 can be dangerous and cause harmful health effects. The OSHA[1] recommends Permissible Exposure Limit (PEL) of 0.5% (5000 ppm) for CO_2 as an 8 hours time weighted average (TWA) [127].

The following safety precautions should be undertaken:
- Laboratories containing CO_2 cylinders must have ventilation system.
- Keep CO_2 cylinder gas-tight. Detect any leak and seal immediately.
- Any CO_2 discharge from cylinder or apparatus must be done within an extraction fumehood or vented outdoors.

As the initial aim of this project sought to investigate phase data for systems with H_2S, its safe handling procedure was adopted into the method. Hydrogen sulfide is a highly flammable hazardous gas, thus, the safety precautions must be followed when attempting to work with such chemicals. The H_2S cylinder must be kept away from heat, sparks and flames. It is heavier than air and it tends to be more highly concentrated in low lying areas and near the ground that are poorly ventilated, therefore, the working space should be well-ventilated. Using a non-sparking ventilation system separated from other exhaust ventilation systems is recommended. In addition, the ventilation system must be connected to a generator during a power outage. Fortunately, hydrogen sulfide can be recognizable by its rotten egg smell. Although the initial perception of its odour varies from person to person, usually a concentration of 0.13 ppm (below its permissible exposure limit) is sufficient for the odour to be detected. Considering the extremely toxic aspects of H_2S, it is not recommended to rely on the sense of smell. In addition, a high level of concentration or continued exposure to low levels for a long period of time eliminates the worker's ability to smell the gas. Consequently, a highly accurate H_2S detector must be used to detect the presence of H_2S in the area.

ACGIH[2] recommends threshold limit value (TLV[3]) of 1 ppm as an 8 hours time weighted average and a short-term exposure limit (STEL) of 5 ppm. NOISH[4] recommended exposure limit (REL) is 10 ppm

---

[1] Occupational Safety and Health Administration
[2] American Conference of Governmental Industrial Hygienists
[3] The threshold limit value (TLV) of a chemical substance is a level to which it is believed a worker can be exposed day after day for a working lifetime without adverse effects. Strictly speaking, TLV is a reserved term of the ACGIH.
[4] National Institute for Occupational Safety and Health

for 10 minutes ceiling. It is most important to use sufficient ventilation to control exposure below the recommended levels.

The following emergency procedure should be undertaken if H_2S is released into the working space:

- Laboratory workers must be aware of the risk. Normally, due to the egg rotten smell of H_2S, it can be recognized by workers at the concentration of 0.13 ppm (very small release). All unnecessary personnel must immediately leave the area when they get aware or sense it.
- Protective equipment must be equipped (air purifying respirator, chemical goggles, face shield and gloves). Self-contained breathing apparatus (SCBA) should be used in a high concentration of leakage that condition is dangerous to life or health.
- Make sure that H_2S cylinder valve and its regulator are closed completely.
- Make sure that the ventilation system is working. If there is a power outage, turn on the generator.
- The equilibrium cell and gas reservoir contents must be flushed into the release emergency container.
- The residue of H_2S present in the cell and gas reservoir must be released to the NaOH trap using nitrogen gas.
- The laboratory would be vacant until the H_2S odour cannot be detected within the lab.
- If the equipment is in need of repair, then these must be attended to urgently.

5. EXPERIMENTAL PROCEDURE

This chapter describes the experimental method applied to obtain accurate solubility data using the equipment detailed in Chapter 4. The experimental procedure includes: leak detection and elimination; calibration of temperature and pressure sensors, along with volume calibration of the liquid within the cell using the depth gauge; measurements of total volume for the equilibrium cell and the gas reservoir; preparation of the solvent; degassing and loading; and phase equilibrium measurements.

5.1 Leak detection and elimination

The equilibrium cell and the gas reservoir were pressurised using N_2 to pressure of approximately 10 MPa to ensure these maintained the pressure and did not leak. By applying Snoop® solution to all suspected joints or submerging these in water, leaks were detected, for which bubbles would be seen if there was any leak. The leaks were eliminated by tightening the joints from which bubbles had originated. Furthermore, the pressure was monitored to ensure that this did not exceed the maximum allowable pressure on the transducers. Hence, leak tests of the equilibrium cell and the gas reservoir at pressures exceeding the transducer ratings were performed with a high-pressure transducer.

In addition, before any measurements could be performed it was necessary to perform a leak test to determine the leak rate and ensure that the equilibrium cell was leak-proof under pressure or that it held a vacuum for system measurements below atmospheric pressure. For this aim, the equilibrium cell was left under vacuum or at high pressure, depending on the minimum and maximum pressures of the measurement system, for approximately 12 hours. The pressures at the beginning and after the time period were recorded. The leak rate (kPa/hour) was obtained by dividing the pressure change by period of time. If it was more than 0.05 kPa/hour (the maximum allowable leak rate is dependent on the period of time required to do experiments), the equipment, joints and fittings had to be rechecked. It was also important to monitor the temperature during leak testing to ensure that an isothermal condition was maintained. For accurate measurements, it was necessary to do the leak test and calculate the leak rate before starting each set of solubility measurements.

5.2 Temperature calibration

Three 100 Ω Platinum Resistance (Pt-l00) probes (WIKA; 1/10 DIN) used in this work were calibrated against a standard digital temperature probe (WIKA Instruments; model CTH 6500). The following steps were performed to calibrate the Pt-100 sensors:

1- The Pt-100 sensors and standard probe were placed in the water bath and held together tightly. The temperature of the water bath was controlled by an immersion circulator (Grant; TX-150).

2- The temperature of the water bath was set to 25° C.

3- When the set temperature was reached and the standard probe and Pt-100 sensors showed almost a constant temperature, the temperature of probes were recorded for at least 2 minutes. Then the average temperature of the standard probe as well as the average temperature of each of the three sensors were recorded separately.

4- The temperature of the water bath was raised by 5 degrees. This procedure was repeated until a set temperature of 100°C was reached.

5- The temperature displayed by the standard probe was converted into the actual temperature using a chart presented by WlKA.

6- Correlations between the actual temperatures and the temperatures displayed by each Pt-100 sensor were performed to obtain the calibration equations of each Pt-100 sensor which is usually linear.

7- The uncertainty of the temperature calibration was the maximum difference between the temperature calculated using the calibration equation and the actual temperature.

8- The calibration equations were used to calculate the actual temperatures from the temperatures displayed by Pt-100 sensors during solubility measurements.

Figure 5-1 shows the calibration graph for the three Pt-100 sensors.

(a) (b) (c)
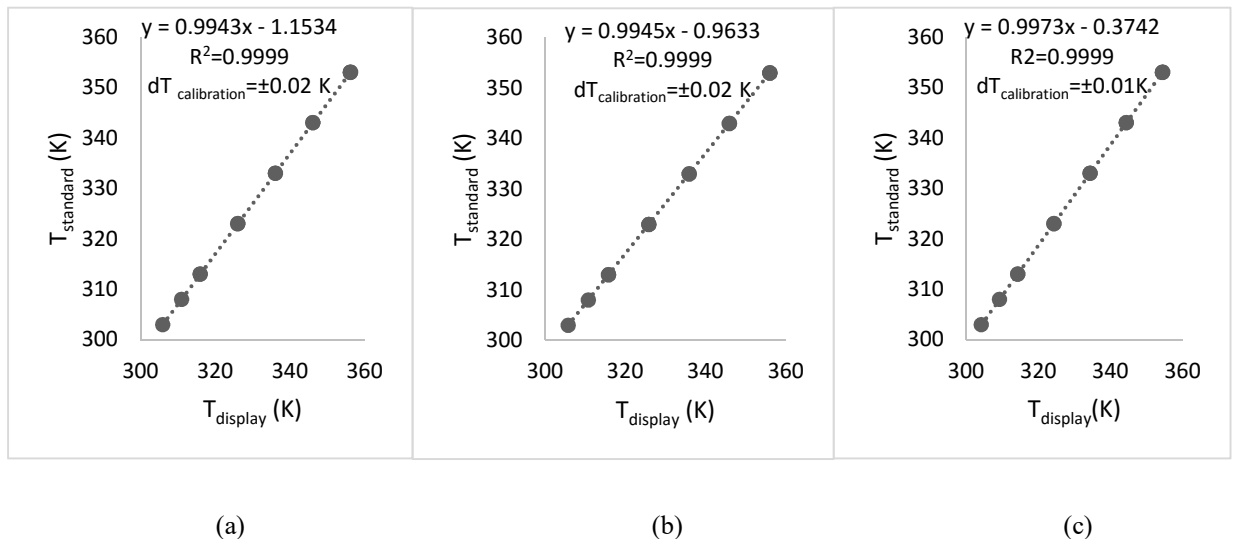
Figure 5-1: Calibration graphs for the Pt-100 sensors: **(a)** and **(b)** sensors of the equilibrium cell; and **(c)** sensor of the gas reservoir.

5.3 Pressure calibration

The gauge pressure transducers were calibrated against a standard pressure transmitter (Mensor CPC 8000; 25 MPa gauge), the data is displayed in Figure 5-2. The following steps were done to calibrate each pressure transducer:

1- The standard pressure transmitter and pressure transducer were connected to the equilibrium cell.

2- The equilibrium cell was left under atmospheric condition by opening its valves and selecting the vent mode of the pressure transmitter. In this condition, the pressure displayed by the pressure transmitter must be zero, otherwise, this was considered as the uncertainty of the pressure transmitter.

3- The pressure of the transmitter was set at 0.5 MPa. When the pressure transducer reading remained approximately constant for at least 10 minutes, this was recorded for 2 minutes and then the average pressure of transducer was determined. The actual pressure was obtained by subtracting the uncertainty determined in step 2 from the pressure transmitter reading.

4- The pressure of the transmitter was raised by 0.5 MPa and the previous step was repeated until a set pressure of 3 MPa was reached.

5- Steps 2 to 4 were repeated three times.

6- Correlation between the actual pressure and the pressure displayed by the pressure transducer was performed to obtain the calibration equation of the pressure transducer which is usually linear.

7- The uncertainty of the pressure calibration was the maximum difference between the pressure calculated using the calibration equation and the actual pressure.

8- The calibration equation was used to calculate the actual pressure from the pressures displayed by the pressure transducer during solubility measurements.

(a) (b)
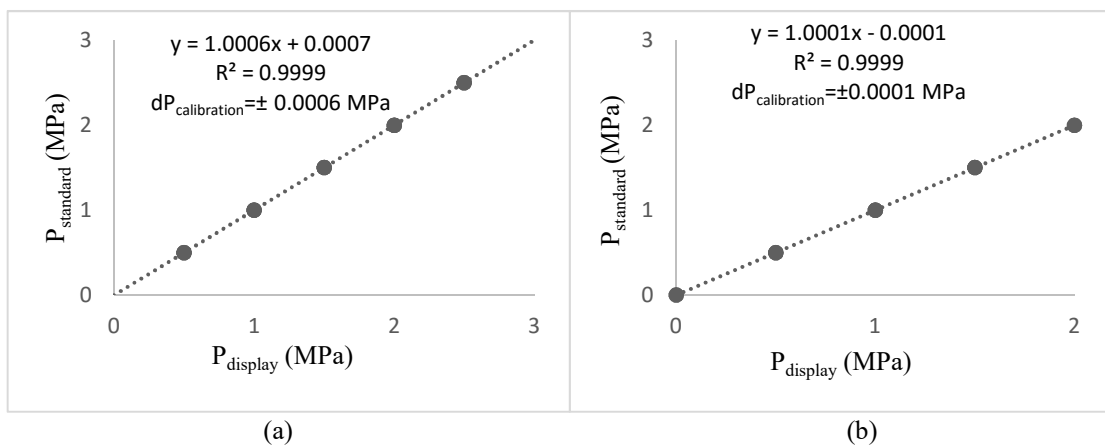
Figure 5-2: Calibration graphs for the pressure transducers: **(a)** transducer of the equilibrium cell; and **(b)** transducer of the gas reservoir.

5.4 Volume measurements

In the static-synthetic method, there is no phase analysis, hence, the total working volumes of the equilibrium cell and gas reservoir are important parameters required to determine the liquid phase compositions. It is therefore crucial that these volumes are measured accurately. The working volume of the equilibrium cell includes the volume of the cavity inside the equilibrium cell, lines between the loading needle valve and the drain ball valve connected to the equilibrium cell, and the pressure transducer BSP fitting welded onto the top flange. The working volume of the gas reservoir refers to the volume of the cavity inside the gas reservoir, all temperature regulated lines, the pressure transducer BSP fitting, and the four-way union fitting attached to the inlet of the gas reservoir. The following steps were performed to measure the working volume of the equilibrium cell:

1- The equilibrium cell was evacuated using a vacuum pump. The cell was then weighed using a mass balance (Ohaus Explorer; maximum capacity of 6100 g; readability of 0.01 g). Deionized water was injected into the cell which was almost full. Then the cell was weighed to determine the amount of water loaded. The density of deionized water was measured using a density and sound velocity meter (Anton Paar, DSA 5000M), and the volume of water loaded into the cell was calculated.

2- Then, to fill the equilibrium cell completely, a known amount of degassed water was metered into the equilibrium cell via a high accuracy syringe pump (Teledyne ISCO; 100 DX; capacity ~ 100 cm^3) at a constant temperature. The volume of water that filled the equilibrium cell was recorded. The uncertainty of the pump was within 0.5% of the recorded volume.

3- The sum of the volumes of water loaded into the equilibrium cell in step 1 and 2 were considered as the working volume of the equilibrium cell.

The above steps were followed to measure the working volume of the gas reservoir as well.

5.5 Calibration of the depth gauge

A depth gauge was designed to allow for accurate measurement of the liquid level in the equilibrium cell. It was built into the top flange of the equilibrium cell and has an adjustable bar moving along the length of the sapphire tube. After adjusting the pointer of the depth gauge to indicate the level of the liquid, the length of the bar on the top of the equilibrium cell is equal to the height of the liquid phase within the sapphire tube. Thus, the volume of liquid phase as a function of the height of the liquid phase within the sapphire tube was determined by calibrating the depth gauge against known volumes of water charged gravimetrically into the equilibrium cell. To calibrate the depth gauge, a known mass of water was injected to the equilibrium cell, and then the pointer of the depth gauge was adjusted to indicate the level of the liquid (the bottom

or top level of meniscus of water). The length of the bar on the top of the equilibrium cell was measured by an electronic precision measuring gauge. The volume of the liquid phase corresponding to the length of the bar on the top of the equilibrium cell (or the liquid level in the equilibrium cell) was calculated from a knowledge of water mass and density. This procedure was repeated with different masses of water. Correlation between the volumes of the liquid phase in the equilibrium cell and the lengths of the bar on the top of the equilibrium cell was performed to obtain the calibration equation of the depth gauge which is linear. Figure 5-3 shows the calibration graph for the depth gauge. It should be mentioned here that the pointer of depth gauge must be adjusted at a determined place (the bottom or top level of meniscus) during calibration and main experiments and it must not be changed.

The depth gauge was calibrated using water that had a special meniscus within the sapphire tube. The difference between the meniscus of water and the meniscus of solvent loaded into the cell and also drops of the solvent splashed on the interior wall of the sapphire tube during loading solvent were sources of uncertainty of the liquid phase volume measurements. To counteract these uncertainties and correct the liquid phase volume measurements, an offset was determined for the depth gauge whenever the solvent was loaded into the cell. The offset was considered in the calculations for each set of solubility measurements. It was the difference between the actual volume of solvent determined by the knowledge of density and mass of the solvent and the volume measured by the depth gauge at a specific temperature and atmospheric pressure.

The graph shows:
$$y = 0.2535x + 17.76$$
$$R^2 = 0.9997$$
$$dV_{calibration} = \pm 0.09 \text{ cm}^3$$
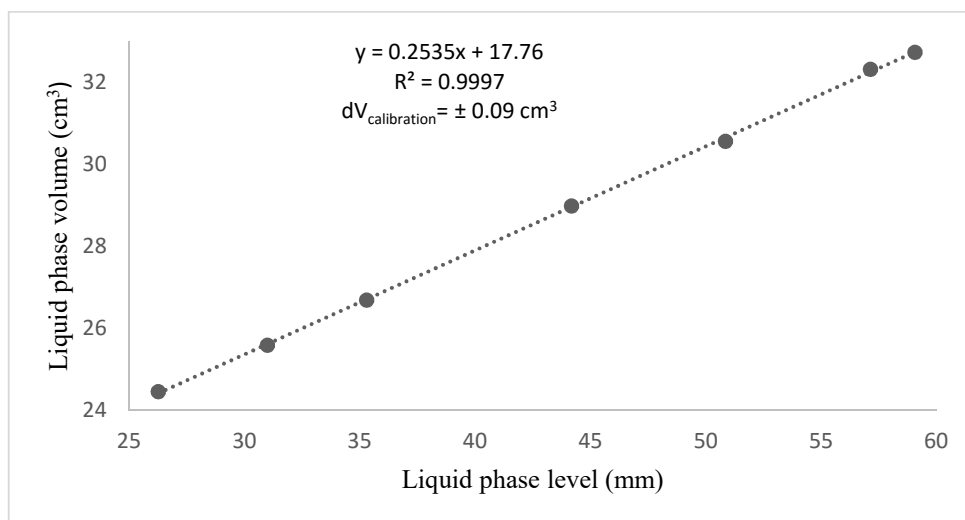
Figure 5-3: Calibration graph of the depth gauge for liquid phase volume measurements.

5.6 Preparation of the solvent and degassing

Liquid chemicals were dried under vacuum. Then their density, viscosity and refractive index were measured and compared with the literature to ensure that chemicals were pure. Dried chemicals were kept in a desiccator to protect them from absorbing any moisture. The gas chemicals were used without any further purification.

To prepare the solvent, the required liquid chemicals were dried and degassed again, and kept separately in glass round-bottom flasks under vacuum. Thus, their exposure to air and CO_2 was minimized to avoid contamination. A mass balance (Ohaus Explorer; maximum capacity of 450 g; readability of 0.001 g) was used for the gravimetric preparation of the hybrid solvent. Based on the composition of the hybrid solvent, the required amounts of chemicals were mixed in the glass round-bottom flask having a high vacuum valve. Photograph 5-1 shows the set-up used for the preparation of hybrid solvents. Two flasks were connected to the vacuum pump by a T-piece fitting, and the glass joints were sealed using high vacuum grease. Before mixing chemicals, air within the line connecting two flasks was evacuated using the vacuum pump for approximately 30 seconds.
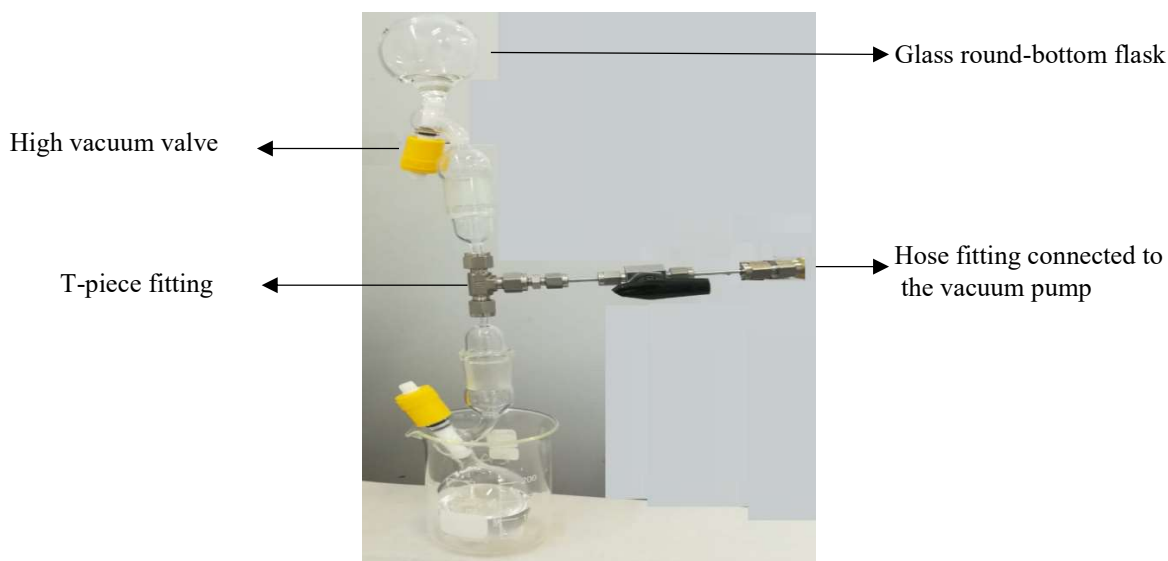
Photograph 5-1: Set-up used to prepare the hybrid solvent.

5.7 Solubility measurement

Following the sensor calibration, leak test and preparation of solvent, solubility measurements were performed in such a way that at first, the equilibrium cell was evacuated using vacuum pump. It was then weighed using a mass balance (Ohaus Explorer; maximum capacity of 6100 g; readability of 0.01 g). The solvent was loaded into the evacuated equilibrium cell, and then degassed again for a short time. Photograph 5-2 shows the set-up used for loading the solvent into

the equilibrium cell. The total mass of solvent charged into the cell was determined by weighing the cell. CO_2 was charged into the evacuated gas reservoir to the lowest applicable pressure and at a constant temperature of 323.15 K. A known amount of gas was then be metered into the equilibrium cell, taking note of the pressure and temperature of the gas reservoir before and after the gas loading. The number of moles of carbon dioxide transferred into the equilibrium cell (n_{CO_2}) was determined using the following equation:

$$n_{CO_2} = \frac{P_1 V_{GR}}{Z_1 R T_1} - \frac{P_2 V_{GR}}{Z_2 R T_2} \tag{5-1}$$

Where P_1 and P_2 are the pressure of the gas reservoir before and after gas loading; T_1 and T_2 are the temperature of the gas reservoir before and after gas loading; V_{GR} is the volume of the gas reservoir, and Z_1 and Z_2 denote the compressibility factors calculated using the Peng-Robinson equation of state (PR EoS). At this point, the total composition of the mixture loaded into the equilibrium cell is known. The contents of the equilibrium cell were then thoroughly agitated at a constant temperature. The pressure drop in the equilibrium cell because of gas absorption was recorded as a function of time until attaining equilibrium state that is distinguished by constant pressure and temperature (within the uncertainty: $\delta P \leqslant U(P)$[1], $\delta T \leqslant U(T)$[2]). Once equilibrium was achieved, the height of the liquid phase was measured with the depth gauge and the volume of the gas phase at equilibrium was determined. Finally, the mole fraction of CO_2, (x_{CO_2}), in the liquid phase was calculated from:

$$x_{CO_2} = \frac{n_{CO_2}^L}{n_{CO_2}^L + n_{solvent}} \tag{5-2}$$

Where:

$$n_{CO_2}^L = n_{CO_2} - n_{CO_2}^V \tag{5-3}$$

$$n_{CO_2}^V = \frac{y_{CO_2} \cdot P_{eq} \cdot V_V}{Z_{eq} \cdot R \cdot T_{eq}} \tag{5-4}$$

Where $n_{CO_2}^L$ and $n_{CO_2}^V$ are total moles of CO_2 in the liquid and gas phases; $n_{solvent}$, V_V and y_{CO_2} are the total moles of solvent within the equilibrium cell, the volume of gas phase, and the mole fraction of CO_2 in the gas phase respectively; P_{eq} and T_{eq} are the pressure and temperature of the equilibrium cell at the equilibrium condition; and Z_{eq} denotes the compressibility factor calculated using the PR EoS. Equations 5-2 to 5-4 can be summarized in the following equation:

$$x_{CO_2} = \frac{n_{CO_2} - y_{CO_2} \cdot V_V \cdot \rho_{g,EOS}}{n_t - V_V \cdot \rho_{g,EOS}} \tag{5-5}$$

---

[1] $U(P) = 0.002$ MPa
[2] $U(T) = 0.02$ K

Where $\rho_{g,EOS}$ is the molar density of the gas phase and n_t is the total moles of gas and solvent within the equilibrium cell. The molar density was calculated using the PR EoS corresponding to the equilibrium condition. It was assumed that the mole fraction of CO_2 in the gas phase was equal to unity when the solvent exhibited a low vapour pressure [128]. For systems including volatile liquids such as water, the partial pressure of solvent was assumed to be equal to the vapour pressure of the solvent, $P^v_{solvent}$, at the equilibrium temperature. Thus, the mole fraction of CO_2 in the gas phase was calculated from [128]:

$$y_{CO_2} = \frac{P_{CO_2}}{P} = \frac{P_{eq} - P^v_{solvent}}{P_{eq}} \qquad (5\text{-}6)$$

The ball valve connected to the bottom flange of the cell had a dead volume of 0.035 ml. Thus, 0.035 ml of solvent was trapped in the ball valve during loading solvent into the cell. The mass of the trapped solvent was determined by the knowledge of solvent density. It was then subtracted from the total mass of solvent loaded into the cell to obtain the actual mass of solvent within the cell.

Photograph 5-2: Set-up for loading solvent into the equilibrium cell; top valve is connected to the vacuum pump.

5.8 Uncertainty analysis

An uncertainty analysis was carried out following the methods outlined by NIST (National Institute of Standards and Technology) [129]. As discussed in the NIST guidelines, when there is a functional relationship between the output quantity, y', and the measured input quantities, x_i',

in the form of $y' = f(x_1', x_2', ..., x_N')$, the combined uncertainty of y', $u_c(y')$, can be calculated through the law of propagation of uncertainty, as follows [113, 129]:

$$u_c^2(y) = \sum_{i=1}^{N} \left(\frac{\partial f}{\partial x_i'}\right)^2 u_c^2(x_i') + 2\sum_{i=1}^{N-1} \sum_{j=i+1}^{N} \frac{\partial f}{\partial x_i'} \frac{\partial f}{\partial x_j'} u(x_i', x_j') \tag{5-7}$$

Equation 5-7often reduces to a simple form and the second term vanishes.

The details to calculate the uncertainty of mole fraction of CO_2 in the liquid phase are presented in Appendix D. The estimates used for the uncertainty calculation are listed in Table 5-1. In this work, a coverage factor of $k = 2$ was used to determine the expanded uncertainties for temperature, pressure and mole fraction of CO_2 as follows:

$$U_c(x_{CO_2}) = 2.\,u_c(x_{CO_2}) \tag{5-8}$$

$$U_c(T) = 2.\,u_c(T) \tag{5-9}$$

$$U_c(P) = 2.\,u_c(P) \tag{5-10}$$

Table 5-1: Standard uncertainty estimates and influences of the variables in this work.

Source of uncertainty	Distribution	Estimate
Pressure (P)		
P reference (MPa): Mensor CPC 8000 (25 MPa)	normal	0.0025
Correlation for P (MPa), (4 MPa), equilibrium cell	rectangular	0.0003
Correlation for P (MPa), (2.5 MPa), gas reservoir	rectangular	0.0001
Temperature (T)		
T reference (K): CTH 6500	rectangular	0.02
Correlation for T (K), equilibrium cell (EC)	rectangular	0.02
Correlation for T (K), gas reservoir (GR)	rectangular	0.01
Non-uniformity of water temperature[a] (K)	rectangular	0.01
Volume of gas phase (V_V) in equilibrium cell		
Total volume of equilibrium cell (cm³)	None[b]	$u(V_{EC}) = 0.03$
Calibration of the depth gauge, V_L (cm³)	rectangular	0.09
Repeatability of volume (cm³)	rectangular	0.12
Liquid density (g/cm³)	rectangular	0.0002
Syringe pump flow accuracy (Q (cm³))	rectangular	$0.005Q$
Total composition[c] (z_i)		
Pressure (MPa), gas reservoir	None[b]	$u(P_{GR}) = 0.0008$

Source of uncertainty	Distribution	Estimate
Total composition[c] (z_i)		
Temperature (K), gas reservoir	None[b]	$u(T_{GR}) = 0.01$
Total volume of gas reservoir (cm³)	None[b]	$u(V_{GR}) = 0.05$
Compressibility factor vapour phase, Z^V	rectangular	$0.006 . Z^V$
Source of uncertainty	Distribution	Estimate
Mass balance uncertainty[d] (g)	rectangular	0.03
Mass balance uncertainty[e] (g)	rectangular	0.003
Liquid phase composition[f] (x_i)		
Pressure (MPa), equilibrium cell	None[b]	$u(P_{EC}) = 0.0009$
Temperature (K), equilibrium cell	None[b]	$u(T_{EC}) = 0.02$
Vapour phase composition	rectangular	$1 - y_{CO_2}$
Volume of gas phase, V_V (cm³)	None[b]	$u(V_V) = 0.09$
Compressibility mixture vapour phase (Z^V)	rectangular	$0.006 . Z^V$

[a] Non-uniformity of water temperature is only for temperature of gas reservoir, it was not considered for the equilibrium cell temperature since it has two temperature sensors.
[b] Combined standard uncertainty.
[c] Total composition of the mixture prepared in the equilibrium cell.
[d] Mass balance uncertainty for loading a known mass of liquid into the equilibrium cell.
[e] Mass balance uncertainty for preparing solvent mixtures.
[f] Composition of the liquid phase calculated from the T-P-z data.

5.9 Viscosity, density, speed of Sound, refractive index and evaporation rate measurements

The viscosity, density, and speed of sound for the liquid components, as well as the liquid mixtures, were measured using a commercial density and sound velocity meter (Anton Paar, DSA 5000M). The device was calibrated by a certified Anton Paar technician. These physical properties were measured simultaneously from a single injected sample (3.5 mL). The apparatus measures the density and speed of sound using the isothermal oscillating U-tube method. The DSA 5000M is also equipped with an auxiliary viscometer (Lovis, 2000 ME). The viscosity of the sample is determined via the "falling sphere" method.

The refractive indices for the liquid components, as well as the liquid mixtures, were measured using a commercial digital refractometer (Atago, RX-7000α). It measures refractive index in a temperature range of 278.15 to 343.15 K. The refractometer has automatic temperature compensation (ATC) for accuracy, a built-in Peltier thermo-module for temperature control eliminating the need for a constant temperature water bath, and manual calibration to adjust standard liquid values and to correct differences in measurement values between instruments. Thus, before measurements, the refractometer was manually calibrated by measuring the refractive index of distilled-deionized water in accordance with the instrument instructions.

In this work, the thermogravimetric analysis method was utilized to investigate the volatility of the liquid mixtures. To this aim, a thermogravimetric analyser TGA (DTG-60AH simultaneous TG-DTA apparatus, Shimadzu) was used to measure the evaporation rates of the solvents. The experiments were conducted at atmospheric pressure (0.101325 KPa). A constant flow of nitrogen, supplied by Afrox, with a flow rate of 100 cm^3/min was maintained throughout the experiment. A small amount of the liquid sample (the initial amount of each sample is reported in Chapter 7) was placed in an aluminium sample pan and placed in the furnace of the thermogravimetric analyser. The furnace was heated to 373.15 K. The temperature of the sample was measured using a thermocouple placed directly under the sample pan. The experimental temperature was held constant during measurements and the mass of the sample versus time was recorded. When the rate of change in the mass of the sample remained zero for at least one hour, the measurement was stopped. The graph of the change in mass of the sample with respect to time was then used to obtain the evaporation rate of the sample.

6. MODELLING AND PREDICTION OF PHASE EQUILIBRIUM DATA

The solubility of acid gases in various solvents takes place physically or/and chemically. This process can be described and analysed by mathematical models. Thermodynamic models are capable of correlating measured phase equilibrium date and predicting data in regions where experimental data are not available. Thus, they are used to provide a full description of the phase behaviour of the process, enabling better design of experiments that can make more applicable and useful results.

In this chapter, applicable and simple methods to analyse the solubility of acid gases in chemical or/and physical solvents are explained in detail. This chapter is presented into two parts: the first covers the Vapour-Liquid Equilibrium (VLE) modelling of the CO_2 + NMP + bmim[BF_4] systems which are physical absorption; and the second presents a short literature review on thermodynamic models developed for chemical absorption of acid gases. Then an applicable method to analyse the solubility of acid gases in chemical solvents is presented in this study.

6.1 Thermodynamic modelling of CO_2 + NMP + bmim[BF_4] systems

Flash calculations were performed to model the CO_2 + NMP + bmim[BF_4] systems and predict compositions of the liquid and gas phases at a given temperature and pressure. The computational steps to determine x_i and y_i which are mole fractions of component i in the liquid phase and gas phase respectively, are explained.

Step 1: A material balance on the ith component and for 1 mol of the mixture of CO_2 + NMP + bmim[BF_4] results in:

$$x_i n_L + y_i n_V = z_i \tag{6-1}$$

Where z_i is the total mole fraction of component i in the mixture; x_i and y_i are the mole fractions of component i in the liquid phase and gas phase; and n_L and n_V are the mole fraction of the mixture presented in the liquid and gas phases respectively. Initial equilibrium ratio of the ith component, k_i, defined as the ratio of y_i to x_i, can be estimated by Wilson's correlation [130, 131]:

$$k_i = \frac{y_i}{x_i} = \frac{P_{ci}}{P_{eq}} exp\left[5.37(1 + \omega_i)(1 - \frac{T_{ci}}{T_{eq}})\right] \tag{6-2}$$

Where ω_i, $P_{ci}(MPa)$ and $T_{ci}(K)$ are acentric factor, critical pressure and critical temperature of the ith component respectively; and $T_{eq}(K)$ and $P_{eq}(MPa)$ are temperature and pressure of the system at equilibrium condition. Combining equations 6-1 and 6-2 results in:

$$x_i = \frac{z_i}{n_L + n_V k_i}$$
(6-3)

$$y_i = \frac{z_i k_i}{n_L + n_V k_i}$$
(6-4)

Inserting the above equations into: $\sum_i y_i - \sum_i x_i = 0$; and replacing n_L with ($1-n_V$) gives [131]:

$$f(n_v) = \sum_i \frac{z_i(k_i - 1)}{n_V(k_i - 1) + 1} = 0$$
(6-5)

Equation 6-5 can be solved by applying the Newton-Raphson iteration method to determine n_v. In this method, an initial guess for n_v, that can be any random value between 0 and 1, is required. A good initial guess can be calculated from the following equation [131]:

$$n_V = \frac{A}{A + B}$$
(6-6)

Where:

$$A = \sum_i z_i(k_i - 1)$$
(6-7)

$$B = \sum_i z_i(\frac{1}{k_i} - 1)$$
(6-8)

Using the initial guess of n_v, the value of $f(n_v)$ given by equation 6-5 is calculated. If the absolute value of $f(n_v)$ is smaller than a determined tolerance, for example 10^{-6}, then the initial value of n_v is acceptable; otherwise a new value of n_v, $(n_v)_{new}$, is calculated from the following equation [131]:

$$(n_V)_{new} = n_V - \frac{f(n_V)}{f'(n_V)}$$
(6-9)

Where $f'(n_v)$ is derived from equation 6-5 as follows:

$$f'(n_V) = -\sum_i \left[\frac{z_i(k_i - 1)^2}{(n_V(k_i - 1) + 1)^2} \right] \tag{6-10}$$

$(n_v)_{new}$ is applied as n_v in the next iteration to calculate $f(n_v)$ from equation 6-5. This procedure is repeated until the absolute value of $f(n_v)$ is less than the tolerance meaning that the newest value of n_v is desirable and can be used in equations 6-3 and 6-4 to calculate x_i and y_i.

Step 2: Compressibility factors of the gas phase, Z_V, and liquid phase, Z_L, are separately calculated using the Peng-Robinson equation of state[1] as follows [130, 131]:

$$Z_\pi{}^3 - (1 - B^*)Z_\pi{}^2 + \left(A^* - 2B^* - 3B^{*2}\right)Z_\pi - \left(A^*B^* - B^{*2} - B^{*3}\right) = 0 \tag{6-11}$$

Where:

$$A^* = \frac{aP_{eq}}{R^2 T_{eq}{}^2} \tag{6-12}$$

$$B^* = \frac{bP_{eq}}{RT_{eq}} \tag{6-13}$$

$$a = \sum_j \sum_i (l_i)(l_j)\left(a_i a_j\right)^{\frac{1}{2}}\left(1 - \overline{k_{\iota J}}\right) \tag{6-14}$$

$$b = \sum_i l_i . b_i \tag{6-15}$$

$$a_i = \frac{0.45724\, R^2 T_{ci}^2}{P_{ci}} \left[1 + fw_i(1 - (\frac{T_{eq}}{T_{ci}})^{\frac{1}{2}})\right]^2 \tag{6-16}$$

$$fw_i = 0.37464 + 1.54226\, \omega_i - 0.2699\, \omega_i{}^2 \tag{6-17}$$

$$b_i = \frac{0.07780 RT_{ci}}{P_{ci}} \tag{6-18}$$

Where π refers to liquid (L) or gas (V) phases; l_i is x_i (liquid phase) or y_i (gas phase); and i and j refer to CO_2, NMP and IL in the respective phase. The binary interaction parameter, $\overline{k_{\iota J}}$, is generally obtained by minimising the difference between predicted and experimental data.

---

[1] Peng-Robinson equation of state was used in the experimental procedure to obtain the solubility of CO_2 in the solvents. The results of the test systems agreed well with the data in the literature. Thus, this equation was used in the modelling part as well.

Step 3: Fugacity coefficients of each component in the gas and liquid phases ($\emptyset_i^\pi$) are calculated from the following equation [130, 131]:

$$\ln \emptyset_i^\pi = \frac{b_i}{b}(Z_\pi - 1) - \ln(Z_\pi - B^*) + \frac{A^*}{B^*\sqrt{8}}\left(\frac{b_i}{b} - \delta_i\right) \ln \frac{2Z_\pi + B^*(2+\sqrt{8})}{2Z_\pi + B^*(2-\sqrt{8})} \tag{6-19}$$

Where:

$$\frac{b_i}{b} = \frac{T_{ci}/P_{ci}}{\sum[(l_i)\frac{T_{cj}}{P_{cj}}]} \tag{6-20}$$

$$\delta_i = \frac{2a_i^{1/2}}{a}\sum_j [(l_i)a_j^{\frac{1}{2}} - (1 - \overline{k_{\iota J}})] \tag{6-21}$$

Step 4: Fugacities of each component in the gas and liquid phases are determined as follows [130-132]:

$$f_i^L = x_i P_{eq} \emptyset_i^L \tag{6-22}$$

$$f_i^V = y_i P_{eq} \emptyset_i^V \tag{6-23}$$

Step 5: the equilibrium state, the component fugacities in the liquid and gas phases must be equal. Thus following relation connects the gas phase to the liquid phase [130-132]:

$$f_i^V = f_i^L \tag{6-24}$$

If $\left|f_i^L - f_i^V\right| < \varepsilon$ is true for all the components, x_i and y_i calculated in step 1 are accurate enough. Otherwise, k_i must be corrected using the following equaion, and then all the steps are repeated until the component fugacities in the liquid and gas phases are equal.

$$(k_i)_{new} = \frac{\emptyset_i^L}{\emptyset_i^V} = \frac{f_i^L}{f_i^V}k_i \tag{6-25}$$

A simplified representation of the flash calculation algorithm is illustrated in Figure 6-1. The solubility of CO_2 in NMP, bmim[BF_4] and their mixtures were modelled using this algorithm and a MATLAB program developed in this study.

The quality of the modelling results was assessed statistically using the absolute average deviation (AAD) and the average absolute relative deviation (AARD). The AAD and AARD are defined as:

$$AAD(x) = \frac{1}{N_p} \sum_{1}^{N_p} |x_{exp} - x_{cal}| \tag{6-26}$$

$$AARD(x) = \frac{1}{N_p} \sum_{1}^{N_p} \frac{|x_{exp} - x_{cal}|}{x_{exp}} \tag{6-27}$$

Where x_{exp} and x_{cal} are the experimental and calculated values of a liquid mole fraction of carbon dioxide, respectively, and N_p is the total number of data points.

Inputs: Temperature (T_{eq}); Pressure (P_{eq}); acentric factor (ω_i), critical temperature (T_{ci}) and critical pressure (P_{ci}) for each component.

↓

Calculate the equilibrium ratio (k_i) for each component (equation 6-2).

↓

Calculate initial value of n_v, (equations 6-6 to 6-8).

↓

Calculate $f(n_v)$ from equation 6-5

Is absolute value of $f(n_V)$ smaller than 10^{-6}?

NO →

Calculate new n_V (equations 6-5, 6-9 and 6-10).

YES ↓

Calculate x_i and y_i using equations 6-3 and 6-4.

↓

Calculate thermodynamic parameters A^* and B^* for each phase using equations 6-12 to 6-18; then separately obtain compressibility factors, Z_V (the maximum root of equation 6-11) and Z_L (the smallest and positive root of equation 6-11).

↓

Calculate fugacity coefficients of each component in the gas and liquid phases using equations 6-19 to 6-21; and then obtain fugacities of each component in the gas and liquid phases using equations 6-22 to 6-23

↓

Is $|f^L_i - f_i^V| \leq \varepsilon$ true for each component?

NO →

Consider new k_i using equation 6-25.

YES ↓

x_i and y_i calculated for the equilibrium state of system are correct

Figure 6-1: VLE flow diagram for physical absorption system.

6.2 Modelling of acid gas solubility in alkanolamine aqueous solution

Thermodynamic modelling of the chemical absorption of acid gases has been a hot and complex topic for many years. Researchers have tried to propose models predicting the behaviour of these systems precisely ensuring their applicability and simplicity for industrial applications. There are two classes of thermodynamics models: 1) simple models based on Kent-Eisenberg model, and 2) rigorous models based on the activity coefficient models [133, 134].

Kent and Eisenberg defined the apparent equilibrium constants for two main reactions of the amine process (amine protonation and carbamate formation reactions); regressed them as a function of temperature by fitting to the experimental data; and assumed an ideal state for the remaining equilibrium constants. Non-ideality of the gas phase was neglected and non-idealities of the liquid phase were lumped into the apparent equilibrium constants. Thus all activity coefficients and fugacity coefficients were set equal to unity [133-141]. In the modified Kent-Eisenberg models developed by different authors, the apparent equilibrium constants were regressed as a function of temperature, partial pressure of acid gas, initial amine concentration and gas solubility in the solvent [134, 142-147]. The Kent-Eisenberg model and its modified versions are the simplest models since all the equations governing the amine process can be merged into one equation that is easily solved using numerical methods [144, 145]. The details of the Kent-Eisenberg model are presented in Appendix E.

Deshmukh and Mather (1980) developed a rigorous model to analyse the acid gas solubility in amine solutions. They proposed to use the Debye–Hückel law and the Guggenheim equation to calculate activity coefficients and consider non-idealities of the system [145, 148]. Other semi-empirical activity coefficient models used in rigorous models include the Pitzer model [132, 149], E-NRTL [150] and E-UNIQUAC model [151]. These models are based on the excess Gibbs free energy while the forces between species are divided to the long-range electrostatic interactions between ionic solutes; and the short-range non-electrostatic interactions between different molecular and ionic solutes. Although in the most of models, the Debye– Hückel expression is applied to consider the long-range forces, the short-range forces are presented by various methods including the NRTL, UNIQUAC, Wilson, Van Laar, Margules equations, etc. [132]. Table 6-1 presents the specifications of the thermodynamics models used in rigorous models to calculate activity coefficient parameters. In rigorous models, a large number of non-linear equations need to be solved simultaneously, thus failure to provide good initial values may result in convergence problems [133-135, 139, 140]. Of the aforementioned models, the Deshmukh-Mather model is widely applied for industrial applications and is simpler compared to other rigorous models having a large number of adjustable binary interaction parameters [53, 152].

Table 6-1: Specifications of activity coefficient models used for electrolyte solutions.

Activity coefficient model	Reference	Remarks
Electrolyte NRTL	Chen et al. (1982) [150], Austgen (1989) [153], Chang et al. (1993) [154], Liu et al. (1999) [155], Aroua et al. (2002) [156], Zhang et al. (2011) [157], Dash et al. (2011) [158], Barreau et al. (2006) [159]	- Two fundamental assumptions: 1. The local composition of cations(anions) around cations (anions)is zero 2. The net local ionic charge around a central solvent molecule is zero - The Pitzer-Debye-Hückel formula proposed by Pitzer (1980) is used to account for long-range ion-ion interactions. - The NRTL model (a local composition concept) is used to represent short-range forces [132, 150]
Pitzer	Pitzer (1973) [149], Edwards et al. (1978) [160], Pitzer and Simonson (1986) [161], Li and Mather (1994) [162], Kuranov et al. (1996) [163], Kamps et al. (2001) [164], Arcis et al. (2009) [165], B¨ottinger et al. (2007) [166], Rumpf et al. (1993) [167], Lemoine et al. (2000) [168]	- Pitzer calculated Excess Gibs energy from the virial expansion and it is subjected to the limitations of the virial model. Debye- Hückel law is used for the electrostatic part and the virial expansion is taken to account for the short-range van der Waals forces [132]. - The model parameters are dependent on temperature and type of solvent [150]. Binary parameters are strong functions of ionic strength providing high convergence for the virial expansion. - Ternary parameters are necessary at a high concentration that makes this model more complicated [160].
Extended UNIQUAC	Sander et al. (1986) [151], Thomsen et al. (1999) [169], Addicks (2002) [170], Faramarzi et al. (2009) [171], Sadegh, N. (2015) [172]	Extended UNIQUAC model consists of three terms: - Two non-electrostatic terms, combinatorial and residual, are the same as the expressions proposed in original UNIQUAC model (by Abrams and Prausnitz, 1975 and Maurer and Prausnitz, 1978). They represent the short-range interactions between different molecular and ionic solutes - Extended Debye- Hückel formula is the electrostatic term used to account the long-range interaction forces between ionic solutes.

Activity coefficient model	Reference	Remarks
Deshmukh-Mather	Deshmukh and Mather (1981) [148], Haji Sulaiman et al. (1995) [173], Jou et al. (1995) [119], Tong et al. (2012) [136], Jane et al. (1997) [174], Macgregor (1991) [175], Hartono et al. (2011) [176], Benamor et al. (2005) [177], Wong et al. (2015) [152], Pahlavanzadeh et al. (2011) [178], Soltani Panah et al. (2015) [53]	• The electrostatic forces are taken into account by Debye- Hückel law • Short-range Van der Waals forces are presented by Guggenheim equation. • It is assumed that water behaviour is ideal and all the interaction parameters including water are set to zero [148]. • Compared with other models, it is simpler to handle and less computational time is required [173].

The new algorithm, presented in this study, uses the concept of the apparent equilibrium constant defined in the Kent-Eisenberg model to simplify equations of the liquid phase and reduce them to a polynomial equation. The Deshmukh-Mather activity model is applied to determine the apparent equilibrium constants of all the reactions. In this approach, at first the calculations of the vapour phase are carried out using Peng-Robinson equation of state. Then the polynomial equation derived from the equations governing the aqueous phase is solved using results obtained for the vapour phase. Similar to the Kent-Eisenberg model, the present approach has the important advantage of computational simplicity since just a few polynomial equations are supposed to be individually solved.

6.2.1 Thermodynamic Model

As explained in Chapter 1, the initial proposal of this PhD thesis was to study H_2S systems. But the objectives were modified to focus on CO_2. Therefore, the modelling part includes the chemical absorption of CO_2 and H_2s in amine solvents. Chemical equilibrium of the solubility of acid gases in the aqueous alkanolamine solutions can be described by the following reactions:

Dissociation of protonated amine [148]:

$$RR'R''NH^+ \overset{K_1}{\leftrightarrow} RR'R''N + H^+ \qquad K_1 = \frac{m_{RR'R''N} \cdot \gamma_{RR'R''N} \cdot m_{H^+} \cdot \gamma_{H^+}}{m_{RR'R''NH^+} \cdot \gamma_{RR'R''NH^+}} \qquad (6\text{-}28)$$
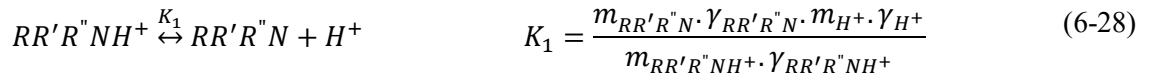
Dissociation of water [148]:

$$H_2O \overset{K_2}{\leftrightarrow} H^+ + OH^- \qquad K_2 = \frac{m_{OH^-} \cdot \gamma_{OH^-} \cdot m_{H^+} \cdot \gamma_{H^+}}{a_{H_2O}} \qquad (6\text{-}29)$$
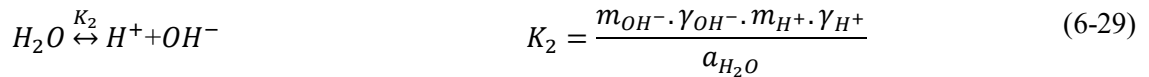
Hydration of carbon dioxide and the formation of bicarbonate [148]:

$$CO_2 + H_2O \overset{K_3}{\leftrightarrow} H^+ + HCO_3^- \qquad K_3 = \frac{m_{H^+} \cdot \gamma_{H^+} \cdot m_{HCO_3^-} \cdot \gamma_{HCO_3^-}}{m_{CO_2} \cdot \gamma_{CO_2} \cdot a_{H_2O}} \qquad (6\text{-}30)$$
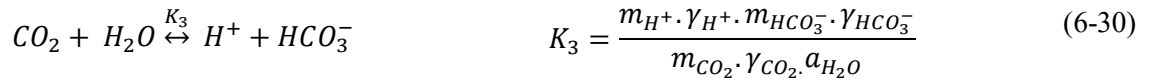
Dissociation of bicarbonate and formation of carbonate [148]:

$$HCO_3^- \overset{K_4}{\leftrightarrow} CO_3^{2-} + H^+ \qquad K_4 = \frac{m_{H^+} \cdot \gamma_{H^+} \cdot m_{CO_3^{2-}} \cdot \gamma_{CO_3^{2-}}}{m_{HCO_3^-} \cdot \gamma_{HCO_3^-}} \qquad (6\text{-}31)$$
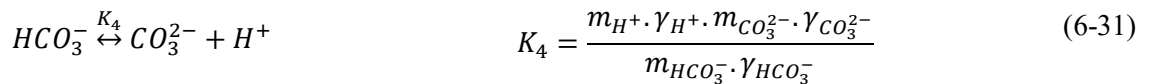
Dissociation of carbamate (except for tertiary amines) [148]:

$$R'R''NCOO^- (\text{carbamate}) + H_2O \overset{K_5}{\leftrightarrow} RR'R''N + HCO_3^-$$

$$K_5 = \frac{m_{HCO_3^-} \cdot \gamma_{HCO_3^-} \cdot m_{RR'R''N} \cdot \gamma_{RR'R''N}}{m_{R'R''NCOO^-} \cdot \gamma_{R'R''NCOO^-} \cdot a_w} \qquad (6\text{-}32)$$
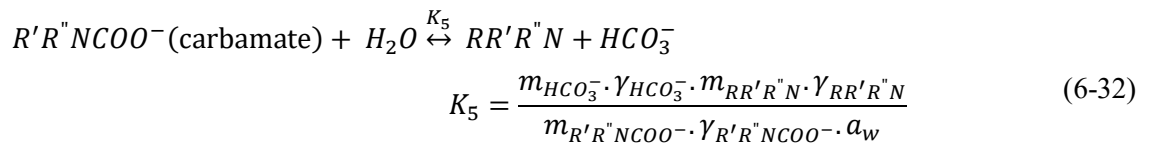
Dissociation of hydrogen sulfide [148]:

$$H_2S \overset{K_6}{\leftrightarrow} H^+ + HS^- \qquad\qquad K_6 = \frac{m_{H^+} \cdot \gamma_{H^+} \cdot m_{HS^-} \cdot \gamma_{HS^-}}{m_{H_2S} \cdot \gamma_{H_2S}} \qquad (6\text{-}33)$$
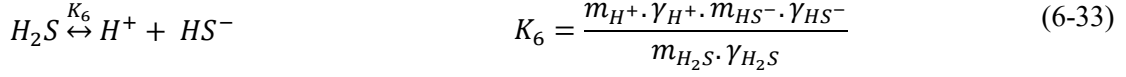
Dissociation of hydrosulfide and formation of sulfide ion [148]:

$$HS^- \overset{K_7}{\leftrightarrow} H^+ + S^{2-} \qquad\qquad K_7 = \frac{m_{H^+} \cdot \gamma_{H^+} \cdot m_{S^{2-}} \cdot \gamma_{S^{2-}}}{m_{HS^-} \cdot \gamma_{HS^-}} \qquad (6\text{-}34)$$
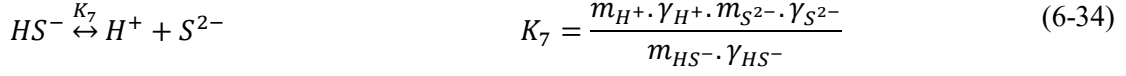
Where a_{H_2O}, m_i (mol/kg water) and γ_i are the activity of water, the molality and activity coefficient of species i, respectively. For all the components except for water, asymmetric activity coefficient is applied that is related to the infinite-diluted state of the component. In addition, the reference state for water is pure-water at the pressure and temperature of the system. Reactions 6-28 to 6-30 occur when CO_2 is captured in the aqueous amines and reactions 6-31 and 6-32 take place when H_2S is present in the system.

At equilibrium condition, the component fugacities in the aqueous and vapour phases must be equal. Thus following relations, written for the volatile components, connect the vapour phase to the aqueous phase [53]:

$$f^V_{CO_2} = f^L_{CO_2}$$

$$P \cdot y_{CO_2} \cdot \emptyset_{CO_2} = \gamma_{CO_2} \cdot m_{CO_2} \cdot H^m_{CO_2} \cdot \exp\left(\frac{v_{CO_2} \cdot (P - P^0)}{RT}\right) \qquad (6\text{-}35)$$

$$f^V_{H_2O} = f^L_{H_2O}$$

$$P \cdot y_{H_2O} \cdot \emptyset_{H_2O} = a_{H_2O} \cdot P^0_{H_2O} \cdot \emptyset^0_{H_2O} \cdot \exp\left(\frac{v_{H_2O} \cdot (P - P^0)}{RT}\right) \qquad (6\text{-}36)$$

$$f^V_{H_2S} = f^L_{H_2S}$$

$$P \cdot y_{H_2S} \cdot \emptyset_{H_2S} = \gamma_{H_2S} \cdot m_{H_2S} \cdot H^m_{H_2S} \cdot \exp\left(\frac{v_{H_2S} \cdot (P - P^0)}{RT}\right) \qquad (6\text{-}37)$$

Where $T(K)$ and $P(bar)$ are the equilibrium temperature and pressure of the system; $\emptyset_i$ is the fugacity coefficient of species i; $H^m_{CO_2}$ and $H^m_{H_2S}$ are Henry's constants (bar. kg water/mol) at temperature of system; v_{CO_2}, v_{H_2S} and v_{H_2O} are the molar volumes (cm^3/mol) at infinite dilution and temperature of system; $P^0_{H_2O}$ (bar) is the vapour pressure of water; $\emptyset^0_{H_2O}$ is the fugacity coefficient of pure water at T and $P^0_{H_2O}$; and R ($\frac{bar.cm^3}{K.mol}$) is the gas constant.

6.2.2 Development of thermodynamic modelling

The approach developed in this study has two main stages. The first stage is to organize the equations in the aqueous phase and derive an overall polynomial equation for this phase. The second stage is to calculate partial pressures and concentrations in the gas phase. The

concentrations in the aqueous phase and the solubility of acid gas are then determined by using the polynomial equation derived in the first stage.

6.2.2.1 Derivation of the overall equation for the aqueous phase

In this section, the procedure to obtain the overall equation for the aqueous MEA (as a primary amine) + CO_2 system, that has maximum reactions in the aqueous phase compared to other systems, is explained in detail.

For the liquid phase of the aqueous MEA + CO_2 system, the following equations exist (from equations 6-28 to 6-32):

$$K_1' = \frac{m_{RR'R''N} \cdot m_{H^+}}{m_{RR'R''NH^+}} = K_1 \frac{\gamma_{RR'R''NH^+}}{\gamma_{H^+} \cdot \gamma_{RR'R''N}} \qquad (6\text{-}38)$$

$$K_2' = m_{OH^-} \cdot m_{H^+} = K_2 \frac{a_{H_2O}}{\gamma_{OH^-} \cdot \gamma_{H^+}} \qquad (6\text{-}39)$$

$$K_3' = \frac{m_{H^+} \cdot m_{HCO_3^-}}{m_{CO_2}} = K_3 \frac{\gamma_{CO_2} \cdot a_{H_2O}}{\gamma_{H^+} \cdot \gamma_{HCO_3^-}} \qquad (6\text{-}40)$$

$$K_4' = \frac{m_{H^+} \cdot m_{CO_3^{2-}}}{m_{HCO_3^-}} = K_4 \frac{\gamma_{HCO_3^-}}{\gamma_{H^+} \cdot \gamma_{CO_3^{2-}}} \qquad (6\text{-}41)$$

$$K_5' = \frac{m_{HCO_3^-} \cdot m_{RR'R''N}}{m_{R'R''NCOO^-}} = K_5 \frac{\gamma_{R'R''NCOO^-} \cdot a_{H_2O}}{\gamma_{HCO_3^-} \cdot \gamma_{RR'R''N}} \qquad (6\text{-}42)$$

Where K_1' to K_5' are the apparent equilibrium constants that can be calculated from the activity models and values of equilibrium constants available in the literature.

Mass balance equation:

$$m_{RR'R''N}^t = m_{RR'R''N} + m_{R'R''NCOO^-} + m_{RR'R''NH^+} \qquad (6\text{-}43)$$

Where $m_{RR'R''N}^t$ ($\frac{mol}{kg\ water}$) is the initial concentration of amine solution.

Charge balance equation:

$$m_{H^+} + m_{RR'R''NH^+} = m_{OH^-} + m_{R'R''NCOO^-} + m_{HCO_3^-} + 2\,m_{CO_3^{2-}} \qquad (6\text{-}44)$$

Equation defining the CO_2 solubility:

$$a_{CO_2} = \frac{m_{CO_2} + m_{HCO_3^-} + m_{CO_3^{2-}}}{m_{RR'R''N}^t} \qquad (6\text{-}45)$$

Overall, there are 8 equations and 9 unknown variables, namely m_{H^+}, $m_{RR'R''NH^+}$, m_{OH^-}, $m_{R'R''NCOO^-}$, $m_{HCO_3^-}$, $m_{CO_3^{2-}}$, m_{CO_2}, $m_{RR'R''N}$ and a_{CO_2}.

Equation 6-38 to 6-42 are rewritten as follows:

$$\frac{m_{RR'R"N}}{m_{RR'R"NH^+}} = \frac{K_1 \cdot \gamma_{RR'R"NH^+}}{m_{H^+} \cdot \gamma_{RR'R"N} \cdot \gamma_{H^+}} = \frac{K_1'}{m_{H^+}} \tag{6-46}$$

$$m_{OH^-} = \frac{K_2 \cdot a_{H_2O}}{\gamma_{OH^-} \cdot m_{H^+} \cdot \gamma_{H^+}} = \frac{K_2'}{m_{H^+}} \tag{6-47}$$

$$m_{HCO_3^-} = \frac{K_3 \cdot m_{CO_2} \cdot \gamma_{CO_2} \cdot a_{H_2O}}{m_{H^+} \cdot \gamma_{H^+} \cdot \gamma_{HCO_3^-}} = \frac{K_3' \cdot m_{CO_2}}{m_{H^+}} = \frac{N}{m_{H^+}} \quad ; where \ N = K_3' \cdot m_{CO_2} \tag{6-48}$$

$$m_{CO_3^{2-}} = \frac{K_4 \cdot \gamma_{HCO_3^-}}{m_{H^+} \cdot \gamma_{H^+} \cdot \gamma_{CO_3^{2-}}} \cdot \frac{N}{m_{H^+}} = \frac{K_4' \cdot N}{m_{H^+}^2} \tag{6-49}$$

$$\frac{m_{RR'R"N}}{m_{R'R"NCOO^-}} = \frac{K_5 \cdot \gamma_{R'R"NCOO^-} \cdot a_{H_2O}}{\gamma_{HCO_3^-} \cdot \gamma_{RR'R"N} \cdot m_{HCO_3^-}} = \frac{m_{H^+}}{N} \cdot K_5' \tag{6-50}$$

By inserting equations 6-46 and 16-50 into equation 6-43, following equations are obtained:

$$m_{R'R"NCOO^-} = \frac{m_{RR'R"N}^t \cdot N \cdot K_1'}{m_{H^+}^2 \cdot K_5' + m_{H^+} \cdot K_5' \cdot K_1' + N \cdot K_1'} \tag{6-51}$$

$$m_{RR'R"NH^+} = \frac{m_{H^+}^2 \cdot m_{RR'R"N}^t \cdot K_5'}{m_{H^+}^2 \cdot K_5' + m_{H^+} \cdot K_5' \cdot K_1' + N \cdot K_1'} \tag{6-52}$$

The aim of the above conversions is to obtain the concentration of all the components as a function of m_{CO_2} and m_{H^+} (m_{CO_2} is present in the equations related to the gas phase and is calculated using them. m_{H^+} is the common component in most equations, thus, it is easy to write other concentrations as a function of m_{H^+}).

Lastly, the overall equation is determined by inserting equations 6-47 to 6-49, 6-51 and 6-52 into equation 6-44 and arranging it, as follows:

$$A_1 \cdot m_{H^+}^5 + A_2 \cdot m_{H^+}^4 + A_3 \cdot m_{H^+}^3 + A_4 \cdot m_{H^+}^2 + A_5 \cdot m_{H^+} + A_6 = 0 \tag{6-53}$$

Where:

$A_1 = K_5'$

$A_2 = K_5' \cdot K_1' + K_5' \cdot m_{RR'R"N}^t$

$A_3 = K_1' \cdot N - K_5' \cdot K_2' - N \cdot K_5'$

$A_4 = -((K_2' + N) \cdot K_5' \cdot K_1' + 2 \cdot N \cdot K_4' \cdot K_5' + N \cdot K_1' \cdot m_{RR'R"N}^t)$

$A_5 = -((K_2' + N) \cdot N \cdot K_1' + 2 \cdot N \cdot K_4' \cdot K_5' \cdot K_1')$

$A_6 = -(2 \cdot N^2 \cdot K_1' \cdot K_4')$

Therefore, all the equations governing the aqueous phase are summarised in equation 6-53 without any simplifying assumption. It is a degree-five polynomial which can be solved easily using numerical methods. The overall equations for MDEA / AMP / DIPA / DEA + CO₂ and MEA / MDEA / AMP / DIPA / DEA + H₂S systems are degree-four polynomials having almost the same derivation procedure for the MEA + CO₂ system.

6.2.2.2 Calculation of solubility of acid gas

In this section, several steps are pursued in order to calculate the composition of the vapour phase, partial pressures, concentrations of the components in the aqueous phase; and finally the solubility of acid gas in the aqueous amine solution.

Step 1: The first step is to compute thermodynamic parameters required in the modelling which are: K_i, equilibrium constants of chemical reactions that are mostly dependent on the temperature; H_i^m, Henry's constants of CO_2 and H_2S dissolved in the amine solution; $P_{H_2O}^0$, vapour pressure of water; and molar volumes $v_{CO_2}(\frac{cm^3}{mol})$, $v_{H_2S}(\frac{cm^3}{mol})$ and $v_{H_2O}(\frac{cm^3}{mol})$. The following equations are applied to state their dependency on the temperature [53, 136, 160, 164, 167]:

$$v_{H_2O} = \frac{18.02}{0.753597 + 1.877465 \times 10^{-3} \times T - 3.563982 \times 10^{-6}T^2} \tag{6-54}$$

$$v_{H_2S} = 0.000599631 \times (T - 273.15)^2 + 0.002899997 \times (T - 273.15) + 34.825 \tag{6-55}$$

$$v_{CO_2} = 0.00056007 \times (T - 273.15)^2 + 0.003296583 \times (T - 273.15) + 32.41271286 \tag{6-56}$$

$$\ln(K_i \, or \, H_i^m \, or \, P_{H_2O}^0) = C_1 + \frac{C_2}{T} + C_3.\ln T + C_4.T + C_5.T^2 \tag{6-57}$$

Values of parameters C_1 to C_5 taken from literatures are listed in Table F-1.

Activity coefficients of solute species (except for water) included in the apparent equilibrium constants and the equilibria phase equations must be determined using the activity coefficient models. The Deshmukh-Mather model using Debye-Hückel theory is applied to calculate the activity coefficients as follows [148]:

$$ln\gamma_i = -\frac{A \, z_i'^2 \sqrt{I}}{1 + B\sqrt{I}} + 2\sum_j \beta_{ij} \, m_j \tag{6-58}$$

The first term represents the contribution of the electrostatic forces and the second term represents the short-range van der Waals forces. z_i' and m_j are the electrical charge and the molality of component, respectively. I is the ionic strength of the solution defined by the following equation [148]:

$$I = \frac{1}{2}\sum_j m_j z_j'^2 \tag{6-59}$$

Parameter B is set to 1.2; and A, the Debye–Hückel proportionality factor, is mostly a function of the temperature [53]:

$$A = 1.306548 + \frac{0.1328238 \times 10^{-1}}{T} - \frac{0.3550803 \times 10^{-4}}{T^2} + \frac{0.3381968 \times 10^{-7}}{T^3} \quad (6\text{-}60)$$

β_{ij} is the binary interaction parameter obtained from the regression of experimental data and minimising the difference between predicted and experimental data. Some of them are temperature-dependent function as follows [53]:

$$\beta_{ij} = a_{ij} + b_{ij}T \quad (6\text{-}61)$$

Literally, it is unnecessary to take into account all the possible interactions between species.

Equation 6-56 shows that the activity coefficient is dependent on the molality of components, m_j, which are unknown. Thus, proper initial guesses for concentrations are required. They can be calculated by considering the system in the ideal state ($\gamma_i \& \emptyset_i = 1$) and solving the related equations [53, 178].

Step 2: In this step, a_{H_2O}, $\varphi^0_{H_2O}$ and φ_{H_2O}, that are activity of water, fugacity coefficient of the saturated vapour of pure water at T and $P^0_{H_2O}$ and fugacity coefficient of water in the vapour phase, respectively, should be determined in order to calculate the mole fraction of the components in the vapour phase. a_{H_2O} can be equal to its mole fraction in the aqueous phase since in most cases the aqueous phase is predominantly water [148]. Thus, a_{H_2O} is obtained by using initial guesses for concentrations calculated in the previous step. $\varphi^0_{H_2O}$ is obtained using the Peng-Robinson equation as follows [131]:

$$\emptyset^0_{H_2O} = \exp((Z - 1) - \ln(Z - B^*) - \frac{A^*}{B^*\sqrt{8}} \ln \frac{2Z + B^*(2 + \sqrt{8})}{2Z + B^*(2 - \sqrt{8})} \quad (6\text{-}62)$$

Where:

$$Z^3 - (1 - B^*)Z^2 + (A^* - 2B^* - 3B^{*2})Z - (A^*B^* - B^{*2} - B^{*3}) = 0 \quad (6\text{-}63)$$

$$A^* = \frac{aP}{R^2T^2} \quad (6\text{-}64)$$

$$B^* = \frac{bP}{RT} \quad (6\text{-}65)$$

$$a = \frac{0.45724\, R^2 T_c^2}{P_c} \left[1 + (0.37464 + 1.54226\, \omega - 0.2699\, \omega^2)(1 - (\frac{T}{T_c})^{\frac{1}{2}})\right]^2 \quad (6\text{-}66)$$

$$b = \frac{0.07780 R T_c}{P_c} \tag{6-67}$$

Z, $P_c(bar)$ and $T_c(K)$ are compressibility factor and critical temperature and pressure of the pure component which is water here. P in equation 6-64 and 6-65 is equal to $P^0_{H_2O}$ to calculate $\emptyset^0_{H_2O}$.

φ_{H_2O} is dependent on the mole fraction of components in the vapour phase. Thus, a trial value for y_{H_2O} should be assumed and then compressibility factor of the vapour phase, Z_V, is obtained by using equations 6-63 to 6-65; while the mixing rule is applied for the calculation of a and b as follows [131]:

$$a = \sum_j \sum_i y_i y_j (a_i a_j)^{\frac{1}{2}} (1 - \overline{k_{ij}}) \tag{6-68}$$

$$b = \sum_i y_i b_i \tag{6-69}$$

Where i and j refer to CO_2 or H_2S and H_2O. a_i and b_i for each component are determined by using equations 6-66 and 6-67. $\overline{k_{ij}}$ or binary interaction coefficients are presented in table G-1 [53]. φ_i, for H_2O and CO_2 or H_2S, is calculated as follows [131]:

$$\ln \emptyset_i = \frac{b_i}{b}(Z_V - 1) - \ln(Z_V - B^*) + \frac{A^*}{B^*\sqrt{8}} \left(\frac{b_i}{b} - \delta_i \right) \ln \frac{2Z_V + B^*(2 + \sqrt{8})}{2Z_V + B^*(2 - \sqrt{8})} \tag{6-70}$$

Where:

$$\frac{b_i}{b} = \frac{T_{ci}/P_{ci}}{\sum y_j T_{cj}/P_{cj}} \tag{6-71}$$

$$\delta_i = \frac{2a_i^{1/2}}{a} \sum_j y_j a_j^{\frac{1}{2}} - (1 - \overline{k_{ij}}) \tag{6-72}$$

Finally, y_{H_2O} can be determined by using equation 6-34:

$$y_{H_2O} = \frac{a_{H_2O} \cdot P^0_{H_2O} \cdot \emptyset^0_{H_2O} \cdot \exp\left(\frac{v_{H_2O} \cdot (P - P^0)}{RT} \right)}{P \cdot \emptyset_{H_2O}} \tag{6-73}$$

If the calculated y_{H_2O} is almost equal to the trial value, the molality of CO_2 or H_2S in the liquid phase is determined using equation 6-35 or 6-37; otherwise step 2 must be repeated with the new calculated y_{H_2O}.

Step 3: In this step, parameters A_1 to A_6 for equation 6-53 are calculated. Then equation 6-53 is solved by a numerical method such as Newton-Raphson. The initial guess calculated in step 1 for the molality of H^+, can be used as the initial point to start the Newton-Raphson method. The concentrations of other components in the aqueous phase are determined by equations 6-47 to 6-49, 6-51 and 6-52. If the new calculated concentrations, m_i, are almost equal to the initial guesses calculated in step 1, the solubility of acid gas in the aqueous solution at given temperature and pressure is calculated using equation 6-45; otherwise, steps 1 to 3 are repeated with the new calculated concentrations as initial guesses.

A simplified representation of the algorithm developed in this section is illustrated in Figure 6-2. The solubility of CO_2 and H_2S in aqueous MEA, MDEA, DEA, DIPA, AMP and MEA + bmim[OTF] solutions are modelled using this algorithm and MATLAB program.

Inputs: T, P, $m^t_{RR'R''N}$

Determine K_i, $H^m_{CO_2/H_2S}$, $P^0_{H_2O}$, v_{CO_2}, v_{H_2S} and v_{H_2O} (equations 6-54 to 6-57). Consider system in the ideal state (γ_i & $\emptyset_i$=1) and calculate initial guesses for concentrations, m^{guess}_i.

Calculate the activity coefficient of components (equations 6-58 to 6-61) using m^{guess}_i. Then calculate activity of water:

$$a_{H_2O} = \frac{\frac{1000}{18.02}}{\frac{1000}{18.02} + \sum_i m^{guess}_i}$$

Calculate $\emptyset^0_{H_2O}$ (equations 6-62 to 6-67). To obtain the root of equation 6-63, use Newton-Raphson method while initial guess is $Z^{guess} = 1$. Guess an initial value for $y^{guess}_{H_2O}$. It must be $0 < y^{guess}_{H_2O} < 1$.

Calculate Peng Robinson's parameters using $y^{guess}_{H_2O}$; and then calculate Z_V, (equations 36-63 to 6-69). Calculate $\emptyset_{H_2O}$ using equations 6-70 to 6-72; then obtain y_{H_2O} via equation 6-73. Is $|y_{H_2O} - y^{guess}_{H_2O}| \leq \mathcal{E} = 10^{-6}$?

NO

Consider: $y^{guess}_{H_2O} = y_{H_2O}$

YES

Calculate $m_{CO_2 \ or \ H_2S}$ (equations 6-35 or 6-37). Calculate parameters of equation 6-53 and solve it. Determine concentrations of other components, m_i, in the aqueous phase (equations 6-47 to 6-49, 6-51 and 6-53). Is $|m_i - m^{guess}_i| \leq \mathcal{E}$ right for each component?

YES

Calculate the solubility of acid gas:

$$\alpha_{CO_2} = \frac{m_{CO_2} + m_{HCO_3^-} + m_{CO_3^{2-}}}{m^t_{RR'R''N}}$$

NO

Consider the new calculated m_i as initial guess:

$$m^{guess}_i = m_i$$

Figure 6-2: Flow diagram of algorithm developed for chemical absorption of acid gases.

7. RESULTS AND DISCUSSION

Experimental phase equilibrium data are an important source of information. Even predictive models require a number of experimental points to adjust the interaction parameters and validate their ability to anticipate the phase equilibrium behaviour. When performing experimental measurements, it is important to make sure the measured data are accurate. This is achieved by preparing the equipment correctly, calibrating the measuring devices, performing reliable VLE test systems, and chemical purity checks. Measurement of the VLE test systems was important to this project since this validated the reliability and the reproducibility of the new equipment and the experimental procedure. Thus, before collecting new sets of data using the equipment described in Chapter 4, measurements were performed on the test systems listed in Table 7-1. The choice of the test systems was based on the presence of consistent data (at least three sets) on the systems in the literature at the desired pressures, and the availability of chemicals required for the test systems in TRU laboratory as well. Once, the results on the test systems were repeatable and consistent with data in the literature, therefore confirming the reliability of the equipment and the experimental procedure, new sets of data on the systems listed in Table 7-1 were collected. Most of these systems had no VLE data available in the literature at the time measurements were carried out.

This chapter presents the results of the experimental measurements on the test systems. The performance and reliability of new equipment are discussed. Then, the experimental data on the solubility of CO_2 in, and densities, viscosities, sound velocity and evaporation rates of, five main systems, viz. (NMP + bmim[BF$_4$], MEA/DGA + water + bmim[OTF] and MEA/DGA + NMP + bmim[TF$_2$N]) are presented. Finally, the ability of modelling method developed in Chapter 6 to predict the solubility of CO_2/H_2S in the aqueous amine solutions and their mixture with ionic liquids is assessed and its limitations and drawbacks are discussed in detail.

Table 7-1: Overview of the test and main VLE systems measured in this work.

Solvent	Temperature (K)	Pressure range (MPa)
Test systems		
CO_2 + Hexane	313.20	0.345 to 2.802
CO_2 + NMP	298.16, 313.14, 323.14, 333.15 348.14	0.130 to 2.090
CO_2 + bmim[BF$_4$]	298.14, 313.15, 323.15, 333.15, 348.16	0.145 to 2.742
Main systems		
CO_2 + bmim[BF$_4$] + NMP	298.15, 313.15, 323.15	0.152 to 2.051
CO_2 + MEA + H_2O	313.15	0.189 to 2.322
CO_2 + MEA + NMP	313.15	0.194 to 2.298
CO_2 + MEA + bmim[OTF]	313.15	0.564 to 2.065
CO_2 + MEA + H_2O + bmim[OTF]	298.15, 313.15	0.093 to 2.322
CO_2 + MEA + NMP + bmim[TF$_2$N]	313.15	0.297 to 1.993
CO_2 + DGA + H_2O	313.15	0.188 to 2.101
CO_2 + DGA + NMP	313.15	0.262 to 1.893
CO_2 + DGA + H_2O + bmim[OTF]	298.15, 313.15	0.271 to 2.301
CO_2 + DGA + NMP + bmim[TF$_2$N]	313.15	0.297 to 1.973

7.1 Chemicals used

The chemicals used, their purities, densities, refractive indices and the suppliers are listed in Table 7-2. All the liquid chemicals, except for deionized water and n-hexane, were dried under the vacuum condition (temperature and duration of drying was dependant on the boiling point of the chemicals). All the liquid components were thoroughly degassed in the round-bottom flasks in the solvent preparation step, and then these were degassed in the equilibrium cell.

Table 7-2: Pure-component parameters, purities, and properties for the chemicals used in this study, as well as the expanded uncertainty ($k = 2$).

Component	Supplier	Density at 318.15 K (g.cm^{-3})		Refractive index at 298.15 K		Supplier purity (wt.%)	Purification
		Experimental[a]	Literature[b]	Experimental[c]	Literature[d]		
CO_2	Afrox	-NA-	-NA-	-NA-	-NA-	99	none
n-hexane	Merck	0.6412[e]	0.642[e]	1.372	1.37242	≥ 99	degassed
NMP	Merck	1.0119	1.0117	1.469	1.4680	≥ 99.5	dried
bmim[BF$_4$]	Sigma Aldrich	1.1882	1.1884 1.1891	1.423[f]	1.423[f]	≥ 98	dried
MEA	Sigma Aldrich	1.0105[g]	1.009[g]	1.4513 1.4532[f]	1.4521 1.4539[f]	≥ 99	dried
DGA	Sigma Aldrich	1.0395[e]	1.03953[e]	1.4582 1.4597[f]	1.4598[f]	98	dried
H_2O	obtained from the analytical lab at the same university	0.9957[g]	0.9957[g]	1.3325 1.333[f]	1.33336[f]		degassed
bmim[OTF]	Sigma Aldrich	1.2833[e]	1.2945[e]	1.4383 1.4395[f]		97	dried
bmim[TF$_2$N]	Sigma Aldrich	1.4162 1.4353[h]	1.440[h]	1.4266 1.4281[f]		≥ 98	dried

[a] $U(T) = 0.02$ K; $U(\rho) = 0.0002$ g.cm^{-3}, data recorded at 0.101 MPa, $U(P) = 0.001$ MPa.

[b] Data for the liquid density (ρ) from literature [111, 179-184].

[c] $U(T) = 0.02$ K ; $U(n_D) = 0.001$; data recorded at 0.101 MPa and a standard wavelength of 589 nm, $U(P) = 0.001$ MPa.

[d] Data for the refractive index (n_D) from the literature [185-188].

[e] Data at 313.15 K.

[f] Data at 293.15 K.

[g] Data at 303.15 K.

[h] Data at 293.15 K.

7.2 Performance of the new equipment

7.2.1 Test system solubility measurements

The equipment and experimental technique were tested by measuring VLE data for three different binary non-ideal test systems, namely: CO_2 + n-hexane at 313.20 K, CO_2 + NMP at 298.16 K and CO_2 + bmim[BF_4] at 298.14 K. The experimental data (*T-P-x*) for the binary system of CO_2 + n-hexane are presented in Figure 7-1 and listed in Table H-1. Additionally, the raw data (*T-P-z*) are reported to enable future modelling of the data. The data presented herein contain six different initial loadings of n-hexane to check for measurement repeatability. The data reported show very good agreement to the data available in the literature that were measured using a variety of different experimental methods. The phase equilibrium data (*T-P-x*) for the CO_2 + NMP binary system are displayed in Figure 7-2 and listed in Table H-2 (at a temperature of 298.16 K). Excellent agreement is observed between the experimental data and the data reported in the literature. The experimental data (*T-P-x*) for the binary system of CO_2 + bmim[BF_4] are listed in Table H-3 and displayed in Figure 7-3. There are some noticeable differences between the experimental data and the data available in the literature. However, there is significant scatter in the data reported in the literature. Furthermore, the experimental solubility data for the binary system of CO_2 + NMP/bmim[BF_4] at temperatures of (313.14, 323.14, 333.15 and 348.14) K were measured. The data expands upon the concentration and temperature range of the data available in the literature. The experimental data were modelled using the flash calculation and the phi-phi approach as previously discussed in Chapter 6. The experimental and modelling results are displayed in Figures 7-3, 7-5 and listed in Tables H-2 and H-3. The modelled predictions agree well with the experimental results, except for the CO_2 + bmim[BF_4] system at 298.15 K which there are some considerable differences among the experimental data, modelled results and data available in literature.

Depending on the apparatus used and the accuracy of measurements, experimental results can be always subjected to small or large errors and uncertainties. It is possible to find large errors when plotting the graphical dependence of data since they come out as deviations from a smooth curve. The large errors are especially obvious in the diagram that is displaying the dependence of the difference between mole fraction in the liquid phase and the mole fraction in the vapour phase (*x-y*) on the composition of the liquid phase (*x*). However, in some cases, the smoothness of the curve does not guarantee the accuracy and reliability of the experimental results, since results can be subjected to a systematic error. Potential errors are mostly caused by improper functioning of the apparatus and do not show up as a scattering of the measured data. In these cases, the accuracy and validity of the measured points can be tested by comparing them with the requirements of some thermodynamically exact relation or reliable data in the literature [4]. Figures 7-1 to 7-5

show that there is extremely low scatter in the measured data, and the test systems were repeated with different initial loadings of solvent (around 3 different initial liquid loadings). Therefore, the smooth curves covering the experimental data and also excellent agreement between the experimental data and the literature data guarantee the accuracy, reliability and repeatability of the equipment and experimental procedure.
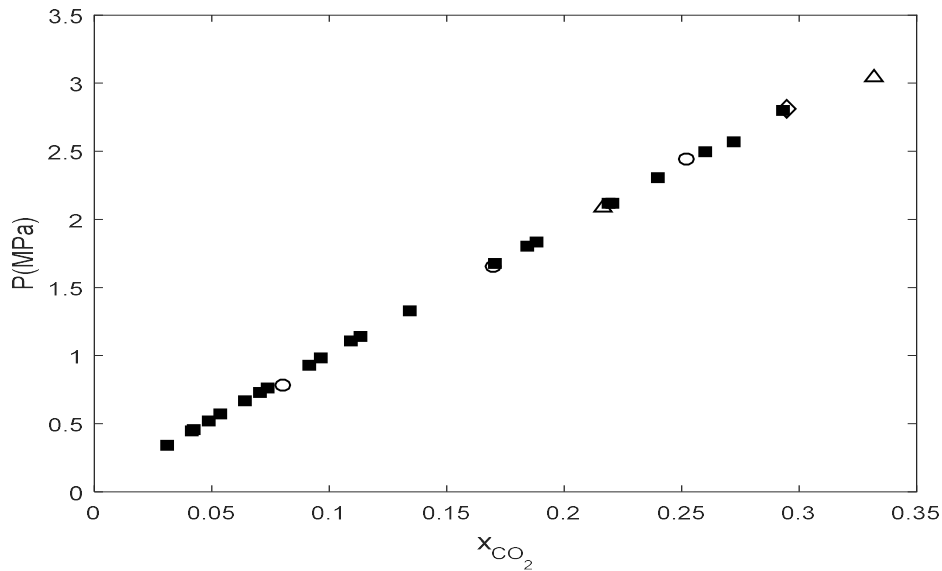
Figure 7-1: Solubility data for the binary system of CO_2 + n-hexane: Exp (this work) at 313.20 K (■); Nelson and Ramjugernath at 313.15 K [125] (◇); Li et al. at 313.14 K [189] (○); and Wagner and Wichterle at 313.14 K [190] (△).
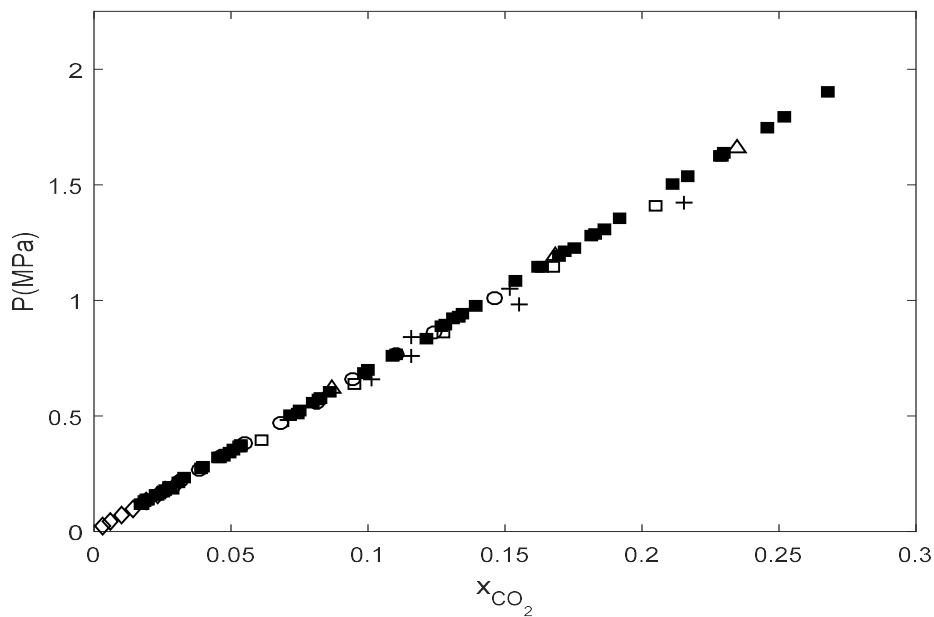
Figure 7-2: Solubility data for the binary system of CO_2 + NMP: Exp (this work) at 298.16 K (■); Murrieta-Guevara and Trejo Rodriguez at 298.144 K [191] (◇); Sweeney at 298 K [192] (○); Tian et al. at 298.15 K [111] (△); Zubchenko et al. at 298.15 [193] (+); and Murrieta-Guevara et al. at 298.15K [194] (□).
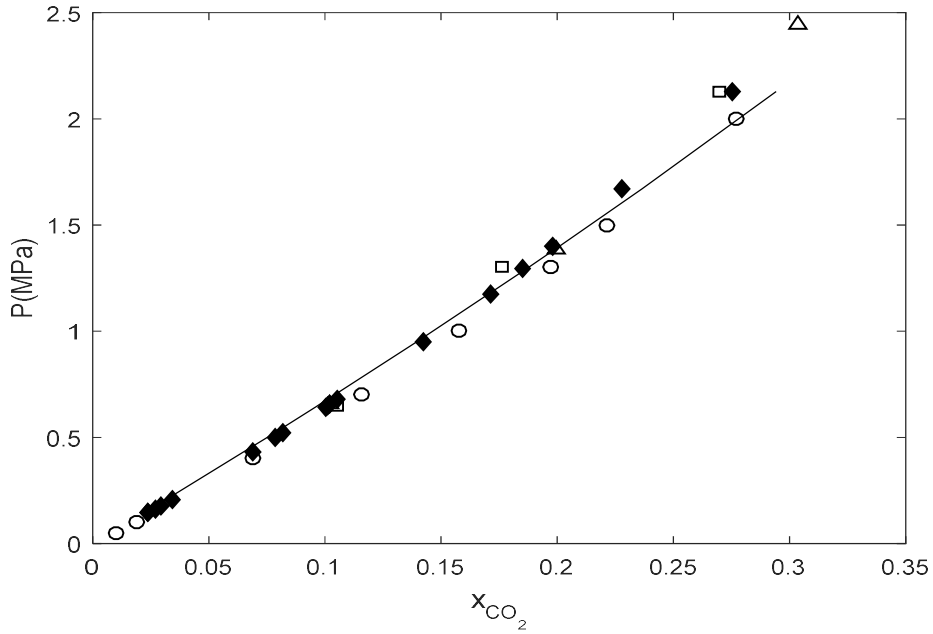
Figure 7-3: Solubility data for the binary system of CO_2 + bmim[BF_4]: Exp (this work) at 298.14 K (◆); Tian et al. at 298.15 K [111] (□); Shiflett and Yokozeki at 298.15, 298.05 and 297.95 K [83] (○); and Kroon et al. at 298.14, 298.17 and 298.47 K [76] (△). The solid line depicts the modelled data using the PR EoS with the vdW mixing rule.
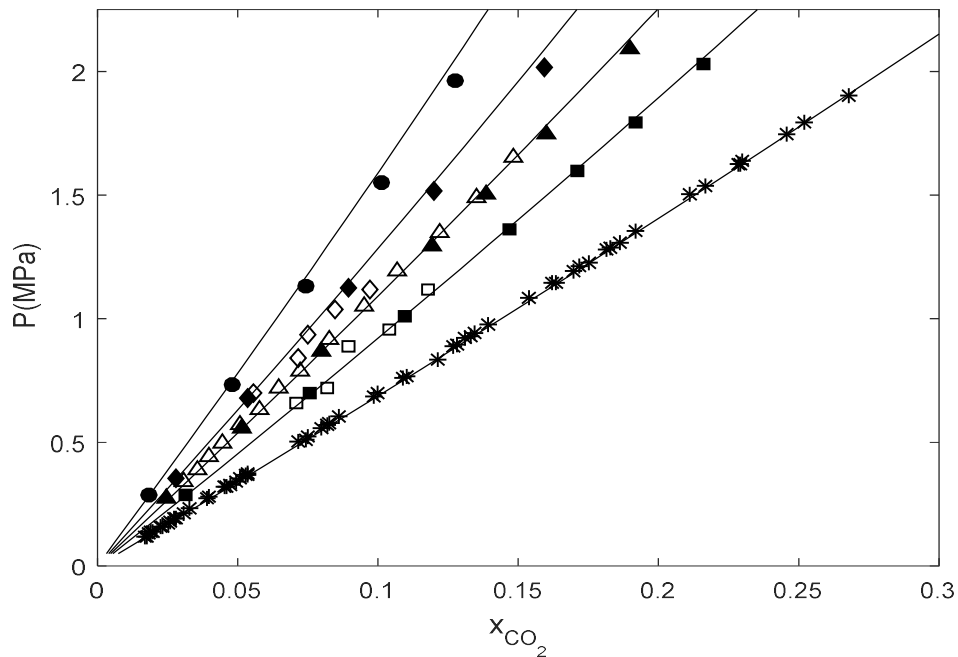
Figure 7-4: Solubility data for the binary system of CO_2 + NMP: Exp (this work) at 298.16 K (✳), 313.14 K (■), 323.14 K (▲), 333.15 K (◆) and 348.14 K (●); Bohloul et al. at 313.15 K (□) and 333.15 K [195] (◇); Sweeney at 323 K [192] (△). The solid line depicts the modelled data using the PR EoS with the vdW mixing rule.

80
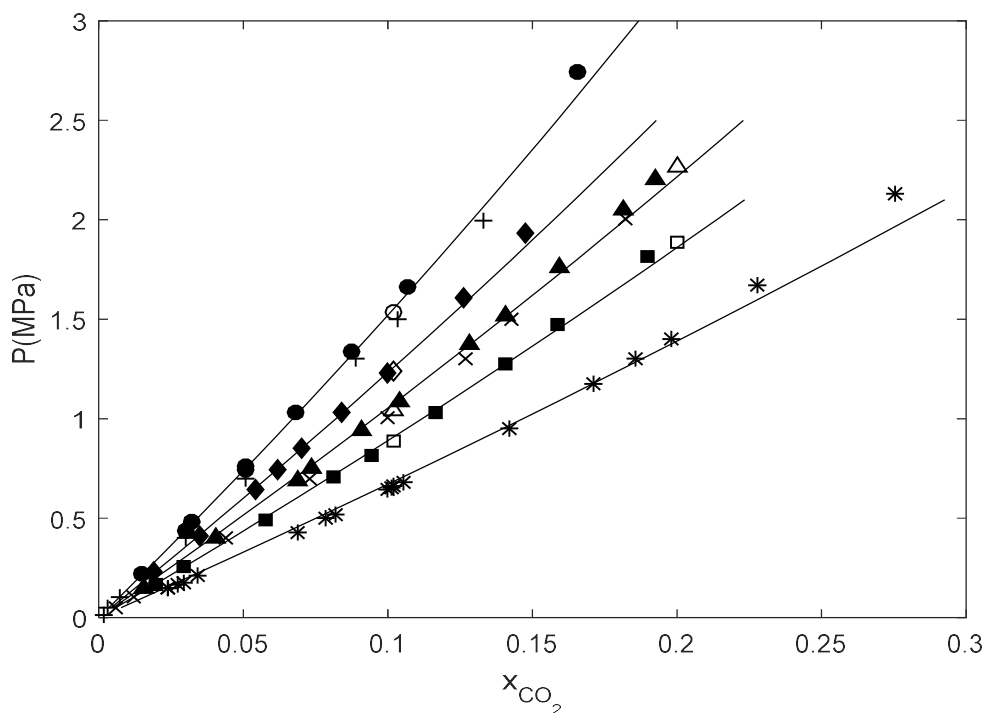
Figure 7-5: Solubility data for the binary system of CO_2 + bmim[BF_4]: Exp (this work) at 298.14 K ($\ast$), 313.15 K (■), 323.15 K (▲), 333.15 K (◆) and 348.16 K (●); Kroon et al. at 313.19 and 313.15 K (□), 323.11 K and 323.15 K (△), 333.16 K (◇) and 348.12 K (○) [76]; Shiflett and Yokozeki at 323.15 K (×) and 348.05 and 348.15 K [83] (+). The solid line depicts the modelled data using the PR EoS with the vdW mixing rule.

7.2.2 Uncertainty analysis

To evaluate the performance of the new equilibrium cell, the uncertainty analysis was carried out for all the studied systems following methods outlined by NIST [196] as previously discussed in Chapter 5. The expanded uncertainty of the mole fraction of CO_2, $U(x_{CO_2})$, and expanded uncertainty of the total fraction of CO_2, $U(z_{CO_2})$ are listed in tables of Appendix H. Additionally, Figure 7-6 compares uncertainties of the NMP + CO_2 system with those of the bmim[BF_4] + CO_2 system at 298.15. It displays that the $U(x_{CO_2})$ and the difference between the $U(z_{CO_2})$ and the $U(x_{CO_2})$ for each system increase with increasing pressure. Although the mole fraction of CO_2 in bmim[BF_4] and NMP is almost same at similar conditions, the $U(x_{CO_2})$ for NMP system is less than that for bmim[BF_4]. This is primarily due to the relatively low volume of the vapour phase during measurements of NMP + CO_2 system. Thus, the $U(x_{CO_2})$ and also difference between $U(x_{CO_2})$ and $U(z_{CO_2})$ decrease with increasing the volume of the liquid phase or the amount of solvent loaded into the equilibrium cell. However, factors, such as viscosity, price and kind (physical or chemical) of solvent, the power of mixing, temperature and pressure of experiment and the time required to reach equilibrium, limit the maximum volume of solvent loaded into the

cell. Therefore, considering these factors, the loading volume of the solvent should be as high as possible; and a determined optimum volume cannot be recommended. Overall, the most accurate measurements can be undertaken by measuring the partial pressure of solvent or its vapour pressure at the equilibrium temperature, by appropriately calibrating the measurement devices, and by loading the maximum allowable volume of solvent into the cell. The depth gauge of the equilibrium cell was calibrated for the liquid levels above the blades of the mixer. Thus, the minimum allowable volume of solvent loaded into the cell is approximately 20 cm^3 which covers the mixer and blades completely.

The designed gas reservoir size and the maximum allowable pressure on the transducer are factors limiting loading of a large amount of the gas into the gas reservoir. For example, CO_2 has a high solubility in chemical solvents such as amine solutions at low pressures and temperatures. Thus, a large amount of gas is required to be loaded into the equilibrium cell at the beginning of the experiment to reach equilibrium condition. In this situation, to get one equilibrium point, the gas has to be charged into the gas reservoir and then into the equilibrium cell at least twice that increases uncertainty.

The solubility of a gas in a liquid solvent is dependent on the pressure and temperature. It decreases with increasing temperature and reducing pressure. The maximum temperature and the minimum pressure that can be measured by the Pt-l00 and the pressure transmitter of the cell are 150 °C[1] and 0.7 bar[2], respectively. Thus, the solubility of the gas in the solvent at these conditions is the lowest solubility that can be measured using the new apparatus. The lowest solubility can have different amounts by changing the solvent and gas. It would be beneficial to have a lower pressure transmitter as well. Therefore, the gas solubility at pressures below 0.7 bar can be measured accurately. Additionally, the vapour pressure of solvent loaded into the cell can be directly measured and, therefore, more accurate measurements are undertaken. The maximum allowable pressure on the transmitter of the equilibrium cell is 40 bar. To measure VLE data at higher pressures, it is required to replace the pressure transmitter with a high-pressure one.

---

[1] The bath fluid must have a boiling point higher than the maximum temperature. Besides, a better tubing for temperature regulation of the GR line will be required.
[2] The minimum pressure is around 0.7 bar due to an error in the pressure transmitter at vacuum pressures.
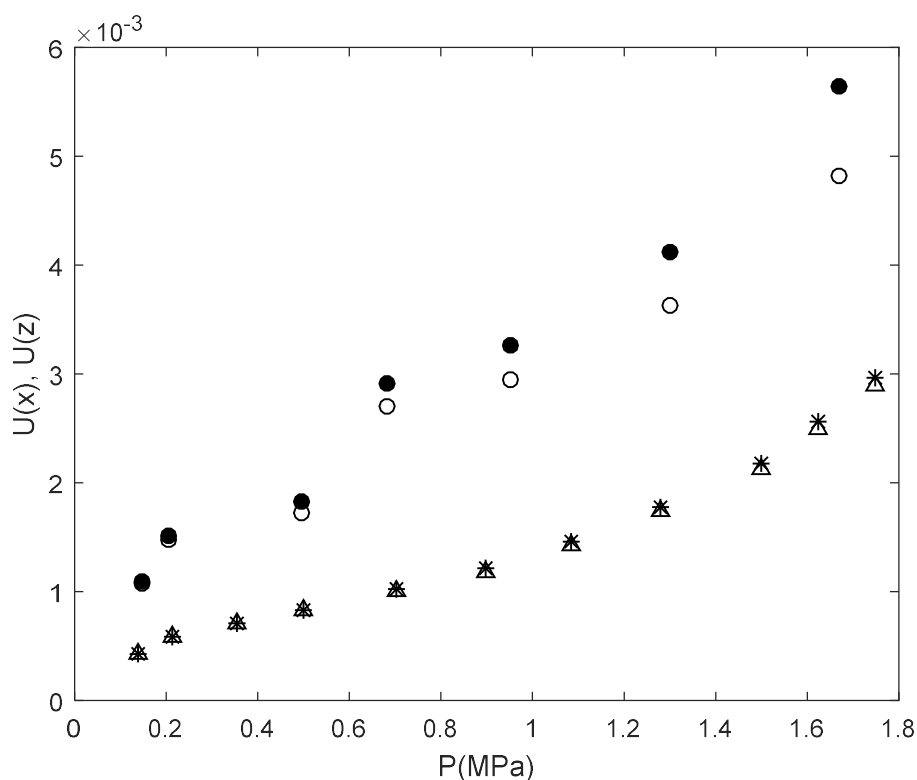
Figure 7-6: Experimental uncertainties of mole fraction of CO_2 ($U(x_{CO_2})$) and total mole fraction of CO_2 ($U(z_{CO_2})$) in bmim[BF$_4$] and NMP at 298.15 K: $U(x_{CO_2})$ for NMP + CO_2 system (*), $U(z_{CO_2})$ for NMP + CO_2 system ($\triangle$), $U(x_{CO_2})$ for bmim[BF$_4$] + CO_2 system ($\bullet$), $U(z_{CO_2})$ for bmim[BF$_4$] + CO_2 system ($\circ$).

7.3 Measurements using physical hybrid solvents

7.3.1 NMP + bmim[BF$_4$] + CO$_2$ system

Characteristics of NMP + bmim[BF$_4$] solutions used to measure the CO_2 solubility, viscosity, density and sound velocity are presented in Table 7-3.

Table 7-3: Overview of the studied bmim[BF$_4$] (1) + NMP (2) solutions.

Initial mass composition	Temperature (K)	Pressure range (MPa)
Solubility measurement		
w_1/w_2 = 0.0986/0.9014 w_1/w_2 = 0.2495/0.7505 w_1/w_2 = 0.4973/0.5027	298.15, 313.15, 323.15	0.152 to 2.051
Viscosity, density and sound velocity measurement		
w_1/w_2 = 0.0986/0.9014 w_1/w_2 = 0.2498/0.7502 w_1/w_2 = 0.4971/0.5029 w_1/w_2 =1.0/0.0 w_1/w_2 = 0.0/1.0	293.15 to 343.15	-

7.3.1.1 Solubility measurements

Isothermal CO_2 solubility data were measured for the samples listed in Table 7-3. The results are displayed in Figures 7-7 to 7-9 and listed in Tables H-4 to H-6. The data complement the higher solvent concentrations available in the literature [111], namely, $w_2 = (0.5000, 0.6999, \text{ and } 0.8981)$ at a temperature of 298.15 K. Figure 7-10 displays the solubility of CO_2 in pure NMP and bmim[BF$_4$], as well as solvent mixtures at a temperature of 298.15 K. From the figure, it is evident that the solubility of CO_2 in each of the pure solvents is very similar. However, the solubility of CO_2 in hybrid solvents shows a decrease of approximately 5% to 25% (dependant on the temperature, pressure and composition of the solvents) in comparison to the pure solvents.

The experimental data were modelled in MATLAB using the flash calculation and the phi-phi approach with the PR EoS and vdW mixing rule as previously discussed in Chapter 6. The new modelled binary interaction parameters, critical properties (T_c and P_c) and acentric factors (ω) of the components are listed in Table 7-4. The modelling results are displayed in Figures 7-7 to 7-9; and listed in Tables H-2 to H-6. The modelling results was evaluated statistically using the absolute average deviation (AAD) and the average absolute relative deviation (AARD) defined in Chapter 6. Statistical deviations are listed in Table 7-5. The percentages of AARD obtained are within 3.5%. AAD (x) are less than the experimental uncertainties, $U(x_{CO_2})$, at all temperatures, except for the temperature of 298.15 K. Excellent compatibility between modelling results and experimental data confirms the ability of model to reproduce the experimental data.
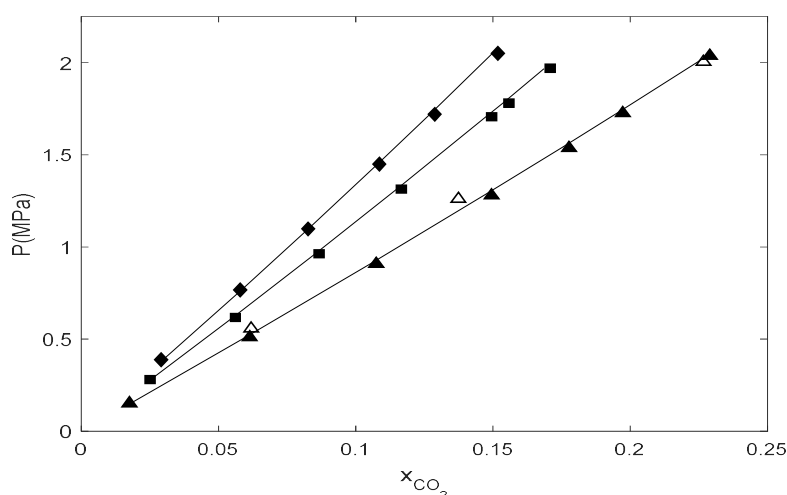
Figure 7-7: Solubility data of CO_2 in bmim[BF$_4$] (1) + NMP (2): Exp (this work) with initial mass composition of $w_1/w_2 = 0.4973/0.5027$ at 298.14 K ($\blacktriangle$), 313.14 K ($\blacksquare$) and 323.15 K ($\blacklozenge$); Literature data with initial mass composition of $w_2/w_3 = 0.5/0.5$ at 298.15 K [111] ($\triangle$). The solid line depicts the modelled data using the PR EoS with the vdW mixing rule.
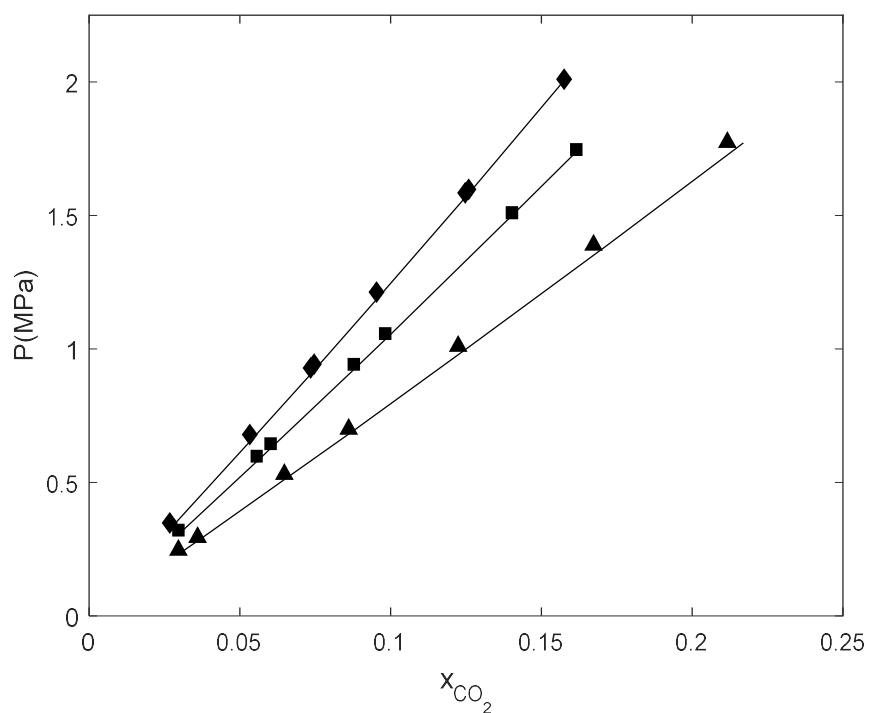
Figure 7-8: Solubility data of CO_2 in bmim[BF_4] (1) + NMP (2): Exp (this work) with initial mass composition of w_1/w_2 = 0.2495/0.7505 at 298.13 K (▲), 313.14 K (■) and 323.13 K (◆). The solid line depicts the modelled data using the PR EoS with the vdW mixing rule.
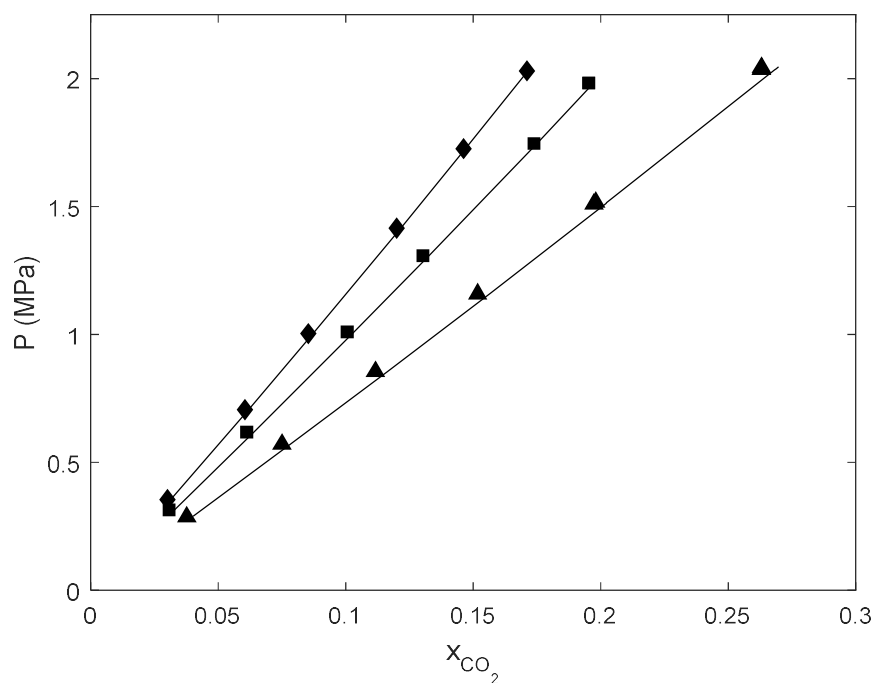
Figure 7-9: Solubility data of CO_2 in bmim[BF_4] (1) + NMP (2): Exp (this work) with initial mass composition of w_1/w_2 = 0.0986/0.9014 at 298.15 K (▲), 313.15 K (■) and 323.16 K (●). The solid line depicts the modelled data using the PR EoS with the vdW mixing rule.
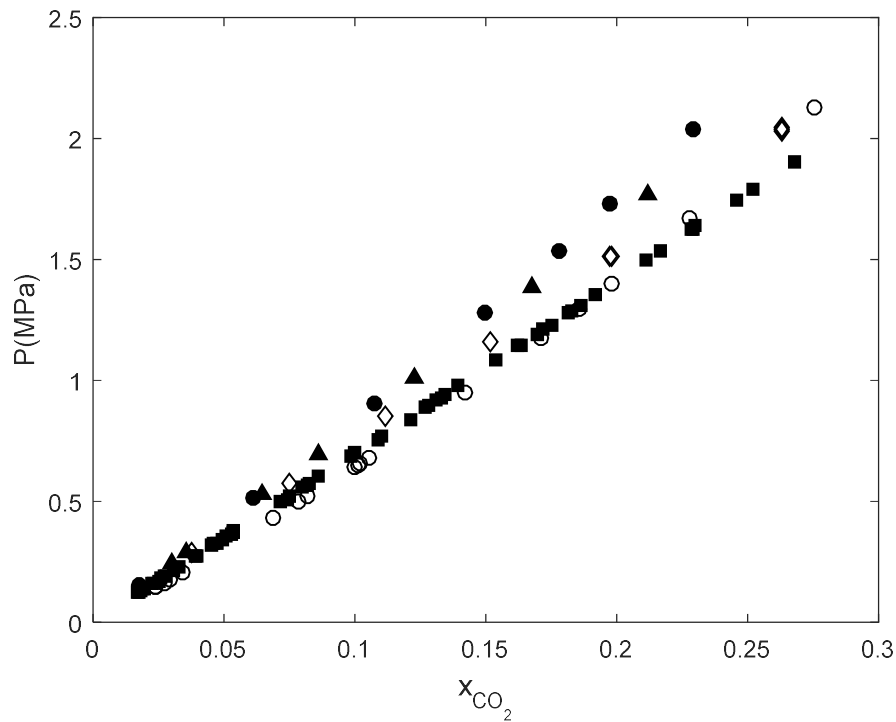
Figure 7-10: Solubility data of CO_2 in bmim[BF_4] (1) + NMP (2) with different initial mass compositions: $w_1/w_2 = 1/0$ at 298.14 K ($\bigcirc$); $w_1/w_2 = 0/1$ at 298.16 K ($\blacksquare$); $w_1/w_2 = 0.4973/0.5027$ at 298.14 K ($\bullet$); $w_1/w_2 = 0.2495/0.7505$ at 298.13 K ($\blacktriangle$); and $w_1/w_2 = 0.0986/0.9014$ at 298.15 K ($\diamondsuit$)

Table 7-4: Binary interaction parameters, critical parameters, and acentric factors required in Peng Robinson EoS[a].

Species	bmim[BF_4]	NMP	CO_2	P_c(MPa)	T_c(K)	ω
bmim[BF_4]	0	$k_{ij} = -0.096$	$k_{ij} = -0.008$	3.457	863.22	0.8156
NMP	$k_{ij} = -0.096$	0	$k_{ij} = 0.00026T - 0.06119$	4.78	724	0.3577
CO_2	$k_{ij} = -0.008$	$k_{ij} = 0.00026T - 0.06119$	0	7.376	304.20	0.225

[a] Data for the critical parameters (T_c, P_c), and acentric factor ω from the literature [195, 197] and from NIST ThermoData Engine (TDE) [198].

Table 7-5: Statistical analysis of the data-fit for the solubility of CO_2 in hybrid solvents of bmim[BF$_4$] (1) + NMP (2) with different initial mass compositions (w).

T (K)	AARD(x_{CO_2})%	AAD(x_{CO_2})	$U(x_{CO_2})^a$
$w_1/w_2 = 0/1$			
298.16	1.57	0.0012	0.0014
313.14	0.99	0.0011	0.0020
323.14	1.45	0.0015	0.0019
333.16	1.72	0.0019	0.0020
348.14	2.81	0.0023	0.0018
$w_1/w_2 = 1/0$			
298.14	4.70	0.0041	0.0031
313.15	1.38	0.0015	0.0035
323.15	1.96	0.0020	0.0042
333.15	1.01	0.0010	0.0037
348.16	2.33	0.0016	0.0035
$w_1/w_2 = 0.4973/0.5027$			
298.14	1.45	0.0018	0.0029
313.14	1.27	0.0015	0.0032
323.15	1.26	0.0010	0.0031
$w_1/w_2 = 0.2495/0.7505$			
298.13	3.25	0.0028	0.0015
313.14	2.43	0.0015	0.0020
323.15	2.62	0.0017	0.0025
$w_1/w_2 = 0.0986/0.9014$			
298.15	3.25	0.0046	0.0025
313.15	2.61	0.0019	0.0024
323.16	1.96	0.0012	0.0024

[a] Expanded uncertainty (average) of the mole fraction of CO_2 in the liquid phase.

Figure 7-11 indicates the total mole fraction of solvent in the gas phase for the CO_2 + NMP + bmim[BF$_4$] system with different initial solvent loading concentrations at 298.15 K which were determined through modelling. The presence of the solvent in the gas phase decreases with an increase in the mass fraction of bmim[BF$_4$], and dramatically with increasing pressure. Consequently, the addition of bmim[BF$_4$] to NMP decreases the volatility of the solvent. Although, the loss of hybrid solvents is less than the NMP and they contaminate the gaseous stream less, the loss of NMP alone is very low due to its relatively high boiling point.
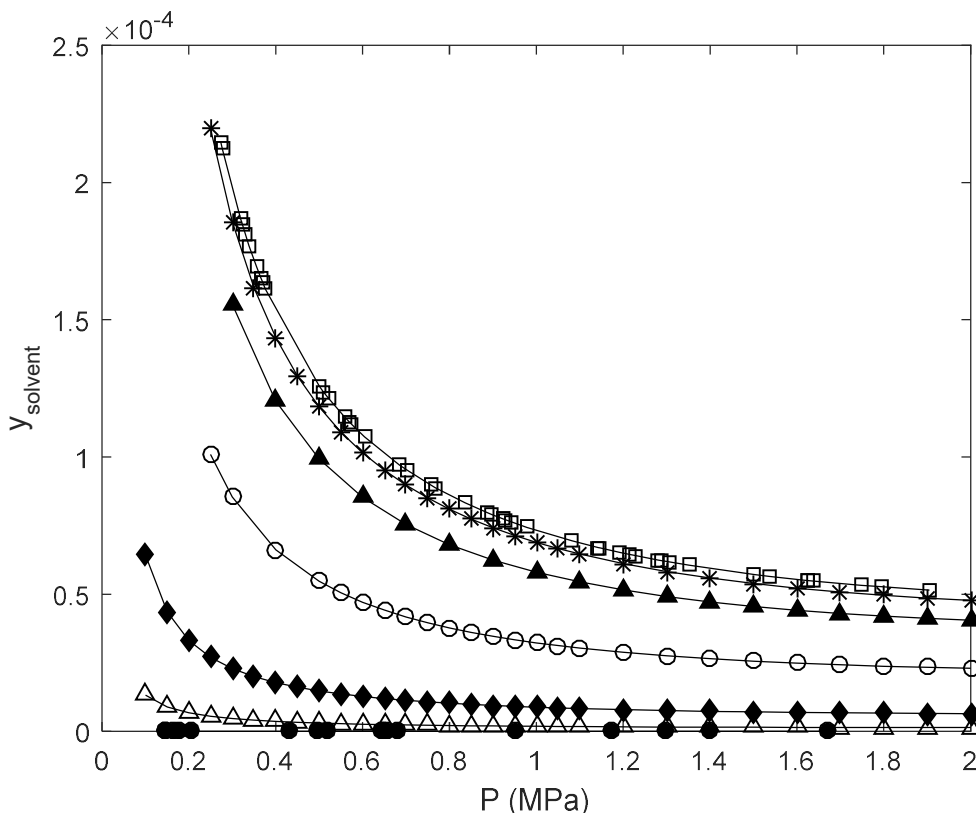
Figure 7-11: Total mole fraction of solvent ($y_{solvent}$) in the gas phase for the system of CO_2 (1) + bmim[BF_4] (2) + NMP (3) with different initial mass compositions at 298.15 K: w_2/w_3 =1/0 (●); w_2/w_3 =0/1 (□); w_2/w_3 = 0.9/0.1 (△); w_2/w_3 = 0.75/0.25 (◆); w_2/w_3 = 0.50/0.50 (○); w_2/w_3 = 0.25/0.75 (▲); and w_2/w_3 = 0.10/0.90 (∗).

7.3.1.2 Viscosity, density and speed of sound measurements

Knowledge of physical properties is required for a full understanding of the thermodynamic properties of liquid mixtures, the design of many industrial and chemical processes and theoretical purposes such as developing and evaluating the models and theories [199-202]. The viscosity of the new solvents which is one of the key properties of solvent should be completely analysed since the studied solvents contain ILs having high viscosity.

Viscosity, density and sound velocity of NMP + bmim[BF_4] solutions described in Table 7-3 were measured. Experimental results are displayed in Figures 7-12 and 7-13 and listed in Table I-1. The measured data show good agreement to the data available in the literature. The density and viscosity decrease with an increase in temperature and also with the addition of NMP to bmim[BF_4]. As observed by Tian et al. NMP notably decreases the viscosity of bmim[BF_4] + NMP liquid mixtures [111]. The addition of NMP to bmim[BF_4], resulting in mixtures with a mass fraction of 0.74 and 0.50 of the IL, reduces the viscosity by 70% and 87% on average, respectively. Thus, the high viscosity of ILs can be approximately avoided for applications

restricted by high viscosity. It is important to note, that a lower viscosity may result in improved mass transport properties such as the diffusion coefficient (dependent on the inverse of viscosity) and the mass transfer rate.

The measured data of viscosity, density and sound velocity were fitted to the equations J-1 to J-3. The fitting parameters and statistical deviations are listed in Table L-1.

In conclusion, NMP outperforms the hybrid solvents with regards to the solubility of CO_2 and the liquid phase viscosity. Given the measured data, the addition of bmim[BF_4] to NMP is not beneficial to CO_2 capture. However, to comprehensively compare the hybrid solvents with NMP, the solubility of other components of petrochemical streams such as heavy hydrocarbons in the hybrid solvents and also the solvent selectivity for CO_2 are required.
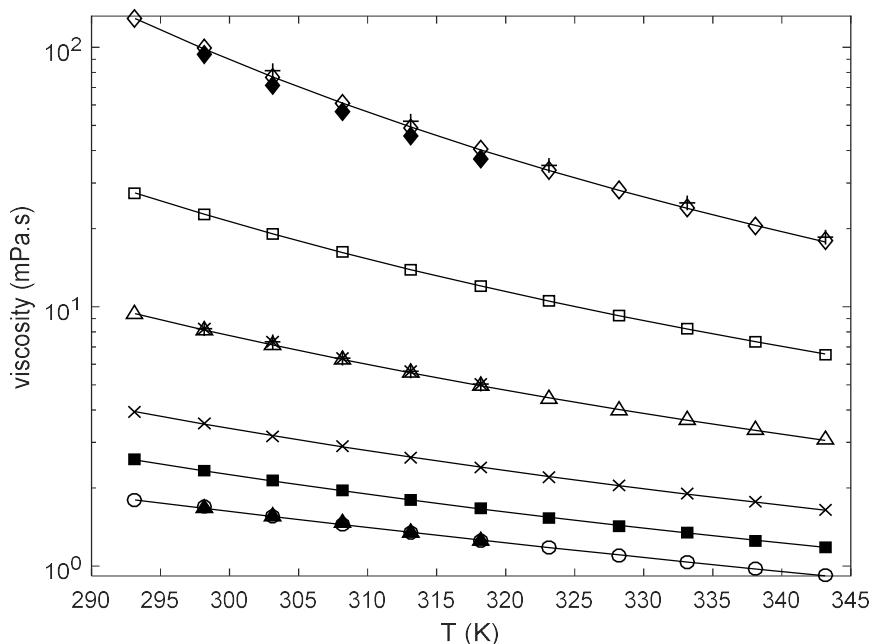
Figure 7-12: Trend analysis showing the effect of temperature on the viscosity of bmim[BF_4] (1) + NMP (2) mixtures with different mass compositions: Exp (this work), $w_1/w_2 = 1/0$ ($\Diamond$), $w_1/w_2 = 0$ ($\bigcirc$), $w_1/w_2 = 0.7413/0.2587$ ($\square$), $w_1/w_2 = 0.4971/0.5029$ ($\triangle$), $w_1/w_2 = 0.2498/0.7502$ ($\times$), and $w_1/w_2 = 0.0986/0.9014$ ($\blacksquare$); Literature data, $w_1/w_2 = 1/0$ ($\blacklozenge$), $w_1/w_2 = 0/1$ ($\blacktriangle$), and $w_1/w_2 = 0.5/0.5$ ($\ast$) [111]; $w_1/w_2 = 1/0$ (+) [203]. Solid line depicts regressed results.
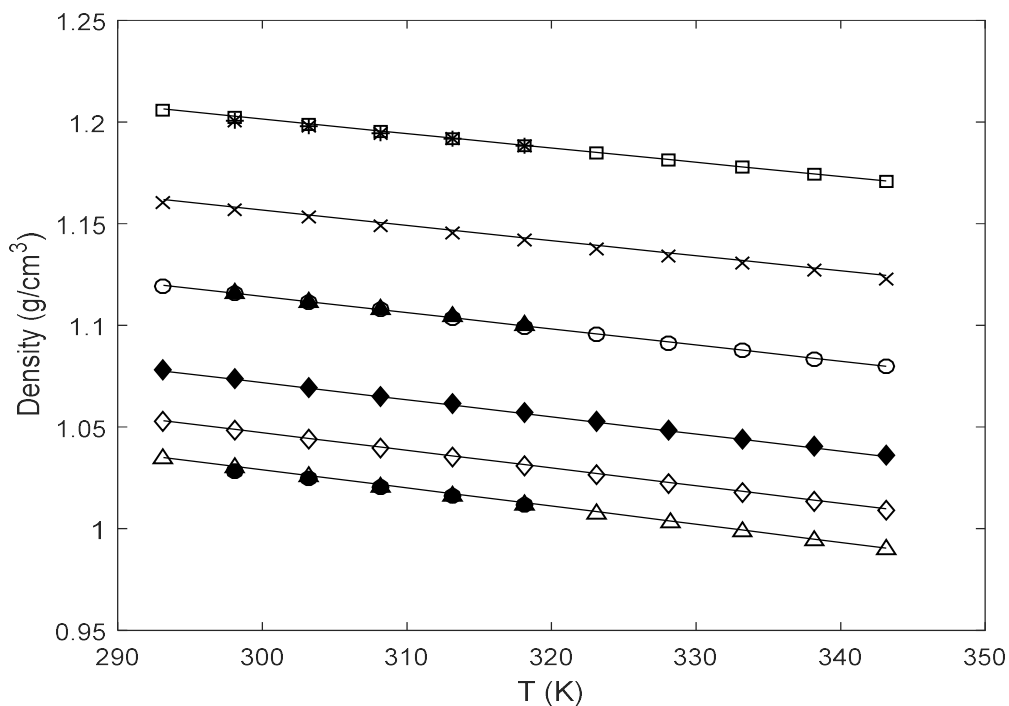
Figure 7-13: Trend analysis showing the effect of temperature on the density of bmim[BF$_4$] (1) + NMP (2) mixtures with different mass compositions: Exp (this work), w_1/w_2 = 1/0 (□), w_1/w_2 = 0/1 (△), w_1/w_2 = 0.7413/0.2587 (×), w_1/w_2 = 0.4971/0.5029 (○), w_1/w_2 = 0.2498/0.7502 (◆), and w_1/w_2 = 0.0986/0.9014 (◇); Literature data, w_1/w_2 = 1/0 (✳), w_1/w_2 = 0/1 (●), and w_1/w_2 = 0.5/0.5 (▲) [111]. Solid line depicts regressed results.

7.4 Measurements with physical–chemical hybrid solvents

As discussed in Chapter 2, the aqueous amine processes have some major disadvantages, namely solvent loss, corrosion and high heat consumption. Each of these problems results from various causes. Amine processes are categorized as chemical absorption with a high heat of reaction and including water which has a high heat capacity. Consequently, they have high energy consumption. Some of the amines, especially the primary amines, degrade causing loss of the solvent and formation of corrosive products. Additionally, the presence of water in the amine processes intensify corrosion. Overall, it seems that water is responsible for some part of the disadvantages of the aqueous amines. Thus, the use of other physical solvent as a substitute for the aqueous media of amine solutions (some or all of it) to reduce the problems of the amines were investigated in this project. With this aim, ILs, namely bmim[OTF] and bmim[TF$_2$N], and NMP were chosen based on the comparison study performed on their ability to absorb the acidic gases, their availability, price, viscosity and selectivity towards H$_2$S. Among the common amines, MEA and DGA are primary amines that were selected since these have higher heat reactions, more degradation products, more corrosive problems, considerable loss of solvent, and lower cost, especially MEA. Additionally, these amines are not selective for H$_2$S. On the other hand, NMP, bmim[OTF] and bmim[TF$_2$N] have a high selectivity for H$_2$S. Therefore, the addition of NMP, bmim[OTF] and bmim[TF$_2$N] to MEA and DGA may increase the solvent selectivity as well. As explained in Chapter 2, the primary amines can chemically absorb acidic gases even in the absence of water, therefore MEA and DGA are appropriate choices for the investigation of the acid gas capture in the free-water physico-chemical hybrid solvent. The aqueous primary amines absorb CO$_2$ through two mechanisms, therefore they are not selective for H$_2$S. Due to this fact, it is reasonable to assume that the removal of water from these solutions, decreases the number of mechanisms occurring during CO$_2$ absorption, hence may alter the selectivity of relevant solvents.

The solubility of CO$_2$ in four hybrid solvents of amines, water, ILs and NMP, viz. (MEA + water + bmim[OTF], DGA + water + bmim[OTF], MEA + NMP + bmim[TF$_2$N], DGA + NMP + bmim[TF$_2$N]), and their viscosity, density, excess properties and evaporation rate were measured. Then, the results are discussed in the following sections. To the best of our knowledge, the systems studied are novel, except for MEA + water + bmim[OTF] system. It should be mentioned that for a complete comparison on the performance of the chosen hybrid solvents, more studies on their corrosion rates, selectivity toward H$_2$S, the solubility of heavy hydrocarbons, and heat of absorption are required.

7.4.1 MEA/DGA + bmim[OTF] + H_2O + CO_2 system

Characteristics of MEA/DGA + bmim[OTF] + H_2O solutions used to measure the CO_2 solubility, viscosity, density, sound velocity and evaporation rates are presented in Table 7-6. The ratio of solvents was done in a manner that water content was reduced, IL was increased and amine was constant.

Table 7-6: Overview of the studied MEA/DGA (1) + H_2O (2) + bmim[OTF] (3) solutions.

Initial mass composition	Temperature (K)	Pressure range (MPa)
Solubility measurement		
MEA (1) + H_2O (2) + bmim[OTF] (3): $w_2/w_1 = 0.7035/0.2965$ $w_3/w_2/w_1 = 0.1003/0.6017/0.2980$ $w_3/w_2/w_1 = 0.2392/0.4614/0.2994$ $w_3/w_2/w_1 = 0.4005/0.3071/0.2924$	298.15, 313.15	0.093 to 2.322
DGA (1) + H_2O (2) + bmim[OTF] (3): $w_2/w_1 = 0.4868/0.5132$ $w_3/w_2/w_1 = 0.1006/0.3878/0.5116$ $w_3/w_2/w_1 = 0.2466/0.2478/0.5056$ $w_3/w_2/w_1 = 0.4024/0.1/0.4976$	298.15, 313.15	0.271 to 2.301
Viscosity, density and sound velocity measurement		
MEA (1) + H_2O (2) + bmim[OTF] (3): $w_2/w_1 = 0.6996/0.3004$ $w_3/w_2/w_1 = 0.1045/0.5836/0.3119$ $w_3/w_2/w_1 = 0.2392/0.4614/0.2994$ $w_3/w_2/w_1 = 0.4311/0.2643/0.3046$	293.15 to 333.15	-
DGA (1) + H_2O (2) + bmim[OTF] (3): $w_2/w_1 = 0.4868/0.5132$ $w_3/w_2/w_1 = 0.1006/0.3878/0.5116$ $w_3/w_2/w_1 = 0.2593/0.2665/0.4742$ $w_3\ w_2/w_1 = 0.4024/0.1/0.4976$	293.15 to 333.15	
Evaporation rate measurement		
MEA (1) + H_2O (2) + bmim[OTF] (3): $w_2/w_1 = 0.6996/0.3004$ $w_3/w_2/w_1 = 0.1045/0.58336/0.3119$ $w_3/w_2/w_1 = 0.2492/0.458/0.2928$ $w_3/w_2/w_1 = 0.3943/0.3178/0.2879$	373.15	Atmospheric pressure
DGA (1) + H_2O (2) + bmim[OTF] (3): $w_2/w_1 = 0.469/0.531$ $w_3/w_2/w_1 = 0.1000/0.4053/0.4947$ $w_3/w_2/w_1 = 0.2507/0.275/0.4743$ $w_3/w_2/w_1 = 0.3887/0.1386/0.4727$	373.15	Atmospheric pressure

7.4.1.1 Solubility measurements

The solubility of CO_2 in the MEA/DGA + bmim[OTF] + H_2O systems listed in Table 7-6 were measured. The initial concentration of amine in the all hybrid solvents of each set was kept fairly constant to provide a proper comparison between solubilities of CO_2 (α_{CO_2}= total moles of CO_2 absorbed in the liquid phase/initial moles of amine) in various solvents. The measured data are displayed in Figures 7-14 and 7-15 and listed in Tables H-7 to H-14. To the best of my knowledge, only one group has studied the MEA (1) + H_2O (2) + bmim[OTF] (3) system with an initial loading concentration of w_3/w_1= 0.3500/0.3000, at atmospheric pressure and temperatures of 298.15 K [21]. As observed by Baj et al. all, the MEA + IL + H_2O solvents with different kinds of ILs have similar capacities to absorb CO_2 at similar conditions of concentration, temperature and pressure [21].

From Figures 7-14 and 7-15, it is evident that the presence of bmim[OTF] in the aqueous amine solution decreases the solubility of CO_2. Compared to the 29.65 wt% MEA aqueous solution at 298.15 K and 313.15 K and pressure range of 0.1 to 2 MPa, the solubility of CO_2 in the hybrid MEA solvents, with an approximate mass fraction of 0.30 of the MEA and mass fractions of 0.1003, 0.2392 and 0.4005 of the IL, decreases by approximately 0.5 % to 4.5 %, 2.5% to 7% and 5% to 11.5%, respectively. As it was stated in Chapter 2, corrosion problems limit the allowable acid gas loading in the amine solutions. Thus, the maximum loading in the MEA solutions is usually 0.3 to 0.35 and 0.7 to 0.9 (moles acid gas/mole of MEA) for carbon steel and stainless steel equipment, respectively. It is clear from the measured data that all studied hybrid MEA solvents are able to achieve the maximum allowable loading of the acid gas even at moderate pressures. Therefore, although the solubility of CO_2 in the bmim[OTF]-containing hybrid MEA solvents is lower than that in the MEA aqueous solution, it does not negatively affect the CO_2 removal processes[1].

Compared to the 51.32 wt.% DGA aqueous solution at 298.15 K and 313.15 K and pressure range of 0.1 to 2 MPa, the solubility of CO_2 in the aqueous hybrid DGA solvents, with an approximate mass fraction of 0.50 of DGA and mass fractions of 0.1006, 0.2466 and 0.4024 of the IL, decreases by approximately 3% to 4.5%, 5% to 8.5% and 8% to 13.5%, respectively. These

---

[1] Gas sweetening is the process of extracting H_2S and CO_2 from natural gas. Natural gas containing sulfur products such as H_2S is called "sour gas" 7. Karadas, F., M. Atilhan, and S. Aparicio, *Review on the Use of Ionic Liquids (ILs) as Alternative Fluids for CO2 Capture and Natural Gas Sweetening.* Energy & Fuels, 2010. **24**(11): p. 5817-5828, 204. Maurice Stewart, K.A., *Gas Sweetening and Processing Field Manual.* 2011: Gulf Professional Publishing-Elsevier, 205. Osman, K.W. and M. Vasagam, *Gas Sweetening Process - Problems And Remedial Measures*, in *Abu Dhabi International Petroleum Exhibition and Conference.* 2002, Society of Petroleum Engineers: Abu Dhabi, United Arab Emirates. p. 7, 206. Fürhacker, M., A. Pressl, and R. Allabashi, *Aerobic biodegradability of methyldiethanolamine (MDEA) used in natural gas sweetening plants in batch tests and continuous flow experiments.* Chemosphere, 2003. **52**(10): p. 1743-1748.

percentages of decrease are more than those of the MEA solutions. The maximum acid gas loading in the DGA solutions should not be more than 0.35 (moles acid gas/mole of DGA). The solubilities of CO_2 in the all studied hybrid DGA solvents are more than 0.35 (mol CO_2/mole DGA), at condition studied. Thus, similar to the bmim[OTF]-containing MEA solutions, the maximum allowable loading of acid gas is achievable for the bmim[OTF]-containing DGA solutions; and the reduced solubility of CO_2 in these solvents compared to the conventional DGA solutions does not affect the CO_2 removal processes.

(a) (b)
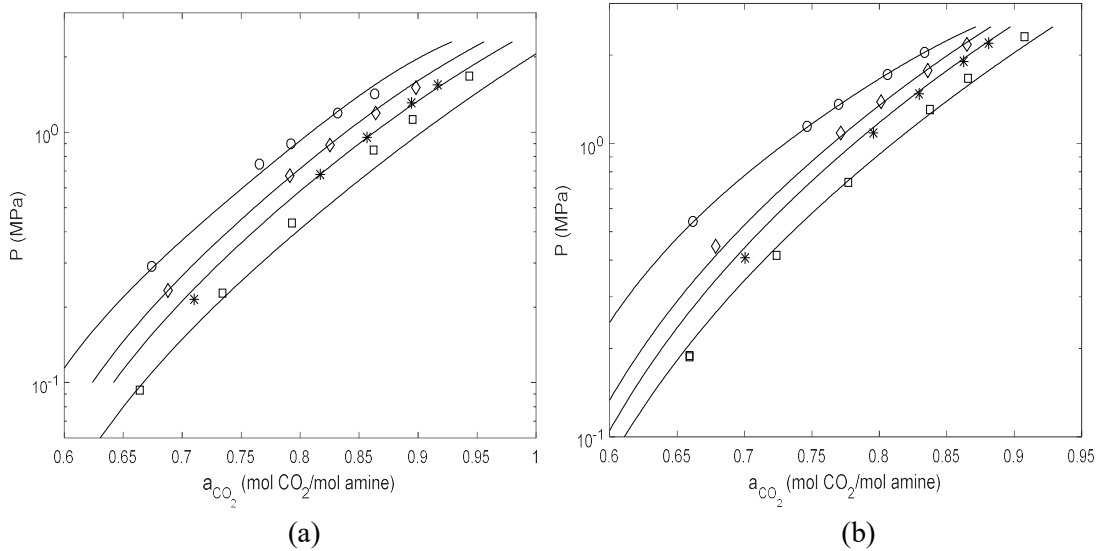
Figure 7-14: Solubility data of CO_2 in MEA (1) + H_2O (2) + bmim[OTF] (3) with different mass compositions: Exp (this work), $w_2/w_1 = 0.7035/0.2965$ (□), $w_3/w_2/w_1 = 0.1003/0.6017/0.2980$ (*), $w_3/w_2/w_1 = 0.2392/0.4614/0.2994$ (◇) and $w_3/w_2/w_1 = 0.4005/0.3071/0.2924$ (○), at **(a)** 298.15 K and **(b)** 313.15 K. The solid line depicts the modelled data using the developed approach.

(a) **(b)**
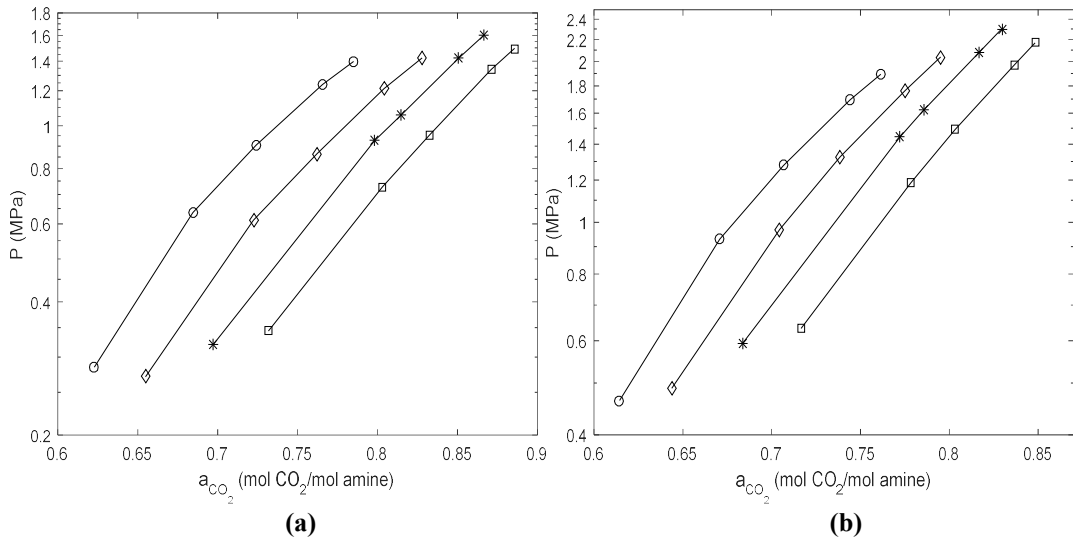
Figure 7-15: Solubility data of CO_2 in DGA (1) + H_2O (2) + bmim[OTF] (3) with different mass compositions: Exp(this work), $w_2/w_1 = 0.4868/0.5132$ (□), $w_3/w_2/w_1 = 0.1006/0.3878/0.5116$ (*), $w_3/w_2/w_1 = 0.2466/0.2478/0.5056$ (◇) and $w_3/w_2/w_1 = 0.4024/0.1/0.4976$ (○), at **(a)** 298.15 K and **(b)** 313.15 K.

The solubility data of CO_2 in the MEA + bmim[OTF] + H_2O solutions were successfully modelled using the approach explained in Chapter 6, and results are displayed in Figure 7-14. The binary interaction parameters, critical parameters, and acentric factors required for equations 6-58, 6-62 and 6-70 are listed in Tables G-1 and G-2. The statistical deviations are shown in Table 7-7. The average absolute relative deviations (AARD) obtained for the present system are less than 1.81%. Almost all of AAD (a_{CO_2}) are less than the experimental uncertainties, $U(a_{CO_2})$, at all temperatures. The compatibility between the modelling results and the experimental data confirms the validity of the modelling approach.

Table 7-7: Statistical analysis of the data-fit for the solubility of CO_2 (a_{CO_2}) in hybrid solvents of MEA (1) + H_2O (2) + bmim[OTF] (3) with different mass compositions (w).

T (K)	AARD(a_{CO_2})%	AAD(a_{CO_2})	$U(a_{CO_2})^a$
$w_2/w_1 = 0.7035/0.2965$			
298.05	1.81	0.0156	0.0109
313.02	0.78	0.0060	0.0104
$w_3/w_2/w_1 = 0.1003/0.6017/0.2980$			
298.07	0.44	0.0035	0.0110
313.12	0.50	0.0039	0.0110
$w_3/w_2/w_1 = 0.2392/0.4614/0.2994$			
298.03	0.33	0.0028	0.0106
313.09	0.42	0.0032	0.0106
$w_3/w_2/w_1 = 0.4005/0.3071/0.2924$			
298.06	0.74	0.0006	0.0096
313.12	0.07	0.0059	0.0096

[a] Expanded uncertainty (average) of the solubility of CO_2 in the liquid phase.

7.4.1.2 Viscosity, density and speed of sound measurements

Viscosity, density and sound velocity of the MEA/DGA + H_2O + bmim[OTF] solutions described in Table 7-6 were measured. The experimental data are displayed in Figures 7-16 and 7-17 and listed in Tables I-2 and I-3. As expected, the density and viscosity decrease with an increase in temperature and increase with increasing concentration of bmim[OTF]. For instance, the addition of bmim[OTF] to the 30 wt.% MEA aqueous solution at 298.15 K, resulting in a mixture with mass fractions of 0.4311 of the IL and 0.3046 of MEA, increases the viscosity by a factor of 3.49. Similarly, the addition of bmim[OTF] to the 51.32 wt.% DGA aqueous solution at 298.15 K to make a mixture with mass fractions of 0.4024 of the IL and 0.4976 of DGA, increases the viscosity by a factor of 3.17.

An increase in the concentration of IL increases the dependency of viscosity on the temperature. For instance, increasing the temperature from 293.15 K to 318.15 reduces the viscosity of the aqueous hybrid MEA solvent with mass fractions of 0.3046 of MEA and 0.4311 of IL by

approximately 58%; while a similar increase in the temperature decreases the viscosity of the 30.04 wt.% MEA aqueous solution by 42%. On the other hand, the dependency of density on the temperature does not change with increasing the concentration of IL, and all solvents have a similar trend (shown in Figures 7-17-b and 7-18 -b). The measured data of viscosity, density and sound velocity were fitted to the equations J-1 to J-3. The fitting parameters and statistical deviations are listed in Tables L-2 and L-3.

The coefficients of thermal expansions (a), the excess coefficients of thermal expansion[1] (α^E), the excess molar volumes (V^E) and the deviations of viscosity ($\Delta\eta$) were calculated from the measured physical properties according to equations J-4 to J-8 and are listed in Table I-2 and I-3.

Results of the MEA + H_2O + bmim[OTF] system (Table I-2) show that the thermal expansion coefficients of bmim[OTF] are higher than those of water at the same temperature. Therefore, as the mass fraction of the IL increases, the thermal expansion coefficient of the mixture increases and shows less dependency on the temperature (similar to the pure IL). The calculated α^E for the MEA + water system shows negative values at temperatures higher than 323.15 K. the negative α^E strongly suggests the presence of hydrogen bond between the components. On the other hand, the addition of the IL into the present system increases the values of α^E considerably and they have positive deviations over the entire range of temperatures indicating the self-association of the components. The V^E shows negative values (Table I-2) for the present systems over the entire range of temperatures. Considering this fact that present systems have positive α^E, it seems reasonable to assume that negative values of V^E are mainly due to structural contributions, beside the self-association of components. Furthermore, the increasing trend of V^E with an increase in the temperature can be attributed to the increase in kinetic energy of components that may have an opposing effect on the structural contribution or the interstitial accommodation. The results listed in Table I-2 show that the $\Delta\eta$ has negative values at low temperatures, but they become positive with increasing temperature for all the systems. Additionally, an increase in the concentration of IL makes the $\Delta\eta$ more negative. Negative values of $\Delta\eta$ indicate that all the components face less resistance to flow upon mixing.

Results of the DGA + H_2O + bmim[OTF] system presented in Table I-3 show that the thermal expansion coefficients of the present systems increase slightly with increasing the mass fraction of the IL and increasing the temperature. The α^E have positive deviations over the entire range of temperatures for all the DGA + H_2O + bmim[OTF] samples indicating the self-association of the components. Additionally, calculated data show that the addition of low concentrations of the IL

---

[1] An excess thermodynamic property (M^E) is equal to the difference between the actual properties (M) and the property in the ideal case (M^{ideal}) of a solution at the same temperature, pressure, and composition.

(10 and 25 wt.% IL) slightly change the α^E, but the addition of IL to the 51.32 wt.% DGA aqueous solution resulting in a mixture with mass fractions of 0.4024 of the IL and 0.4976 of DGA decrease this property by 54% on average. The V^E show negative values for all the samples studied. The negative values can be reasonably attributed to the structural contributions of components or the geometrical fitting of one component into the other. Considering this fact that present systems have positive α^E, the assumption of the presence of chemical contributions or the specific intermolecular interactions, causing the negative values for V^E, is unlikely. Additionally, the increasing trend of V^E with an increase in the temperature can be attributed to the increase in kinetic energy of the components. The results listed in Table I-3 show that $\Delta\eta$ are positive values for all the systems. Positive values of $\Delta\eta$ indicate that all the components face more resistance to flow upon mixing.
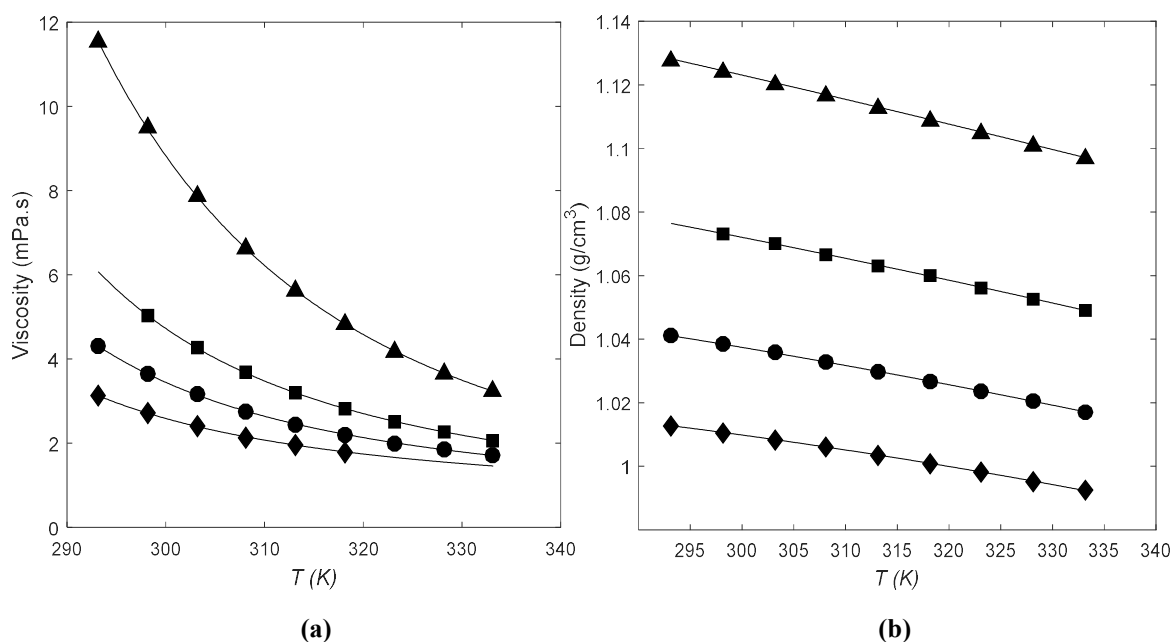
Figure 7-16: Trend analysis showing the effect of temperature on: **(a)** viscosity and **(b)** density of MEA (1) + H_2O (2) + bmim[OTF] (3) mixtures with different mass compositions: Exp (this work) w_2/w_1 = 0.6996/0.3004 (◆), $w_3/w_2/w_1$ = 0.1045/0.5836/0.3119 (●), $w_3/w_2/w_1$ = 0.2392/0.4614/0.2994 (■) and $w_3/w_2/w_1$ = 0.4311/0.2643/0.3046 (▲). Solid line depicts regressed results.

97
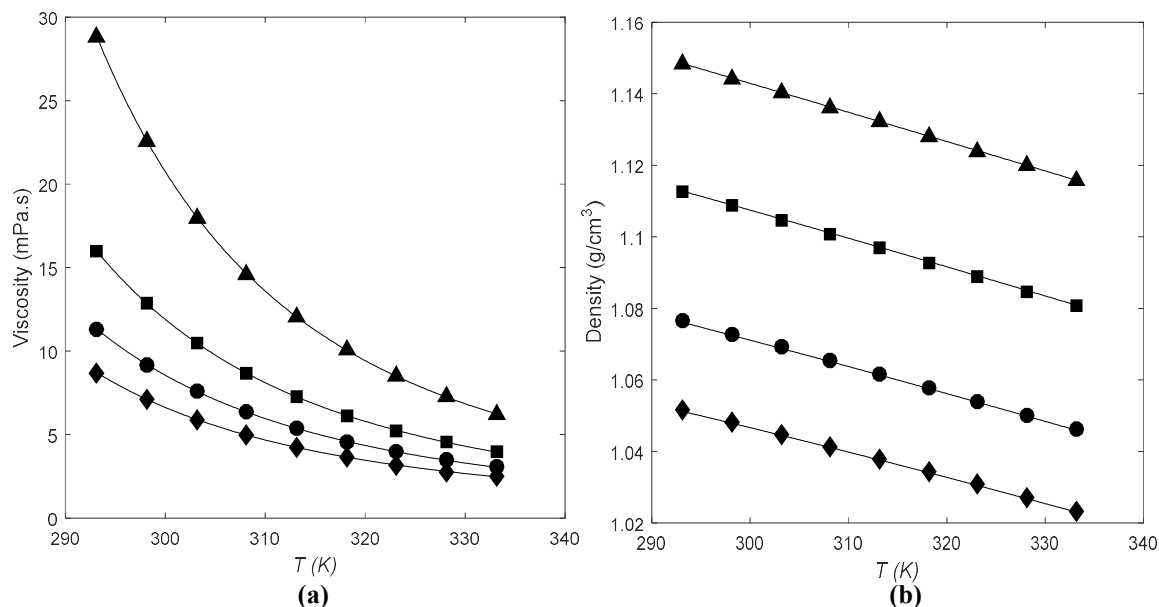
Figure 7-17: Trend analysis showing the effect of temperature on: **(a)** viscosity and **(b)** density of DGA (1) + H_2O (2) + bmim[OTF] (3) mixtures with different mass compositions: Exp (this work), w_2/w_1 = 0.4868/0.5132 (◆), $w_3/w_2/w_1$ = 0.1006/0.3878/0.5116 (●), $w_3/w_2/w_1$ = 0.2593/0.2665/0.4742 (■) and $w_3/w_2/w_1$ = 0.4024/0.1/0.4976 (▲). Solid line depicts regressed results.

7.4.1.3 Measurement of evaporation rate

The volatility of amine solutions leading to the release of amine and water into the gas phase and air during the desorption process is one of the disadvantages of the amine process. Consequently, a part of the solvent is lost and must be replaced regularly in each cycle [10, 18]. TGA analysis or Thermogravimetry was used to compare the vapour pressure or evaporation rate[1] of the hybrid solvents introduced in this project and investigate the potential of the ILs to increase the stability of solvent during the desorption step. To this aim, samples of MEA/DGA + H_2O + bmim[OTF] listed in Table 7-6 were prepared. The experimental method is explained in Chapter 5. Figures 7-18 and 7-19 display the sample mass versus the time at a temperature of 373.15 K. Experimental data are summarized in Tables 7-8 and 7-9. It is clear from the figures that the samples with 30 wt.% of MEA and 53.10 wt.% of DGA had evaporated completely after 38 minutes and 4 hours respectively, but the rate of mass loss or the evaporation rate for the samples containing the IL is less than that of the IL-free sample. Additionally, the evaporation rate decreases with respect to time and becomes zero for the IL-containing samples after some time. Afterwards, the mass of samples remains constant. Tables 7-8 and 7-9 shows that the final mass of the IL-containing samples is approximately equal to the mass of IL present in the initial sample loaded in the TGA apparatus. Therefore, it is reasonable to conclude that the loss of IL in the mentioned conditions

---

[1]According to the Langmuir equation that is based on the kinetic gas theory, the vapour pressure of the liquid has a straight relation with the evaporation rate of the liquid.207. Aschenbrenner, O., et al., *Measurement of vapour pressures of ionic liquids and other low vapour pressure solvents.* Green Chemistry, 2009. **11**(8): p. 1217-1221.

which are close to the desorption conditions (high temperature and low pressure) is almost zero, and the entire amount of IL can be recovered and reused.

Considering that the boiling point of MEA (443.15 K) and DGA (494.15 K) are much greater than the boiling point of water (373.15 K) and the experiment was done at 373.15 K; it was assumed that the sample drying (evaporation of water content) happened at first, and afterwards the amine present in the sample evaporated. Based on this assumption, the evaporation rate of water and MEA/DGA were calculated and listed in Tables 7-8 and 7-9. Results show that addition of IL, especially 10 wt.% IL, into the aqueous solution with 30.04 wt.% of MEA or 53.1 wt.% of DGA decreases the evaporation rate of MEA or DGA. The evaporation rate of MEA in the 31.19 wt.% MEA solution with 10.45 wt.% IL is almost half of the evaporation rate of MEA in the IL-free 30.04 wt.% MEA solution; which is evident in Figure 7-18 as well. The evaporation rate of DGA in the 49.47 wt.% DGA solution with 10 wt.% IL is almost 0.75 of the evaporation rate of DGA in the IL-free 53.10 wt.% DGA solution. The addition of IL into the amine solutions, not only decreases the volatile part of the solvent, but it also decelerates the evaporation rate of amine part, while the loss of IL as the expensive part of the hybrid solvent is almost zero.

In conclusion, although the aqueous IL-free amine solutions outperform the IL-containing amine solvents with regards to the solubility of CO_2 and viscosity, all the IL-containing amine solvents can achieve the maximum allowable loading of the acid gas at the conditions studied. Given the measured data for solubility and evaporation rate, the inclusion of 10 wt.% of bmim[OTF] in the aqueous amine solutions with 30 wt.% MEA or 53.10% DGA is beneficial to CO_2 extraction since it reduces the solvent volatility by approximately 50% for the MEA solvents and %25 for the DGA solvents. The addition of 10% of IL decreases the solubility of CO_2 in the MEA and DGA solvents by 0.5 % to 4.5 % and 3% to 4.5%, respectively. These reduced solubilities are not considerable because the maximum absorption capacity of the amine solvent is not used in the industry.
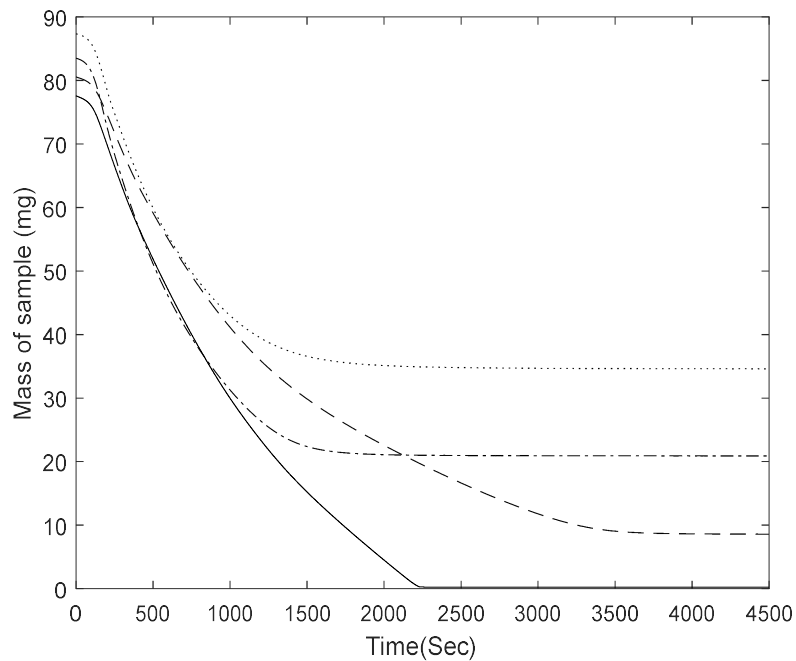
Figure 7-18: Sample mass versus time at a temperature of 373.15 K for MEA (1) + H_2O (2) + bmim[OTF] (3) mixtures with different mass compositions: w_2/w_1 = 0.6996/0.3004 (solid line), $w_3/w_2/w_1$ = 0.1045/0.58336/0.3119 (dashed line), $w_3/w_2/w_1$ = 0.2492/0.458/0.2928 (dash-dot line) and $w_3/w_2/w_1$ = 0.3943/0.3178/0.2879 (dotted line).
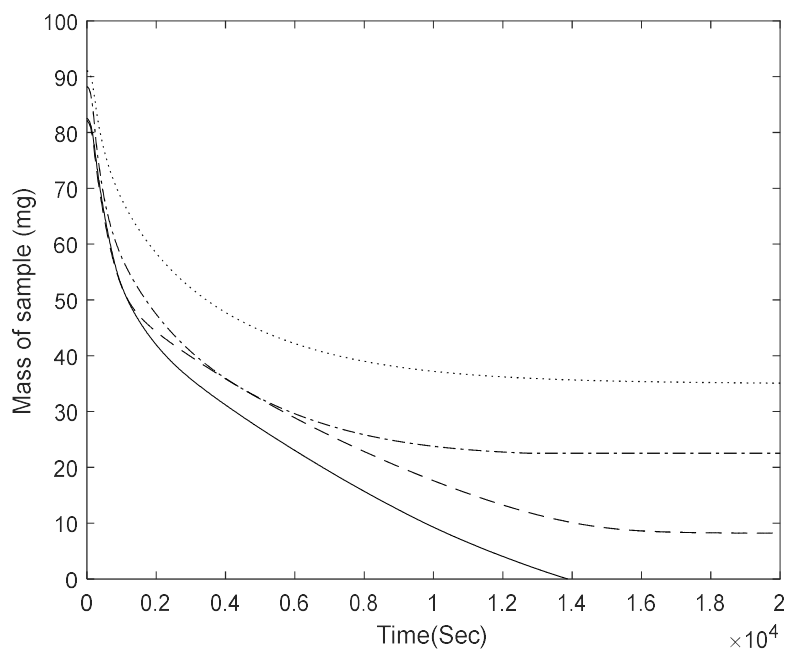
Figure 7-19: Sample mass versus time at a temperature of 373.15 K for DGA (1) + H_2O (2) + bmim[OTF] (3) mixtures with different mass compositions: w_2/w_1 = 0.469/0.531 (solid line), $w_3/w_2/w_1$ = 0.1000/0.4053/0.4947 (dashed line), $w_3/w_2/w_1$ = 0.2507/0.275/0.4743 (dash-dot line) and $w_3/w_2/w_1$ = 0.3887/0.1386/0.4727 (dotted line).

Table 7-8: Experimental data describing the samples of MEA (1) + H_2O (2) + bmim[OTF] (3) mixtures with different initial mass compositions used for TGA measurements[a].

Sample	Initial mass (mg)	Initial MEA (mg)	Initial water (mg)	Initial IL (mg)	Final mass after 75 mins (mg)	Evaporation rate of water (mg/sec)	Evaporation rate of MEA (mg/sec)
$w_1 = 0.3004$, $w_2 = 0.6996$	77.5779	23.3048	54.2731	0	0.2042	0.04517	0.0221
$w_1 = 0.3119$, $w_2 = 0.5837$, $w_3 = 0.1045$	80.5632	25.1242	47.0215	8.4175	8.5727	0.03602	0.0106
$w_1 = 0.2928$, $w_2 = 0.4581$, $w_3 = 0.2492$	83.5133	24.4488	38.2565	20.8080	20.8975	0.06226	0.0191
$w_1 = 0.2879$, $w_2 = 0.3177$, $w_3 = 0.3943$	87.3554	25.1520	27.7565	34.4469	34.5976	0.05484	0.0150

[a]Readability = 0.0001 mg, sensitivity = 0.001 mg

Table 7-9: Experimental data describing the samples of DGA (1) + H_2O (2) + bmim[OTF] (3) mixtures with different initial mass compositions used for TGA measurements[a].

Sample	Initial mass (mg)	Initial DGA (mg)	Initial water (mg)	Initial IL (mg)	Final mass (mg) after 5.56 hour	Evaporation rate of water (mg/sec)	Evaporation rate of DGA (mg/sec)
$w_1 = 0.5310$, $w_2 = 0.4690$	82.5615	43.8387	38.7229	0	0.0004[b]	0.0219	0.0036
$w_1 = 0.4947$, $w_2 = 0.4052$, $w_3 = 0.10$	82.1506	40.6412	33.2914	8.2180	8.2139	0.0257	0.0027
$w_1 = 0.4743$, $w_2 = 0.2750$, $w_3 = 0.2507$	88.2386	41.8529	24.2676	22.1181	22.5344	0.0372	0.0036
$w_1 = 0.4727$, $w_2 = 0.1385$, $w_3 = 0.3887$	91.1062	43.0693	12.6223	35.4145	35.0823	0.02920	0.0032

[a]Readability = 0.0001 mg, sensitivity = 0.001 mg

[b] final mass (mg) after 3.85 hour

7.4.2 MEA + (NMP + bmim[TF$_2$N])/H$_2$O + CO$_2$ system

Characteristics of MEA + (NMP + bmim[TF$_2$N])/H$_2$O/bmim[OTF] solutions used to measure the CO$_2$ solubility, viscosity, density, sound velocity and evaporation rates are presented in Table 7-10. In this section, the aqueous solvents with different concentration of MEA are studied. Then, the entire aqueous media of the MEA samples is replaced with NMP or bmim[OTF]. Finally, the inclusion of different concentration of IL in the NMP-containing 10% MEA is studied.

Table 7-10: Overview of the measured MEA + (NMP + bmim[TF$_2$N])/H$_2$O/bmim[OTF] solutions.

Initial mass composition	Temperature (K)	Pressure range (MPa)
Solubility measurement		
MEA (1) + H$_2$O (2): w_1/w_2 = 0.1034/ 0.8966 w_1/w_2 = 0.1997/ 0.8003 w_1/w_2 = 0. 2965/ 0.7034	313.15	0.189 to 2.322
MEA (1) + NMP (2): w_1/w_2 = 0.1025/ 0.8975 w_1/w_2 = 0.2032/ 0.7968 w_1/w_2 = 0.3037/ 0.6963	313.15	0.194 to 2.298
MEA (1) + bmim[OTF] (2): w_1/w_2 = 0.0912/ 0.9088	313.15	0.564 to 2.065
MEA (1) + NMP (2) + bmim[TF$_2$N] (3): $w_1/w_2/w_3$ = 0.1039/ 0.7966/ 0.0995 $w_1/w_2/w_3$ = 0.0977/ 0.6492/ 0.2531 $w_1/w_2/w_3$ = 0.1162/ 0.4932/ 0.3906	313.15	0.297 to 1.993
Viscosity, density and sound velocity measurement		
MEA (1) + H$_2$O (2): w_1/w_2 =0.1034/ 0.8966 w_1/w_2 = 0.2008/ 0.7992 w_1/w_2 = 0.3004/ 0.6996	293.15 to 333.15	-
MEA (1) + NMP (2): w_1/w_2 = 0.1021/ 0.8979 w_1/w_2 = 0.2090/ 0.791 w_1/w_2 = .03089/ 0.6911	293.15 to 333.15	-
MEA (1) + bmim[OTF] (2): w_1/w_2 = 0.0912/ 0.9088	293.15 to 333.15	-
MEA (2) + NMP (3) + bmim[TF$_2$N] (4): $w_1/w_2/w_3$ = 0.0976/ 0.8032/ 0.0992 $w_1/w_2/w_3$ = 0.1138/ 0.6414/ 0.2448 $w_1/w_2/w_3$ =0.1162/ 0.4932/ 0.3906	293.15 to 333.15	-

Initial mass composition	Temperature (K)	Pressure range (MPa)
Evaporation rate measurement		
MEA (1) + H$_2$O (2): $w_1/w_2 = 0.0997/ 0.9003$ $w_1/w_2 = 0.1985/ 0.8015$ $w_1/w_2 = 0.3004/ 0.6996$	373.15	Atmospheric pressure
MEA (1) + NMP (2): $w_1/w_2 = 0.1129/ 0.8871$ $w_1/w_2 = 0.2070/ 0.793$ $w_1/w_2 = 0.3050/ 0.695$	373.15	Atmospheric pressure
MEA (1) + bmim[OTF] (2): $w_1/w_2 = 0.0912/0.9088$	373.15	Atmospheric pressure
MEA (1) + NMP (2) + bmim[TF$_2$N] (3): $w_1/w_2/w_3 = 0.1039/0.7966/0.0995$ $w_1/w_2/w_3 = 0.0977/0.6492/0.2531$ $w_1/w_2/w_3 = 0.1162/0.4932/0.3906$	373.15	Atmospheric pressure

7.4.2.1 Solubility Measurements

The solubility of CO_2 in the samples listed in Table 7-10 were measured. The data are presented in Figure 7-20 and listed in Tables H-15 to H-23. Figures 7-20-a, 7-20-b and 7-20-c compare the solubility of CO_2 in an MEA aqueous solution with a water-free NMP-containing MEA solution at the approximate temperature of 313.15 K. The concentration of MEA is approximately constant in each comparison, and measurements for three concentrations of MEA, viz. $w \sim$ (0.1, 0.2 and 0.3), were performed. It is evident from the figures that there is a turning point or a pressure point for each set of measurements. The turning point shows that the solubility of CO_2 in the MEA aqueous solution is less than that in the free-water MEA solution at pressures higher than the turning point, and the solubility in the aqueous solutions is more than that in the free-water MEA solutions at pressures lower than the turning point. It seems that the turning point is dependent on the initial concentration of MEA and decreases with reducing the concentration of MEA. The turning point for the CO_2 + MEA ($w \sim 0.3$) + H$_2$O/NMP ($w \sim 0.7$) systems, displayed in Figure 7-20-a, is around 1.4 MPa. Results show that the solubility of CO_2 in the 29.65 wt.% MEA aqueous solution is maximum 5.5% higher than that in the NMP-containing 30.37 wt.% MEA solution at pressures between 0.3 to 1.4 MPa. Besides, the replacement of water with NMP in the MEA aqueous solution increases the CO_2 solubility maximum by 6.5% at pressures between 1.4 to 2 MPa. The turning point for the CO_2 + MEA ($w \sim 0.2$) + H$_2$O/NMP ($w \sim 0.8$) systems, shown in Figure 7-20-b, is around 0.6 MPa. Data show that the solubility of CO_2 in the 19.97 wt.% MEA aqueous solution is maximum 4.5% higher than that in the NMP-containing 20.32 wt.% MEA solution at pressures between 0.2 to 0.6 MPa. Additionally, the replacement of water with NMP in the 19.97 wt.% MEA aqueous solution increases the CO_2 solubility maximum by 25% at

pressures between 0.6 to 2 MPa. Finally, The turning point for the CO_2 + MEA ($w \sim 0.1$) + H_2O/NMP ($w \sim 0.9$) systems, shown in Figure 7-26-c, is less than 0.213 MPa definitely (more data at lower pressures are required to obtain the turning point more accurately). Data show that the replacement of water with NMP in the 10.34 wt.% MEA aqueous solution increases the CO_2 solubility maximum by 81% at pressures between 0.213 to 2 MPa.

In addition, Figure 7-20-c shows the solubility of CO_2 in the water-free bmim[OTF]-containing MEA solution. It is clear from the figure that bmim[OTF] does not improve the ability of the MEA solution to absorb CO_2 at low pressures. The turning point for the CO_2 + MEA ($w \sim 0.1$) + H_2O/bmim[OTF] ($w \sim 0.9$) systems is around 1.5 MPa. The solubility of CO_2 in the 10.34 wt.% MEA aqueous solution is maximum 20% higher than that in the bmim[OTF]-containing 9.11 wt.% MEA solution at pressures between 0.6 to 1.5 MPa. Additionally, the replacement of water with bmim[OTF] in the 10.34 wt.% MEA aqueous solution increases the CO_2 solubility maximum by approximately 12% at pressures between 1.5 to 2 MPa. The measured data listed in Table H-20 show that the bmim[OTF]-containing solvent is able to achieve the maximum allowable loading of acid gas (0.3 to 0.35 and 0.7 to 0.9 moles acid gas per mole of MEA for the carbon steel and stainless steel equipment, respectively) at pressures higher than 0.55 MPa.

Figure 7-27-d clearly presents the effect of the addition of bmim[TF_2N] to the NMP-containing MEA solvents on the solubility of CO_2. Bmim[TF_2N] was chosen since it has less viscosity and a higher ability to absorb CO_2 in comparison to bmim[OTF]. From the figure, it is evident that an increase in the concentration of bmim[TF_2N] present in the NMP-containing MEA solutions decreases the solubility of CO_2. Compared to the NMP-containing 10.25 wt.% MEA solution at 313.15 K and pressure range of 0.4 to 2 MPa, the solubility of CO_2 in the hybrid solvents of NMP + MEA + bmim[TF_2N], with an approximate mass fraction of 0.10 of the MEA and mass fractions of 0.0995, 0.2531 and 0.3906 of the IL, decreases approximately by 5% to 9%, 10% to 14% and 23.5% to 33%, respectively. The turning point for the CO_2 + MEA ($w \sim 0.1$) + (bmim[TF_2N] (w =0.0995) + NMP) / H_2O (w = 0.8966) systems is less than 0.341 MPa definitely. The replacement of aqueous media with the mixture of bmim[TF_2N] (w = 0.0995) + NMP in the 10.34 wt. % MEA aqueous solution increases the CO_2 solubility maximum by 65% at pressures between 0.341 to 2 MPa. The turning point for the CO_2 + MEA ($w \sim 0.1$) + (bmim[TF_2N] (w = 0.2531) + NMP)/ H_2O (w = 0.8966) systems is less than 0.413 MPa. Additionally, the replacement of entire water with the mixture of bmim[TF_2N] (w = 0.2531) + NMP in the 10.34 wt.% MEA aqueous solution increases the CO_2 solubility maximum by 56% at pressures between 0.4 to 2 MPa. Finally, The turning point for the CO_2 + MEA ($w \sim 0.1$) + (bmim[TF_2N] (w = 0.3906) + NMP) / H_2O (w = 0.8966) systems is around 1.1 MPa. The solubility of CO_2 in the 10.34 wt.% MEA aqueous solution is maximum 17% higher than that in the solvent containing 39.06 wt.% bmim[TF_2N] at

pressures between 0.3 to 1.1 MPa. Additionally, the replacement of whole water with the mixture of bmim[TF$_2$N] (w =0.3906) + NMP in the 10.34 wt.% MEA aqueous solution increases the CO$_2$ solubility maximum by 22% at pressures between 1.1 to 2 MPa.

(a)

(b)

(c)

(d)
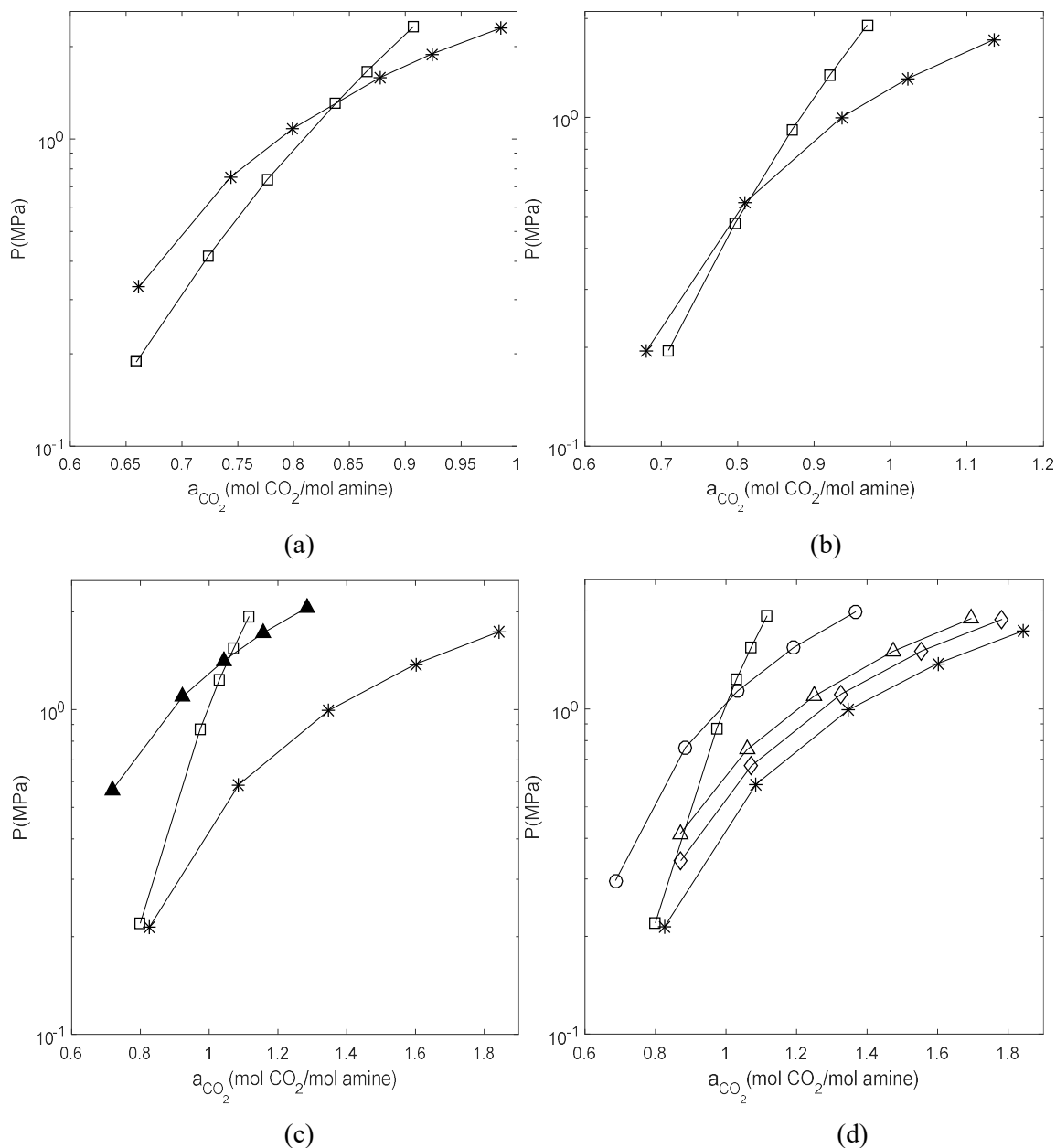
Figure 7-20: Comparison of experimental data for the solubility of CO$_2$ in: **(a)** MEA (1) +H$_2$O (2) with mass composition of w_1/w_2 = 0. 2965/0.7034 (□), and MEA (1) + NMP (2) with w_1/w_2 = 0.3037/0.6963 (*); **(b)** MEA (1) + H$_2$O (2) with w_1/w_2 = 0.1997/0.8003 (□); and MEA (1) + NMP (2) with w_1/w_2 = 0.2032/0.7968 (*); **(c)** MEA (1) + H$_2$O (2) with w_1/w_2 = 0.1034/0.8966 (□), MEA (1) + NMP (2) with w_1/w_2 = 0.1025/0.8975 (*), and MEA (1) + bmim[OTF] (2) with w_1/w_2 = 0.0912/0.9088 (▲); and **(d)** MEA (1) + H$_2$O (2) with w_1/w_2 = 0.1034/0.8966 (□), MEA (1) + NMP (2) with of w_1/w_2 = 0.1025/0.8975 (*), and MEA (1) + NMP (2) + bmim[TF$_2$N] (3) with different mass compositions: $w_1/w_2/w_3$ = 0.1039/0.7966/ 0.0995 (◇), $w_1/w_2/w_3$ = 0.0977/ 0.6492/0.2531 (△), and $w_1/w_2/w_3$ = 0.1162/ 0.4932/ 0.3906 (○), at 313.15 K.

7.4.2.2 Viscosity, density and speed of sound measurements

Viscosity, density and sound velocity of samples listed in Table 7-10 were measured. Experimental data are presented in Figures 7-21 and 7-22 and listed in Table I-4. Similar to other systems, the density and viscosity decrease with an increase in the temperature. Figure 7-21 shows that the use of IL instead of water considerably increases the viscosity. The viscosity of the water-free bmim[OTF]-containing 9.12 wt.% MEA solution is greater than the viscosity of the 10.34 wt.% MEA aqueous solution by a factor of 21 to 38.1, over the entire range of tested temperatures. On the other hand, the replacement of the aqueous media with NMP in the MEA aqueous solutions with different mass fractions of MEA, viz. (0.1034, 0.2008, 0.3004), resulting in the NMP + MEA solutions with mass fractions of MEA, viz. (0.1021, 0.2090, 0.3089), increases the viscosity by a maximum factor of 2.6. Figure 7-21 shows that the addition of bmim[TF$_2$N] to a NMP-containing MEA solution increases the viscosity. For instance, the addition of bmim[TF$_2$N] to the NMP solution containing 10.21 wt.% MEA to make a mixture with mass fractions of 0.3906 of the bmim[TF$_2$N] and 0.1162 of MEA, increases the viscosity by a factor of 1.6 to 2.1. Additionally, the viscosity becomes more dependent on the temperature with an increase in the concentration of the IL. The fitting parameters and statistical deviations are listed in Table L-4.

Results presented in Table I-4 show that the thermal expansion coefficients (α) of the MEA aqueous systems are considerably lower than those of the NMP-containing MEA systems since the α of NMP is greater than water by 2.5 times on average. The α slightly decreases with increasing the mass fractions of the IL. The effect of changing the concentration of MEA on the α is more visible in the MEA aqueous solutions than that in the NMP-containing solvents. Additionally, the α of the NMP-containing MEA systems show less dependency on the temperature compared to the aqueous systems.

The excess coefficients of thermal expansion (α^E) are considerably changed by replacing water with NMP in the MEA aqueous solutions. Although most of the MEA aqueous solutions have negative values indicating the specific intermolecular interactions, all of the NMP-containing MEA solutions have positive values showing the self-association of components.

The excess molar volume (V^E) shows negative values for the MEA aqueous systems that can be attributed to the specific intermolecular interactions or the structural contributions of the components present in the solvents. Because the aqueous 30.04 wt.% MEA solvent has positive α^E at temperatures below 318.15 K, it is reasonable to assume that negative values of V^E for this system is mostly because of the structural contributions of the components. All the NMP-containing MEA solvents, except one with 39.06 wt.% IL, show negative values for V^E indicating

the structural contributions of components. Additionally, changing the temperature has a slight effect on the excess molar volume for all the present systems.

Results listed in Table I-4 show that the deviation of viscosity ($\Delta\eta$) has negative values for all the systems (except for the 30.04 wt.% MEA aqueous solution at temperatures more than 308.15 K) indicating that all the components face less resistance to flow upon mixing. Furthermore, the addition of bmim[TF$_2$N] to the MEA + NMP system decreases the $\Delta\eta$.
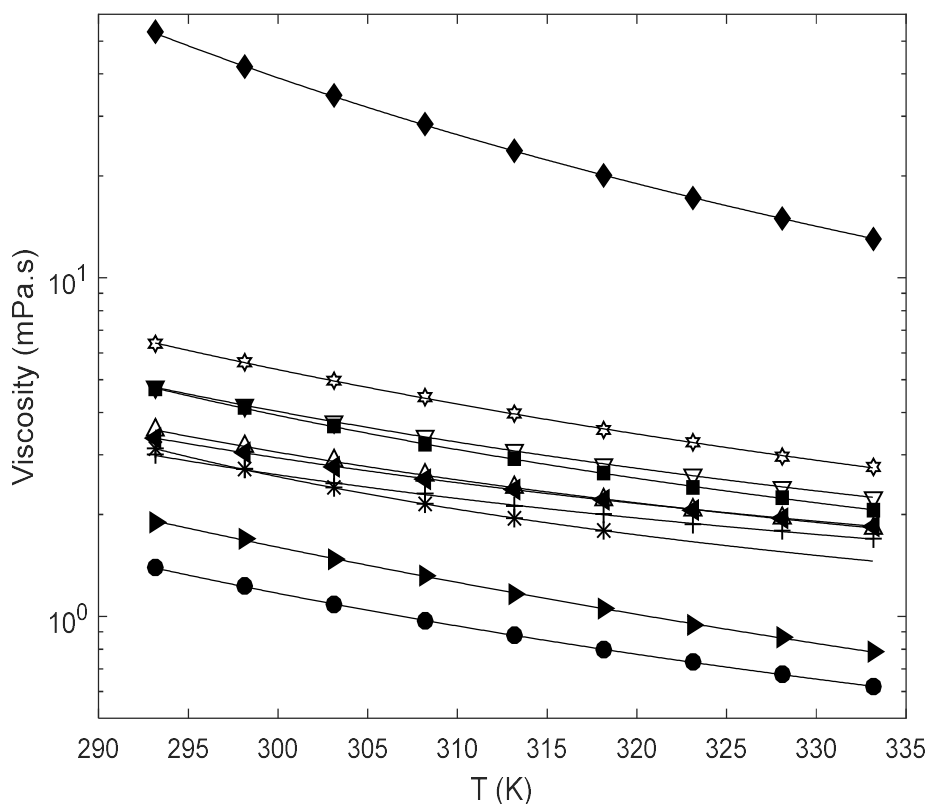
Figure 7-21: Trend analysis showing the effect of temperature on the viscosity of MEA (1) + NMP (2) + bmim[TF$_2$N] (3) mixtures with different mass compositions: w_1/w_2 = 0.1021/0.8979 (+), w_1/w_2 = 0.2090/ 0.791 ($\triangle$), w_1/w_2 = 0.3089/0.6911 (■), $w_1/w_2/w_3$ = 0.0976/0.8032/0.0992 (◄), $w_1/w_2/w_3$ = 0.1138/0.6414/ 0.2448 ($\triangledown$), $w_1/w_2/w_3$ =0.1162/0.4932/0.3906 (✳); MEA (1) + bmim[OTF] (2) with mass fraction w_1/w_2 = 0.0912/0.9088 (◆); and mixtures of MEA (1) + H$_2$O (2) with mass fractions: w_1/w_2 = 0.1034/0.8966 (●), w_1/w_2 = 0.2008/0.7992 (▶), w_1/w_2 = 0.3004/ 0.6996 (✳), Solid line depicts regressed results.
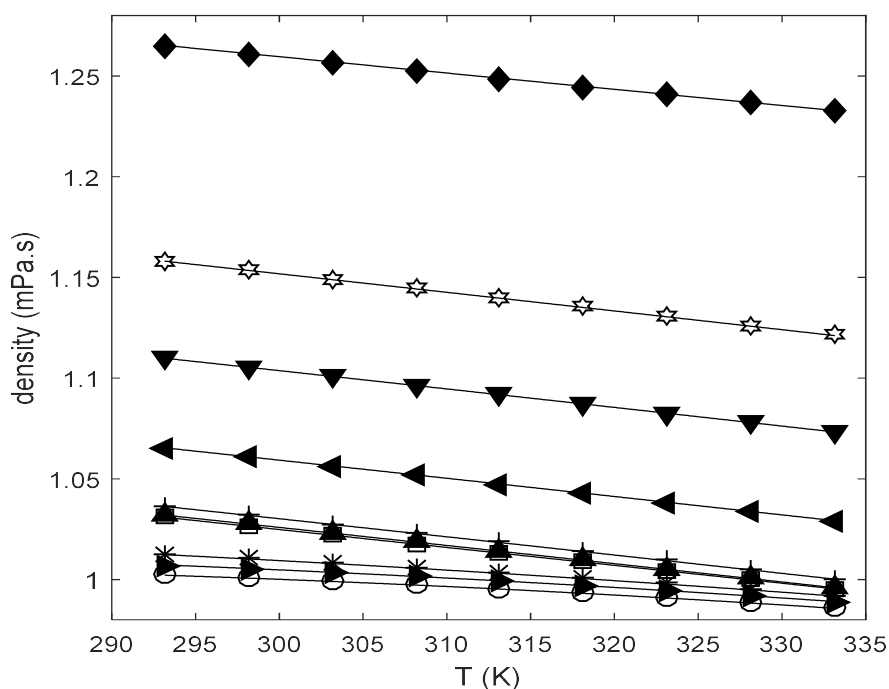
Figure 7-22: Trend analysis showing the effect of temperature on the density of MEA (1) + NMP (2) + bmim[TF$_2$N] (3) mixtures with different mass compositions: w_1/w_2 = 0.1021/0.8979 (+), w_1/w_2 = 0.2090/ 0.791 (▲), w_1/w_2 = 0.3089/0.6911 (□), $w_1/w_2/w_3$ = 0.0976/ 0.8032/0.0992 (◄), $w_1/w_2/w_3$ = 0.1138/ 0.6414/ 0.2448 (▼), $w_1/w_2/w_3$ =0.1162/0.4932/0.3906 (✳); MEA (2) + bmim[OTF] (3) with mass fraction w_1/w_2 = 0.0912/0.9088 (◆); and mixtures of MEA (1) + H$_2$O (2) with mass fractions: w_1/w_2 =0.1034/0.8966 (○), w_1/w_2 = 0.2008/0.7992 (►), w_1/w_2 = 0.3004/ 0.6996 (✳); Solid line depicts regressed results.

7.4.2.3 Measurement of evaporation rate

Evaporation rate of samples of MEA + (NMP + bmim[TF$_2$N]) / H$_2$O / bmim[OTF] listed in Table 7-10 were measured. Figures 7-23 and 7-24 show the sample mass versus the time at 373.15 K. Experimental data are listed in Table 7-11. The boiling point of NMP (475.15 K) and MEA (443.15 K) are close and calculation of the evaporation rates of NMP and MEA separately may have considerable uncertainty, thus, only the total average evaporation rate was determined. It is clear from Figure 7-23 that replacing water with NMP in the MEA aqueous solutions with different concentrations of MEA decreases the evaporation rate of samples. For instance, the evaporation rate of the NMP-containing 20.70 wt.% MEA solution is approximately 58% of the evaporation rate of MEA in the 19.85 wt.% MEA aqueous solution. Figure 7-24 and Table 7-11 show that the addition of IL to the NMP-containing 11.29 wt.% MEA sample, to make solutions with 25.31% and 39.06% of IL, decreases the average evaporation rate; and the sample loss becomes zero after a period of time. Interestingly, the evaporation rate of MEA in the 9.12 wt.% MEA solution with 90.88 wt.% of bmim[OTF] is 9.85% of the evaporation rate of MEA in the 9.97 wt.% MEA aqueous solution. Table 7-11 shows that the final mass of the IL-containing samples is approximately equal to the mass of IL present in the initial loaded sample (after 6 to 9

hours approximately). Therefore, the loss of IL, as the most expensive component of the studied hybrid solvents, is almost zero in the mentioned conditions, and the entire amount of IL can be recovered and reused.

In conclusion, the NMP-containing solvents with 10 or 20 wt.% of MEA outperform the aqueous MEA solutions with regards to solubility and evaporation rate, especially for the NMP-containing 10 % MEA solution which its absorption capacity is 81% higher than the aqueous MEA. The NMP-containing 10% MEA solvents with 10 or 25 wt.% bmim[TF_2N] can absorb more CO_2 compared to the aqueous 10% MEA solution. But the inclusion of 10 wt.% of IL in the NMP-containing 10% MEA solvent does not improve the solubility and evaporation rate of solvent, thus it is not recommended. Given the measured data, among all the solvents studied in this section, the NMP-containing 10% MEA solutions, the NMP-containing 10% MEA solvent with 25% of bmim[TF_2N] and the NMP-containing 20% MEA solvent are recommended, respectively.
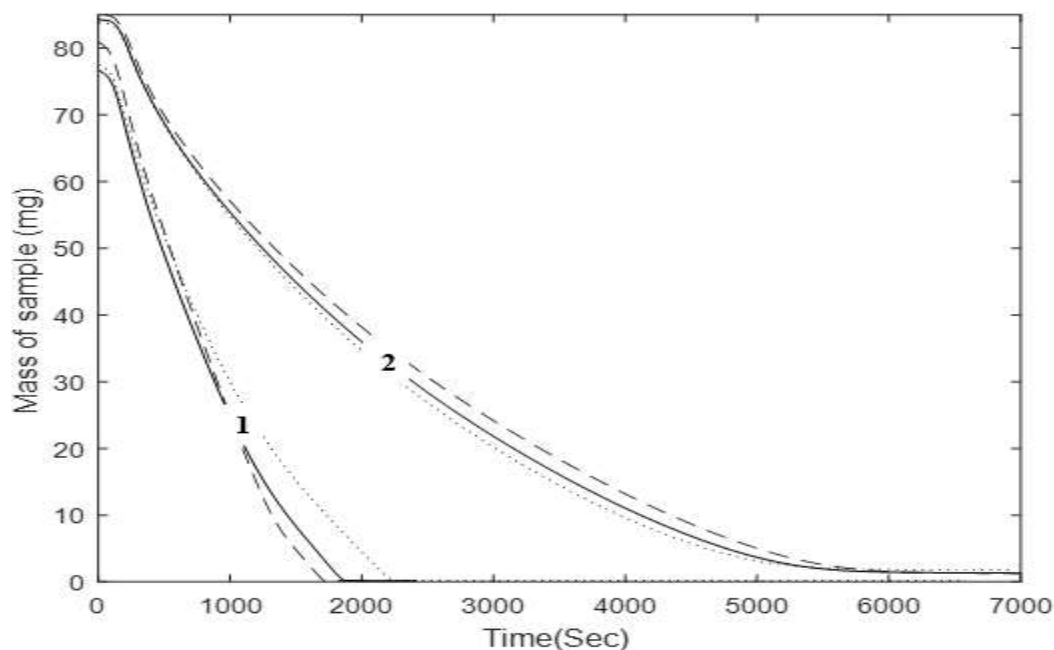
Figure 7-23: Sample mass versus time at a temperature of 373.15 K for MEA (1) + H_2O (2) mixtures with different mass compositions (group 1): w_1/w_2 = 0.0997/0.9003 (dashed line), w_1/w_2 = 0.1985/0.8015 (solid line), w_1/w_2 = 0.3004/0.6996 (dotted line), and mixtures of MEA (1) + NMP (2) with mass fractions (group 2): w_1/w_2 =0.1129/0.8871 (dashed line), w_1/w_2 = 0.2070/0.793 (solid line), w_1/w_2 = 0.3050/0.695 (dotted line).
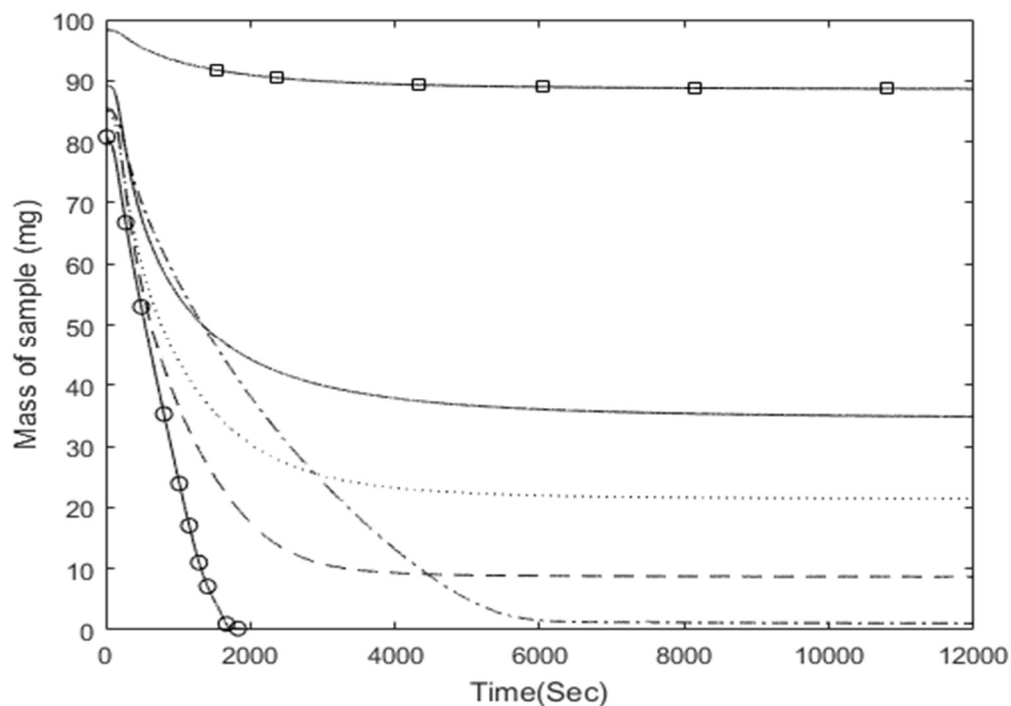
Figure 7-24: Sample mass versus time at a temperature of 373.15 K for MEA (1) + NMP (2) + bmim[TF$_2$N] (3) mixtures with different mass compositions: w_1/w_2 =0.1129/0.8871 (dash-dot line), $w_1/w_2/w_3$= 0.1039/0.7966/0.0995 (dashed line), $w_1/w_2/w_3$= 0.0977/0.6492/0.2531 (dotted line) and $w_1/w_2/w_3$= 0.1162/0.4932/0.3906 (solid line); MEA (1) + bmim[OTF] (2) with mass fraction w_1/w_2 = 0.0912/0.9088 (□); and mixture of MEA (2) + H$_2$O (3) with mass fraction: w_1/w_2 = 0.0997/ 0.900 (○).

110

Table 7-11: Experimental data describing the samples of MEA (1) + H_2O (2)/(NMP (2) + bmim[TF_2N] (3)) / bmim[OTF] (2) mixtures with different initial mass compositions used for TGA measurements[a].

Sample	initial mass (mg)	Initial MEA (mg)	Initial NMP/water (mg)	Initial IL (mg)	Final mass (mg)	Final point for time (hour)	Total evaporation rate of MEA and NMP (mg/sec)
w_1 = 0.0912, $w_{bmim[OTF]}$ = 0.9088	98.29878	8.96037	0.00000	89.33841	88.50572	6.44	0.00232
w_1 = 0.0997, w_{water} = 0.9003	80.97307	8.07455	72.89851	0.00000	0.21842	0.53	0.02349
w_1 = 0.1985, w_{water} = 0.8015	76.72352	15.22757	61.49595	0.00000	0.15123	0.67	0.02469
w_1 = 0.3004, w_{water} = 0.6996	77.57794	23.30484	54.27310	0.00000	0.20422	1.25	0.02211
w_1 = 0.1129, w_{NMP} = 0.8871	85.06101	9.60082	75.46018	0.00000	0.93371	6.36	0.01392
w_1 = 0.2070, w_{NMP} = 0.7930	84.26213	17.44124	66.82089	0.00000	1.30810	1.95	0.01439
w_1 = 0.3050, w_{NMP} = 0.6950	83.75638	25.54462	58.21176	0.00000	1.77797	1.93	0.01509
w_1 = 0.1039, w_{NMP} = 0.7966, $w_{bmim[TF2N]}$ = 0.0995	85.43335	8.87631	68.05904	8.49800	8.45506	8.36	0.01903
w_1 = 0.0977, w_{NMP} = 0.6492, $w_{bmim[TF2N]}$ = 0.2531	84.1945	8.22570	54.66030	21.30850	21.25250	8.36	0.01128
w_1 = 0.1162, w_{NMP} = 0.4932, $w_{bmim[TF2N]}$ = 0.3906	89.17671	10.36181	43.98229	34.83261	34.43819	9.55	0.00858

[a]Readability = 0.0001 mg, sensitivity = 0.001 mg

7.4.3 DGA + (NMP + bmim[TF$_2$N])/H$_2$O + CO$_2$ system

Characteristics of DGA + (NMP + bmim[TF$_2$N])/H$_2$O solutions used to measure the CO$_2$ solubility, viscosity, density, sound velocity and evaporation rates are presented in Table 7-12. In this section, the aqueous DGA solvents with different concentration of amine are studied. Then, the aqueous media of the DGA samples is replaced with NMP. Finally, the addition of different concentration of IL to the NMP-containing 30% DGA is studied.

Table 7-12: Overview of the studied DGA+ (NMP + bmim[TF$_2$N])/H$_2$O solutions.

Initial mass composition	Temperature (K)	Pressure range (MPa)
Solubility measurement		
DGA (1) + H$_2$O (2): $w_1/w_2 = 0.5132/ 0.4868$ $w_1/w_2 = 0.3101/ 0.6899$	313.15	0.188 to 2.168
DGA (1) + NMP (2): $w_1/w_2 = 0.4964/ 0.5036$ $w_1/w_2 = 0.3020/0.6980$	313.15	0.262 to 1.893
DGA (1) + NMP (2) + bmim[TF$_2$N] (3): $w_1/w_2/w_3 = 0.3108/ 0.5864/ 0.1028$ $w_1/w_2/w_3 = 0.3035/ 0.4462/ 0.2503$ $w_1/w_2/w_3 = 0.2981/ 0.3096/ 0.3923$	313.15	0.297 to 1.973
Viscosity, density and sound velocity measurement		
DGA (1) + H$_2$O (2): $w_1/w_2 = 0.2923/0.7077$ $w_1/w_2 = 0.5132/0.4868$	293.15 to 333.15	-
DGA (1) + NMP (2): $w_1/w_2 = 0.4981/0.5019$ $w_1/w_2 = 0.3102/0.6898$	293.15 to 333.15	-
DGA (1) + NMP (2) + bmim[TF$_2$N] (3): $w_1/w_2/w_3 = 0.2981/0.3096/0.3923$ $w_1/w_2/w_3 = 0.3035/0.4462/0.2503$ $w_1/w_2/w_3 = 0.2840/ 0.6166/0.0994$	293.15 to 333.15	-
Evaporation rate measurement		
DGA (1) + H$_2$O (2): $w_1/w_2 = 0.5310/0.4690$ $w_1/w_2 = 0.2923/0.7077$	373.15	Atmospheric pressure
DGA (1) + NMP (2): $w_1/w_2 = 0.4915/0.5085$ $w_1/w_2 = 0.2923/0.7077$	373.15	Atmospheric pressure
DGA (1) + NMP (2) + bmim[TF$_2$N] (3): $w_1/w_2/w_3 = 0.2840/0.6166/0.0994$ $w_1/w_2/w_3 = 0.3035/0.4462/0.2503$ $w_1/w_2/w_3 = 0.2981/0.3096/0.3923$	373.15	Atmospheric pressure

7.4.3.1 Solubility measurements

Solubility data were isothermally measured for the systems listed in Table 7-12. The data are showed in Figures 7-25 and 7-26 and listed in Tables H-24 to H-29. Figures 7-31 and 7-32 separately compare the solubility of CO_2 in a DGA aqueous solution with a water-free NMP-containing DGA solution. The concentration of DGA is approximately constant in each comparison, and measurements for two concentrations of DGA, viz. $w\sim$ (0.3 and 0.5), were performed. Similar to the MEA systems, the turning point of the DGA solvents is dependent on the concentration of DGA. The turning point for the CO_2 + DGA ($w \sim 0.5$) + H_2O/NMP ($w \sim 0.5$) systems, displayed in Figure 7-25-a, is definitely less than 0.433 MPa (more data at lower pressures are required to obtain the turning pressure more accurately). Results show that the replacement of aqueous media with NMP in the 51.32 wt.% DGA aqueous solution increases the solubility of CO_2 approximately 2% to 12% at pressures between 0.4 to 2 MPa. The turning point for the CO_2 + DGA ($w \sim 0.3$) + H_2O/NMP ($w \sim 0.7$) systems, shown in Figure 7-25-b, is around 0.262 MPa. Data show that the replacement of water with NMP in the 31.01 wt.% DGA aqueous solution increases the CO_2 solubility maximum by 30% at pressures between 0.26 to 2 MPa.

Figure 7-26 clearly shows the effect of the addition of bmim[TF_2N] to the DGA solvents on the solubility of CO_2. From the figure, it is evident that an increase in the concentration of bmim[TF_2N] decreases the solubility of CO_2. Compared to the NMP-containing 30.20 wt.% DGA solution at 313.15 K and pressure range of 0.4 to 2 MPa, the solubility of CO_2 in the hybrid solvents of NMP, DGA and bmim[TF_2N], with an approximate mass fraction of 0.30 of DGA and mass fractions of 0.1029, 0.2503 and 0.3923 of the IL, decreases approximately by 3% to 7%, 8% to 13% and 11% to 17%, respectively. The turning point for the CO_2 + DGA ($w\sim$ 0.3) + (bmim[TF_2N] ($w = 0.1029$) + NMP) / H_2O ($w = 0.6899$) systems is around 0.6 MPa. The solubility of CO_2 in the 31.01 wt.% DGA aqueous solution is maximum 1% higher than that in the solvent containing 10.29 wt.% bmim[TF_2N] at pressures between 0.35 to 0.6 MPa. Additionally, the replacement of entire water with the mixture of bmim[TF_2N] ($w = 0.1029$) + NMP in the 30.01 wt.% DGA aqueous solution increases the CO_2 solubility maximum by 21% at pressures between 0.6 to 2 MPa. The turning point for the CO_2 + DGA ($w\sim$ 0.3) + (bmim[TF_2N] ($w = 0.2503$) + NMP) / H_2O ($w = 0.6899$) systems is around 1.1 MPa. The solubility of CO_2 in the 31.01 wt.% DGA aqueous solution is maximum 6% higher than that in the solvent containing 25.03 wt.% bmim[TF_2N] at pressures between 0.35 to 1.1 MPa. Additionally, the replacement of aqueous media with the mixture of bmim[TF_2N] ($w = 0.2503$) + NMP in the 31.01 wt.% DGA aqueous solution increases the CO_2 solubility maximum by 13.5% at pressures between 1.1 to 2 MPa. Finally, The turning point for the CO_2 + DGA ($w\sim$ 0.3) + (bmim[TF_2N] ($w = 0.3923$) + NMP) / H_2O ($w = 0.6899$) systems is around 1.5 MPa. The solubility of CO_2 in the 31.01 wt.% DGA

aqueous solution is maximum 9% higher than that in the solvent containing 39.23% bmim[TF$_2$N] at pressures between 0.3 to 1.5 MPa. Besides, the replacement of whole water with the mixture of bmim[TF$_2$N] ($w = 0.3923$) + NMP in the 31.01 wt.% DGA solution increases the CO$_2$ solubility maximum by 8% at pressures between 1.5 to 2 MPa.
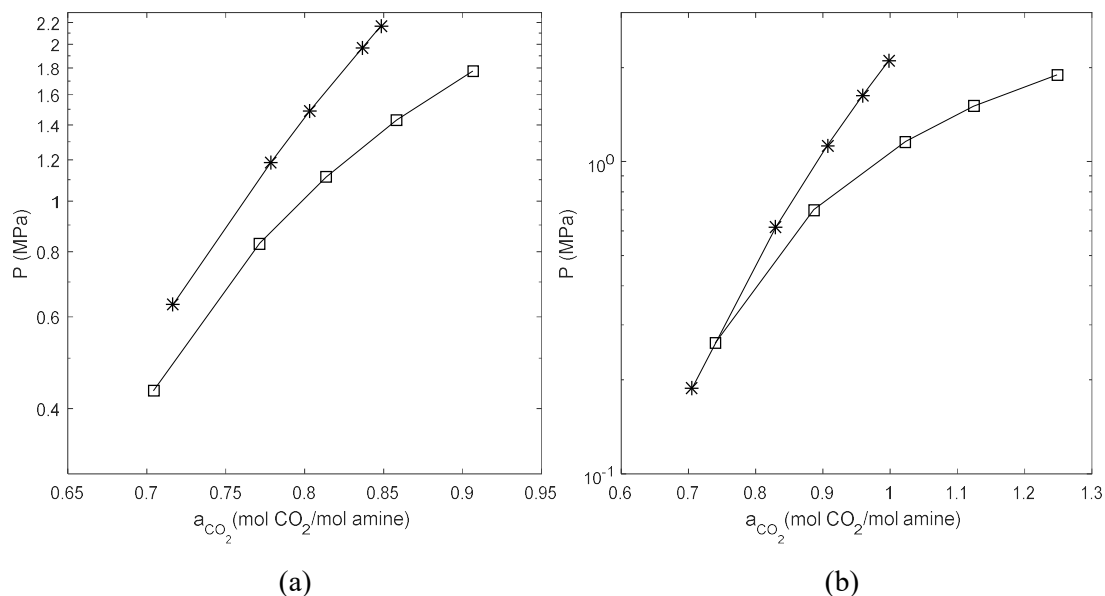
Figure 7-25: Comparison of experimental data for the solubility of CO$_2$ in: **(a)** DGA (1) + H$_2$O (2) with mass composition of $w_1/w_2 = 0.5132/0.4868$ (*), and DGA (1) + NMP (2) with mass composition of $w_1/w_2 = 0.4964/0.5036$ ($\square$); and **(b)** DGA (1) + H$_2$O (2) with mass composition of $w_1/w_2 = 0.3101/0.6899$ (*); and DGA (1) + NMP (2) with mass composition of $w_1/w_2 = 0.3020/0.6980$ ($\square$), at 313.15 K.
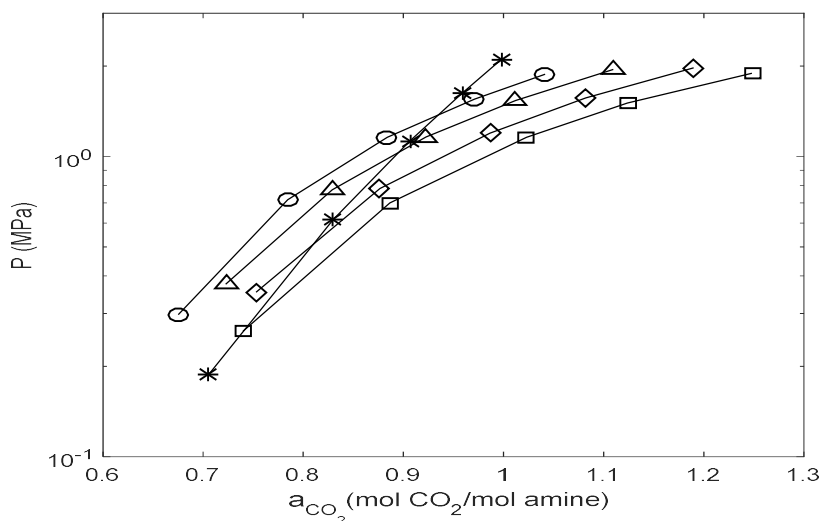
Figure 7-26: Comparison of experimental data for the solubility of CO$_2$ in: DGA (1) + H$_2$O (2) with mass composition of $w_1/w_2 = 0.3101/0.6899$ (*); DGA (1) + NMP (2) with mass composition of $w_1/w_2 = 0.3020/0.6980$ ($\square$); and DGA (1) + NMP (2) + bmim[TF$_2$N] (3) with different mass compositions: $w_1/w_2/w_3 = 0.3108/0.5864/0.1028$ ($\diamond$), $w_1/w_2/w_3 = 0.3035/0.4462/0.2503$ ($\triangle$), and $w_1/w_2/w_3 = 0.2981/0.3096/0.3923$ ($\bigcirc$) at 313.15 K.

114

7.4.3.2 Viscosity, density and speed of sound measurements

Viscosity, density and sound velocity of samples listed in Table 7-12 were measured. Experimental data are displayed in Figures 7-27 and 7-28 and listed in Table I-5. Results show that the viscosity of the water-free NMP-containing 31.02 wt.% DGA solution is greater than the viscosity of the 29.23 wt.% DGA aqueous solution by a factor of 1.7 to 2, over the entire range of measured temperatures. On the other hand, the replacement of water with NMP in a 51.32 wt.% DGA aqueous solution has a different trend compared to the 29.23 wt.% DGA aqueous solution. The water-free NMP-containing 49.81 wt.% DGA solution is less viscose than the 51.32 wt. % DGA aqueous solution at temperatures below 313.15. Overall, the viscosities of these solvents are very similar. Figure 7-27 shows that the addition of bmim[TF$_2$N] to a NMP-containing DGA solvent increases the viscosity. For instance, the addition of bmim[TF$_2$N] to the 31.02 wt.% DGA solution at 298.15 K to make a mixture with mass fractions of 0.3923 of the IL and 0.2981of DGA, increases the viscosity by a factor of 2.5. Additionally, the viscosity becomes more dependent on the temperature with an increase in the concentration of the IL. On the other hand, the dependency of density on the temperature for the all present systems is similar (shown in Figure 7-28). It is an interesting point that the NMP-containing 31.02 wt.% DGA solvent and the one with 9.94 wt.% IL are less viscous than the 51.32 wt.% DGA aqueous solvent as a commonly used solvent in the industry. In addition, the viscosities of the solvent with 25.03 wt.% IL and the NMP-containing 49.81 wt.% DGA solvent are quite close to those of the 51.32 wt.% DGA aqueous solvent. The fitting parameters and statistical deviations are listed in Table L-5.

Results listed in Table I-5 show that the thermal expansion coefficients (α) of the DGA aqueous systems are considerably lower than those of the NMP-containing DGA systems. The α slightly decreases with increasing the mass fractions of the IL and DGA present in the NMP-containing solvents. The excess coefficients of thermal expansion (α^E) have different trends for the DGA aqueous solutions. Although the 51.32 wt.% DGA aqueous solution has positive values indicating the self-association of components, the 29.23 wt. % DGA aqueous solution has negative values at temperatures below 303.15 K showing the specific intermolecular interactions. Replacement of water with NMP in the aqueous DGA solution, and an increase in the mass fraction of IL decrease the α^E resulting in solvents similar to their ideal cases, especially solvents containing 25 wt.% and 40 wt.% IL. The excess molar volume (V^E) has negative values for the aqueous systems that can be attributed to the structural contributions of components present in the solvents. The NMP-containing DGA solvents have different trends in comparison to the aqueous solvents. The values of V^E are very close to zero indicating the similarity of the NMP-containing solvents with their ideal cases. Deviations of viscosity ($\Delta\eta$) are negative values for all the NMP-containing

systems indicating that all the components face less resistance to flow upon mixing. Furthermore, the addition of the IL to the DGA systems slightly changes the $\Delta\eta$.
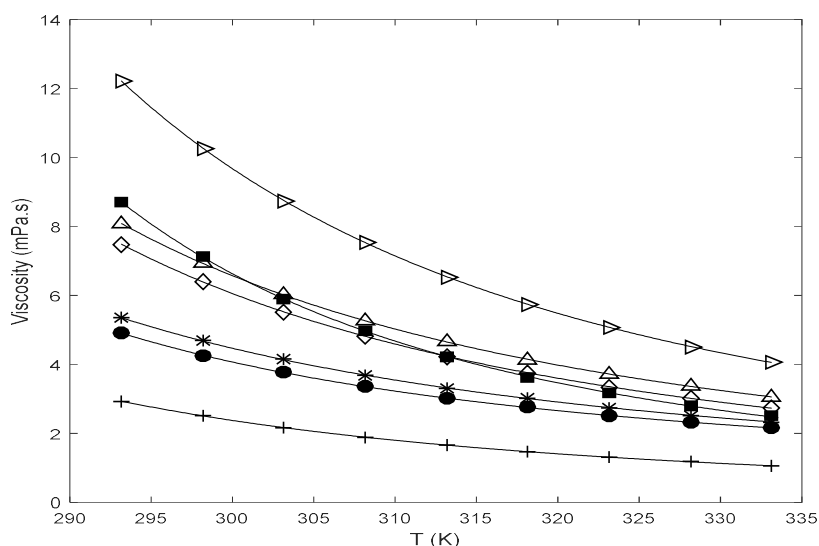
Figure 7-27: Trend analysis showing the effect of temperature on the viscosity of DGA (1) + NMP (2) + bmim[TF$_2$N] (3) mixtures with different mass compositions: $w_1/w_2 = 0.4981/0.5019$ ($\Diamond$), $w_1/w_2 = 0.3102/0.6898$ ($\bullet$), $w_1/w_2/w_3 = 0.2981/0.3096/0.3923$ ($\triangleright$), $w_1/w_2/w_3 = 0.3035/0.4462/0.2503$ ($\triangle$) and $w_1/w_2/w_3 = 0.2840/0.6166/0.0994$ ($\ast$); and mixtures of DGA (1) + H$_2$O (2) with mass fractions of $w_1/w_2 = 0.2923/0.7077$ ($+$) and $w_1/w_2 = 0.5132/0.4868$ ($\blacksquare$). Solid line depicts regressed results.
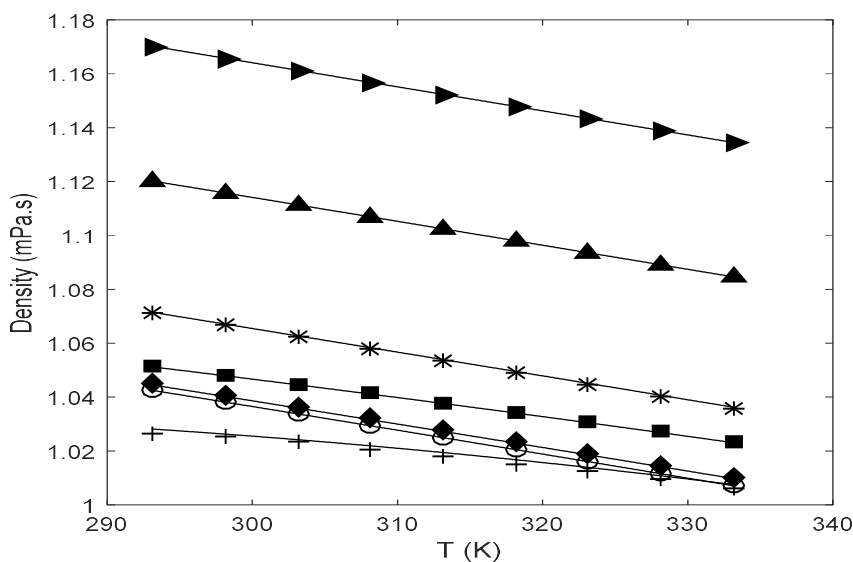

Figure 7-28: Trend analysis showing the effect of temperature on the density of DGA (1) + NMP (2) + bmim[TF$_2$N] (3) mixtures with different mass compositions: $w_1/w_2 = 0.4981/0.5019$ ($\blacklozenge$), $w_1/w_2 = 0.3102/0.6898$ ($\bigcirc$), $w_1/w_2/w_3 = 0.2981/0.3096/0.3923$ ($\blacktriangleright$), $w_1/w_2/w_3 = 0.3035/0.4462/0.2503$ ($\blacktriangle$) and $w_1/w_2/w_3 = 0.2840/0.6166/0.0994$ ($\ast$); and mixtures of DGA (1) + H$_2$O (2) with mass fractions of $w_1/w_2 = 0.2923/0.7077$ ($+$) and $w_1/w_2 = 0.5132/0.4868$ ($\blacksquare$). Solid line depicts regressed results.

7.4.3.3 Measurement of evaporation rate

The evaporation rate of samples listed in Table 7-12 were measured. Figure 7-29 shows the evaporation of sample versus the time at 373.15 K and atmospheric pressure. Experimental data are listed in Table 7-13. The boiling point of NMP (475.15 K) and DGA (494.15 K) are close, thus, the evaporation rates of NMP and DGA were not calculated separately, and only the total average evaporation rate was determined. It is clear from the figure that replacing water with NMP decreases the evaporation rate of samples. The evaporation rate of the water-free 29.23wt.% DGA solution containing NMP is approximately 44% of the evaporation rate of the 29.23 wt.% DGA aqueous solution. Furthermore, the addition of IL to the NMP-containing samples decreases the evaporation rate and the mass loss becomes zero for the IL-containing samples after a period of time. Table 7-13 shows that the final mass of the IL-containing samples is approximately equal to the mass of IL present in the initial loaded sample. Therefore, the loss of IL is almost zero, and the whole initial amount of IL can be recovered and reused.

In conclusion, the NMP-containing DGA solvents outperform the aqueous DGA solutions with regards to solubility. Additionally, replacing water with NMP in the 30% DGA solvent decreases the volatility considerably. The addition of IL also has a positive effect on the volatility, but a high concentration of IL is not recommended because it decreases the solubility. Among all the solvents introduced in this section, the NMP-containing solutions with 30% and 50% of DGA and the NMP-containing 30% DGA solvent with 10% of IL are recommended to extract CO_2.
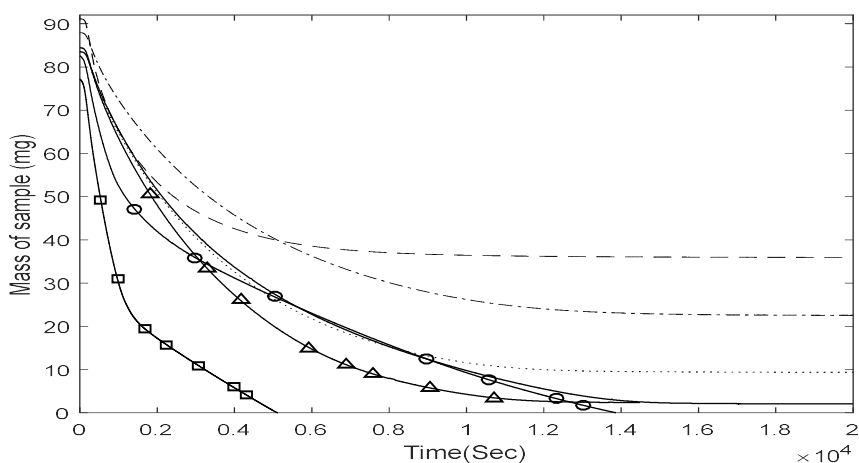
Figure 7-29: Sample mass versus time at a temperature of 373.15 K for DGA (1) + NMP (2) + bmim[TF$_2$N] (3) mixtures with different mass compositions: $w_1/w_2 = 0.4915/0.5085$ (solid line), $w_1/w_2 = 0.2923/0.7077$ ($\triangle$), $w_1/w_2/w_3 = 0.2840/0.6166/0.0994$ (dotted line), $w_1/w_2/w_3 = 0.3035/0.4462/0.2503$ (dash-dot line), $w_1/w_2/w_3 = 0.2981/0.3096/0.3923$ (dashed line); and DGA (1) + H$_2$O (2) mixtures with mass fractions: $w_1/w_2 = 0.5310/0.4690$ ($\bigcirc$), $w_1/w_2 = 0.2923/0.7077$ ($\square$).

Table 7-13: Experimental data describing the samples of DGA (1) + H_2O (2)/(NMP(2) + bmim[TF_2N] (3)) mixtures with different initial mass compositions used for TGA measurements[a].

Sample	initial mass (mg)	Initial DGA (mg)	Initial NMP/water (mg)	Initial IL (mg)	Final mass (mg)	Final point for time (hour)	Total evaporation rate (mg/sec)
$w_1 = 0.5310$, $w_{H2O} = 0.4690$	82.56154	43.83867	38.72286	0.00000	0.00045	3.85	0.00595
$w_1 = 0.4915$, $w_{NMP} = 0.5085$	83.48496	41.03640	42.44856	0.00000	2.07640	5.56	0.00548
$w_1 = 0.2923$, $w_{H2O} = 0.7077$	77.19712	22.56702	54.63010	0.00000	0.00124	1.42	0.01517
$w_1 = 0.2923$, $w_{NMP} = 0.7077$	84.43588	24.67858	59.75729	0.00000	2.36128	4.02	0.00674
$w_1 = 0.2840$, $w_{NMP} = 0.6166$, $W_3 = 0.0994$	83.57021	23.73162	51.52857	8.31001	9.28561	6.94	0.00582
$w_1 = 0.3035$, $w_{NMP} = 0.4462$, $w_3 = 0.2503$	87.93480	26.69060	39.23428	22.00992	22.44307	6.94	0.00456
$w_1 = 0.2981$, $w_{NMP} = 0.3096$, $w_3 = 0.3923$	91.12931	27.16703	28.21118	35.75110	35.85961	6.94	0.00572

[a]Readability = 0.0001 mg, sensitivity = 0.001 mg

7.5 Data modelling results

In order to examine the validity of the method developed in Chapter 6, the solubility of CO_2 and H_2S in five aqueous amines, viz., MEA, DEA, DIPA, MDEA and AMP were modelled and results were compared with the literature values over a wide variety of temperature, pressure and initial concentration of amine. In this section, only some of the results obtained for the MEA + H_2O + CO_2 system are presented. The modelled results for the solubility of CO_2 and H_2S in MEA, DEA, DIPA, MDEA and AMP are explained in Appendix M. In addition, the isothermal solubility data measured for the systems of CO_2 + MEA + H_2O + bmim[OTF] and CO_2 + bmim[BF_4] + NMP were successfully modelled, and the results were discussed in sections 7.3.1 and 7.4.1.

Figures 7-30 to 7-32 present the modelled results compared with experimental data for the MEA + H_2O + CO_2 system with two different initial concentrations of amines viz. w = (0.153 and 0.3). The figures show that there is significant scatter in the data reported in the literature, especially for the system with a high concentration of amine, but the present method is able to give relatively good predictions on the CO_2 solubility. Figure 7-31 displays that although the Deshmukh-Mather activity coefficient model was used in the present method, there is a noticeable difference between the modelled data and the literature data obtained using the Deshmukh-Mather model. Figure 7-32 shows the results predicted with the present model and the results of the original Kent-Eisenberg model which the apparent equilibrium constants reported by Kent and Eisenberg (1976) [135] were used in. Kent and Eisenberg regressed the parameters of apparent equilibrium constants for the MEA + CO_2 system by forcing a fit between the experimental results measured over the 15.3 wt.% MEA aqueous solution. Thus, as it is clear from Figure 7-32, there is an excellent agreement between the experimental data and the results of Kent-Eisenberg model for CO_2 + MEA system with the initial concentration of 15.3 wt.% of MEA.

In order to assess further the validity of the developed method, the solubility of acid gases in pure water was modelled by setting the initial concentration of amine equal to zero as the input of the proposed algorithm. The results shown in Figure 7-33, perfectly match with the experimental data reported in the literature.
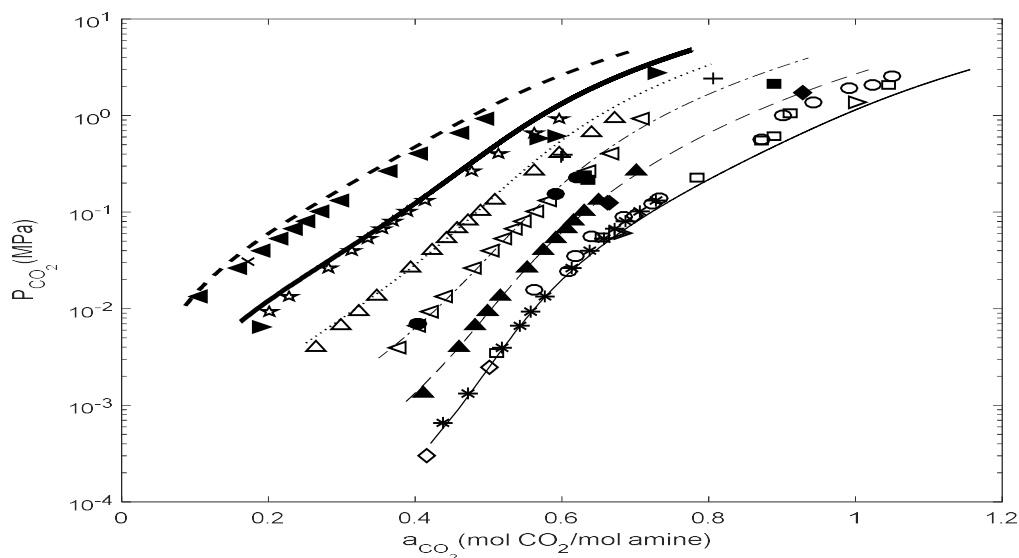
Figure 7-30: Comparison between experimental data [153, 208-211] and modelled results for the solubility of CO_2 in the aqueous 15.3% MEA solution. Exp (literature): Jones et al. at 313.15 K (✳), 333.15 K (▲), 353.15 K (◁), 373.15 K (△), 393.15 K (✳) and 413.15 K (◀) [208]; Shen and Li at 313.15 K (○) [209]; Park et al. at 313.15 K (□) [210]; Austgen and Rochelle at 313.15 K (◇) and 353.15 K (●) [153]; and Lawson and Garst at 313.15 K (▷), 333.15 K (◆), 353.15 K (■), 373.15 K (+), 393.15 K (▶) and 413.15 K (×) [211]. Modelled data (this work): at 313.15 K (solid line), 333.15 K (dashed line), 353.15 K (dash-dot line), 373.15 K (dotted line), 393.15 K (bold solid line) and 413.15 K (bold dashed line).
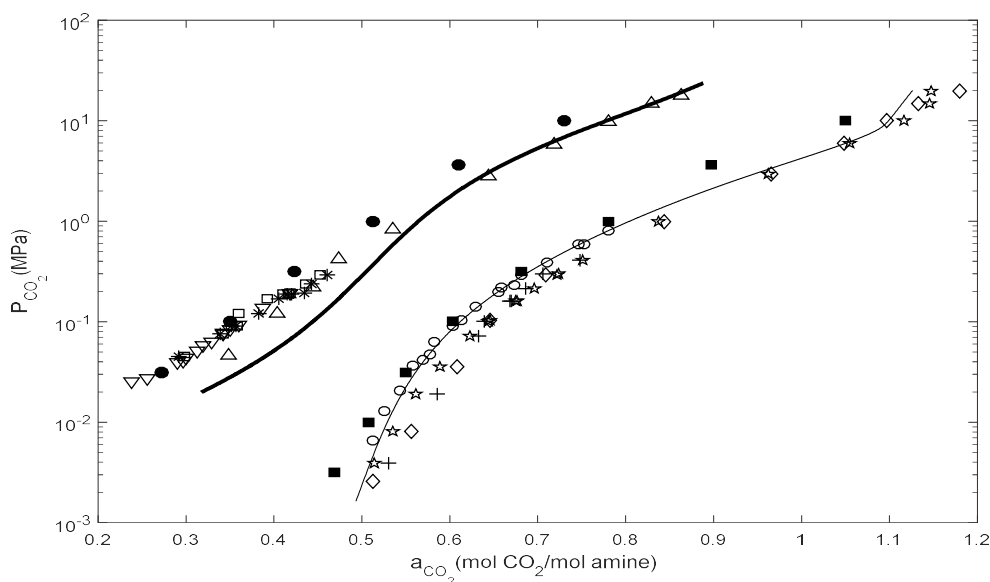
Figure 7-31: Comparison between experimental data [119, 136, 212-214] and modelled results for the solubility of CO_2 in the aqueous 30% MEA solution. Exp (literature): Xu et al. at 313.15 K (○) [213]; Lee et al. at 313.15 K (■) and 393.15 K (●) [214]; Tong et al. at 313.15 K (+) and 393.15 K (✳) [136]; Jou et al. at 313.15 K (◇) and 393.15 K (△) [119]; and Ma'mun et al. 393.15 K (▽) [212]. Deshmukh-Mather model data: Tong et al. at 313.15 K (✳) and 393.1 K (□) [119, 136]. Modelled data (this work): at 313.15 K (solid line) and 393.15 K (bold solid line).
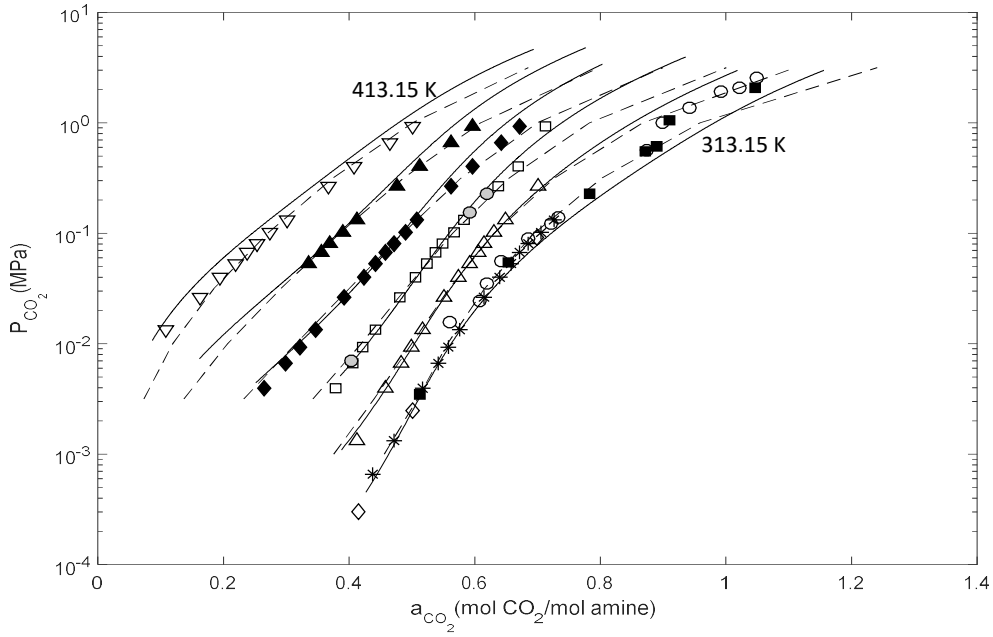
Figure 7-32: Comparison between experimental data [153, 208-210] and modelled results for the solubility of CO_2 in the aqueous 15.3% MEA solution. Exp (literature): Jones et al. at 313.15 K (✳), 333.15 K (△), 353.15 K (□), 373.15 K (◆), 393.15 K (▲) and 413.15 K (▽) [208]; Shen and Li at 313.15 K (○) [209]; Park et al. at 313.15 K (■) [210]; and Austgen and Rochelle at 313.15 K (◇) and 353.15 K (◕) [153]. The solid lines and dashed lines depict results of present model and Kent-Eisenberg model, respectively.
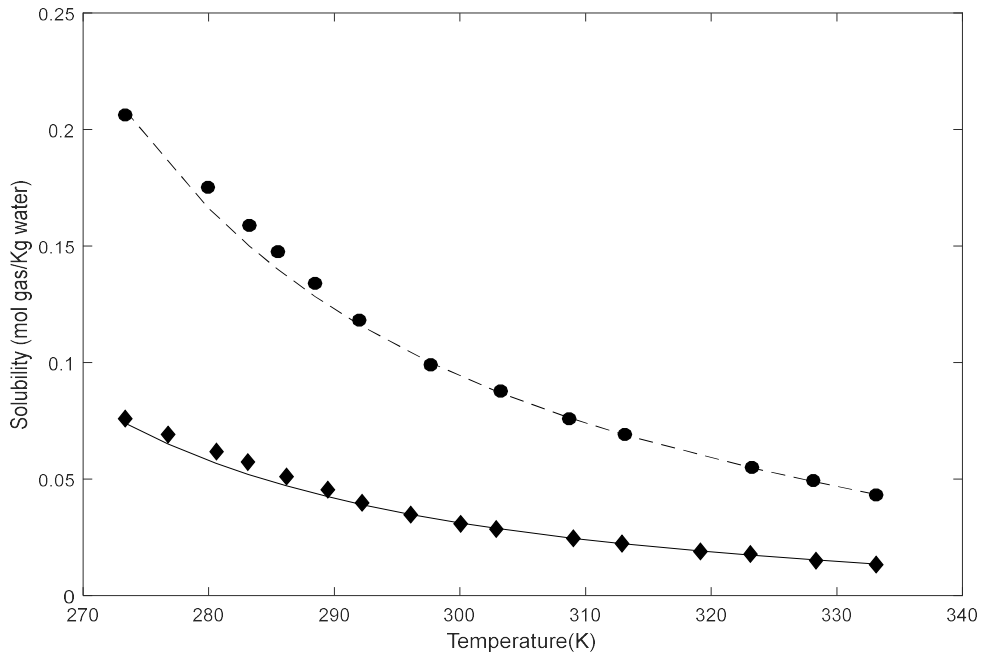
Figure 7-33: Comparison between experimental data and modelled results for the solubility of H_2S and CO_2 in water at 0.101325 MPa. Exp (literature): solubility of CO_2 (◆) and H_2S (●). Lines depict results of present model.

121

Good agreement obtained between the modelled data and that reported in the literature indicates the validity of the modelling method, but the accuracy and deviation of the modelled data are changed in the different systems and conditions. Similar to other rigorous models, the accuracy and convergence of the developed method are strongly dependant on the binary interactions that are mostly considered as a function of temperature. Binary interaction parameters listed in Table G-2 are applicable over a wide range of temperature, pressure and initial concentrations of amine. Considering the dependency of interaction parameters on pressure and initial concentrations of amine could improve the modelled results especially at low pressures where the present model is limited to predict the gas loadings. Similarly, equilibrium constants have an important role in the accuracy of the modelled results. Thus, considering dependency of the equilibrium constants on pressure could improve the results as well.

8. CONCLUSION

To measure the solubility of acid gas in solvents with a high boiling point, a new experimental apparatus based on the static-synthetic method was designed and commissioned. The apparatus has a low volume equilibrium cell (36.29 cm^3) equipped with a depth gauge to measure the volume of liquid phase within the equilibrium cell. The low volume of the equilibrium cell is beneficial for measurements involving chemicals such as ionic liquids which are expensive and/or difficult to synthesize at high purity. The new apparatus and experimental method were assessed by performing three test systems, vis (hexane + CO_2, NMP + CO_2 and bmim[BF$_4$] + CO_2). The measured data agreed well with the data available in the literature. Overall, by the end of test systems measurements, the apparatus had been validated and its accuracy and reproducibility were proved.

The solubility of CO_2 in five new systems viz. (NMP + bmim[BF$_4$], MEA/DGA + water + bmim[OTF] and MEA/DGA + (NMP + bmim[TF$_2$N])/water) was measured in the main work. Experimental measurements also included the evaporation rate, viscosity, density and speed of sound. Besides, the coefficient of thermal expansions, the excess coefficient of thermal expansion, the excess molar volume and the deviation of viscosity of the hybrid solutions were discussed.

The data measured for the NMP + bmim[BF$_4$] + CO_2 system show that the addition of bmim[BF$_4$] to NMP does not improve the ability of solvent to absorb CO_2. On the other hand, it increases the viscosity of solvent. The experimental data were modelled using a flash calculation method with the PR EoS and vdW mixing rule.

The second and third systems were MEA + water + bmim[OTF] + CO_2 and DGA + water + bmim[OTF] + CO_2. The effects of addition of the IL to the aqueous amine solutions were studied. The ratio of solvents contents was done in a manner that water content was reduced, the IL was increased and the amine was constant. Overall, the addition of the IL to amine solvents decreases the CO_2 solubility, but it decreases the solvent volatility as well. The measured data show that the inclusion of 10% of the IL in the aqueous 30% MEA solution and the aqueous 50% DGA solution decreases the CO_2 solubility in these solvents by 0.5% to 4.5% and 3% to 4.5%, respectively. The addition of 10% of the IL to theses solvents is recommended since it reduces the solvent volatility by approximately 50% for the MEA solvents and %25 for the DGA solvents, while the reduced solubility is not considerable.

The fourth system studied was MEA + H$_2$O/(NMP + bmim[TF$_2$N])/bmim[OTF] + CO_2. The aqueous media of the MEA solvents was replaced with bmim[OTF], NMP and NMP + bmim[TF$_2$N] and the results of the free-water MEA solutions were compared with those of the

aqueous MEA solutions. In conclusion, the replacement of the entire water with NMP in the aqueous MEA solvents with 10% or 20% MEA improves the gas solubility and decreases the volatility of solvents. The absorption capacity of the NMP-containing 10% MEA solvent is maximum 81% higher than the aqueous 10% MEA at pressures between 0.213 to 2 MPa. Although the addition of 10% or 25% of bmim[TF_2N] to the NMP-containing MEA solvents decreases the solubility, these IL-containing solvents outperform the aqueous 10% MEA solvents with regards to the solubility of CO_2. The inclusion of 10% of the IL in the NMP-containing MEA solvents is not recommended since it does not improve the solubility and solvent volatility. Given the measured data, the NMP-containing 10% MEA solution, the NMP-containing 10% MEA solvent with 25% of bmim[TF_2N] and the NMP-containing 20% MEA solvent are beneficial to CO_2 extraction compared to the aqueous MEA solvents with 10% or 20% MEA.

The last system was DGA + H_2O / (NMP + bmim[TF_2N]). Similar to the MEA solvents, the water-free DGA solvents were compared with the aqueous ones with different concentrations of amine. At the same condition, the NMP-containing DGA solvents can absorb more CO_2 in comparison to the aqueous DGA solvents. Furthermore, the replacement of entire water with NMP in the aqueous 30% DGA solvent and then the addition of the IL reduce the solvent volatility. Overall, among all the DGA solvents introduced in this section, the NMP-containing solutions with 30% or 50% of DGA and the NMP-containing 30% DGA solvent with 10% of the IL are recommended for CO_2 removal.

A new approach using Kent-Eisenberg and Deshmukh–Mather models was developed to predict the solubility of acid gas in the aqueous amine solution. A comparative study was performed among the modelled results of this work, experimental data and the modelled data reported in the literature to check the validity of proposed method. Agreement between the modelled results and experimental data indicates the accuracy of method followed in this study. But present model with interaction parameters determined in this study is limited to predict gas loading at very low pressures depending on the temperature and initial concentration of amine.

9. RECOMMENDATIONS

This study can be continued in many aspects. The following remarks are recommended to be investigated for future research wok:

- Study the corrosion problems. As previously explained, some of the amines, especially the primary amines, degrade forming the corrosive product. Besides, the presence of water in the amine processes intensify corrosion. Thus, it is recommended to investigate the potential of physical solvents (NMP, bmim[OTF] and bmim[TF_2N]) to reduce the corrosion rates when these are used as additives to the aqueous amine solutions or as a substitute for water in these solutions.

- Study the heat consumption of the gas absorption processes introduced in this project. Aqueous amine processes as chemical absorption processes have high energy consumption compared to the physical absorption processes since they have a high heat of reaction and high heat capacity. Therefore, it is recommended to investigate the energy consumption of chemical-physical processes studied in this thesis. Additionally, there is a need for the heat of absorption and heat capacity data.

- Measure the freezing point data of the hybrid solvents of this study.

- Investigate the kinetics of absorption processes using the hybrid solvents introduced in this study and the potential of these solvents to accelerate the absorption process.

- Perform the H_2S solubility measurements in the hybrid solvents of MEA/DGA + NMP/water + bmim[OTF]/bmim[TF_2N] to determine the selectivity of these solvents toward H_2S.

- Perform the light and heavy hydrocarbons solubility measurements in the hybrid solvents of MEA/DGA + NMP/water + bmim[OTF]/bmim[TF_2N] to compare the loss of hydrocarbons in the conventional absorption processes and the processes introduced in this study.

- Acquisition of further accurate data for the solubility of acid gas (CO_2/H_2S) in hybrid solvents studied in this project at more temperatures and high pressures where there are no experimental data.

- Study the acid gas (CO_2/H_2S) solubility in the hybrid solvents including secondary and tertiary amines.

- It should be mentioned that MEA is used in aqueous solutions with concentrations between 10% and 20 wt.% MEA; and problems such as foaming happen for higher concentrations of amine. On the other hand, the use of MEA solutions with higher concentrations results in lower circulation rates and also lower freezing points. In section 7.4.1, the concentration of MEA was higher than the commonly used concentrations.

During experiments, problems such as foaming were not noticed. It can be because of the viscosity of the hybrid solvents that increases with the addition of ILs. Therefore, the relation between viscosity, surface tension and harmful phenomenon such as foaming, as well as, the potential of ILs to increase the maximum concentration of MEA allowed to be used in industry, avoiding current problems, can be investigated in the future works.

- Improve the modelling approach developed in this study for more complicated systems, such as water-free hybrid solvent + H_2S/CO_2, $H_2S + CO_2$ + hybrid solvents, and aqueous mixture of amines + H_2S/CO_2, etc.

APPENDIX A. COMMON CATIONS AND ANIONS USED IN IL SYNTHESIS

Table A-1: List of common cations and anions [18, 71, 95, 215].

Ion name	Abbreviation	M (g/mol)	Structure
Tetrafluoroborate	BF_4	86.8	
Hexafluorophosphate	PF_6	144.96	
Bis(trifluoromethylsulfonyl)-imide	TF_2N	280.147	
Trifluoromethanesulfonate	OTF	149.070	
Methylsulfate	CH_3SO_4	111.098	
Nitrate	NO_3	62.005	
Acetate	Ac	59.04	
Trifluoroacetate	TFA	113.016	
Tris(pentafluoroethyl)trifluorophosphate	FEP	445.010	
tris(pentafluoroethyl)trifluorophosphate	eFAP	445.0092	
tris(heptafluoropropyl)trifluorophosphate	pFAP	595.032	

Ion name	Abbreviation	M (g/mol)	Structure
tris(nonafluorobutyl)trifluorophosphate	bFAP	745.05	
pentadecafluorooctanoate	$C_7F_{15}CO_2$	413.062	
docusate	doc	444.56	
saccharinate	SAC	466.725	
acesulfame	ACE	163.147	
methide	methide	411.22	
Tricyanomethanide	TCA	90.063	
Lactate or 2-hydroxypropanoate	L	89.070	
Chloride	Cl	35.453	Cl^-
Diethylphosphate	DEP	153.094	
1,3-Dimethylimidazolium; R = CH_3	dmim	97.14	
1-Ethyl-3-methylimidazolium; R = C_2H_5	emim	111.17	
1-Butyl-3-methylimidazolium; R = C_4H_9	bmim	139.22	
1-Pentyl-3-methylimidazolium; R = C_5H_{11}	pmim	153.24	
1-Hexyl-3-methylimidazolium; R = C_6H_{13}	hmim	167.27	
1-octyl-3-methylimidazolium; R = C_8H_{17}	Omim	195.3256	
1-ethyl-2,3-dimethylimidazolium	emmim	125.1922	

Ion name	Abbreviation	M (g/mol)	Structure
1-Methoxymethyl-3-methylimidazolium	C_2Omim	127.16	
1-(2-Methoxyethyl)-3-methylimidazolium	C_3Omim	153.2	
1-(1,1,2,2-Tetrafluoroethyl)-3-methylimidazolium	TFEmim	183.13	
1-Pentafluoroethyl-3-trifluoromethylimidazolium	FEFmim	255.09	
1-N-Butyl-3-methylpyridinium; R = C_4H_9 1-N-hexyl-3-methylpyridinium; R = C_5H_{11}	bmpy hmpy	150.24 164.27	
1-Butyl-1-methylpyrrolidinium	bmpyrr	142.26	
Tetrabutylphosphonium	P(C_4)$_4$	259.43	
1-butylpyridinium	N-bupy	136.215	

APPENDIX B. STUDIES RELATED TO CO_2 + ILs + AMINE + H_2O

Table B-1: A brief review of studies related to CO_2 + IL + amine + H_2O^a.

Absorbent	Composition of solvent	Temperature & pressure	Method	Results	Ref.
bmim[BF$_4$] + MDEA + H$_2$O & bmim[BF$_4$] + MEA + H$_2$O	aqueous amine (50 wt.% water) + 0/ 10/ 25/ 35/ 50/ 100 wt.% IL	318.15 K 0.1−2.7 MPa	magnetic suspension balance (MSB)	*reduction of corrosion rate for MEA by up to 72%. *addition of IL increases viscosity that helps to reduce corrosion. *reduction of the corrosion rate for MDEA is 25% by adding 10 wt.% IL. *absorption capacity (mol CO$_2$/g solvent) of mixtures is between those of aqueous amine and pure IL.	[100]
MDEA + piperazine + bmim[BF$_4$] / bmim[NO$_3$] / bmim[Cl] + H$_2$O	30 wt.% amine + 3 wt.% PZ + 57 wt.% water + 10 wt.% IL 0 - 1MPa	313 to 373 K	drop pressure method using equilibrium cell	*use of ILs especially with fluorinated as additives is helpful in saving energy consumption. *bmim[BF$_4$] as an additive to amine increases the CO$_2$ cyclic capacity (mol CO$_2$/mol amine). *cation and anion of ILs influence the CO$_2$ absorption enthalpy. *the heat of absorption of CO$_2$ can be tailored by the choice of anions of ILs.	[102]

Absorbent	Composition of solvent	Temperature & pressure	Method	Results	Ref.
bmim[OAc] / emim[OcSO$_4$] / bmim[OcSO$_4$] / emim[EtSO4] / bmim[BF$_4$] / bmim[OTf] + MEA & bmim[OAc] / emim[OcSO$_4$] / bmim[OcSO$_4$] / emim[EtSO$_4$] / bmim[BF$_4$] / bmpr[BF$_4$] / bmim[OTf] + MEA + H$_2$O & bmim[OAc] + H$_2$O	30 wt.% amine + 70 wt.% IL 30 wt.% amine + 35 wt.% IL + 35 wt.% water 0 to 100 wt.% IL	298.15 to 338.15 K 0.1 MPa	gasometric apparatus	*formation of heterogeneous mixture for some hybrid solvents of IL + MEA after absorption. *the CO$_2$ absorption capacity is dependent on the composition of solvent. *the increase of temperature increases the rate of absorption, and decreases viscosity. *addition of water decreases the viscosity, and therefore facilitates the application of IL and increases rate of absorption. *addition of water leads to a decreased ability of bmim[OAc]/water systems to capture CO$_2$.	[21]
P$_{66614}$[Bentriz], P$_{66614}$[Benzim], P$_{66614}$[123Triz], P$_{66614}$[124Triz], P$_{66614}$[Im] (reactive ILs) + MEA	Equimolar mixtures	295.15 K 0.1 MPa	gravimetric technique	*presence of MEA improves the CO$_2$ capture ability of some ILs. *presence of MEA decreases the viscosity of ILs. *CO$_2$ absorption into hybrid solvents results in a large increase in viscosity.	[105]
bmim[BF$_4$] + MEA + H$_2$O	C$_{bmim[BF4]}$/ C$_{MEA}$: 0:1, 1:9, 2:8, 4:6, 3:7,5:5. C$_t$: 1 mol/litter.	303.15 to 333.15 K 0.015 MPa	double stirred cell	*absorption capacity of the hybrid absorbent (mole CO$_2$/mol MEA) is higher than that of aqueous MEA, approaching 0.638 mol CO$_2$/mol MEA. *the regenerate rate of mixed absorbent is slightly higher than aqueous MEA solution.	[22]
bmim[BF$_4$] + MEA + H$_2$O	C$_{bmim[BF4]}$/ C$_{MEA}$: 0:1, 1:9, 2:8, 4:6, 3:7,5:5. C$_t$: 1 mol/litter.	303.15 to 333.15 K 0.015 MPa	double Stirred Cell	*IL improves mass transfer of CO$_2$. *values of the enhancement factor and the second-order reaction rate constant for CO$_2$ absorption into mixed solution are higher than those into aqueous MEA.	[216]

Absorbent	Composition of solvent	Temperature & pressure	Method	Results	Ref.
bmim[BF$_4$] + MEA + H$_2$O	40 wt.% IL + 30 wt.% MEA + 30 wt.% H$_2$O	323.15 K 0.1016 MPa	absorption−desorption loop system	*addition of IL decreases the energy consumption for absorbent regeneration by 37.2%. *addition of IL decreases the MEA loss by 67.3%. *no ionic liquid loss. *addition of IL increases slightly CO$_2$removal efficiency.	[103]
bmim[acetate] + MDEA	70 wt.% IL + 30 wt.% MEA & 50 wt.% IL + 50 wt.% MEA +	303.15 to 343.15 K 0.1 to 3.9 MPa	static equilibrium cell	*a rise in the concentration of IL in the hybrid solvent enhances CO$_2$ absorption. *addition of IL decreases the energy required for solvent regeneration.	[97]
MDEA / DEA / DIPA / AMP+ bmim[acetate] + H$_2$O	40 wt.% amine and IL (40 + 0,35 + 5, 30 + 10) + 60 wt.% H$_2$O & 30 wt.% amine + 70 wt.% H$_2$O	323.15 K 0.1 to 4 MPa	static equilibrium cell	* increasing concentration of IL while total concentration of amine and IL are fixed decreases the CO$_2$ molality. *addition of 10 wt. % IL into the fixed concentration of 30 wt. % amine increases the mole fraction of CO$_2$ in the hybrid solvent.	[98]
MDEA + H$_2$O + bmim[BF$_4$]	Aqueous 4 mol/liter MDEA + 0 to 2.02 mol/liter IL	303 to 333 K 0 to 0.110 MPa	*stirred cell reactor *equilibrium cell	*addition of a low concentration of IL into aqueous amine enhances the initial absorption rate. *addition of IL into amine solvent has no considerable effect on the loading capacity of solvent.	[217]
MDEA + H$_2$O + bmim[Ac] / bmim[BF$_4$] / bmim[DCA]	Aqueous 4 mol/liter MDEA + 0 to 2 mol/liter IL	303 to 333 K 0.1 to 0.7 MPa	equilibrium cell	*CO$_2$ loading (mol CO$_2$/kg solvent) decreases with increasing of IL concentration.	[106]

Absorbent	Composition of solvent	Temperature & pressure	Method	Results	Ref.
gua[OTF] + MDEA + H_2O	Aqueous 4 mol/liter MDEA + 1 mol/liter IL	303.2 to 333.2 K 0.5 to 3 MPa	batch reactor cell	*addition of IL into aqueous amine decreases slightly the loading capacity (mol CO_2/total mol of amine and IL)	[218]
gua[FAP] + MDEA + H_2O	Aqueous 4.01 mol/liter MDEA + 0 to 2.011 mol/liter IL & Aqueous 2.01 mol/liter MDEA + 0 to 2.012 mol/liter IL	313.15 to 353.15 K 0 to 3 MPa.	high-pressure equilibrium equipment	*addition of IL into aqueous MDEA decreases the absorption capacity (mol CO_2/total mol of amine and IL). *addition of IL into aqueous amine enhances the absorption rate within a certain limit of IL concentration. *addition of IL into amine solvent can be helpful in reducing the energy consumption for CO_2 capture.	[107]
hmim[TF_2N] + DEA	0.5, 1 and 2 mole DEA/ liter IL	298.15 to 314.15 K	scale gas–liquid/liquid stirred-cell reactor	*the liquid–solid–liquid mass transfer coefficient increases with the increase of CO_2 concentration and with the reduction of the amine concentration.	[108]
N_{1111}[Gly] / N_{2222}[Gly] / N_{1111}[Lys] / N_{2222}[Lys] + MDEA + H_2O	30 wt.% amine + 0/ 5/ 10/ 15/ 30/ 100 wt.% IL & 30/ 50/ 65/ 80/ 100 wt.% IL + H_2O & 15 wt.% amine + 15 wt.% IL + H_2O	298 to 318 K 0.004 to 0.4 MPa	equilibrium cell	*addition of IL into aqueous amine enhances the absorption process and increases absorption rate. *addition of H_2O into IL increases absorption rate. *lysine-based ILs could absorb more CO_2 than glycine-based ILs. *temperature has a slight effect on the absorption of CO_2 in hybrid solvents. *solubility of N_2 in hybrid solvents is very small.	[219]

Absorbent	Composition of solvent	Temperature & pressure	Method	Results	Ref.
$N_{1111}[Gly]$ + MDEA + H_2O	2.5/ 5/ 7.5/ 10/ 12.5/ 15 wt.% IL + 30/ 40/ 50 wt.% MDEA	298.15 K

0.097 MPa | equilibrium cell | *addition of IL into the 30 wt.% MDEA aqueous solvent increases dramatically the absorption rate of CO_2
*similar to the case of 30 wt.% MDEA solution, addition of IL into 40 and 50 wt.% MDEA aqueous solvents enhances the absorption rate, but the absorption rate is lower and it takes longer time to reach the equilibrium state than 30 wt.% MDEA aqueous solution, due to the higher viscosity.
*the increase of IL concentration increases slightly the absorption capacity (mol CO_2/mol amine) | [220] |
| hmim[Tf_2N] + DEA | 0.5, 1 and 2 mol DEA/ liter IL | 298.15 to 314.15 K 0.101 MPa | double jacketed stirred-cell reactor | *during absorption process, precipitation of CO_2-captured carbamate is produced that may result in an efficient CO_2 absorption process. | [221] |
| Emim[Ac] + PZ + H_2O | 30 wt.% PZ + 0/ 10/ 20/ 30 wt.% IL & 20/ 10/ 0 wt.% PZ + 30 wt.% IL | 313.15 to 343.15 K

0 to 1 MPa. | isothermal synthetic method | *addition of PZ enhances highly the absorption capacity (mol CO_2/mol IL) of hybrid solvents.
*Emim[Ac] slightly improves the absorption capacity (mol CO_2/mol amine) of a highly concentrated PZ aqueous solution.
*viscosity of the hybrid solvents is much lower than that of pure Emim[Ac].
*addition of IL into amine solvent is helpful in reducing the energy required for solvent regeneration. | [104] |

Absorbent	Composition of solvent	Temperature & pressure	Method	Results	Ref.
MDEA + N_{1111}[Gly] + H_2O	15/10 wt.% IL + 30 wt.% MDEA & 10 wt.% IL + 40 wt.% MDEA	363, 373, 378 K 0 to 0.3 MPa	apparatus for the thermal regeneration	*CO_2 absorption in regenerated solutions reveals that under same pressure, the absorption capacity of CO_2 increases with an increase in regeneration temperature.	[222]
N_{1111}[Gly] + MDEA + H_2O	2.5 to 20 wt.% IL + 30/ 40 wt.% MDEA & 15 wt.% IL + 15/ 40/ 50 wt.% MDEA & 10 wt.% IL + 40 wt.% MDEA	298.15, 308.15, 318.15 K 0 to 0.3 MPa	dual-vessel absorption equilibrium system	*with the rise of IL or MDEA concentration, the density of solvent increases slightly, but the viscosity increases dramatically. *with the increase of MDEA concentration up to a certain value, CO_2 absorption (mol CO_2/g solvent) into hybrid solvent enhances considerably.	[223]
C_2OHmim[DCA] / bmim[DCA] + MEA + H_2O	30 wt.% MEA + 10/ 20/ 30/ 50 wt.% IL	313.15, 333.15 K 0.01 to 0.8 MPa	absorption apparatus using equilibrium cell	*addition of IL into amine solvent decreases solubility (mol CO_2/mol amine)	[213]
mmim[dmp] / emim[dep] + MDEA + H_2O	0 to 0.2 mole fraction MDEA + 1 to 0.1 mole fraction IL + 0 to 0.7 mole fraction water	293.15 to 343.15 K 0.1 MPa	*densimeter *tensiometer *rheometer	*with increase of mmim[dmp] concentration, viscosity, density and surface tension of hybrid solvent increase *with increase of emim[dep], viscosity and density increase but the surface tension of solvent decreases.	[224]

Absorbent	Composition of solvent	Temperature & pressure	Method	Results	Ref.
hmim[Tf$_2$N] + MDEA	0 to 1 mole fraction of IL	303.15 to 323.15 K	*densimeter *viscometer *refractometer	*with increasing IL concentration up to 0.5012, the viscosity of hybrid solvent decreases, but after that viscosity increases with rising mole fraction of IL	[99]
HE$_3$MA[LAC] / 3HEMA[MS] + H$_2$O		303 K 2.5 MPa	classical molecular dynamics simulations	*addition of water to the CO$_2$–ionic liquid systems results in remarkable ion–water interactions, especially strong for the LAC and MS anions. *CO$_2$ absorption should not be remarkably affected by the presence of water.	[225]
bmim[BF$_4$] + MDEA + H$_2$O	Aqueous 4 mol/litre MDEA + 0/ 0.2/ 0.5/ 1/ 1.5/ 2 mol/litre IL	303 to 333 K	stirred cell reactor	*addition of IL into aqueous amine solution leads to a significant reduction in the activation energy.	[101]
beim[BF$_4$] / bmim[BF$_4$] + MDEA/MEA	30 wt.% amine + ionic liquid	298, 308, 318 K	* stirred round-bottom flask cell. * electronic analytical balance to detect weight change (the absorbed CO$_2$)	the CO$_2$ absorption performance of ionic liquids is increased via adding amines	[59]

Absorbent	Composition of solvent	Temperature & pressure	Method	Results	Ref.
MEA / TEA + hmim[Tf$_2$N] / bmim[BF$_4$] + H$_2$O	30 wt.% MEA + 0/40/40 wt.% bmim[BF$_4$] or 70 wt.% hmim[Tf$_2$N]; 5 wt.% MEA + 90 wt.% bmim[BF$_4$]; 5 wt.% TEA + 90 wt.% bmim[BF$_4$]	323 K	Ab-desorption loop system having two columns	*addition of IL into aqueous amine solution decreases thermal energy required by CO$_2$ desorption. *addition of bmim[BF$_4$] to the MEA aqueous solution decreases MEA and water losses by reducing the vapour pressure of the hybrid absorbent. *effects of O$_2$ and SO$_2$ are relatively insignificant for MEA and water losses.	[226]

[a] This information is my own work, and summarised looking at the past 6 year information available in the open literature.

APPENDIX C. OPTIMIZATION PROCEDURE TO ESTIMATE VOLUMES

To obtain the approximate volumes of the equilibrium cell and gas reservoir, uncertainty analysis was done. To this aim, physical system of NMP + CO_2 was selected. The procedure had four parts to calculate uncertainties of solubility of CO_2 in solvent, and total mole fraction of CO_2, with different volumes for equilibrium cell and gas reservoir. Uncertainties were compared with literature data and finally the lowest volumes that can produce accurate and reliable phase equilibrium data were determined. Four computational steps are explained in the following.

1) First part is to calculate x_i, y_i at T_{eq} and P_{eq} and molar volumes of gas and liquid phase, v_L, v_V. Algorithm is illustrated in Figure C-1.

Inputs: Teq, Peq, overall composition (z), acentric factor (ω), critical temperature and pressure (Tc & Pc), molecular weights (M_i), interaction coefficients ($\overline{k_{ij}}$).
Calculate parameters of PR EOS, a_i and b_i, for each component (equations 6-16 and 6-18).
Estimate initial equilibrium ratio of the ith component, k_i, (equation 6-2).

Calculate the n_V and n_l which are the mole fraction of the mixture in the liquid and gas phases, respectively (equation 6-5 to 6-10).
Calculate PR EOS parameters of gas and liquid phases, then Z_V and Z_L (equation 6-11 to 6-15).
Calculate the fugacity and fugacity coefficient for each component in each phase (equation 6-19 to 6-23).

Is $\left| f_i^L - f_i^V \right| < \varepsilon$ true for each component?

NO

Consider new K_i:

$$(k_i)^{k+1} = (\frac{f_i^L}{f_i^V} \, k_i)^k$$

YES

Calculate molar volume of gas and liquid phase:

$$v_V = \frac{RT_{eq}Z_v}{P_{eq}}$$

$$v_L = \frac{RT_{eq}Z_L}{P_{eq}}$$

Figure C-1: Flow diagram to calculate phase composition and molar volumes at equilibrium state (part 1) [130-132].

2) Second part is to calculate the volume of the equilibrium cell, as a function of total moles of CO_2 loaded into the equilibrium cell at Teq, Peq and a certain amount of solvent. Algorithm is illustrated in Figure C-2.

Inputs:
Mass of solvent (NMP), for example: 20 g

Total moles of CO_2 existing in the cell when z_{CO_2} changes from 0.002 to 0.9, and mass of solvent is constant

Calculate the total moles in gas and liquid phase:

$$n_{gas} = \frac{n_t z_1 - n_t x_1}{y_1 - x_1}$$

$$n_{liquid} = n_t - n_{gas}$$

$$V_{cell} = n_{liquid} v_L + n_{gas} v_V$$

Thus, V_{cell} at different total moles of CO_2 loaded into the cell is obtained as $V_{cell} = f(n_{tCO_2})$. This function is used to calculate n_{tCO2} when the volume of cell is known.

Figure C-2: Flow diagram to calculate the volume of equilibrium cell, as a function of total moles of CO_2 (part 2).

3) Third part is to calculate the uncertainty of overall composition of CO_2, $U(z_1)$. n_{NMP}, T_{GR} and V_{GR} are known. n_{tCO_2} is calculated using algorithm of part 2 at certain V_{cell}, T_{eq}, P_{eq} and n_{NMP}. The pressure of the gas reservoir before loading CO_2 into the equilibrium cell, P_1, is known and has different values. Algorithm is illustrated in Figure C-3.

Inputs:

T_{GR}, V_{GR}, n_{NMP}, V_{cell}, T_{eq}, P_{eq}, n_{tCO_2}, P_1= [4, 6, 8, 10, 12, 14, 16, 20, 22, 25, 30] bar

Uncertainty of the mass of solvent loaded into the equilibrium cell = $u\ (m_2)$ = 0.02 g

Uncertainty of the volume of gas reservoir = $u(V)$ = 0.5 mL

Uncertainty of the temperature of gas reservoir = $u(T)$ = 0.05 K

Uncertainty of compressibility factor of gas phase = $u(Z)$ = 0.002

Uncertainty of the pressure of gas reservoir = $u(P)$ = 0.008 bar

---

Calculate the moles of CO_2 in gas reservoir before loading CO_2 into the cell equilibrium:

$$n_1 = \frac{P_1 V_{GR}}{Z_1 R T_{GR}}$$

While, Z_1 is calculated from PR EOS.

n_2 is the moles of CO_2 in the gas reservoir after loading CO_2 in to the equilibrium cell:

$$n_2 = n_1 - n_{tCO_2 injected}$$

$$n_{tCO_2 injected} = n_{tCO_2} - n_{tCO_2}^0$$

$n_{tCO_2}^0$ is moles of CO_2 in the equilibrium cell from previous step. It is equal to zero in the first step. $n_{tCO_2 injected}$ is total moles of CO_2 injected into the equilibrium cell.

Pressure of the gas reservoir after loading, P_2:

$$P_2 = n_2 * \frac{Z_2 R T_{GR}}{V_{GR}}$$

Z_2 is not known and is a function of P_2. Assume $Z0_2 = Z_1$

Calculate $P0_2$:

$$P0_2 = n_2 * \frac{Z0_2 R T_{GR}}{V_{GR}}$$

Calculate Z_{New} using PR EOS and $P0_2$. If $| Z_{New} - Z0_2| \leq \varepsilon$ is true, $Z_2 = Z0_2$ and P_2 is:

$$P_2 = n_2 * \frac{Z_2 R T_{GR}}{V_{GR}}$$

Otherwise, repeat calculation with: $Z0_2 = Z_{New}$

Calculate $f_{P1}, f_{P2}, f_{Vgasbomb}, f_T, f_{Z1}, f_{Z2}$ from:

$$n_{tCO_2 injected} = \frac{V_{GR}}{R T_{GR}} \left(\frac{P_1}{Z_1} - \frac{P_2}{Z_2} \right) = f(P_1, P_2, T, V_{GR}, Z_1, Z_2)$$

Calculate the uncertainty of $n_{tCO_2 injected}$:

$$u(n_{tCO_2 injected})$$
$$= \sqrt{(f_{P1} * u(P_1))^2 + (f_{P2} * u(P_2))^2 + (f_{V_{GR}} * u(V_{GR}))^2 + (f_T * u(T_{GR}))^2 + (f_{Z1} * u(Z_1))^2 + (f_{Z2} * u(Z_2))^2}$$

Calculate the uncertainty of total mole of CO_2 in the cell while:

$$n_{tCO_2} = n_{tCO_2 injected} + n_{tCO_2}^0 = h$$

$$u(n_{tC\,2}) = \sqrt{(h_{n_{tCO_2}^0} * u(n_{tCO_2}^0))^2 + (h_{n_{tCO_2 injected}} * u(n_{tCO_2 injected}))^2}$$

Finally calculate the uncertainty in overall composition of CO_2:

$$z_{CO_2} = \frac{n_{tCO_2}}{(n_{tCO_2} + \frac{mass_{NMP}}{Mw_{NMP}})} = g$$

$$u(z_{CO_2}) = \sqrt{(g_{n_{tC\,2}} * u(n_{tCO_2}))^2 + (g_{mass_{NMP}} * u(mass_{NMP}))^2}$$

$$U(z_{CO_2}) = 2 * u(z_{CO_2})$$

Figure C-3: Flow diagram to calculate the uncertainty of overall composition of CO_2 (part 3).

4) Fourth part is to calculate the uncertainty of solubility of CO_2 in solvent, $u(a_{CO_2})$. Algorithm is illustrated in Figure C-4.

Inputs:

T_{eq}, n_{NMP}, V_{cell}, V_L, P_{eq}

$V_V = V_{cell} - V_L$

Uncertainty of the volume of cell = *0.5 mL*

Uncertainty of T_{eq} = *0.05 K*

Uncertainty of the volume of liquid phase = *0.5 ml*

Uncertainty of total moles of CO_2 = $u(n_{tCO_2})$

Uncertainty of compressibility factor of gas phase, *u(Z) = 0.002*

Calculate the moles of CO_2 in the gas phase within the cell:

$$n_{gas} = \frac{P_{eq}V_V}{ZR\ _{eq}}$$

Z is calculated from PR EOS at P_{eq} and T_{eq}.

Thus, the solubility of the gas in solvent is:

$$a_{CO_2} = \frac{n_{tCO_2} - n_{gas}}{\left(\frac{mass_{NMP}}{M_{NMP}}\right)}$$

Obtain the uncertainty of a_{CO_2} as follow:

$$u(V_V) = \sqrt{(u(V_{cell}))^2 + u(V_L)^2}$$

If $\quad n_{gas} = \frac{P_{eq}V_V}{ZR\ _{eq}} = f$

$$u(n_{gas}) = \sqrt{(f_{P_{eq}} * u(P_{eq}))^2 + (f_{V_V} * u(V_V))^2 + (f_{T_{eq}} * u(T_{eq}))^2 + (f_Z * u(Z))^2}$$

And if:

$$a_{CO_2} = \frac{n_{tCO_2} - n_{gas}}{\left(\frac{mass_{NMP}}{M_{NMP}}\right)} = g$$

$$u(a_{CO_2}) = \sqrt{(g_{n_{tCO_2}} * u(n_{tCO_2}))^2 + (g_{n_{gas}} * u(n_{gas}))^2 + (g_{mass_{NMP}} * u(mass_{NMP}))^2}$$

$$U(a_{CO_2}) = 2 * u(a_{CO_2})$$

Figure C-4: Flow diagram to calculate the uncertainty of solubility of CO_2 (part 4).

APPENDIX D. UNCERTAINTY ANALYSIS

The combined uncertainty of the measured variable (Θ) showing temperature, pressure or volume measurement, can be estimated by [113]:

$$u_c^2(\Theta) = \sum_i u_i^2(\Theta) \tag{D-1}$$

Where $u_c(\Theta)$ is the combined uncertainty of Θ and $u_i(\Theta)$ is the standard uncertainty for the variable Θ due to the non-negligible source of error i present in the Θ measurement; such as an error in calibration correlations.

Based on the above equation and equation 5-7, the uncertainty of the mole fraction of CO_2 in the liquid phase was calculated by inserting equations 5-1 to 5-4 into simple form of equation 5-7 as follows:

$$u_c(x_{CO_2}) = ((\frac{\partial x_{CO_2}}{\partial n_{CO_2}^L})^2 . u_c{}^2(n_{CO_2}^L) + (\frac{\partial x_{CO_2}}{\partial n_{solvent}})^2 . u_c{}^2(n_{solvent}))^{0.5} \tag{D-2}$$

Where:

$$u_c(n_{solvent}) = (2.(\frac{1}{M_{solvent}})^2 . u^2(mass\ balance))^{0.5} \tag{D-3}$$

$$u_c(n_{CO_2}^L) = (u_c{}^2(n_{CO_2}) + u_c{}^2(n_{CO_2}^V))^{0.5} \tag{D-4}$$

Where:

$$u_c(n_{CO_2}^V) = ((\frac{\partial n_{CO_2}^V}{\partial P_{eq}})^2 . u_c{}^2(P_{eq}) + (\frac{\partial n_{CO_2}^V}{\partial V^V})^2 . u_c{}^2(V^V) + (\frac{\partial n_{CO_2}^V}{\partial Z_{eq}})^2 . u^2(Z_{eq}) +$$

$$(\frac{\partial n_{CO_2}^V}{\partial T_{eq}})^2 . u_c{}^2(T_{eq}) + (\frac{\partial n_{CO_2}^V}{\partial y_{CO_2}})^2 . u_c{}^2(y_{CO_2}))^{0.5} \tag{D-5}$$

And:

$$u_c(n_{CO_2}) = ((\frac{\partial n_{CO_2}}{\partial P_1})^2 . u_c{}^2(P_1) + (\frac{\partial n_{CO_2}}{\partial V_{GR}})^2 . u_c{}^2(V_{GR}) + (\frac{\partial n_{CO_2}}{\partial Z_1})^2 . u^2(Z_1) +$$

$$(\frac{\partial n_{CO_2}}{\partial T_1})^2 . u_c{}^2(T_1) + (\frac{\partial n_{CO_2}}{\partial P_2})^2 . u_c{}^2(P_2) + (\frac{\partial n_{CO_2}}{\partial Z_2,})^2 . u^2(Z_2) + (\frac{\partial n_{CO_2}}{\partial T_2})^2 . u_c{}^2(T_2))^{0.5} \tag{D-6}$$

APPENDIX E. KENT-EISENBERG MODEL

Equations 6-28 to 6-32 describe CO_2 + MEA system equilibrium. The apparent equilibrium constants for reaction 6-28 and 6-32 are expressed in terms of concentrations only, as follow [135]:

$$K_1' = \frac{c'_{RR'R''N} \cdot c'_{H^+}}{c'_{RR'R''NH^+}} = A + \frac{B}{T} + \frac{C}{T^2} + \frac{D}{T^3} + \frac{E}{T^4} \tag{E-1}$$

$$K_5' = \frac{c'_{HCO_3^-} \cdot c'_{RR'R''N}}{c'_{R'R''NCOO^-}} = A + \frac{B}{T} + \frac{C}{T^2} + \frac{D}{T^3} + \frac{E}{T^4} \tag{E-2}$$

Where c_i is the molarity (mol/liter solution) of species i. K_1' and K_5' are the apparent equilibrium constants regressed as a function of temperature with parameters determined by forcing a fit with the experimental data. Equilibrium constants of reactions 6-29 to 6-31 and equation 6-35 are set to be equal to those of an ideal solution as follows [135, 227]:

$$K_2 = c'_{OH^-} \cdot c'_{H^+} \tag{E-3}$$

$$K_3 = \frac{c'_{H^+} \cdot c'_{HCO_3^-}}{c'_{CO_2}} \tag{E-4}$$

$$K_4 = \frac{c'_{H^+} \cdot c'_{CO_3^{2-}}}{c'_{HCO_3^-}} \tag{E-5}$$

$$P \cdot y_{CO_2} = P_{CO_2} = c'_{CO_2} \cdot H^c_{CO_2} \tag{E-6}$$

Thus, the literature values for equilibrium constants K_2 to K_4 and Henry's law constants are used [135, 139, 140]. Equations E-1 to E-6, 6-43 and 6-44 are reduced into fewer equations, and finally solubility of CO_2 in aqueous MEA is determined using equation 6-45.

APPENDIX F. PARAMETERS REQUIRED FOR HENRY'S CONSTANTS AND EQUILIBRIUM CONSTANTS OF CHEMICAL REACTIONS

Table F-1: Parameters required for equation 6-55 (molality based) [136, 144, 160, 164, 167, 228]

$$\ln(K_i \text{ or } H_i^m \text{ or } P_{H_2O}^0) = C_1 + \frac{C_2}{T} + C_3.\ln T + C_4 T + \frac{C_5}{T^2} + C_6 T^2$$

	C_1	C_2 (K)	C_3	C_4 (K^{-1})	C_5 (K^2)	C_6 (K^{-2})
K_1 (MEA)	-38.846	-17.3	0	0.05764	0	0
K_1 (MDEA)	-79.474	-819.7	10.9756	0	0	0
K_1 (AMP)	-18.0751	-4317.27	1.88	0	0	0
K_1 (DEA)	-48.7594	- 3071.15	6.776904	0	0	0
K_1 (DIPA)	-9.279	-4214.076	0	0.0099612	0	0
K_2	140.932	-13445.9	-22.4773	0	0	0
K_3	235.482	-12092.1	-36.7816	0	0	0
K_4	175.360	-7230.60	-30.6509	0.0131478	-3.72805×10^5	0
K_5 (MEA)	2.151	-1545.3	0	0	0	0
K_6 (T=>373.15) K_6 (T=<373.15)	461.7162 210.8976	-18034.72 -1.2358×10^4	-78.07186 -32.5337	0.0919824 0	0 0	0
K_7	-214.5592	-406.0035	33.88898	-0.05411082	0	0
$H_{CO_2}^m (kg.\frac{MPa}{mol})$	192.876	-9624.4	-28.749	0.01441	0	0
$H_{H_2S}^m (kg.\frac{MPa}{mol})$	340.305	-13236.8	-55.0551	0.0595651	0	0
$10^6 P_{H_2S}^0$ (MPa)	72.55	-7206.7	-7.1385	0	0	0.4046×10^{-5}

APPENDIX G. INTERACTION PARAMETERS

Table G-1: Binary interaction parameters, critical parameters, and acentric factors required in Peng Robinson equation (equation 6-60 and 6-68) [53].

Species i and j	H_2O	H_2S	CO_2	$P_c(MPa)$	$T_c(K)$	ω
H_2O	0	0.5	0.5	22.055	647.13	0.344861
H_2S	0.5	0	0.097	8.9629	373.53	0.0941677
CO_2	0.5	0.097	0	7.376	304.20	0.225

Table G-2: Ions or molecules binary interaction parameters required for equation 6-56 [136, 137, 152, 160, 174, 175].

Species interactions	$\beta_{ij}\ (kg\ water/mol)$	Species interactions	$\beta_{ij}\ (kg\ water/mol)$
$CO_2 - CO_3^{2-}$	0.489	$HCO_3^- - H^+$	0.071
$CO_2 - MEA$	$-0.171 + 2.086 \times 10^{-4} \times T$	$MEACOO^- - CO_3^{2-}$	-0.26
$HCO_3^- - CO_3^{2-}$	7.816×10^{-3}	$OH^- - CO_3^{2-}$	0.054
$HCO_3^- - MEAH^+$	$-0.192 + 4.140 \times 10^{-4} \times T$	$OH^- - H^+$	0.208
$CO_2 - MEACOO^-$	-0.12	$CO_2 - MEAH^+$	$0.000125 \times T - 0.03914375$
$HCO_3^- - MEACOO^-$	$-0.00218 \times T + 0.701101$	$MDEA - HCO_3^-$	-0.01379
$HCO_3^- - OH^-$	4.2815×10^{-3}	$MDEAH^+ - HCO_3^-$	$0.0000233 \times T - 0.009206833$
$CO_3^{2-} - MEA$	-0.202	$HS^- - S^{2-}$	0.081
$CO_3^{2-} - MEAH^+$	-0.328	$HS^- - H^+$	0.194
$MEA - HCO_3^-$	-1.1226×10^{-3}	$HS^- - OH^-$	0.162
$MEA - MEAH^+$	12.493×10^{-3}	$H^+ - S^{2-}$	0.127
$MEA - MEACOO^-$	1.1159×10^{-3}	$OH^- - S^{2-}$	0.095
$MEA - H^+$	-3.8228×10^{-3}	$H^+ - H_2S$	0.017
$MEA - OH^-$	-1.8050×10^{-3}	$OH^- - H_2S$	$0.26 - 1.72 \times 10^{-3} \times T + 3.07 \times 10^{-6} \times T^2$
$MEAH^+ - MEACOO^-$	$-0.001529 \times T + 0.45343405$	$AMP - AMPH^+$	-0.024549
$MEAH^+ - H^+$	-1.1601×10^{-3}	$AMP - HS^-$	$0.00266667 \times T - 0.93506667$

Species interactions	β_{ij} (kg water/mol)	Species interactions	β_{ij} (kg water/mol)
$MEAH^+ - OH^-$	0.23100×10^{-3}	$AMPH^+ - HS^-$	$0.00285 \times T - 0.9634775$
$MEACOO^- - H^+$	7.5028×10^{-3}	$AMPH^+ - H_2S$	$-0.0012 \times T + 0.33778$
$MEACOO^- - OH^-$	6.0378×10^{-3}	$AMP - HCO_3^-$	$0.00475 \times T - 1.5924625$
$MEAH^+ - HS^-$	$-0.00035 \times T + 0.0986025$	$DEA - HCO_3^-$	0.1
$MDEAH^+ - MDEA$ $T < 393.15\ K$	$0.000663806 \times T - 0.16$	$DEA - CO_3^{2-}$	0.2
$MDEAH^+ - MDEA$ $T > 393.15\ K$	$-0.0009 \times T + 0.4537$	$DEAH^+ - CO_2$	0.03
$MDEAH^+ - H_2S$	$0.000125 \times T - 0.11914375$	$DEAH^+ - CO_3^{2-}$	$-0.63853273 + 0.068298236 \times m_A^t$
$MDEAH^+ - HS^-$	$0.000594642 \times T - 0.191783582$	$DEAH^+ - HCO_3^-$	-0.03
$MDEAH^+ - CO_2$	-0.08868	$DEA - DEAH^+$	-0.207674
$CO_3^{2-} - H^+$	5.7164×10^{-3}	$DEA - HS^-$	0.141
$DEAH^+ - H_2S$	$a \times T + b$ $a = 0.0003977 m_A^{t\,2} - 0.002185 m_A^t + 0.0001699$ $b = -0.1142 m_A^{t\,2} + 0.5962 m_A^t + 0.1286$	$DEAH^+ - HS^-$	$a \times T + b$ $a = -0.0005787 m_A^{t\,2} - 0.003271 m_A^t - 0.001549$ $b = 0.2747 m_A^{t\,2} - 1.756 m_A^t + 1.741$
$AMPH^+ - CO_2$	$-0.0021667 \times T + 0.708491667$	$DEA - H_2S$	-0.05
$AMPH^+ - HCO_3^-$	$0.00275 \times T - 0.9311625$	$DIPAH^+ - CO_2$	$0.03119 \times m_A^t - 0.1881$
$DIPAH^+ - DIPA$	$0.0227 \times m_A^t - 0.11525$	$DIPAH^+ - HCO_3^-$	$-0.0104 \times m_A^t + 0.1327$
$[OTF]^- - HCO_3^-$	$a \times T + b$ $a = 0.00004427 C_{IL}^t(w\%) - 0.004413$ $b = -0.013196017 C_{IL}^t + 1.20542$	$[OTF]^- - CO_2$	-0.09
$[OTF]^- - MEAH^+$	0.35	$[OTF]^- - MEACOO^-$	-0.08

APPENDIX H. TABULATED EXPERIMENTAL VAPOUR-LIQUID EQUILIBRIUM DATA

H.1 Tabulated test system vapour-liquid equilibrium data

Table H-1: Experimental (exp) and modelled (model) data for the solubility of CO_2 in n-hexane, including the measured temperature (T), pressure (P), volume of gas phase (V_V), total number of moles of solvent ($n_{solvent}$), number of moles of CO_2 (n_{CO_2}), total mole fraction of CO_2 (z_{CO_2}) and mole fraction of CO_2 in liquid phase(x_{CO_2}), including the expanded uncertainties ($k = 2$), $U(T) = 0.02$ K, $U(P) = 0.002$ MPa.

T (K)	P(MPa)	V_V(cm^3)	n_{CO_2}(mol)	$n_{solvent}$ (mol)	z_{CO_2}	$U(z_{CO_2})$	$x_{CO_2}^{exp}$	$U(x_{CO_2})$	$x_{CO_2}^{model}$
313.19	0.345	5.81	0.0079	0.2263	0.0339	0.0006	0.0310	0.0006	0.0322
313.22	0.450	10.17	0.0101	0.1948	0.0491	0.0007	0.0414	0.0007	0.0431
313.19	0.515	5.62	0.0126	0.2263	0.0527	0.0009	0.0485	0.0009	0.0499
313.22	0.672	9.88	0.0158	0.1948	0.0750	0.0010	0.0640	0.0011	0.066
313.22	0.731	7.29	0.0181	0.2122	0.0786	0.0011	0.0705	0.0012	0.0722
313.22	0.760	5.17	0.0195	0.2277	0.0790	0.0010	0.0734	0.0011	0.0752
313.19	0.929	5.00	0.0246	0.2263	0.0981	0.0013	0.0916	0.0014	0.0926
313.22	0.981	9.46	0.0244	0.1948	0.1112	0.0015	0.0964	0.0016	0.0980
313.23	1.105	6.74	0.0290	0.2122	0.1201	0.0017	0.1093	0.0018	0.1106
313.22	1.145	4.60	0.0312	0.2277	0.1204	0.0012	0.1134	0.0013	0.1147
313.19	1.331	4.30	0.0373	0.2263	0.1416	0.0021	0.1341	0.0021	0.1338
313.21	1.681	3.65	0.0493	0.2277	0.1778	0.0015	0.1703	0.0016	0.1695
313.19	1.798	3.41	0.0537	0.2263	0.1918	0.0033	0.1844	0.0034	0.1814
313.23	1.838	5.40	0.0532	0.2122	0.2005	0.0036	0.1880	0.0037	0.1855
313.17	2.122	2.74	0.0664	0.2263	0.2268	0.0046	0.2203	0.0049	0.2144
313.18	2.310	3.78	0.0726	0.2177	0.2500	0.0050	0.2403	0.0051	0.2336
313.23	2.494	4.01	0.0790	0.2122	0.2714	0.0055	0.2604	0.0057	0.2521
313.21	2.572	7.09	0.0787	0.1920	0.2908	0.0055	0.2719	0.0058	0.2601
313.20	2.802	1.58	0.0967	0.2277	0.2981	0.0026	0.2934	0.0027	0.2836

Table H-2: Experimental (exp) and modelled (model) data for the solubility of CO_2 in NMP, including the measured temperature (T), pressure (P), volume of gas phase (V_V), total number of moles of solvent ($n_{solvent}$), number of moles of CO_2 (n_{CO_2}), total mole fraction of CO_2 (z_{CO_2}) and mole fraction of CO_2 in liquid phase(x_{CO_2}), including the expanded uncertainties ($k = 2$) $U(T) = 0.02$ K, $U(P) = 0.002$ MPa.

T (K)	P(MPa)	V_V(cm^3)	n_{CO_2}(mol)	$n_{solvent}$ (mol)	z_{CO_2}	$U(z_{CO_2})$	$x_{CO_2}^{exp}$	$U(x_{CO_2})$	$x_{CO_2}^{model}$
298.14	0.130	13.63	0.0050	0.2323	0.0211	0.0005	0.0182	0.0005	0.0192
298.14	0.158	14.07	0.0063	0.2323	0.0263	0.0005	0.0226	0.0005	0.0234
298.14	0.214	9.13	0.0096	0.2813	0.0330	0.0006	0.0303	0.0006	0.0315
298.16	0.274	9.17	0.0125	0.2799	0.0427	0.0006	0.0393	0.0006	0.0404
298.16	0.319	6.06	0.0156	0.3118	0.0476	0.0007	0.0453	0.0007	0.0470
298.15	0.356	8.83	0.0164	0.2813	0.0550	0.0007	0.0509	0.0007	0.0523
298.18	0.376	9.35	0.0173	0.2781	0.0585	0.0005	0.0539	0.0005	0.0552
298.20	0.509	7.06	0.0252	0.2958	0.0784	0.0009	0.0741	0.0009	0.0745
298.17	0.558	9.78	0.0259	0.2706	0.0872	0.0007	0.0802	0.0008	0.0815
298.18	6.043	8.87	0.0285	0.2781	0.0928	0.0007	0.0861	0.0008	0.0881
298.16	0.684	8.40	0.0329	0.2799	0.1053	0.0009	0.0983	0.0009	0.0996
298.14	0.702	8.23	0.0338	0.2813	0.1072	0.0010	0.1002	0.0010	0.1021
298.13	0.758	12.65	0.0324	0.2323	0.1223	0.0011	0.1087	0.0011	0.1100
298.19	0.836	6.39	0.0430	0.2958	0.1268	0.0011	0.1210	0.0011	0.1210
298.17	0.887	8.66	0.0430	0.2730	0.1361	0.0010	0.1271	0.0011	0.1283
298.18	0.922	8.20	0.0451	0.2781	0.1396	0.0012	0.1310	0.0012	0.1332
298.17	0.943	8.99	0.0457	0.2706	0.1444	0.0012	0.1333	0.0012	0.1361
298.14	1.083	7.39	0.0546	0.2813	0.1626	0.0014	0.1539	0.0015	0.1556
298.15	1.142	12.42	0.0512	0.2323	0.1805	0.0017	0.1624	0.0018	0.1639
298.17	1.213	7.57	0.0616	0.2781	0.1814	0.0016	0.1717	0.0016	0.1737
298.13	1.280	6.94	0.0661	0.2813	0.1903	0.0017	0.1812	0.0018	0.1829
298.15	1.307	7.01	0.0679	0.2799	0.1953	0.0018	0.1860	0.0018	0.1866
298.17	1.352	8.08	0.0690	0.2706	0.2032	0.0020	0.1918	0.0021	0.1927

T (K)	P(MPa)	V_V(cm^3)	n_{CO_2}(mol)	$n_{solvent}$ (mol)	z_{CO_2}	$U(z_{CO_2})$	$x_{CO_2}^{exp}$	$U(x_{CO_2})$	$x_{CO_2}^{model}$
298.15	1.500	6.40	0.0797	0.2813	0.2207	0.0021	0.2114	0.0022	0.2130
298.17	1.536	7.67	0.0802	0.2706	0.2287	0.0024	0.2170	0.0025	0.2178
298.15	1.624	6.02	0.0877	0.2813	0.2377	0.0025	0.2286	0.0026	0.2297
298.15	1.748	5.71	0.0960	0.2813	0.2545	0.0029	0.2455	0.0030	0.2464
298.17	1.793	6.92	0.0969	0.2706	0.2636	0.0029	0.2522	0.0030	0.2524
298.17	1.905	6.14	0.1051	0.2730	0.2780	0.0029	0.2677	0.0030	0.2674
313.12	0.290	9.45	0.0099	0.2741	0.0350	0.0005	0.0313	0.0005	0.0322
313.12	0.700	8.87	0.0250	0.2741	0.0836	0.0008	0.0760	0.0008	0.0766
313.15	1.012	8.39	0.0371	0.2741	0.1193	0.0013	0.1095	0.0013	0.1097
313.14	1.362	7.80	0.0515	0.2741	0.1583	0.0018	0.1468	0.0019	0.1460
313.14	1.597	7.42	0.0616	0.2741	0.1835	0.0024	0.1712	0.0025	0.1701
313.15	1.796	7.09	0.0704	0.2741	0.2044	0.0031	0.1918	0.0032	0.1902
313.15	2.031	6.65	0.0813	0.2741	0.2286	0.0038	0.2159	0.0039	0.2136
323.11	0.273	8.44	0.0081	0.2840	0.0278	0.0004	0.0249	0.0004	0.0256
323.15	0.556	8.00	0.0170	0.2840	0.0566	0.0006	0.0512	0.0007	0.0518
323.14	0.867	7.65	0.0272	0.2840	0.0874	0.0010	0.0798	0.0001	0.0800
323.16	1.292	7.04	0.0419	0.2840	0.1287	0.0016	0.1190	0.0017	0.1177
323.14	1.506	6.71	0.0496	0.2840	0.1488	0.0022	0.1384	0.0023	0.1364
323.15	1.750	6.37	0.0586	0.2840	0.1709	0.0029	0.1599	0.0030	0.1574
323.15	2.090	5.84	0.0715	0.2840	0.2010	0.0038	0.1896	0.0040	0.1862
333.16	0.357	12.48	0.0086	0.2404	0.0345	0.0005	0.0281	0.0005	0.0285
333.14	0.678	12.20	0.0168	0.2404	0.0652	0.0010	0.0539	0.0011	0.0537
333.15	1.124	11.77	0.0286	0.2404	0.1062	0.0016	0.0893	0.0017	0.0880
333.16	1.518	11.32	0.0394	0.2404	0.1409	0.0025	0.1202	0.0026	0.1175
333.17	2.018	10.77	0.0540	0.2404	0.1835	0.0039	0.1591	0.0041	0.1542
348.13	0.288	9.08	0.0060	0.2714	0.0216	0.0005	0.0183	0.0005	0.0187

T (K)	P (MPa)	V_V (cm^3)	n_{CO_2} (mol)	$n_{solvent}$ (mol)	z_{CO_2}	$U(z_{CO_2})$	$x_{CO_2}^{exp}$	$U(x_{CO_2})$	$x_{CO_2}^{model}$
348.16	0.732	8.69	0.0159	0.2714	0.0553	0.0009	0.0478	0.0009	0.0470
348.11	1.129	8.30	0.0251	0.2714	0.0845	0.0015	0.0740	0.0015	0.0718
348.17	1.553	7.99	0.0351	0.2714	0.1144	0.0023	0.1011	0.0024	0.0978
348.14	1.960	7.53	0.0450	0.2714	0.1423	0.0035	0.1272	0.0036	0.1222

Table H-3: Experimental (exp) and modelled (model) data for the solubility of CO_2 in bmim[BF$_4$], including the measured temperature (T), pressure (P), volume of gas phase (V_V), total number of moles of solvent ($n_{solvent}$), number of moles of CO_2 (n_{CO_2}), total mole fraction of CO_2 (z_{CO_2}) and mole fraction of CO_2 in liquid phase(x_{CO_2}), including the expanded uncertainties ($k = 2$) $U(T) = 0.02$ K, $U(P) = 0.002$ MPa.

T (K)	P (MPa)	V_V (cm^3)	n_{CO_2} (mol)	$n_{solvent}$ (mol)	z_{CO_2}	$U(z_{CO_2})$	$x_{CO_2}^{exp}$	$U(x_{CO_2})$	$x_{CO_2}^{model}$
298.14	0.145	15.42	0.0037	0.1121	0.0318	0.0011	0.0242	0.0011	0.0222
298.14	0.146	15.98	0.0036	0.1090	0.0324	0.0011	0.0242	0.0011	0.0224
298.15	0.164	15.45	0.0042	0.1126	0.0357	0.0011	0.0271	0.0011	0.0250
298.13	0.177	15.38	0.0045	0.1121	0.0386	0.0015	0.0294	0.0015	0.0270
298.13	0.207	15.90	0.0052	0.1090	0.0455	0.0015	0.0341	0.0015	0.0317
298.15	0.429	15.22	0.0110	0.1126	0.0891	0.0021	0.0688	0.0022	0.0647
298.13	0.496	15.72	0.0125	0.1090	0.1031	0.0017	0.0786	0.0018	0.0746
298.14	0.520	15.76	0.0131	0.1089	0.1074	0.0013	0.0818	0.0014	0.0781
298.14	0.644	14.54	0.0167	0.1148	0.1270	0.0017	0.1001	0.0018	0.0961
298.13	0.650	15.02	0.0167	0.1121	0.1296	0.0018	0.1011	0.0020	0.0969
298.15	0.658	15.03	0.0169	0.1126	0.1305	0.0023	0.1018	0.0025	0.0981
298.14	0.681	15.57	0.0173	0.1090	0.1369	0.0027	0.1054	0.0029	0.1014
298.14	0.952	15.33	0.0243	0.1090	0.1823	0.0030	0.1423	0.0033	0.1399
298.18	1.174	15.26	0.0302	0.1089	0.2172	0.0081	0.1711	0.0091	0.1703
298.14	1.298	15.09	0.0334	0.1090	0.2343	0.0036	0.1855	0.0041	0.1872
298.15	1.396	14.00	0.0369	0.1143	0.2437	0.0043	0.1983	0.0049	0.2004

T (K)	P (MPa)	V_V (cm^3)	n_{CO_2} (mol)	$n_{solvent}$ (mol)	z_{CO_2}	$U(z_{CO_2})$	$x_{CO_2}^{exp}$	$U(x_{CO_2})$	$x_{CO_2}^{model}$
298.13	1.671	14.82	0.0432	0.1090	0.2839	0.0048	0.2278	0.0056	0.2365
298.12	2.128	14.46	0.0556	0.1090	0.3377	0.0066	0.2753	0.0079	0.2943
313.10	0.171	15.29	0.0033	0.1123	0.0283	0.0011	0.0198	0.0011	0.0198
313.14	0.252	15.26	0.0049	0.1123	0.0419	0.0015	0.0296	0.0015	0.0292
313.16	0.493	15.10	0.0098	0.1123	0.0800	0.0019	0.0575	0.0020	0.0564
313.16	0.709	15.01	0.0142	0.1123	0.1121	0.0031	0.0814	0.0033	0.0803
313.17	0.819	14.39	0.0167	0.1148	0.1270	0.0022	0.0945	0.0023	0.0923
313.16	1.035	14.28	0.0212	0.1148	0.1556	0.0031	0.1168	0.0034	0.1155
313.15	1.277	14.11	0.0262	0.1148	0.1856	0.0039	0.1407	0.0044	0.1409
313.14	1.473	14.04	0.0303	0.1148	0.2085	0.0050	0.1590	0.0056	0.1611
313.14	1.813	13.78	0.0374	0.1148	0.2456	0.0067	0.1896	0.0077	0.1951
323.15	0.152	14.64	0.0026	0.1141	0.0225	0.0010	0.0155	0.0011	0.0150
323.14	0.398	14.50	0.0070	0.1141	0.0577	0.0015	0.0404	0.0015	0.0389
323.13	0.692	14.32	0.0122	0.1141	0.0966	0.0019	0.0686	0.0020	0.0668
323.14	0.753	15.46	0.0131	0.1089	0.1074	0.0017	0.0734	0.0018	0.0724
323.17	0.943	14.29	0.0167	0.1148	0.1270	0.0019	0.0908	0.0021	0.0899
323.14	1.085	14.13	0.0192	0.1141	0.1442	0.0027	0.1040	0.0030	0.1028
323.14	1.374	13.97	0.0244	0.1141	0.1763	0.0041	0.1285	0.0046	0.1286
323.13	1.520	13.91	0.0271	0.1141	0.1918	0.0052	0.1405	0.0059	0.1414
323.14	1.762	13.80	0.0315	0.1141	0.2161	0.0068	0.1594	0.0078	0.1621
323.17	2.052	13.77	0.0369	0.1143	0.2437	0.0044	0.1811	0.0052	0.1863
323.15	2.201	13.52	0.0395	0.1141	0.2569	0.0090	0.1924	0.0107	0.1986
333.13	0.225	14.05	0.0035	0.1178	0.0286	0.0013	0.0192	0.0013	0.0191
333.15	0.414	13.96	0.0064	0.1178	0.0517	0.0017	0.0352	0.0018	0.0348
333.15	0.6470	13.87	0.0101	0.1178	0.0789	0.0021	0.0544	0.0022	0.0539
333.13	0.743	13.82	0.0116	0.1178	0.0897	0.0024	0.0620	0.0026	0.0616

T (K)	P(MPa)	V_V(cm^3)	n_{CO_2}(mol)	$n_{solvent}$ (mol)	z_{CO_2}	$U(z_{CO_2})$	$x_{CO_2}^{exp}$	$U(x_{CO_2})$	$x_{CO_2}^{model}$
333.17	0.850	15.37	0.0131	0.1089	0.1074	0.0020	0.0703	0.0022	0.0701
333.15	1.029	13.67	0.0161	0.1178	0.1205	0.0031	0.0843	0.0034	0.0843
333.15	1.234	13.58	0.0194	0.1178	0.1416	0.0041	0.0999	0.0046	0.1003
333.16	1.606	15.16	0.0251	0.1089	0.1871	0.0051	0.1259	0.0060	0.1285
333.15	1.928	15.06	0.0302	0.1089	0.2172	0.0081	0.1477	0.0096	0.1523
348.17	0.225	15.09	0.0028	0.1106	0.0248	0.0011	0.0146	0.0011	0.0155
348.14	0.439	9.85	0.0058	0.1378	0.0405	0.0009	0.0303	0.0009	0.0301
348.15	0.479	15.02	0.0062	0.1106	0.0530	0.0016	0.0321	0.0017	0.0328
348.17	0.744	9.68	0.0099	0.1378	0.0673	0.0015	0.0509	0.0016	0.0504
348.15	0.766	14.94	0.0100	0.1106	0.0830	0.0025	0.0511	0.0026	0.0519
348.15	1.036	14.87	0.0136	0.1106	0.1097	0.0035	0.0684	0.0039	0.0695
348.21	1.339	14.71	0.0177	0.1106	0.1381	0.0055	0.0874	0.0062	0.0887
348.13	1.664	14.66	0.0222	0.1106	0.1668	0.0071	0.1067	0.0082	0.1090
348.15	2.742	13.52	0.0369	0.1143	0.2437	0.0044	0.1658	0.0055	0.1727

H.2 Tabulated Vapour-Liquid Equilibrium Data of Main Systems

H.2.1 NMP + bmim[BF$_4$] + CO$_2$

Table H-4: Experimental (exp) and modelled[a] (model) data for the solubility of CO_2 in hybrid solvents of bmim[BF_4] (1) + NMP (2) with $w_1 = 0.4973 \pm 0.0001$, including the measured temperature (T), pressure (P), volume of gas phase (V_V), total number of moles of solvent ($n_{solvent}$), number of moles of CO_2 (n_{CO_2}), total mole fraction of CO_2 (z_{CO_2}) and mole fraction of CO_2 in liquid phase(x_{CO_2}), including the expanded uncertainties ($k = 2$) $U(T) = 0.02$ K, $U(P) = 0.002$ MPa.

T (K)	P(MPa)	V_V(cm³)	n_{CO_2}(mol)	$n_{solvent}$ (mol)	z_{CO_2}	$U(z_{CO_2})$	$x_{CO_2}^{exp}$	$U(x_{CO_2})$	$x_{CO_2}^{model}$
298.15	0.152	13.86	0.0042	0.1839	0.0223	0.0007	0.0179	0.0007	0.0180
298.16	0.511	13.53	0.0149	0.1839	0.0750	0.0010	0.0614	0.0010	0.0600
298.15	0.906	13.11	0.0272	0.1839	0.1288	0.0015	0.1075	0.0016	0.1050
298.15	1.282	12.70	0.0394	0.1839	0.1765	0.0023	0.1495	0.0025	0.1469
298.13	1.538	13.08	0.0475	0.1785	0.2103	0.0050	0.1779	0.0054	0.1749
298.13	1.729	12.16	0.0547	0.1839	0.2292	0.0035	0.1975	0.0038	0.1955
298.13	2.036	11.82	0.0657	0.1839	0.2632	0.0049	0.2292	0.0054	0.2280
313.12	0.278	14.18	0.0062	0.1785	0.0333	0.0007	0.0252	0.0007	0.0252
313.15	0.616	14.00	0.0140	0.1785	0.0727	0.0011	0.0560	0.0012	0.0551
313.15	0.960	13.70	0.0222	0.1785	0.1106	0.0017	0.0865	0.0018	0.0850
313.15	1.312	13.45	0.0308	0.1785	0.1472	0.0026	0.1166	0.0028	0.1148
313.15	1.708	13.15	0.0408	0.1785	0.1861	0.0038	0.1496	0.0041	0.1476
313.12	1.780	12.89	0.0429	0.1799	0.1924	0.0057	0.1558	0.0062	0.1535
313.14	1.967	12.91	0.0475	0.1785	0.2103	0.0050	0.1706	0.0055	0.1686
323.17	0.388	13.85	0.0074	0.1799	0.0394	0.0007	0.0289	0.0007	0.0299
323.17	0.765	13.60	0.0151	0.1799	0.0775	0.0013	0.0581	0.0013	0.0583
323.14	1.097	13.39	0.0220	0.1799	0.1090	0.0021	0.0829	0.0022	0.0826
323.14	1.447	13.15	0.0295	0.1799	0.1408	0.0031	0.1086	0.0034	0.1077
323.14	1.718	12.93	0.0355	0.1799	0.1648	0.0043	0.1286	0.0047	0.1269
323.16	2.051	12.71	0.0429	0.1799	0.1924	0.0057	0.1517	0.0063	0.1498

Table H-5: Experimental (exp) and modelled[a] (model) data for the solubility of CO_2 in hybrid solvents of bmim[BF$_4$] (1) + NMP (2) with $w_1 = 0.2495 \pm 0.0001$, including the measured temperature (T), pressure (P), volume of gas phase (V_V), total number of moles of solvent ($n_{solvent}$), number of moles of CO_2 (n_{CO_2}), total mole fraction of CO_2 (z_{CO_2}) and mole fraction of CO_2 in liquid phase(x_{CO_2}), including the expanded uncertainties ($k = 2$)· $U(T) = 0.02$ K, $U(P) = 0.002$ MPa.

T (K)	P(MPa)	V_V(cm^3)	n_{CO_2}(mol)	$n_{solvent}$ (mol)	z_{CO_2}	$U(z_{CO_2})$	$x_{CO_2}^{exp}$	$U(x_{CO_2})$	$x_{CO_2}^{model}$
298.08	0.246	13.73	0.0078	0.2105	0.0359	0.0006	0.0298	0.0006	0.0315
298.11	0.291	13.54	0.0095	0.2120	0.0430	0.0006	0.0359	0.0006	0.0373
298.17	0.529	13.41	0.0176	0.2105	0.0770	0.0009	0.0649	0.0009	0.0671
298.10	0.698	13.09	0.0238	0.2120	0.1011	0.0010	0.0862	0.0010	0.0881
298.15	1.007	12.81	0.0350	0.2105	0.1424	0.0015	0.1227	0.0016	0.1260
298.15	1.388	12.29	0.0498	0.2105	0.1914	0.0023	0.1675	0.0024	0.1718
298.16	1.771	11.73	0.0660	0.2105	0.2386	0.0032	0.2120	0.0035	0.2169
313.14	0.320	13.62	0.0080	0.2096	0.0370	0.0006	0.0294	0.0006	0.0310
313.15	0.597	13.72	0.0154	0.2064	0.0694	0.0008	0.0556	0.0008	0.0573
313.15	0.645	13.35	0.0168	0.2096	0.0743	0.0010	0.0600	0.0011	0.0619
313.14	0.945	13.04	0.0252	0.2096	0.1071	0.0015	0.0879	0.0016	0.0899
313.15	1.056	13.27	0.0282	0.2064	0.1200	0.0015	0.0982	0.0016	0.1001
313.16	1.510	12.77	0.0418	0.2064	0.1682	0.0028	0.1405	0.0030	0.1412
313.09	1.749	14.20	0.0476	0.1929	0.1980	0.0046	0.1616	0.0051	0.1626
323.14	0.350	14.34	0.0075	0.2013	0.0359	0.0006	0.0271	0.0006	0.0289
323.14	0.680	14.13	0.0151	0.2013	0.0696	0.0012	0.0534	0.0013	0.0555
323.04	0.927	14.90	0.0207	0.1929	0.0967	0.0015	0.0734	0.0015	0.0753
323.13	0.946	13.93	0.0213	0.2013	0.0957	0.0017	0.0744	0.0018	0.0766
323.16	1.214	13.73	0.0278	0.2013	0.1213	0.0026	0.0954	0.0028	0.0976
323.16	1.581	13.40	0.0371	0.2013	0.1556	0.0036	0.1245	0.0039	0.1258
323.15	1.599	14.41	0.0370	0.1929	0.1608	0.0030	0.1257	0.0033	0.1271
323.15	2.012	14.07	0.0476	0.1929	0.1980	0.0046	0.1575	0.0051	0.1581

Table H-6: Experimental (exp) and modelled (model) data for the solubility of CO_2 in hybrid solvents of bmim[BF$_4$] (1) + NMP (2) with $w_1 = 0.0986 \pm 0.0001$, including the measured temperature (T), pressure (P), volume of gas phase (V_V), total number of moles of solvent ($n_{solvent}$), number of moles of CO_2 (n_{CO_2}), total mole fraction of CO_2 (z_{CO_2}) and mole fraction of CO_2 in liquid phase(x_{CO_2}), including the expanded uncertainties ($k = 2$) $U(T) = 0.02$ K, $U(P) = 0.002$

T (K)	P(MPa)	V_V(cm^3)	n_{CO_2}(mol)	$n_{solvent}$ (mol)	z_{CO_2}	$U(z_{CO_2})$	$x_{CO_2}^{exp}$	$U(x_{CO_2})$	$x_{CO_2}^{model}$
298.14	0.289	14.03	0.0104	0.2221	0.0446	0.0005	0.0377	0.0006	0.0401
298.14	0.571	13.64	0.0212	0.2221	0.0873	0.0009	0.0749	0.0009	0.0785
298.14	0.854	13.27	0.0327	0.2221	0.1283	0.0012	0.1116	0.0013	0.1162
298.14	1.160	12.73	0.0462	0.2221	0.1722	0.0018	0.1520	0.0019	0.1566
298.14	1.512	12.16	0.0626	0.2221	0.2200	0.0025	0.1971	0.0026	0.2021
298.22	1.516	8.79	0.0684	0.2526	0.2130	0.0035	0.1983	0.0036	0.2023
298.14	2.034	11.11	0.0897	0.2221	0.2878	0.0037	0.2633	0.0039	0.2682
298.14	2.039	11.11	0.0897	0.2221	0.2878	0.0036	0.2633	0.0039	0.2688
298.13	2.046	11.11	0.0897	0.2221	0.2878	0.0037	0.2632	0.0039	0.2697
313.16	0.311	10.65	0.0092	0.2526	0.0352	0.0005	0.0305	0.0005	0.0324
313.15	0.617	10.34	0.0191	0.2526	0.0702	0.0008	0.0615	0.0008	0.0639
313.16	1.008	9.83	0.0323	0.2526	0.1134	0.0013	0.1008	0.0013	0.1032
313.16	1.309	9.41	0.0430	0.2526	0.1454	0.0018	0.1305	0.0019	0.1328
313.13	1.746	12.17	0.0557	0.2218	0.2007	0.0045	0.1741	0.0048	0.1749
313.16	1.980	8.45	0.0684	0.2526	0.2130	0.0034	0.1952	0.0036	0.1970
323.15	0.353	13.6745	0.0086	0.2218	0.0375	0.0006	0.0298	0.0006	0.0313
323.15	0.709	13.37	0.0179	0.2218	0.0746	0.0010	0.0603	0.0010	0.0622
323.16	1.003	13.12	0.0259	0.2218	0.1045	0.0015	0.0856	0.0016	0.0871
323.16	1.416	12.66	0.0374	0.2218	0.1444	0.0023	0.1202	0.0024	0.1216
323.16	1.729	12.31	0.0466	0.2218	0.1738	0.0034	0.1465	0.0036	0.1472
323.15	2.029	11.99	0.0557	0.2218	0.2007	0.0045	0.1710	0.0049	0.1713

H.2.2 MEA + bmim[OTF] + H₂O + CO₂ system

Table H-7: Experimental (exp) and modelled (model) data for the solubility of CO_2 in solvent of MEA (1) + H_2O (2) with $w_2 = 0.2965 \pm 0.0001$, including the measured temperature (T), pressure (P), volume of gas phase (V_V), total number of moles of solvent ($n_{solvent}$), number of moles of CO_2 (n_{CO_2}), total mole fraction of CO_2 (z_{CO_2}), apparent mole fraction of CO_2 in liquid phase(x_{CO_2}), and solubility of CO_2 (a_{CO_2}), including the expanded uncertainties ($k = 2$)· $U(T) = 0.02$ K, $U(P) = 0.002$.

T (K)	P(MPa)	V_V(cm³)	n_{CO_2}(mol)	$n_{solvent}$ (mol)	z_{CO_2}	$U(z_{CO_2})$	$x_{CO_2}^{exp}$	$U(x_{CO_2})$	$a_{CO_2}^{exp}$	$U(a_{CO_2})$	$a_{CO_2}^{model}$
313.10	0.189	15.00	0.0676	0.9128	0.0690	0.0007	0.0680	0.0007	0.6592	0.0074	0.6526
313.09	0.188	15.00	0.0676	0.9128	0.0690	0.0007	0.0680	0.0007	0.6593	0.0076	0.6522
312.99	0.417	14.93	0.0755	0.9128	0.0764	0.0008	0.0741	0.0008	0.7237	0.0085	0.7181
313.00	0.739	14.84	0.0828	0.9128	0.0831	0.0008	0.0791	0.0009	0.7767	0.0091	0.7758
312.98	1.304	14.72	0.0924	0.9128	0.0919	0.0009	0.0848	0.0009	0.8377	0.0103	0.8417
313.01	1.660	14.68	0.0975	0.9128	0.0965	0.0012	0.0874	0.0013	0.8654	0.0137	0.8725
312.98	2.322	14.57	0.1063	0.9128	0.1043	0.0014	0.0912	0.0015	0.9075	0.0161	0.9183
298.05	0.093	15.17	0.0676	0.9128	0.0690	0.0007	0.0684	0.0007	0.6643	0.0077	0.6614
298.06	0.229	15.06	0.0755	0.9128	0.0764	0.0008	0.0751	0.0008	0.7338	0.0083	0.7397
298.04	0.433	14.99	0.0828	0.9128	0.0831	0.0009	0.0807	0.0009	0.7932	0.0092	0.8058
298.05	0.851	14.85	0.0924	0.9128	0.0919	0.0009	0.0871	0.0009	0.8624	0.0101	0.8833
298.04	1.127	14.77	0.0975	0.9128	0.0965	0.0012	0.0901	0.0013	0.8951	0.0138	0.9181
298.05	1.687	14.69	0.1063	0.9128	0.1043	0.0014	0.0945	0.0015	0.9431	0.0160	0.9717

Table H-8: Experimental (exp) and modelled (model) data for the solubility of CO_2 in hybrid solvent of MEA (1) + H_2O (2) + bmim[OTF] (3) with $w_3/w_1 =$ 0.1003/0.2980, including the measured temperature (T), pressure (P), volume of gas phase (V_V), total number of moles of solvent ($n_{solvent}$), number of moles of CO_2 (n_{CO_2}), total mole fraction of CO_2 (z_{CO_2}), apparent mole fraction of CO_2 in liquid phase(x_{CO_2}), and solubility of CO_2 (a_{CO_2}), including the expanded uncertainties ($k = 2$). $U(T) = 0.02$ K, $U(P) = 0.002$.

T (K)	P(MPa)	V_V(cm^3)	n_{CO_2}(mol)	$n_{solvent}$ (mol)	z_{CO_2}	$U(z_{CO_2})$	$x_{CO_2}^{exp}$	$U(x_{CO_2})$	$a_{CO_2}^{exp}$	$U(a_{CO_2})$	$a_{CO_2}^{model}$
313.14	0.406	14.74	0.0757	0.8293	0.0836	0.0008	0.0813	0.0008	0.7004	0.0072	0.6929
313.12	1.089	14.58	0.0898	0.8293	0.0977	0.0008	0.0913	0.0009	0.7957	0.0082	0.7910
313.11	1.473	14.55	0.0958	0.8293	0.1035	0.0010	0.0949	0.0011	0.8298	0.0102	0.8266
313.12	1.910	14.46	0.1020	0.8293	0.1095	0.0012	0.0983	0.0012	0.8625	0.0120	0.8600
313.10	2.206	14.43	0.1060	0.8293	0.1133	0.0017	0.1002	0.0018	0.8814	0.0175	0.8796
298.08	0.215	14.90	0.0757	0.8293	0.0836	0.0008	0.0823	0.0008	0.7101	0.0074	0.7013
298.05	0.676	14.73	0.0898	0.8293	0.0977	0.0008	0.0936	0.0008	0.8171	0.0081	0.8165
298.08	0.960	14.67	0.0958	0.8293	0.1035	0.0010	0.0977	0.0011	0.8569	0.0103	0.8577
298.08	1.310	14.61	0.1020	0.8293	0.1095	0.0012	0.1015	0.0012	0.8944	0.0118	0.8975
298.05	1.554	14.53	0.1060	0.8293	0.1133	0.0017	0.1038	0.0018	0.9167	0.0175	0.9208

Table H-9: Experimental (exp) and modelled (model) data for the solubility of CO_2 in hybrid solvent of MEA (1) + H_2O (2) + bmim[OTF] (3) with $w_3/w_1 =$ 0.2392/0.2994, including the measured temperature (T), pressure (P), volume of gas phase (V_V), total number of moles of solvent ($n_{solvent}$), number of moles of CO_2 (n_{CO_2}), total mole fraction of CO_2 (z_{CO_2}), apparent mole fraction of CO_2 in liquid phase(x_{CO_2}), and solubility of CO_2 (a_{CO_2}), including the expanded uncertainties ($k = 2$). $U(T) = 0.02$ K, $U(P) = 0.002$.

T (K)	P(MPa)	V_V(cm^3)	n_{CO_2}(mol)	$n_{solvent}$ (mol)	z_{CO_2}	$U(z_{CO_2})$	$x_{CO_2}^{exp}$	$U(x_{CO_2})$	$a_{CO_2}^{exp}$	$U(a_{CO_2})$	$a_{CO_2}^{model}$
313.08	0.448	14.41	0.0779	0.7106	0.0988	0.0010	0.0959	0.0010	0.6782	0.0080	0.6853
313.09	1.081	14.17	0.0920	0.7106	0.1146	0.0011	0.1077	0.0011	0.7717	0.0087	0.7741
313.09	1.389	14.14	0.0971	0.7106	0.1203	0.0012	0.1114	0.0012	0.8014	0.0099	0.8036
313.09	1.780	14.01	0.1034	0.7106	0.1271	0.0013	0.1157	0.0014	0.8362	0.0110	0.8351
313.10	2.171	13.96	0.1092	0.7106	0.1332	0.0018	0.1192	0.0019	0.8653	0.0156	0.8622

T (K)	P(MPa)	V_V(cm^3)	n_{CO_2}(mol)	$n_{solvent}$ (mol)	z_{CO_2}	$U(z_{CO_2})$	$x_{CO_2}^{exp}$	$U(x_{CO_2})$	$a_{CO_2}^{exp}$	$U(a_{CO_2})$	$a_{CO_2}^{model}$
298.03	0.232	14.60	0.0779	0.7106	0.0988	0.0010	0.0972	0.0010	0.6884	0.0081	0.6875
298.02	0.672	14.36	0.0920	0.7106	0.1146	0.0010	0.1101	0.0011	0.7910	0.0085	0.7930
298.05	0.889	14.24	0.0971	0.7106	0.1203	0.0012	0.1144	0.0012	0.8256	0.0100	0.8247
298.03	1.200	14.15	0.1034	0.7106	0.1271	0.0013	0.1191	0.0013	0.8644	0.0108	0.8609
298.04	1.509	14.04	0.1092	0.7106	0.1332	0.0018	0.1232	0.0019	0.8982	0.0156	0.8912

Table H-10: Experimental (exp) and modelled (model) data for the solubility of CO_2 in hybrid solvent of MEA (1) + H_2O (2) + bmim[OTF] (3) with w_3/w_1= 0.4005/0.2924, including the measured temperature (T), pressure (P), volume of gas phase (V_V), total number of moles of solvent ($n_{solvent}$), number of moles of CO_2 (n_{CO_2}), total mole fraction of CO_2 (z_{CO_2}), apparent mole fraction of CO_2 in liquid phase(x_{CO_2}), and solubility of CO_2 (a_{CO_2}), including the expanded uncertainties (k = 2) $U(T)$ = 0.02 K, $U(P)$ = 0.002.

T (K)	P(MPa)	V_V(cm^3)	n_{CO_2}(mol)	$n_{solvent}$ (mol)	z_{CO_2}	$U(z_{CO_2})$	$x_{CO_2}^{exp}$	$U(x_{CO_2})$	$a_{CO_2}^{exp}$	$U(a_{CO_2})$	$a_{CO_2}^{model}$
313.12	0.540	14.57	0.0764	0.5371	0.1245	0.0011	0.1201	0.0011	0.6619	0.0071	0.6619
313.12	1.142	14.33	0.0893	0.5371	0.1426	0.0012	0.1334	0.0012	0.7466	0.0078	0.7471
313.13	1.362	14.29	0.0932	0.5371	0.1479	0.0013	0.1370	0.0014	0.7697	0.0089	0.7711
313.11	1.727	14.17	0.0995	0.5371	0.1563	0.0014	0.1425	0.0015	0.8058	0.0099	0.8060
313.11	2.036	14.09	0.1045	0.5371	0.1629	0.0020	0.1467	0.0021	0.8335	0.0142	0.8329
298.06	0.290	14.77	0.0764	0.5371	0.1245	0.0011	0.1220	0.0012	0.6739	0.0072	0.6759
298.06	0.742	14.53	0.0893	0.5371	0.1426	0.0012	0.1364	0.0012	0.7655	0.0076	0.7749
298.04	0.901	14.45	0.0932	0.5371	0.1479	0.0013	0.1404	0.0014	0.7918	0.0090	0.7970
298.05	1.189	14.35	0.0995	0.5371	0.1563	0.0014	0.1464	0.0015	0.8317	0.0098	0.8296
298.07	1.426	14.24	0.1045	0.5371	0.1629	0.0021	0.1511	0.0021	0.8634	0.0143	0.8525

H.2.3 DGA + bmim[OTF] + H₂O + CO₂ system

Table H-11: Experimental (exp) data for the solubility of CO_2 in solvent of DGA (1) + H_2O (2) with w_1= 0.5132± 0.0001, including the measured temperature (*T*), pressure (*P*), volume of gas phase (V_V), total number of moles of solvent ($n_{solvent}$), number of moles of CO_2 (n_{CO_2}), total mole fraction of CO_2 (z_{CO_2}), apparent mole fraction of CO_2 in liquid phase(x_{CO_2}), and solubility of CO_2 (a_{CO_2}), including the expanded uncertainties ($k = 2$) $U(T) = 0.02$ K, $U(P) = 0.002$.

T (K)	P(MPa)	V_V(cm³)	n_{CO_2}(mol)	$n_{solvent}$ (mol)	z_{CO_2}	$U(z_{CO_2})$	$x_{CO_2}^{exp}$	$U(x_{CO_2})$	$a_{CO_2}^{exp}$	$U(a_{CO_2})$
313.06	0.633	14.99	0.0785	0.6823	0.1032	0.0010	0.0988	0.0010	0.7165	0.0083
313.08	1.185	14.87	0.0884	0.6823	0.1147	0.0011	0.1064	0.0011	0.7783	0.0091
313.07	1.491	14.82	0.0930	0.6823	0.1199	0.0013	0.1095	0.0014	0.8033	0.0112
313.09	1.972	14.72	0.0997	0.6823	0.1275	0.0015	0.1135	0.0015	0.8367	0.0128
313.09	2.168	14.71	0.1023	0.6823	0.1303	0.0020	0.1149	0.0021	0.8483	0.0176
297.98	0.344	15.06	0.0785	0.6823	0.1032	0.0010	0.1007	0.0010	0.7318	0.0084
298.02	0.728	14.94	0.0884	0.6823	0.1147	0.0011	0.1094	0.0011	0.8030	0.0090
298.03	0.955	14.90	0.0930	0.6823	0.1199	0.0013	0.1130	0.0014	0.8326	0.0113
298.03	1.342	14.84	0.0997	0.6823	0.1275	0.0015	0.1177	0.0015	0.8712	0.0127
298.05	1.496	14.83	0.1023	0.6823	0.1303	0.0020	0.1194	0.0021	0.8857	0.0176

Table H-12: Experimental (exp) data for the solubility of CO_2 in hybrid solvent of DGA (1) + H_2O (2) + bmim[OTF] (3) with w_3/w_1 = 0.1006/0.5116, including the measured temperature (*T*), pressure (*P*), volume of gas phase (V_V), total number of moles of solvent ($n_{solvent}$), number of moles of CO_2 (n_{CO_2}), total mole fraction of CO_2 (z_{CO_2}), apparent mole fraction of CO_2 in liquid phase(x_{CO_2}), and solubility of CO_2 (a_{CO_2}), including the expanded uncertainties ($k = 2$) $U(T) = 0.02$ K, $U(P) = 0.002$.

T (K)	P(MPa)	V_V(cm³)	n_{CO_2}(mol)	$n_{solvent}$ (mol)	z_{CO_2}	$U(z_{CO_2})$	$x_{CO_2}^{exp}$	$U(x_{CO_2})$	$a_{CO_2}^{exp}$	$U(a_{CO_2})$
313.08	0.593	14.56	0.0777	0.5974	0.1151	0.0010	0.1106	0.0010	0.6835	0.0072
313.07	1.443	14.33	0.0925	0.5974	0.1340	0.0013	0.1232	0.0013	0.7721	0.0096
313.11	1.622	14.32	0.0950	0.5974	0.1373	0.0016	0.1251	0.0016	0.7855	0.0117
313.11	2.077	14.23	0.1014	0.5974	0.1451	0.0018	0.1294	0.0018	0.8166	0.0134

T (K)	P(MPa)	V_V(cm^3)	n_{CO_2}(mol)	$n_{solvent}$ (mol)	z_{CO_2}	$U(z_{CO_2})$	$x_{CO_2}^{exp}$	$U(x_{CO_2})$	$a_{CO_2}^{exp}$	$U(a_{CO_2})$
313.11	2.301	14.22	0.1043	0.5974	0.1487	0.0024	0.1312	0.0025	0.8296	0.0185
298.01	0.320	14.70	0.0777	0.5974	0.1151	0.0010	0.1126	0.0010	0.6970	0.0073
298.01	0.926	14.43	0.0925	0.5974	0.1340	0.0013	0.1268	0.0013	0.7982	0.0094
298.06	1.055	14.42	0.0950	0.5974	0.1373	0.0016	0.1291	0.0016	0.8144	0.0117
298.02	1.420	14.36	0.1014	0.5974	0.1451	0.0018	0.1340	0.0018	0.8504	0.0133
298.05	1.601	14.31	0.1043	0.5974	0.1487	0.0024	0.1362	0.0025	0.8663	0.0184

Table H-13: Experimental (exp) data for the solubility of CO$_2$ in hybrid solvent of DGA (1) + H$_2$O (2) + bmim[OTF] (3) with $w_3/w_1 = 0.2466/0.5056$, including the measured temperature (T), pressure (P), volume of gas phase (V_V), total number of moles of solvent ($n_{solvent}$), number of moles of CO$_2$ (n_{CO_2}), total mole fraction of CO$_2$ (z_{CO_2}), apparent mole fraction of CO$_2$ in liquid phase(x_{CO_2}), and solubility of CO$_2$ (a_{CO_2}), including the expanded uncertainties ($k = 2$) $U(T) = 0.02$ K, $U(P) = 0.002$.

T (K)	P(MPa)	V_V(cm^3)	n_{CO_2}(mol)	$n_{solvent}$ (mol)	z_{CO_2}	$U(z_{CO_2})$	$x_{CO_2}^{exp}$	$U(x_{CO_2})$	$a_{CO_2}^{exp}$	$U(a_{CO_2})$
313.07	0.489	15.03	0.0724	0.4361	0.1424	0.0012	0.1375	0.0013	0.6438	0.0068
313.07	0.969	14.88	0.0819	0.4361	0.1580	0.0013	0.1485	0.0013	0.7044	0.0075
313.03	1.326	14.79	0.0878	0.4361	0.1676	0.0015	0.1546	0.0016	0.7386	0.0090
313.08	1.765	14.69	0.0946	0.4361	0.1782	0.0017	0.1611	0.0018	0.7752	0.0102
313.06	2.038	14.65	0.0986	0.4361	0.1844	0.0024	0.1645	0.0026	0.7951	0.0148
298.01	0.271	15.22	0.0724	0.4361	0.1424	0.0013	0.1396	0.0013	0.6548	0.0069
298.03	0.612	15.04	0.0819	0.4361	0.1580	0.0013	0.1518	0.0013	0.7224	0.0073
298.05	0.865	14.94	0.0878	0.4361	0.1676	0.0016	0.1588	0.0016	0.7622	0.0091
298.01	1.213	14.78	0.0946	0.4361	0.1782	0.0017	0.1661	0.0017	0.8040	0.0101
298.00	1.423	14.72	0.0986	0.4361	0.1844	0.0024	0.1701	0.0025	0.8278	0.0148

Table H-14: Experimental (exp) data for the solubility of CO_2 in hybrid solvent of DGA (1) + H_2O (2) + bmim[OTF] (3) with $w_3/w_1 = 0.4024/0.4976$, including the measured temperature (T), pressure (P), volume of gas phase (V_V), total number of moles of solvent ($n_{solvent}$), number of moles of CO_2 (n_{CO_2}), total mole fraction of CO_2 (z_{CO_2}), apparent mole fraction of CO_2 in liquid phase(x_{CO_2}), and solubility of CO_2 (a_{CO_2}), including the expanded uncertainties ($k = 2$) $U(T) = 0.02$ K, $U(P) = 0.002$.

T (K)	P(MPa)	V_V(cm^3)	n_{CO_2}(mol)	$n_{solvent}$ (mol)	z_{CO_2}	$U(z_{CO_2})$	$x_{CO_2}^{exp}$	$U(x_{CO_2})$	$a_{CO_2}^{exp}$	$U(a_{CO_2})$
313.08	0.464	14.84	0.0711	0.2750	0.2055	0.0015	0.1994	0.0015	0.6143	0.0059
313.09	0.930	14.69	0.0802	0.2750	0.2258	0.0016	0.2137	0.0017	0.6707	0.0067
313.07	1.278	14.54	0.0863	0.2750	0.2390	0.0021	0.2227	0.0021	0.7067	0.0088
313.12	1.695	14.43	0.0931	0.2750	0.2530	0.0023	0.2317	0.0024	0.7441	0.0102
313.07	1.892	14.35	0.0963	0.2750	0.2595	0.0030	0.2359	0.0033	0.7615	0.0137
298.03	0.285	15.01	0.0711	0.2750	0.2055	0.0015	0.2015	0.0016	0.6227	0.0060
298.01	0.637	14.82	0.0802	0.2750	0.2258	0.0016	0.2172	0.0016	0.6844	0.0066
298.06	0.905	14.70	0.0863	0.2750	0.2390	0.0021	0.2269	0.0021	0.7241	0.0088
298.05	1.241	14.56	0.0931	0.2750	0.2530	0.0023	0.2368	0.0024	0.7655	0.0101
298.03	1.397	14.51	0.0963	0.2750	0.2595	0.0031	0.2413	0.0032	0.7849	0.0138

H.2.4 MEA + (NMP + bmim[TF$_2$N]) / H$_2$O / bmim[OTF] + CO$_2$ system

Table H-15: Experimental (exp) data for the solubility of CO_2 in hybrid solvent of MEA (1) + NMP (2) with $w_1/w_2 = 0.3037/0.6963$, including the measured temperature (T), pressure (P), volume of gas phase (V_V), total number of moles of solvent ($n_{solvent}$), number of moles of CO_2 (n_{CO_2}), total mole fraction of CO_2 (z_{CO_2}), apparent mole fraction of CO_2 in liquid phase(x_{CO_2}), and solubility of CO_2 (a_{CO_2}), including the expanded uncertainties ($k = 2$) $U(T) = 0.02$ K, $U(P) = 0.002$.

T (K)	P(MPa)	V_V(cm^3)	n_{CO_2}(mol)	$n_{solvent}$ (mol)	z_{CO_2}	$U(z_{CO_2})$	$x_{CO_2}^{exp}$	$U(x_{CO_2})$	$a_{CO_2}^{exp}$	$U(a_{CO_2})$
313.034	0.330	14.41	0.0718	0.2550	0.2196	0.0017	0.2151	0.0017	0.6614	0.0066
313.039	0.751	14.11	0.0828	0.2550	0.2451	0.0017	0.2355	0.0017	0.7434	0.0072
313.032	1.081	13.88	0.0905	0.2550	0.2620	0.0019	0.2488	0.0019	0.7991	0.0083

T (K)	P(MPa)	V_V(cm³)	n_{CO_2}(mol)	$n_{solvent}$ (mol)	z_{CO_2}	$U(z_{CO_2})$	$x_{CO_2}^{exp}$	$U(x_{CO_2})$	$a_{CO_2}^{exp}$	$U(a_{CO_2})$
313.076	1.583	13.62	0.1017	0.2550	0.2850	0.0024	0.2666	0.0025	0.8770	0.0113
313.065	1.889	13.42	0.1084	0.2550	0.2982	0.0030	0.2768	0.0032	0.9238	0.0148
313.084	2.298	13.19	0.1173	0.2550	0.3151	0.0039	0.2901	0.0042	0.9859	0.0201

Table H-16: Experimental (exp) data for the solubility of CO_2 in hybrid solvent of MEA (1) + NMP (2) with $w_1/w_2 = 0.2032/0.7968$, including the measured temperature (T), pressure (P), volume of gas phase (V_V), total number of moles of solvent ($n_{solvent}$), number of moles of CO_2 (n_{CO_2}), total mole fraction of CO_2 (z_{CO_2}), apparent mole fraction of CO_2 in liquid phase(x_{CO_2}), and solubility of CO_2 (a_{CO_2}), including the expanded uncertainties ($k = 2$) $U(T) = 0.02$ K, $U(P) = 0.002$.

T (K)	P(MPa)	V_V(cm³)	n_{CO_2}(mol)	$n_{solvent}$ (mol)	z_{CO_2}	$U(z_{CO_2})$	$x_{CO_2}^{exp}$	$U(x_{CO_2})$	$a_{CO_2}^{exp}$	$U(a_{CO_2})$
313.04	0.194	14.55766	0.0494	0.2428	0.1691	0.0008	0.1660	0.0008	0.6798	0.0041
313.05	0.551	14.28135	0.0606	0.2428	0.1998	0.0009	0.1915	0.0010	0.8093	0.0051
313.04	1.001	13.92646	0.0722	0.2428	0.2291	0.0012	0.2151	0.0013	0.9360	0.0070
313.07	1.314	13.68563	0.0800	0.2428	0.2479	0.0017	0.2303	0.0018	1.0221	0.0104
313.00	1.726	13.38904	0.0904	0.2428	0.2712	0.0028	0.2494	0.0030	1.1348	0.0183

Table H-17: Experimental (exp) data for the solubility of CO_2 in hybrid solvent of MEA (1) + NMP (2) with $w_1/w_2 = 0.1025/0.8975$, including the measured temperature (T), pressure (P), volume of gas phase (V_V), total number of moles of solvent ($n_{solvent}$), number of moles of CO_2 (n_{CO_2}), total mole fraction of CO_2 (z_{CO_2}), apparent mole fraction of CO_2 in liquid phase(x_{CO_2}), and solubility of CO_2 (a_{CO_2}), including the expanded uncertainties ($k = 2$) $U(T) = 0.02$ K, $U(P) = 0.002$.

T (K)	P(MPa)	V_V(cm³)	n_{CO_2}(mol)	$n_{solvent}$ (mol)	z_{CO_2}	$U(z_{CO_2})$	$x_{CO_2}^{exp}$	$U(x_{CO_2})$	$a_{CO_2}^{exp}$	$U(a_{CO_2})$
313.04	0.213	15.07	0.0309	0.2304	0.1184	0.0007	0.1142	0.0007	0.8247	0.0059
313.10	0.588	14.30	0.0424	0.2304	0.1555	0.0009	0.1451	0.0009	1.0860	0.0082
313.08	0.993	13.92	0.0541	0.2304	0.1901	0.0013	0.1739	0.0013	1.3467	0.0126

T (K)	P(MPa)	V_V(cm³)	n_{CO_2}(mol)	$n_{solvent}$ (mol)	z_{CO_2}	$U(z_{CO_2})$	$x_{CO_2}^{exp}$	$U(x_{CO_2})$	$a_{CO_2}^{exp}$	$U(a_{CO_2})$
313.06	1.381	13.52	0.0653	0.2304	0.2209	0.0021	0.2001	0.0022	1.6003	0.0222
313.05	1.741	13.18	0.0760	0.2304	0.2481	0.0030	0.2237	0.0032	1.8438	0.0342

Table H-18: Experimental (exp) data for the solubility of CO_2 in hybrid solvent of MEA (1) + H_2O (2) with w_1/w_2 = 0.1997/ 0.8003, including the measured temperature (T), pressure (P), volume of gas phase (V_V), total number of moles of solvent ($n_{solvent}$), number of moles of CO_2 (n_{CO_2}), total mole fraction of CO_2 (z_{CO_2}), apparent mole fraction of CO_2 in liquid phase(x_{CO_2}), and solubility of CO_2 (a_{CO_2}), including the expanded uncertainties (k = 2) $U(T)$ = 0.02 K, $U(P)$ = 0.002.

T (K)	P(MPa)	V_V(cm³)	n_{CO_2}(mol)	$n_{solvent}$ (mol)	z_{CO_2}	$U(z_{CO_2})$	$x_{CO_2}^{exp}$	$U(x_{CO_2})$	$a_{CO_2}^{exp}$	$U(a_{CO_2})$
312.99	0.196	15.44	0.0486	0.9764	0.0474	0.0003	0.0464	0.0003	0.7095	0.0050
313.04	0.475	15.40	0.0561	0.9764	0.0544	0.0004	0.0518	0.0004	0.7962	0.0060
313.03	0.917	15.30	0.0639	0.9764	0.0614	0.0005	0.0564	0.0005	0.8711	0.0079
313.01	1.348	15.22	0.0700	0.9764	0.0669	0.0007	0.0594	0.0008	0.9207	0.0125
312.99	1.911	15.18	0.0771	0.9764	0.0732	0.0012	0.0623	0.0012	0.9693	0.0207

Table H-19: Experimental (exp) data for the solubility of CO_2 in hybrid solvent of MEA (1) + H_2O (2) with w_1/w_2 = 0.1034/ 0.8966, including the measured temperature (T), pressure (P), volume of gas phase (V_V), total number of moles of solvent ($n_{solvent}$), number of moles of CO_2 (n_{CO_2}), total mole fraction of CO_2 (z_{CO_2}), apparent mole fraction of CO_2 in liquid phase(x_{CO_2}), and solubility of CO_2 (a_{CO_2}), including the expanded uncertainties (k = 2) $U(T)$ = 0.02 K, $U(P)$ = 0.002.

T (K)	P(MPa)	V_V(cm³)	n_{CO_2}(mol)	$n_{solvent}$ (mol)	z_{CO_2}	$U(z_{CO_2})$	$x_{CO_2}^{exp}$	$U(x_{CO_2})$	$a_{CO_2}^{exp}$	$U(a_{CO_2})$
313.04	0.220	15.70	0.0295	1.0718	0.0268	0.0002	0.0256	0.0002	0.7994	0.0062
313.01	0.871	15.59	0.0397	1.0718	0.0357	0.0004	0.0310	0.0004	0.9737	0.0127
313.06	1.239	15.56	0.0442	1.0718	0.0396	0.0005	0.0328	0.0006	1.0303	0.0183
313.03	1.550	15.51	0.0477	1.0718	0.0426	0.0008	0.0341	0.0008	1.0716	0.0271
313.01	1.936	15.51	0.0521	1.0718	0.0463	0.0012	0.0354	0.0012	1.1165	0.0395

Table H-20: Experimental (exp) data for the solubility of CO_2 in hybrid solvent of MEA (1) + bmim[OTF] (2) with w_1/w_2= 0.0912/0.9088, including the measured temperature (T), pressure (P), volume of gas phase (V_V), total number of moles of solvent ($n_{solvent}$), number of moles of CO_2 (n_{CO_2}), total mole fraction of CO_2 (z_{CO_2}), apparent mole fraction of CO_2 in liquid phase(x_{CO_2}), and solubility of CO_2 (a_{CO_2}), including the expanded uncertainties ($k = 2$) $U(T) = 0.02$ K, $U(P) = 0.002$.

T (K)	P(MPa)	V_V(cm^3)	n_{CO_2}(mol)	$n_{solvent}$ (mol)	z_{CO_2}	$U(z_{CO_2})$	$x_{CO_2}^{exp}$	$U(x_{CO_2})$	$a_{CO_2}^{exp}$	$U(a_{CO_2})$
313.04	0.564	15.18	0.0310	0.1198	0.2057	0.0048	0.1875	0.0050	0.7183	0.0238
313.03	1.099	14.90	0.0422	0.1198	0.2605	0.0049	0.2288	0.0054	0.9235	0.0282
313.00	1.414	14.73	0.0487	0.1198	0.2891	0.0054	0.2509	0.0060	1.0423	0.0332
313.02	1.724	14.56	0.0551	0.1198	0.3151	0.0060	0.2712	0.0068	1.1579	0.0397
313.01	2.065	14.40	0.0622	0.1198	0.3419	0.0070	0.2924	0.0081	1.2861	0.0505

Table H-21: Experimental (exp) data for the solubility of CO_2 in hybrid solvent of MEA (1) + NMP (2) + bmim[TF$_2$N] (3) with $w_1/w_2/w_3$ = 0.1039/ 0.7966/ 0.0995, including the measured temperature (T), pressure (P), volume of gas phase (V_V), total number of moles of solvent ($n_{solvent}$), number of moles of CO_2 (n_{CO_2}), total mole fraction of CO_2 (z_{CO_2}), apparent mole fraction of CO_2 in liquid phase(x_{CO_2}), and solubility of CO_2 (a_{CO_2}), including the expanded uncertainties ($k = 2$) $U(T) = 0.02$ K, $U(P) = 0.002$.

T (K)	P(MPa)	V_V(cm^3)	n_{CO_2}(mol)	$n_{solvent}$ (mol)	z_{CO_2}	$U(z_{CO_2})$	$x_{CO_2}^{exp}$	$U(x_{CO_2})$	$a_{CO_2}^{exp}$	$U(a_{CO_2})$
313.09	0.341	14.4634	0.0349	0.2215	0.1360	0.0009	0.1294	0.0009	0.8719	0.0070
313.10	0.669	14.1744	0.0443	0.2215	0.1665	0.0011	0.1546	0.0011	1.0720	0.0092
313.09	1.113	13.8069	0.0564	0.2215	0.2029	0.0017	0.1846	0.0018	1.3275	0.0160
313.06	1.507	13.4773	0.0672	0.2215	0.2326	0.0026	0.2096	0.0028	1.5547	0.0263
313.05	1.886	13.0768	0.0778	0.2215	0.2599	0.0037	0.2331	0.0039	1.7827	0.0393

Table H-22: Experimental (exp) data for the solubility of CO_2 in hybrid solvent of MEA (1) + NMP (2) + bmim[TF_2N] (3) with $w_1/w_2/w_3 = 0.0977/ 0.6492/ 0.2531$, including the measured temperature (T), pressure (P), volume of gas phase (V_V), total number of moles of solvent ($n_{solvent}$), number of moles of CO_2 (n_{CO_2}), total mole fraction of CO_2 (z_{CO_2}), apparent mole fraction of CO_2 in liquid phase(x_{CO_2}), and solubility of CO_2 (a_{CO_2}), including the expanded uncertainties ($k = 2$) $U(T) = 0.02$ K, $U(P) = 0.002$.

T (K)	P(MPa)	V_V(cm^3)	n_{CO_2}(mol)	$n_{solvent}$ (mol)	z_{CO_2}	$U(z_{CO_2})$	$x_{CO_2}^{exp}$	$U(x_{CO_2})$	$a_{CO_2}^{exp}$	$U(a_{CO_2})$
313.05	0.413	14.8732	0.0343	0.2002	0.1461	0.0010	0.1373	0.0010	0.8705	0.0075
313.05	0.750	14.5969	0.0431	0.2002	0.1772	0.0012	0.1622	0.0013	1.0591	0.0102
313.04	1.095	14.3561	0.0521	0.2002	0.2064	0.0017	0.1858	0.0018	1.2490	0.0152
313.07	1.501	13.9936	0.0626	0.2002	0.2382	0.0025	0.2121	0.0027	1.4730	0.0242
313.05	1.898	13.6742	0.0730	0.2002	0.2674	0.0037	0.2366	0.0040	1.6961	0.0380

Table H-23: Experimental (exp) data for the solubility of CO_2 in hybrid solvent of MEA (1) + NMP (2) + bmim[TF_2N] (3) with $w_1/w_2/w_3 = 0.1162/ 0.4932/ 0.3906$, including the measured temperature (T), pressure (P), volume of gas phase (V_V), total number of moles of solvent ($n_{solvent}$), number of moles of CO_2 (n_{CO_2}), total mole fraction of CO_2 (z_{CO_2}), apparent mole fraction of CO_2 in liquid phase(x_{CO_2}), and solubility of CO_2 (a_{CO_2}), including the expanded uncertainties ($k = 2$) $U(T) = 0.02$ K, $U(P) = 0.002$.

T (K)	P(MPa)	V_V(cm^3)	n_{CO_2}(mol)	$n_{solvent}$ (mol)	z_{CO_2}	$U(z_{CO_2})$	$x_{CO_2}^{exp}$	$U(x_{CO_2})$	$a_{CO_2}^{exp}$	$U(a_{CO_2})$
313.01	0.297	15.7075	0.0322	0.1817	0.1506	0.0011	0.1433	0.0011	0.6869	0.0061
313.00	0.762	15.3805	0.0439	0.1817	0.1944	0.0013	0.1774	0.0014	0.8853	0.0084
313.04	1.136	15.1371	0.0527	0.1817	0.2249	0.0019	0.2010	0.0021	1.0328	0.0132
313.03	1.542	14.8735	0.0622	0.1817	0.2552	0.0027	0.2249	0.0030	1.1911	0.0205
313.01	1.993	14.6327	0.0730	0.1817	0.2866	0.0040	0.2500	0.0044	1.3683	0.0324

H.2.5 DGA + (NMP + bmim[TF₂N])/H₂O + CO₂ system

Table H-24: Experimental (exp) data for the solubility of CO_2 in hybrid solvent of DGA (1) + NMP (2) with $w_1/w_2 = 0.4964/0.5036$, including the measured temperature (T), pressure (P), volume of gas phase (V_V), total number of moles of solvent ($n_{solvent}$), number of moles of CO_2 (n_{CO_2}), total mole fraction of CO_2 (z_{CO_2}), apparent mole fraction of CO_2 in liquid phase(x_{CO_2}), and solubility of CO_2 (a_{CO_2}), including the expanded uncertainties ($k = 2$) $U(T) = 0.02$ K, $U(P) = 0.002$.

T (K)	P(MPa)	V_V(cm³)	n_{CO_2}(mol)	$n_{solvent}$ (mol)	z_{CO_2}	$U(z_{CO_2})$	$x_{CO_2}^{exp}$	$U(x_{CO_2})$	$a_{CO_2}^{exp}$	$U(a_{CO_2})$
313.01	0.433	14.46	0.0740	0.2110	0.2597	0.0024	0.2533	0.0024	0.7042	0.0091
313.00	0.830	14.21	0.0831	0.2110	0.2826	0.0025	0.2709	0.0026	0.7714	0.0101
313.00	1.112	14.08	0.0891	0.2110	0.2968	0.0027	0.2816	0.0029	0.8137	0.0116
313.03	1.432	13.90	0.0954	0.2110	0.3115	0.0032	0.2925	0.0034	0.8583	0.0139
313.03	1.776	13.74	0.1024	0.2110	0.3267	0.0039	0.3039	0.0042	0.9064	0.0178

Table H-25: Experimental (exp) data for the solubility of CO_2 in hybrid solvent of DGA (1) + NMP (2) with $w_1/w_2 = 0.3020/0.6980$, including the measured temperature (T), pressure (P), volume of gas phase (V_g), total number of moles of solvent ($n_{solvent}$), number of moles of CO_2 (n_{CO_2}), total mole fraction of CO_2 (z_{CO_2}), apparent mole fraction of CO_2 in liquid phase(x_{CO_2}), and solubility of CO_2 (a_{CO_2}), including the expanded uncertainties ($k = 2$) $U(T) = 0.02$ K, $U(P) = 0.002$.

T (K)	P(MPa)	V_V(cm³)	n_{CO_2}(mol)	$n_{solvent}$ (mol)	z_{CO_2}	$U(z_{CO_2})$	$x_{CO_2}^{exp}$	$U(x_{CO_2})$	$a_{CO_2}^{exp}$	$U(a_{CO_2})$
313.07	0.262	14.83	0.0469	0.2118	0.1813	0.0010	0.1765	0.0010	0.7397	0.0053
313.05	0.701	14.49	0.0584	0.2118	0.2162	0.0012	0.2043	0.0012	0.8864	0.0066
313.02	1.159	14.18	0.0694	0.2118	0.2470	0.0017	0.2286	0.0018	1.0230	0.0107
313.00	1.505	13.96	0.0776	0.2118	0.2683	0.0024	0.2456	0.0026	1.1237	0.0159
313.01	1.893	13.66	0.0875	0.2118	0.2924	0.0037	0.2656	0.0040	1.2481	0.0259

Table H-26: Experimental (exp) data for the solubility of CO_2 in hybrid solvent of DGA (1) + H_2O (2) with $w_1/w_2 = 0.3101/0.6899$, including the measured temperature (T), pressure (P), volume of gas phase (V_V), total number of moles of solvent ($n_{solvent}$), number of moles of CO_2 (n_{CO_2}), total mole fraction of CO_2 (z_{CO_2}), apparent mole fraction of CO_2 in liquid phase(x_{CO_2}), and solubility of CO_2 (a_{CO_2}), including the expanded uncertainties ($k = 2$) $U(T) = 0.02$ K, $U(P) = 0.002$.

T (K)	P(MPa)	V_V(cm^3)	n_{CO_2}(mol)	$n_{solvent}$ (mol)	z_{CO_2}	$U(z_{CO_2})$	$x_{CO_2}^{exp}$	$U(x_{CO_2})$	$a_{CO_2}^{exp}$	$U(a_{CO_2})$
313.04	0.188	14.59	0.0462	0.8960	0.0491	0.0004	0.0480	0.0004	0.7055	0.0055
313.04	0.617	14.52	0.0567	0.8960	0.0595	0.0005	0.0560	0.0005	0.8300	0.0072
313.01	1.126	14.39	0.0646	0.8960	0.0673	0.0006	0.0609	0.0006	0.9064	0.0101
313.01	1.625	14.30	0.0711	0.8960	0.0735	0.0011	0.0642	0.0011	0.9588	0.0174
313.02	2.101	14.29	0.0768	0.8960	0.0789	0.0017	0.0666	0.0017	0.9978	0.0278

Table H-27: Experimental (exp) data for the solubility of CO_2 in hybrid solvent of DGA (1) + NMP (2) + bmim[TF_2N] (3) with $w_1/w_2/w_3 = 0.3108/0.5864/0.1028$, including the measured temperature (T), pressure (P), volume of gas phase (V_V), total number of moles of solvent ($n_{solvent}$), number of moles of CO_2 (n_{CO_2}), total mole fraction of CO_2 (z_{CO_2}), apparent mole fraction of CO_2 in liquid phase(x_{CO_2}), and solubility of CO_2 (a_{CO_2}), including the expanded uncertainties ($k = 2$) $U(T) = 0.02$ K, $U(P) = 0.002$.

T (K)	P(MPa)	V_V(cm^3)	n_{CO_2}(mol)	$n_{solvent}$ (mol)	z_{CO_2}	$U(z_{CO_2})$	$x_{CO_2}^{exp}$	$U(x_{CO_2})$	$a_{CO_2}^{exp}$	$U(a_{CO_2})$
313.03	0.353	14.86	0.0508	0.1995	0.2028	0.0013	0.1962	0.0013	0.7529	0.0062
313.02	0.782	14.62	0.0613	0.1995	0.2349	0.0015	0.2213	0.0016	0.8766	0.0080
313.01	1.197	14.32	0.0708	0.1995	0.2620	0.0021	0.2424	0.0023	0.9867	0.0121
313.02	1.566	14.08	0.0792	0.1995	0.2841	0.0028	0.2598	0.0030	1.0823	0.0167
313.03	1.973	13.81	0.0886	0.1995	0.3074	0.0039	0.2784	0.0042	1.1898	0.0249

Table H-28: Experimental (exp) data for the solubility of CO_2 in hybrid solvent of DGA (1) + NMP (2) + bmim[TF$_2$N] (3) with $w_1/w_2/w_3$ = 0.3035/ 0.4462/ 0.2503, including the measured temperature (T), pressure (P), volume of gas phase (V_V), total number of moles of solvent ($n_{solvent}$), number of moles of CO_2 (n_{CO_2}), total mole fraction of CO_2 (z_{CO_2}), apparent mole fraction of CO_2 in liquid phase(x_{CO_2}), and solubility of CO_2 (a_{CO_2}), including the expanded uncertainties (k = 2) $U(T)$ = 0.02 K, $U(P)$ = 0.002.

T (K)	P (MPa)	V_V (cm^3)	n_{CO_2} (mol)	$n_{solvent}$ (mol)	z_{CO_2}	$U(z_{CO_2})$	$x_{CO_2}^{exp}$	$U(x_{CO_2})$	$a_{CO_2}^{exp}$	$U(a_{CO_2})$
312.99	0.375	14.69	0.0503	0.1843	0.2144	0.0013	0.2072	0.0013	0.7227	0.0059
313.02	0.775	14.43	0.0597	0.1843	0.2446	0.0016	0.2306	0.0017	0.8289	0.0076
313.01	1.160	14.24	0.0682	0.1843	0.2701	0.0023	0.2502	0.0024	0.9227	0.0116
313.03	1.536	14.01	0.0764	0.1843	0.2930	0.0031	0.2679	0.0033	1.0120	0.0171
313.00	1.950	13.75	0.0853	0.1843	0.3165	0.0040	0.2863	0.0044	1.1097	0.0238

Table H-29: Experimental (exp) data for the solubility of CO_2 in hybrid solvent of DGA (1) + NMP (2) + bmim[TF$_2$N] (3) with $w_1/w_2/w_3$ = 0.2981/ 0.3096/ 0.3923, including the measured temperature (T), pressure (P), volume of gas phase (V_V), total number of moles of solvent ($n_{solvent}$), number of moles of CO_2 (n_{CO_2}), total mole fraction of CO_2 (z_{CO_2}), apparent mole fraction of CO_2 in liquid phase(x_{CO_2}), and solubility of CO_2 (a_{CO_2}), including the expanded uncertainties (k = 2) $U(T)$ = 0.02 K, $U(P)$ = 0.002

T (K)	P (MPa)	V_V (cm^3)	n_{CO_2} (mol)	$n_{solvent}$ (mol)	z_{CO_2}	$U(z_{CO_2})$	$x_{CO_2}^{exp}$	$U(x_{CO_2})$	$a_{CO_2}^{exp}$	$U(a_{CO_2})$
313.03	0.297	15.02	0.0473	0.1641	0.2238	0.0013	0.2173	0.0013	0.6752	0.0052
313.01	0.717	14.78	0.0572	0.1641	0.2584	0.0014	0.2440	0.0015	0.7846	0.0063
313.01	1.158	14.56	0.0665	0.1641	0.2884	0.0020	0.2666	0.0021	0.8839	0.0095
313.01	1.551	14.34	0.0748	0.1641	0.3130	0.0029	0.2853	0.0032	0.9708	0.0150
313.02	1.877	14.15	0.0816	0.1641	0.3319	0.0039	0.2999	0.0043	1.0415	0.0214

APPENDIX I.   TABULATED PHYSICAL PROPERTIES DATA OF SOLVENTS

Table I-1: Experimental data of the viscosity (η), density (ρ) and sound velocity (c) at different mass compositions (w) for the binary system of bmim[BF$_4$] (1) + NMP (2)[a].

Sample	Temperature (K)										
	293.15	298.15	303.15	308.15	313.15	318.15	323.15	328.15	333.15	338.15	343.15
	Viscosity (mPa.s)										
$w_1 = 1$	129.340	98.951	77.000	60.901	49.205	40.267	33.435	28.117	23.941	20.619	17.924
	136.9[e]	110.308[c]	74.21[b]	58.18[b]	46.51[b]	37.79[b]	31.08[b]		21.52[b]		15.61[b]
		93.814[f]	68.9[d]	56.407[f]	44.73[d]	37.322[f]	30.81[d]		22.28[d]		16.75[d]
			81.4[e]		51.79[e]		35.23[e]		24.97[e]		18.49[e]
			71.763[f]		45.602[f]						
$w_1 = 0$	1.786	1.693	1.564	1.448	1.3463	1.258	1.176	1.103	1.037	0.9769	0.923
		1.683[f]	1.558[f]	1.47[f]	1.337[f]	1.248[f]	1.175[g]		1.035[g]		0.921[g]
		1.656[g]	1.554[i]		1.322[g]		1.16[i]		1.022[i]		0.908[i]
		1.687[h]			1.332[i]						
		1.683[i]									
$w_1 = 0.7413$	27.487	22.732	19.070	16.260	13.880	12.040	10.540	9.281	8.224	7.318	6.555
$w_1 = 0.4971$	9.374	8.144	7.116	6.257	5.544	4.948	4.444	4.015	3.636	3.340	3.064
		8.196[j]	7.291[j]	6.382[j]	5.63[j]	5.045[j]					
$w_1 = 0.2498$	3.938	3.528	3.180	2.884	2.627	2.405	2.214	2.043	1.892	1.760	1.641
$w_1 = 0.0986$	2.568	2.330	2.129	1.953	1.798	1.662	1.542	1.435	1.341	1.258	1.182

sample	Temperature (K)										
	293.15	298.15	303.15	308.15	313.15	318.15	323.15	328.15	333.15	338.15	343.15
Density (g/cm^3)											
$w_1 = 1$	1.2060 1.20444[e]	1.2024 1.21105[c] 1.20089[e] 1.2006[f]	1.1988 1.1984[b] 1.195698[d] 1.19734[e] 1.1977[f]	1.1952 1.1954[b] 1.1948[f]	1.1917 1.1922[b] 1.188618[d] 1.19027[e] 1.1915[f]	1.1881 1.189[b] 1.1884[f]	1.1846 1.186[b] 1.181591[d] 1.18324[e]	1.1811	1.1776 1.1798[b] 1.174603[d] 1.17625[e]	1.1742	1.1707 1.1735[b] 1.167672[d] 1.16932[e]
$w_1 = 0$	1.0341	1.0297 1.0283[f] 1.02872[g] 1.0279[h] 1.02794[i]	1.0252 1.0245[f] 1.02347[i]	1.0208 1.0201[f]	1.0163 1.0158[f] 1.01519[g] 1.01455[i]	1.0119 1.0117[f]	1.0074 1.00627[g] 1.00566[i]	1.0029	0.9984 0.99741[g] 0.99671[i]	0.9939	0.9894 0.98846[g] 0.98775[i]
$w_1 = 0.7413$	1.1606	1.1568	1.1530	1.1492	1.1454	1.1417	1.1379	1.1342	1.1305	1.1267	1.123
$w_1 = 0.4971$	1.1195	1.1155 1.1156[j]	1.1115 1.1118[j]	1.1075 1.1079[j]	1.1035 1.1041[j]	1.0995 1.1003[j]	1.0955	1.0916	1.0876	1.0836	1.0796
$w_1 = 0.2498$	1.0779	1.0737	1.0695	1.0654	1.0612	1.057	1.0528	1.0486	1.0444	1.0402	1.036
$w_1 = 0.0986$	1.0527	1.0484	1.0440	1.0397	1.0354	1.0310	1.0266	1.0223	1.0180	1.0136	1.0092
Sound Velocity (m/s)											
$w_1 = 1$	1576.7	1564.7	1552.8	1541.2	1529.6	1518.2	1506.9	1495.7	1484.5	1473.2	1461.7
$w_1 = 0$	1565.7	1546.1	1526.7	1507.5	1488.3	1469.2	1450.4	1431.4	1412.8	1394.4	1376.0
$w_1 = 0.7413$	1580.1	1566.6	1552.8	1539.2	1525.6	1512.2	1498.9	1485.6	1472.4	1459.3	1445.8
$w_1 = 0.4971$	1585.5	1570.1	1554.5	1539.0	1523.7	1508.4	1493.2	1478.1	1463.2	1448.1	1432.9
$w_1 = 0.2498$	1582.0	1564.5	1546.8	1529.4	1512.0	1494.8	1478.0	1461.1	1444.4	1427.8	1411.34

Sample	Temperature (K)										
	293.15	298.15	303.15	308.15	313.15	318.15	323.15	328.15	333.15	338.15	343.15
	Sound Velocity (m/s)										
$w_1 = 0.0986$	1579.2	1560.5	1541.8	1523.2	1504.8	1486.6	1468.4	1450.5	1432.6	1414.6	1396.4

[a] Expanded uncertainties are: $U(T) = 0.02$ K; $U(\rho) = 0.0002$ g.cm^{-3}, $U(\eta) = 0.003$ mPa.s and $U(c) = 0.7$ m.s^{-1}. Data recorded at 101 kPa, $U(P) = 1$ kPa.

[b] Data for the viscosity and density from literature [179]; [c] [229]; [d] [230]; [e] [203]; [f] [111]; [g] [231]; [h] [232]; [i] [233].

[j] literature data for the viscosity and density of binary system of [bmim][BF4] (1) + NMP (2), $w_1 = 0.5000$ [111]

Table I-2: Data of the viscosity (η), density (ρ), sound velocity (c), refractive index (n_D), coefficients of thermal expansion (α), the excess coefficients of thermal expansion (α^E), the excess molar volume (V^E) and the deviations of viscosity ($\Delta\eta$) at different mass compositions (w) for the system of MEA (1) + H$_2$O (2) + bmim[OTF] (3) [a].

property	Temperature (K)								
	293.15	298.15	303.15	308.15	313.15	318.15	323.15	328.15	333.15
	$w_{3/}\ w_2/w_1 = 0/0.6996/0.3004$								
η (mPa.s)	3.125 2.990[b]	2.714 2.48[b] 2.489[b]	2.397 2.195[b]	2.143	1.950 1.67[b] 1.671[b]	1.795	-	-	-
ρ (g/cm^3)	1.0127	1.0106 1.0106[b]	1.0084	1.0060	1.0035 1.0034[b]	1.0009	0.9981 0.9981[b]	0.9953	0.9923
c (m/s)	1672.7	1672.6	1671.6	1669.8	1667.3	1664.0	1659.8	1655.2	1649.8
n_D	1.37097	1.3701	1.3692	1.3682	1.3672	1.3663	1.3652	1.3642	1.3631
α (1/K)	0.000406	0.000431	0.000457	0.000483	0.000509	0.000535	0.000562	0.000588	0.000615
α^E (1/K)	0.000020	0.000016	0.000013	0.000009	0.000006	0.000002	-0.000001	-0.000004	-0.000008
V^E (cm^3.mol^{-1})	-0.1909	-0.1885	-0.1871	-0.1863	-0.1864	-0.1869	-0.1864	-0.1873	-0.1884
$\Delta\eta$ (mPa.s)	-0.555	-0.280	-0.080	0.057	0.171	0.250	-	-	-

property	Temperature (K)								
	293.15	298.15	303.15	308.15	313.15	318.15	323.15	328.15	333.15
$w_3/w_2/w_1$= 0.1045/0.5836/0.3119									
η (mPa.s)	4.300	3.656	3.152	2.758	2.447	2.198	2.004	1.847	1.718
ρ (g/cm^3)	1.0411	1.0385	1.0357	1.0328	1.0299	1.0269	1.0237	1.0205	1.0172
c (m/s)	1701.8	1696.6	1691.0	1685.0	1678.5	1671.7	1664.3	1656.4	1648.0
n_D	1.3832	1.3821	1.3810	1.3799	1.3787	1.3775	1.3763	1.3752	1.3742
α (1/K)	0.000505	0.000524	0.000543	0.000562	0.000582	0.000601	0.000621	0.000641	0.000661
α^E (1/K)	0.000076	0.000070	0.000063	0.000057	0.000051	0.000045	0.000039	0.000033	0.000027
V^E (cm^3.mol^{-1})	-0.2860	-0.2764	-0.2684	-0.2614	-0.2555	-0.2503	-0.2459	-0.2416	-0.2376
$\Delta\eta$ (mPa.s)	-0.895	-0.525	-0.267	-0.088	0.045	0.128	0.220	0.287	0.342
$w_3/w_2/w_1$= 0.2392/0.4614/0.2994									
η (mPa.s)	-	5.025	4.267	3.670	3.186	2.805	2.511	2.269	2.073
ρ (g/cm^3)	-	1.0732	1.0700	1.0666	1.0633	1.0598	1.0563	1.0527	1.0490
c (m/s)	-	1685.7	1677.4	1668.9	1659.9	1650.7	1641.1	1631.2	1621.2
n_D	1.3955	1.3947	1.3931	1.3918	1.3905	1.3891	1.3878	1.3863	1.3852
α (1/K)	-	0.000598	0.000613	0.000628	0.000643	0.000658	0.000674	0.000689	0.000705
α^E (1/K)	-	0.000106	0.000099	0.000093	0.000087	0.000081	0.000075	0.000069	0.000064
V^E (cm^3.mol^{-1})	-	-0.3428	-0.3284	-0.3149	-0.3025	-0.2909	-0.2798	-0.2695	-0.2595
$\Delta\eta$ (mPa.s)	-	-0.916	-0.548	-0.301	-0.137	-0.043	0.073	0.154	0.221
$w_3/w_2/w_1$= 0.4311/0.2643/0.3046									
η (mPa.s)	11.545	9.477	7.866	6.611	5.618	4.823	4.182	3.665	3.242
ρ (g/cm^3)	1.1277	1.1240	1.1202	1.1164	1.1125	1.1086	1.1047	1.1007	1.0967
c (m/s)	1651.0	1640.3	1629.3	1618.2	1606.8	1595.3	1583.6	1571.6	1559.5
n_D	1.4165	1.4151	1.4137	1.4121	1.4106	1.4093	1.4082	1.4066	1.4054

Property	Temperature (K)								
	293.15	298.15	303.15	308.15	313.15	318.15	323.15	328.15	333.15
$w_{3/}$ w_2/w_1= 0.4311/0.2643/0.3046									
α (1/K)	0.000657	0.000667	0.000677	0.000687	0.000698	0.000708	0.000719	0.000730	0.000741
α^E(1/K)	0.000105	0.000102	0.000099	0.000096	0.000093	0.000090	0.000087	0.000084	0.000081
V^E (cm^3.mol^{-1})	-0.4215	-0.4001	-0.3800	-0.3605	-0.3417	-0.3237	-0.3058	-0.2885	-0.2710
$\Delta\eta$ (mPa.s)	-2.320	-1.501	-0.944	-0.582	-0.343	-0.252	-0.126	-0.037	0.030

[a] Expanded uncertainties are: $U(T)$ = 0.02 K; $U(\rho)$ = 0.0002 g.cm^{-3}, $U(\eta)$ = 0.003 mPa.s, $U(c)$ = 0.7 m.s^{-1} (Data recorded at 101 kPa, $U(P)$ = 1 kPa), and $U(n_D)$ = 0.001 (data recorded at 101 kPa and a standard wavelength of 589 nm, $U(P)$ = 1 kPa).
[b] Literature data for the viscosity and density of binary system of MEA (1) + H$_2$O (2), w_1 = 0.3000 [234, 235].

Table I-3: Data of the viscosity (η), density (ρ), sound velocity (c), refractive index (n_D), coefficients of thermal expansion (α), the excess coefficients of thermal expansion (α^E), the excess molar volume (V^E) and the deviations of viscosity ($\Delta\eta$) at different mass compositions (w) for the system of DGA (1) + H$_2$O (2) + bmim[OTF] (3) [a].

property	Temperature (K)								
	293.15	298.15	303.15	308.15	313.15	318.15	323.15	328.15	333.15
$w_{3/}$ w_2/w_1= 0/0.4868/0.5132									
η (mPa.s)	8.691	7.123	5.908	4.964	4.215	3.629	3.167	2.794	2.498
ρ (g/cm^3)	1.0515	1.0482	1.0449	1.0414	1.0380	1.0344	1.0308	1.0271	1.0234
c (m/s)	1784.1	1772.5	1760.7	1748.9	1736.8	1724.6	1712.1	1699.1	1685.8
n_D	1.4039	1.4026	1.4012	1.3998	1.3984	1.3971	1.3956	1.3941	1.3932
α (1/K)	0.000621	0.000635	0.000649	0.000663	0.000677	0.000692	0.000706	0.000721	0.000736
α^E (1/K)	0.000131	0.000122	0.000114	0.000106	0.000098	0.000090	0.000082	0.000074	0.000066
V^E (cm^3.mol^{-1})	-0.7163	-0.6980	-0.6819	-0.6674	-0.6542	-0.6422	-0.6311	-0.6209	-0.6115
$\Delta\eta$ (mPa.s)	2.683	2.348	2.054	1.794	1.563	1.371	1.233	1.111	1.020
$w_{3/}$ w_2/w_1=0.1006/0.3878/0.5116									
η (mPa.s)	11.305	9.197	7.591	6.337	5.366	4.581	3.959	3.457	3.052
ρ (g/cm^3)	1.0764	1.0728	1.0691	1.0654	1.0617	1.0579	1.0541	1.0502	1.0463

property	Temperature (K)								
	293.15	298.15	303.15	308.15	313.15	318.15	323.15	328.15	333.15
$w_{3/}\,w_2/w_1$=0.1006/0.3878/0.5116									
c (m/s)	1762.7	1750.3	1737.5	1724.5	1711.5	1698.3	1684.7	1670.8	1656.7
n_D	1.4140	1.4134	1.4111	1.4096	1.4081	1.4065	1.4051	1.4039	1.4026
α (1/K)	0.000665	0.000676	0.000687	0.000698	0.000709	0.000721	0.000732	0.000744	0.000756
α^E (1/K)	0.000137	0.000129	0.000121	0.000114	0.000107	0.000099	0.000092	0.000085	0.000077
V^E (cm^3.mol^{-1})	-0.8064	-0.7843	-0.7643	-0.7461	-0.7293	-0.7137	-0.6991	-0.6853	-0.6722
$\Delta\eta$ (mPa.s)	3.012	2.638	2.330	2.037	1.792	1.549	1.375	1.225	1.104
$w_{3/}\,w_2/w_1$=0.2593/0.2665/0.4742									
η (mPa.s)	15.971	12.843	10.477	8.661	7.252	6.139	5.248	4.534	3.956
ρ (g/cm^3)	1.1125	1.1086	1.1047	1.1008	1.0968	1.0928	1.0888	1.0847	1.0806
c (m/s)	1700.4	1687.5	1674.3	1661.1	1647.8	1634.3	1620.7	1607.0	1593.0
n_D	1.4251	1.4236	1.4220	1.4205	1.4189	1.4174	1.4157	1.4140	1.4135
α (1/K)	0.000690	0.000699	0.000708	0.000717	0.000726	0.000736	0.000745	0.000754	0.000764
α^E (1/K)	0.000119	0.000114	0.000109	0.000104	0.000100	0.000095	0.000090	0.000085	0.000081
V^E (cm^3.mol^{-1})	-0.8367	-0.8121	-0.7894	-0.7679	-0.7477	-0.7282	-0.7095	-0.6917	-0.6743
$\Delta\eta$ (mPa.s)	3.099	2.706	2.388	2.089	1.823	1.544	1.354	1.189	1.055
$w_{3/}\,w_2/w_1$= 0.4024/0.1/0.4976									
η (mPa.s)	28.789	22.548	17.986	14.603	12.008	10.049	8.519	7.249	6.179
ρ (g/cm^3)	1.1483	1.1442	1.1402	1.1361	1.1321	1.1280	1.1239	1.1198	1.1157
c (m/s)	1612.4	1598.9	1585.4	1572.0	1558.5	1545.0	1531.6	1517.9	1504.7
n_D	1.4422	1.4409	1.4391	1.4375	1.4359	1.4342	1.4326	1.4292	-
α (1/K)	0.000699	0.000704	0.000709	0.000715	0.000720	0.000725	0.000730	0.000735	0.000741
α^E (1/K)	0.000052	0.000050	0.000048	0.000046	0.000044	0.000042	0.000040	0.000038	0.000036
V^E (cm^3.mol^{-1})	-0.8935	-0.8762	-0.8604	-0.8457	-0.8318	-0.8180	-0.8056	-0.7926	-0.7807
$\Delta\eta$ (mPa.s)	2.285	1.775	1.504	1.292	1.082	0.842	0.761	0.632	0.478

Table I-4: Data of the viscosity (η), density (ρ), sound velocity (c), refractive index (n_D), coefficients of thermal expansion (α), the excess coefficients of thermal expansion (α^E), the excess molar volume (V^E) and the deviations of viscosity ($\Delta\eta$) at different mass compositions (w) for the system of MEA (1) + H₂O (2) / bmim[OTF] (2) / (NMP (2) + bmim[TF₂N] (3)) ᵃ.

property	Temperature (K)								
	293.15	298.15	303.15	308.15	313.15	318.15	323.15	328.15	333.15
$w_1=0.091$, $w_{bmim[OTF]}=0.9088$									
η (mPa.s)	52.922	41.987	34.402	28.383	23.755	20.13	17.249	14.939	13.046
ρ (g/cm³)	1.2649	1.2608	1.2568	1.2527	1.2486	1.2446	1.2406	1.2366	1.2326
c (m/s)	1440.6	1428.8	1417.0	1405.2	1393.6	1382.1	1370.6	1359.2	1348.0
n_D	1.4405	1.4391	1.4377	1.4363	1.4348	1.4333	1.4319	1.4303	1.4287
α (1/K)	0.000649	0.000649	0.000648	0.000648	0.000648	0.000648	0.000647	0.000647	0.000647
α^E (1/K)	0.000012	0.000011	0.000019	0.000018	0.000017	0.000016	0.000015	0.000014	0.000013
V^E (cm³.mol⁻¹)	0.3245	0.3402	0.3534	0.3670	0.3796	0.3926	0.4050	0.4174	0.4288
$\Delta\eta$ (mPa.s)	-25.305	-19.468	-14.386	-11.004	-8.527	-7.315	-5.850	-4.738	-3.889
$w_1=0.1034$, $w_{water}=0.8966$									
η (mPa.s)	1.389	1.224	1.087	0.973	0.878	0.798	0.731	0.673	0.622
	1.442ᶜ	1.299ᶜ	1.121ᶜ		0.909ᶜ		.0715ᶜ		0.626ᶜ
ρ (g/cm³)	1.0024	1.0010	0.9993	0.9975	0.9956	0.9934	0.9911	0.9886	0.9860
c (m/s)	1546.0	1555.2	1563.0	1569.4	1574.6	1578.6	1581.5	1583.4	1584.1
n_D	1.3455	1.3449	1.3443	1.3435	1.3428	1.3420	1.3413	1.3404	1.3395
α (1/K)	0.000273	0.000308	0.000342	0.000377	0.000412	0.000447	0.000483	0.000519	0.000554
α^E (1/K)	-0.000007	-0.000007	-0.000008	-0.000009	-0.000010	-0.000011	-0.000012	-0.000013	-0.000013
V^E (cm³.mol⁻¹)	-0.0398	-0.0404	-0.0411	-0.0423	-0.0433	-0.0443	-0.0456	-0.0469	-0.0482
$\Delta\eta$ (mPa.s)	-0.401	-0.288	-0.210	-0.156	-0.118	-0.097	-0.068	-0.053	-0.042
$w_1=0.1021$, $w_{NMP}=0.8979$									
η (mPa.s)	2.990	2.712	2.484	2.293	2.133	1.996	1.880	1.782	1.695

property	Temperature (K)								
	293.15	298.15	303.15	308.15	313.15	318.15	323.15	328.15	333.15
w_1=0.1021, w_{NMP}=0.8979									
ρ (g/cm^3)	1.0366	1.0321	1.0276	1.0231	1.0186	1.0141	1.0096	1.0050	1.0004
c (m/s)	1584.9	1566.3	1547.1	1528.1	1509.2	1490.4	1471.8	1453.5	1435.6
α (1/K)	0.000859	0.000866	0.000872	0.000879	0.000886	0.000893	0.000900	0.000907	0.000914
α^E (1/K)	0.000010	0.000012	0.000013	0.000015	0.000016	0.000018	0.000020	0.000021	0.000023
V^E (cm^3.mol^{-1})	-0.3585	-0.3473	-0.3395	-0.3394	-0.3382	-0.3273	-0.3223	-0.3146	-0.3044
$\Delta\eta$ (mPa.s)	-2.378	-1.757	-1.273	-0.915	-0.644	-0.437	-0.269	-0.135	-0.028
w_1=0.2008, w_{water}=0.7992									
η (mPa.s)	1.903 2.005[d]	1.689 1.70[b] 1.702[d]	1.482 1.501[d]	1.310	1.168 1.18[b] 1.169[d]	1.048	0.948 0.95[b] 0.945[d]	0.863	0.789 0.775[d]
ρ (g/cm^3)	1.0071	1.0054 1.0053[b]	1.0035	1.0014	0.9992 0.9991[b]	0.9968	0.9943 0.9943[b]	0.9917	0.9889
c (m/s)	1609.0	1614.5	1618.4	1620.9	1622.3	1622.7	1622.0	1620.4	1617.9
n_D	1.3579	1.3572	1.3564	1.3556	1.3548	1.3538	1.3528	1.3519	1.3508
α (1/K)	0.000336	0.000365	0.000395	0.000426	0.000456	0.000487	0.000517	0.000548	0.000580
α^E (1/K)	0.000003	0.000001	-0.000002	-0.000004	-0.000006	-0.000008	-0.000011	-0.000013	-0.000015
V^E (cm^3.mol^{-1})	-0.1013	-0.1009	-0.1010	-0.1016	-0.1024	-0.1036	-0.1049	-0.1063	-0.1078
$\Delta\eta$ (mPa.s)	-0.746	-0.497	-0.352	-0.253	-0.185	-0.142	-0.098	-0.072	-0.053
w_1=0.2090, w_{NMP}=0.7910									
η (mPa.s)	3.547	3.176	2.869	2.612	2.397	2.218	2.065	1.938	1.830
ρ (g/cm^3)	1.0322	1.0277	1.0233	1.0188	1.0143	1.0098	1.0052	1.0007	0.9961
c (m/s)	1595.0	1576.1	1557.1	1538.2	1519.4	1500.7	1482.6	1464.4	1446.5
α (1/K)	0.000862	0.000868	0.000875	0.000882	0.000889	0.000896	0.000903	0.000910	0.000918
α^E (1/K)	0.000023	0.000024	0.000026	0.000027	0.000028	0.000030	0.000032	0.000033	0.000035
V^E (cm^3.mol^{-1})	-0.1167	-0.1047	-0.0918	-0.0847	-0.0760	-0.0592	-0.0430	-0.0323	-0.0216
$\Delta\eta$ (mPa.s)	-5.140	-3.867	-2.920	-2.229	-1.705	-1.303	-0.987	-0.733	-0.528

property	Temperature (K)								
	293.15	298.15	303.15	308.15	313.15	318.15	323.15	328.15	333.15
w_1=0.3004, w_{water}=0.6996									
η (mPa.s)	3.125	2.714	2.397	2.143	1.950	1.795			
ρ (g/cm^3)	1.0127	1.0106	1.0084	1.0060	1.0035	1.0009	0.9981	0.9953	0.9923
c (m/s)	1672.7	1672.6	1671.6	1669.8	1667.3	1664.0	1659.8	1655.2	1649.8
α (1/K)	0.000406	0.000431	0.000457	0.000483	0.000509	0.000535	0.000562	0.000588	0.000615
α^E(1/K)	0.000020	0.000016	0.000013	0.000009	0.000006	0.000002	-0.000001	-0.000004	-0.000008
V^E (cm^3.mol^{-1})	-0.1909	-0.1885	-0.1871	-0.1863	-0.1864	-0.1869	-0.1864	-0.1873	-0.1884
$\Delta\eta$ (mPa.s)	-0.555	-0.280	-0.080	0.057	0.171	0.250			
w_1=0.3089, w_{NMP}=0.6911									
η (mPa.s)	4.720	4.121	3.633	3.236	2.909	2.638	2.415	2.228	2.075
ρ (g/cm^3)	1.0310	1.0266	1.0222	1.0177	1.0133	1.0088	1.0043	0.9999	0.9956
c (m/s)	1612.3	1593.9	1575.1	1556.5	1538.0	1519.7	1501.8	1484.1	1467.1
α (1/K)	0.000866	0.000868	0.000871	0.000874	0.000877	0.000880	0.000883	0.000886	0.000889
α^E(1/K)	0.000036	0.000033	0.000030	0.000028	0.000025	0.000022	0.000020	0.000016	0.000014
V^E (cm^3.mol^{-1})	-0.1452	-0.1311	-0.1182	-0.1098	-0.1012	-0.0862	-0.0764	-0.0685	-0.0732
$\Delta\eta$ (mPa.s)	-6.731	-5.065	-3.848	-2.963	-2.297	-1.789	-1.389	-1.070	-0.812
w_1=0.0976, w_{NMP}=0.8032, $w_{bmim[TF2N]}$=0.0992									
η (mPa.s)	3.357	3.042	2.776	2.553	2.364	2.204	2.068	1.950	1.848
ρ (g/cm^3)	1.0653	1.0608	1.0564	1.0519	1.0474	1.0428	1.0383	1.0337	1.0291
c (m/s)	1553.8	1535.6	1517.2	1498.9	1480.9	1463.0	1445.3	1427.9	1410.8
α (1/K)	0.000837	0.000844	0.000850	0.000856	0.000863	0.000870	0.000876	0.000883	0.000890
α^E(1/K)	0.000002	0.000004	0.000005	0.000007	0.000008	0.000010	0.000012	0.000013	0.000015
V^E (cm^3.mol^{-1})	-0.2766	-0.2725	-0.2680	-0.2699	-0.2704	-0.2627	-0.2600	-0.2566	-0.2509
$\Delta\eta$ (mPa.s)	-3.277	-2.435	-1.845	-1.370	-1.011	-0.737	-0.518	-0.345	-0.204
w_1=0.1138, w_{NMP}=0.6414, $w_{bmim[TF2N]}$=0.2448									
η (mPa.s)	4.749	4.206	3.761	3.388	3.089	2.818	2.599	2.410	2.252

property	Temperature (K)								
	293.15	298.15	303.15	308.15	313.15	318.15	323.15	328.15	333.15
w_1=0.1138, w_{NMP}=0.6414, $w_{bmim[TF2N]}$=0.2448									
ρ (g/cm^3)	1.1099	1.1055	1.1009	1.0964	1.0918	1.0872	1.0826	1.0780	1.0733
c (m/s)	1512.4	1495.3	1478.3	1461.3	1444.5	1427.8	1411.3	1395.1	1379.1
α (1/K)	0.000808	0.000816	0.000823	0.000831	0.000838	0.000846	0.000854	0.000862	0.000870
α^E(1/K)	-0.000003	0.000000	0.000003	0.000007	0.000009	0.000013	0.000017	0.000020	0.000024
V^E (cm^3.mol^{-1})	-0.1143	-0.1161	-0.1119	-0.1122	-0.1107	-0.1004	-0.0951	-0.0876	-0.0778
$\Delta\eta$ (mPa.s)	-5.004	-3.735	-2.924	-2.227	-1.695	-1.309	-0.995	-0.751	-0.553
w_1=0.1162, w_{NMP}=0.4932, $w_{bmim[TF2N]}$=0.3906									
η (mPa.s)	6.416	5.617	4.959	4.413	3.958	3.575	3.254	2.982	2.752
ρ (g/cm^3)	1.1583	1.1538	1.1492	1.1446	1.1400	1.1353	1.1307	1.1261	1.1214
c (m/s)	1463.2	1447.3	1431.4	1415.6	1399.9	1384.3	1368.8	1353.5	1338.4
n_D	1.4544	1.4526	1.4507	1.4489	1.4470	1.4447	1.4431	1.4412	1.4393
α (1/K)	0.000789	0.000794	0.000799	0.000805	0.000810	0.000816	0.000821	0.000827	0.000833
α^E(1/K)	0.000001	0.000003	0.000005	0.000007	0.000008	0.000010	0.000012	0.000014	0.000016
V^E (cm^3.mol^{-1})	0.1349	0.1343	0.1404	0.1431	0.1467	0.1570	0.1624	0.1686	0.1761
$\Delta\eta$ (mPa.s)	-6.735	-5.017	-4.008	-3.079	-2.392	-1.875	-1.471	-1.155	-0.901

[a] Expanded uncertainties are: $U(T)$ = 0.02 K; $U(\rho)$ = 0.0002 g.cm^{-3}, $U(\eta)$ = 0.003 mPa.s, $U(c)$ = 0.7 m.s^{-1} (Data recorded at 101 kPa, $U(P)$ = 1 kPa), and $U(n_D)$ = 0.001 (data recorded at 101 kPa and a standard wavelength of 589 nm, $U(P)$ = 1 k.

[b] Literature data for the viscosity and density of binary system of MEA (1) + H$_2$O (2), w_1 = 0.2000 [234].

[c] Literature data for the viscosity of binary system of MEA (1) + H$_2$O (2), w_1 = 0.1000 [235].

[d] Literature data for the viscosity of binary system of MEA (1) + H$_2$O (2), w_1 = 0.2000 [235].

Table I-5: Data of the viscosity (η), density (ρ), sound velocity (c), refractive index (n_D), coefficients of thermal expansion (α), the excess coefficients of thermal expansion (α^E), the excess molar volume (V^E) and the deviations of viscosity ($\Delta\eta$) at different mass compositions (w) for the system of DGA (1) + H$_2$O/NMP (2) + bmim[TF$_2$N] (3) [a].

property	Temperature (K)								
	293.15	298.15	303.15	308.15	313.15	318.15	323.15	328.15	333.15
$w_{NMP}/w_1 = 0.5019/0.4981$									
η (mPa.s)	7.477	6.414	5.530	4.816	4.229	3.746	3.344	3.019	2.743
ρ (g/cm^3)	1.0450	1.0407	1.0364	1.0321	1.0277	1.0234	1.0190	1.0146	1.0102
c (m/s)	1595.7	1579.1	1561.9	1544.7	1527.6	1510.6	1493.7	1476.9	1460.4
α (1/K)	0.000818	0.000824	0.000831	0.000838	0.000844	0.000851	0.000858	0.000865	0.000872
α^E (1/K)	0.000010	0.000011	0.000012	0.000014	0.000015	0.000017	0.000018	0.000020	0.000021
V^E (cm^3.mol^{-1})	-0.0258	-0.0210	-0.0145	-0.0086	-0.0016	0.0066	0.0161	0.0249	0.0347
$\Delta\eta$ (mPa.s)	-9.729	-7.137	-5.285	-3.981	-3.048	-2.360	-1.842	-1.434	-1.118
$w_{NMP}/w_1 = 0.6898/0.3102$									
η (mPa.s)	4.923	4.260	3.770	3.360	3.031	2.752	2.518	2.325	2.159
ρ (g/cm^3)	1.0426	1.0382	1.0339	1.0295	1.0251	1.0207	1.0162	1.0117	1.0072
c (m/s)	1585.3	1569.0	1552.3	1534.9	1517.7	1500.6	1483.7	1466.7	1450.0
α (1/K)	0.000832	0.000839	0.000847	0.000854	0.000862	0.000869	0.000877	0.000885	0.000893
α^E (1/K)	0.000012	0.000014	0.000017	0.000019	0.000021	0.000023	0.000026	0.000028	0.000031
V^E (cm^3.mol^{-1})	-0.0368	-0.0299	-0.0211	-0.0129	-0.0035	0.0067	0.0194	0.0327	0.0481
$\Delta\eta$ (mPa.s)	-8.608	-6.465	-4.841	-3.685	-2.832	-2.198	-1.712	-1.330	-1.029
$w_{H2O}/w_1 = 0.7077/0.2923$									
η (mPa.s)	2.927	2.515	2.167	1.885	1.656	1.466	1.308	1.176	1.063
ρ (g/cm^3)	1.0266	1.0256	1.0232	1.0207	1.0181	1.0153	1.0124	1.0094	1.0063
c (m/s)	1676.1	1674.5	1672.1	1669.2	1665.6	1661.4	1656.5	1651.0	1644.8
n_D	1.3722	1.3712	1.3703	1.3693	1.3683	1.3673	1.3662	1.3651	1.364005
α (1/K)	0.000354	0.000393	0.000434	0.000474	0.000515	0.000556	0.000597	0.000638	0.000680
α^E (1/K)	-0.000020	-0.000010	0.000000	0.000011	0.000022	0.000033	0.000045	0.000056	0.000068
V^E (cm^3.mol^{-1})	-0.2792	-0.3023	-0.2969	-0.2923	-0.2883	-0.2849	-0.2818	-0.2791	-0.2768

property	Temperature (K)								
	293.15	298.15	303.15	308.15	313.15	318.15	323.15	328.15	333.15
$w_{H2O}/w_1 = 0.7077/0.2923$									
$\Delta\eta$ (mPa.s)	-0.241	-0.059	0.042	0.099	0.129	0.135	0.147	0.145	0.139
$w_3/w_{NMP}/w_1 = 0.3923/0.3096/0.2981$									
η (mPa.s)	12.206	10.270	8.744	7.522	6.541	5.736	5.069	4.517	4.053
ρ (g/cm^3)	1.1700	1.1655	1.1610	1.1566	1.1521	1.1476	1.1431	1.1387	1.1342
c (m/s)	1467.0	1452.1	1436.9	1421.9	1407.0	1392.3	1377.6	1363.0	1348.5
n_D	1.4534	1.4515	1.4497	1.4480	1.4461	1.4443	1.4424	1.4406	1.438875
α (1/K)	0.000764	0.000767	0.000770	0.000773	0.000777	0.000780	0.000783	0.000786	0.000790
α^E(1/K)	-0.000001	-0.000001	-0.000002	-0.000002	-0.000002	-0.000002	-0.000003	-0.000004	-0.000003
V^E (cm^3.mol^{-1})	0.0771	0.0759	0.0769	0.0760	0.0747	0.0736	0.0733	0.0704	0.0689
$\Delta\eta$ (mPa.s)	-9.257	-6.744	-5.212	-3.922	-2.999	-2.326	-1.825	-1.442	-1.145
$w_3/w_{NMP}/w_1 = 0.2503/0.4462/0.3035$									
η (mPa.s)	8.078	6.927	6.008	5.260	4.651	4.139	3.714	3.359	3.062
ρ (g/cm^3)	1.1200	1.1156	1.1112	1.1067	1.1023	1.0978	1.0934	1.0889	1.0845
c (m/s)	1511.9	1495.7	1479.1	1462.9	1447.0	1431.1	1415.3	1399.6	1383.9
n_D	1.4588	1.4568	1.45487	1.452985	1.45107	1.449225	1.44726	1.44528	1.44337
α (1/K)	0.000789	0.000793	0.000797	0.000802	0.000806	0.000811	0.000815	0.000820	0.000824
α^E(1/K)	0.000000	0.000000	0.000000	0.000001	0.000000	0.000001	0.000001	0.000001	0.000001
V^E (cm^3.mol^{-1})	0.0052	0.0044	0.0057	0.0055	0.0062	0.0061	0.0068	0.0066	0.0077
$\Delta\eta$ (mPa.s)	-8.853	-6.517	-4.965	-3.746	-2.865	-2.221	-1.731	-1.354	-1.057
$w_3/w_{NMP}/w_1 = 0.0994/0.6166/0.2840$									
η (mPa.s)	5.359	4.682	4.146	3.690	3.316	3.017	2.747	2.523	2.335
ρ (g/cm^3)	1.0712	1.0668	1.0624	1.0580	1.0536	1.0492	1.0447	1.0403	1.0358
c (m/s)	1554.7	1537.5	1519.9	1502.1	1485.2	1467.9	1450.8	1433.8	1416.9
n_D	1.4640	1.46216	1.460165	1.458215	1.45617	1.454135	1.45217	1.45	1.44793
α (1/K)	0.000816	0.000822	0.000827	0.000833	0.000838	0.000844	0.000850	0.000856	0.000861

property	Temperature (K)								
	293.15	298.15	303.15	308.15	313.15	318.15	323.15	328.15	333.15
$w_3/w_{NMP}/w_1$ = 0.0994/0.6166/0.2840									
α^E (1/K)	0.000001	0.000002	0.000003	0.000004	0.000003	0.000005	0.000006	0.000007	0.000007
V^E (cm^3.mol^{-1})	-0.0825	-0.0813	-0.0791	-0.0791	-0.0769	-0.0756	-0.0731	-0.0712	-0.0666
$\Delta\eta$ (mPa.s)	-7.086	-5.244	-3.925	-2.956	-2.249	-1.710	-1.315	-1.006	-0.761
w_{H2O}/w_1 = 0.4868/0.5132									
η (mPa.s)	8.691	7.123	5.908	4.964	4.215	3.629	3.167	2.794	2.498
ρ (g/cm^3)	1.0515	1.0482	1.0449	1.0414	1.0380	1.0344	1.0308	1.0271	1.0234
c (m/s)	1784.1	1772.5	1760.7	1748.9	1736.8	1724.6	1712.1	1699.1	1685.8
n_D	1.4039	1.4026	1.4012	1.3998	1.3984	1.3971	1.3956	1.3941	1.3932
α (1/K)	0.000621	0.000635	0.000649	0.000663	0.000677	0.000692	0.000706	0.000721	0.000736
α^E (1/K)	0.000131	0.000122	0.000114	0.000106	0.000098	0.000090	0.000082	0.000074	0.000066
V^E (cm^3.mol^{-1})	-0.7163	-0.6980	-0.6819	-0.6674	-0.6542	-0.6422	-0.6311	-0.6209	-0.6115
$\Delta\eta$ (mPa.s)	2.683	2.348	2.054	1.794	1.563	1.371	1.233	1.111	1.020

[a] Expanded uncertainties are: $U(T)$ = 0.02 K; $U(\rho)$ = 0.0002 g.cm^{-3}, $U(\eta)$ = 0.003 mPa.s, $U(c)$ = 0.7 m.s^{-1} (Data recorded at 101 kPa, $U(P)$ = 1 kPa), and $U(n_D)$ = 0.001 (data recorded at 101 kPa and a standard wavelength of 589 nm, $U(P)$ = 1 kPa).

APPENDIX J. REGRESSION OF THE PHYSICAL PROPERTIES OF SOLVENTS

The viscosity data were fitted to the Vogel–Fulcher–Tammann (VFT) equation [236-238]:

$$\eta = A_1 . \exp[\frac{A_2}{T - A_3}]$$ (J-1)

The measured data of density and sound velocity were regressed using the following equations [230, 238]:

$$\rho = B_1 T^2 + B_2 T + B_3$$ (J-2)

$$c = D_1 T + D_2$$ (J-3)

Where η(mPa.s), ρ(g.cm^3) and c(m/s) are viscosity, density and sound velocity respectively. T is the temperature with the unit Kelvin, and A, B and D are fitting parameters.

The coefficients of thermal expansions, the excess coefficients of thermal expansion, the excess molar volumes and the deviations of viscosity were calculated from the physical properties measured. These properties provide information about the intermolecular interactions between the components of the hybrid solvent [199, 201, 202, 239]. The coefficient of thermal expansion,α (1/K), represents the effect of temperature on the volume of solution, as follows [99, 240-243]:

$$\alpha = \frac{1}{V}\left(\frac{\delta V}{\delta T}\right) = -\frac{1}{\rho}(\frac{\delta \rho}{\delta T})_P$$ (J-4)

The excess coefficient of thermal expansion, α^E (1/K), is calculated using the following equations [99, 240, 242, 243]:

$$\alpha^E = \alpha - \sum_{i=1}^{N} \varphi_i \alpha_i$$ (J-5)

$$\varphi_i = x_i v_i / \sum_{i=1}^{N} x_i v_i$$ (J-6)

Where N is the number of components, and α_i (1/K), φ_i, x_i and v_i (cm^3.mol^{-1}) are thermal expansion coefficient, volumetric fraction, mole fraction and molar volume of the ith component of solution, respectively. The measured data for the pure components are listed in Table K-1. The α^E can

describe the packing of components present in a mixture and their orientation. The positive α^E shows the self-association of the components and the negative α^E strongly suggests the presence of hydrogen bond between the components [99, 242, 244].

Excess molar volume, V^E (cm³.mol⁻¹), is computed as follows [99, 199, 200, 202, 241, 245, 246]:

$$V^E = \sum_{i=1}^{N} x_i M_i \left(\frac{1}{\rho} - \frac{1}{\rho_i} \right) \tag{J-7}$$

Where ρ_i and M_i (g/mol) are density and molar mass of the ith component of solution. The excess molar volume results from contributions of several opposing effects. They can be divided into three types: chemical, physical, and structural. Physical contributions, which are non-specific interactions between the components of the mixture, result in a positive V^E. The chemical or specific intermolecular interactions contribute a volume decrease and a negative V^E. Finally, the structural contributions mostly lead to negative values of V^E. They arise from several effects, especially from the geometrical fitting (interstitial accommodation) of one component into the other because of the differences in the free volume and molar volume between components [99, 199, 244].

Deviation of viscosity, $\Delta\eta$ (mPa.s), is obtained by applying the following equation [201, 202, 239, 246]:

$$\Delta\eta = \eta - \sum_{i=1}^{N} x_i \eta_i \tag{J-8}$$

Where η_i is viscosity of the ith component of solution. Negative values of $\Delta\eta$ indicate that components face less resistance to flow upon mixing [246].

APPENDIX K. TABULATED PHYSICAL PROPERTIES OF PURE CHEMICALS

Table K-1: Data of the viscosity (η), density (ρ), sound velocity (c), coefficients of thermal expansion (α), and the molar volume (v) for pure components present in the hybrid solvents[a].

property	Temperature (K)								
	293.15	298.15	303.15	308.15	313.15	318.15	323.15	328.15	333.15
MEA									
η (mPa.s)	24.777 24.085[b]	19.516 18.924[b]	15.639 15.151[b] 15[b]	12.749	10.528 10.006[b] 9.94[b]	8.798	7.426 6.962[b] 6.87[b]	6.326	5.436 5.037[b]
ρ (g/cm³)	1.0184	1.0145	1.0105 1.009[b]	1.0066	1.0026 0.9999[b]	0.9986	0.9946 0.9918[b]	0.9906	0.9866
c (m/s)	1738.8	1722.6	1706.3	1690.1	1674.0	1658.0	1642.0	1626.3	1610.7
α (1/K)	0.000768	0.000775	0.000781	0.000787	0.000793	0.0008	0.000806	0.000813	0.000819
v (cm³.mol⁻¹)	59.9776	60.2092	60.4441	60.6814	60.9216	61.1647	61.4106	61.6596	61.9122
DGA									
η (mPa.s)	33.682	26.222 26.658[c]	20.702	16.649	13.614 13.432[c]	11.286	9.470 9.155[c]	8.034	6.880 6.530[c]
ρ (g/cm³)	1.0555	1.0515 1.05156[c]	1.0475	1.0435	1.0395 1.03953[c]	1.0354	1.0314 1.03137[c]	1.0273	1.0232 1.02321[c]
c (m/s)	1646.5	1630.7	1614.7	1598.7	1582.7	1566.8	1551.0	1535.3	1519.8
α (1/K)	0.000757	0.000762	0.000767	0.000773	0.000778	0.000783	0.000788	0.000794	0.000799
v (cm³.mol⁻¹)	99.6083	99.9875	100.3708	100.7581	101.1493	101.5444	101.9440	102.3480	102.7571
Bmim[OTF]									
η (mPa.s)	103.530	81.309	64.480 63.453[d]	51.997	42.580 42.112[d]	36.272	30.519 28.354[d]	25.997	22.379 20.911[d]

property	Temperature (K)								
	293.15	298.15	303.15	308.15	313.15	318.15	323.15	328.15	333.15
Bmim[OTF]									
ρ (g/cm^3)	1.2992	1.2952	1.2912 1.3054[d]	1.2873	1.2833 1.2945[d]	1.2794	1.2755 1.2865[d]	1.2716	1.2677 1.2791[d]
c (m/s)	1408	1396.74	1385.5	1374.42	1363.54	1352.87	1342.66	1332.43	1322.61
α (1/K)	0.000616	0.000615	0.000615	0.000614	0.000614	0.000613	0.000613	0.000612	0.000612
v(cm^3.mol^{-1})	221.8960	222.5789	223.2655	223.9521	224.6411	225.3311	226.0231	226.7158	227.41077
Bmim[TF$_2$N]									
η (mPa.s)	50.113 63.8[e] 62.83[e]	40.251 51[e] 49.95[e]	34.876 41.5[e] 40.64[e]	29.036 33.35[e]	24.545 28.5[e]	21.009	18.17 20.5[e]	15.875	13.991 15.43[e]
ρ (g/cm^3)	1.4401 1.44143[e] 1.4426[e] 1.44148[e] 1.43889[e] 1.44051[e] 1.43927[e]	1.4353 1.440[e] 1.436[e] 1.43664[e] 1.4373[e] 1.43676[e] 1.43410[e] 1.43573[e] 1.43430[e] 1.4366[e]	1.4305 1.430[e] 1.43186[e] 1.4335[e] 1.42931[e] 1.43094[e] 1.42940[e]	1.4257 1.423[e] 1.4283[e] 1.42454[e] 1.42617[e] 1.42457[e] 1.4270[e]	1.4210 1.417[e] 1.42234[e] 1.42266[e] 1.41978[e] 1.42140[e] 1.41961[e]	1.4162 1.410[e] 1.41504[e] 1.41666[e] 1.41467[e] 1.4174[e]	1.4115 1.404[e] 1.41287[e] 1.41031[e] 1.41194[e] 1.40965[e]	1.4068 1.40560[e] 1.40723[e] 1.40464[e] 1.4079[e]	1.4021 1.40348[e] 1.40391[e] 1.40092[e] 1.40255[e] 1.39960[e]
c (m/s)	1238.5	1228.0	1217.1	1206.2	1195.5	1184.8	1174.3	1163.8	1153.5
α (1/K)	0.000671	0.000671	0.00067	0.00067	0.00067	0.000669	0.000669	0.000668	0.000668
v(cm^3.mol^{-1})	291.1957	292.1761	293.1585	294.1408	295.1246	296.112	297.1036	298.1007	299.09848

property	Temperature (K)								
	293.15	298.15	303.15	308.15	313.15	318.15	323.15	328.15	333.15
water									
η (mPa.s)	1.008	0.900 0.890[f]	0.810 0.800[f]	0.734	0.672 0.653[f] 0.655[f]	0.627	0.573 0.547[f] 0.549[f]	0.535	0.502 0.466[f]
ρ (g/cm^3)	0.9983	0.9971 0.99704[f]	0.9957 0.9957[f]	0.9941	0.9923 0.99221[f] 0.9923[f]	0.9903	0.9881 0.98804[f] 0.9881[f]	0.9858	0.9833 0.98312[f]
c (m/s)	1483.2	1497.2	1509.4	1519.0	1527.9	1535.4	1541.6	1546.8	1551.0
α (1/K)	0.000225	0.000263	0.000302	0.000341	0.00038	0.000419	0.000459	0.000499	0.000539
v (cm^3.mol^{-1})	18.0512	18.0721	18.0974	18.1267	18.1598	18.1965	18.2365	18.2799	18.3263
NMP									
η (mPa.s)	1.786	1.693	1.564	1.448	1.346	1.258	1.176	1.103	1.037
ρ (g/cm^3)	1.0341	1.0297	1.0253	1.0208	1.0163	1.0119	1.0074	1.0029	0.9984
c (m/s)	1565.7	1546.1	1526.7	1507.5	1488.3	1469.2	1450.4	1431.4	1412.8
α (1/K)	0.000858	0.000863	0.000868	0.000873	0.000879	0.000884	0.000889	0.000895	0.000900
v (cm^3.mol^{-1})	95.8590	96.2724	96.6886	97.1110	97.5372	97.9684	98.4033	98.8446	99.2890

[a] Expanded uncertainties are: $U(T) = 0.02$ K; $U(\rho) = 0.0002$ g.cm^{-3}, $U(\eta) = 0.003$ mPa.s, $U(c) = 0.7$ m.s^{-1} (Data recorded at 101 kPa, $U(P) = 1$ kPa).

[b] Literature data for the viscosity and density of MEA [183, 235].

[c] Literature data for the viscosity and density of DGA [184].

[d] Literature data for the viscosity and density of bmim[OTF] [181].

[e] Literature data for the viscosity and density of bmim[TF$_2$N] [182, 236, 247-252].

[f] Literature data for the viscosity and density of water [183, 184].

APPENDIX L. STATISTICAL DEVIATIONS FOR VISCOSITY, DENSITY AND SOUND VELOCITY

Table L-1: Regressed parameters and statistical deviations (AAD) for viscosity (η), density (ρ) and sound velocity (c) of bmim[BF$_4$] (1) + NMP (2) with different mass compositions (w).

Sample	A_1	A_2	A_3	AAD(η)	B_1	B_2	B_3	AAD(ρ)	D_1	D_2	AAD(c)
$w_1/w_2 = 1/0$	0.1635	788.5	175	0.091	3.243E-07	-0.0009123	1.446	0.0004	-2.291	2247	0.5
$w_1/w_2 = 0/1$	0.002561	2854	-142.2	0.006	-1.451E-07	-0.0008021	1.282	0.0003	-3.794	2677	0.5
$w_1/w_2 = 0.7413/0.2587$	0.1317	731.2	156.2	0.023	2.412E-07	-0.0009038	1.405	0.0002	-2.684	2366	0.5
$w_1/w_2 = 0.4971/0.5029$	0.08983	729.4	136.3	0.010	3.597E-08	-0.0008199	1.357	0.0003	-3.05	2479	0.3
$w_1/w_2 = 0.2498/0.7502$	0.08094	668.5	121.1	0.002	-2.115E-09	-0.0008379	1.324	0.0002	-3.414	2582	0.6
$w_1/w_2 = 0.0986/0.9014$	0.06933	659.7	110.5	0.001	-7.56E-08	-0.0008223	1.300	0.0003	-3.65	2648	0.5

Table L-2: Regressed parameters and statistical deviations (AAD) for viscosity (η), density (ρ) and sound velocity (c) of MEA (1) + H$_2$O (2) + bmim[OTF] (3) with different mass compositions (w).

Sample	A_1	A_2	A_3	AAD(η)	B_1	B_2	B_3	AAD(ρ)	D_1	D_2	AAD(c)
$w_1 = 0.3004, w_2 = 0.6996$	0.4156	132.5	227.5	0.003	-2.50E-06	0.001052	0.9188	0.0001	-0.5773	1846	1.9
$w_1 = 0.3119, w_2 = 0.5837, w_3 = 0.1045$	0.3102	193.5	219.6	0.008	-1.84E-06	0.0006	1.037	0.00003	-1.343	2097	1.3
$w_1 = 0.2994, w_2 = 0.4614, w_3 = 0.2392$	0.2081	286.6	208.2	0.009	-1.40E-06	0.0002	1.14	0.0001	-1.846	2237	0.6
$w_1 = 0.3046, w_2 = 0.2642, w_3 = 0.4311$	0.0446	746.6	158.8	0.007	-8.99E-07	-0.0002	1.268	0.0005	-2.287	2322	0.6

Table L-3: Regressed parameters and statistical deviations (AAD) for viscosity (η), density (ρ) and sound velocity (c) of DGA (1) + H$_2$O (2) + bmim[OTF] (3) with different mass compositions (w).

Sample	A_1	A_2	A_3	AAD(η)	B_1	B_2	B_3	AAD(ρ)	D_1	D_2	AAD(c)
$w_1 = 0.5132$, $w_2 = 0.4868$	0.06539	565.3	177.6	0.013	-0.0000012	0.000075	1.1360	0.0003	-2.5	2503.0	0.7
$w_1 = 0.5116$, $w_2 = 0.3878$, $w_3 = 0.1006$	0.04477	710.2	164.8	0.009	-0.0000009	-0.000164	1.2050	0.0003	-2.6	2540.0	0.6
$w_1 = 0.4742$, $w_2 = 0.2664$, $w_3 = 0.2593$	0.03604	818.9	158.8	0.009	-0.00000072	-0.00034580	1.2760	0.0003	-2.7	2488.0	0.5
$w_1 = 0.4976$, $w_2 = 0.1000$, $w_3 = 0.4024$	0.05911	753.7	171.4	0.037	-0.00000029	-0.00063360	1.3590	0.0002	-2.7	2402.0	0.4

Table L-4: Regressed parameters and statistical deviations (AAD) for viscosity (η), density (ρ) and sound velocity (c) of MEA (1) + H_2O (2)/(NMP (2) + bmim[TF$_2$N] (3)) / bmim[OTF] (3) with different mass compositions (w).

Sample	A_1	A_2	A_3	AAD(η)	B_1	B_2	B_3	AAD(ρ)	D_1	D_2	AAD(c)
w_1= 0.0912, $w_{bmim[OTF]}$ = 0.9088	0.2244	635.8	176.7	0.076	0.0000003	-0.0009929	1.531	0.0002	-2.318	2120	0.3
w_1 = 0.1034, w_{water} = 0.8966	0.05118	409.9	169	0.001	-0.0000034	0.001724	0.7898	0.0001	0.9452	1275	3.1
w_1 = 0.1021, w_{NMP} = 0.8979	0.4923	156.6	206.3	0.002	-0.0000003	-0.0007106	1.271	0.0002	-3.746	2683	0.5
w_1 = 0.2008, w_{water} = 0.7992	0.01185	956.6	105	0.005	-0.0000029	0.001387	0.8533	0.0001	0.208	1554	2.8
w_1 = 0.2090, w_{NMP} = 0.7910	0.3834	208.5	199.5	0.004	-0.0000003	-0.0007071	1.266	0.0002	-3.719	2684	0.6
w_1 = 0.3004, w_{water} = 0.6996	0.4156	132.5	227.5	0.003	-0.0000025	0.001052	0.9188	0.0001	-0.577	1846	1.9
w_1 = 0.3089, w_{NMP} = 0.6911	0.2703	281.1	194.9	0.005	0.0000001	-0.0009501	1.301	0.0001	-3.646	2680	0.6
w_1 = 0.0976, w_{NMP} = 0.8032, $w_{bmim[TF2N]}$ = 0.0992	0.4296	200.1	195.9	0.002	-0.0000003	-0.0007155	1.301	0.0001	-3.583	2604	0.6
w_1 = 0.1138, w_{NMP} = 0.6414, $w_{bmim[TF2N]}$ = 0.2448	0.2899	305.8	183.8	0.003	-0.0000005	-0.0006251	1.333	0.00004	-3.338	2490	0.4
w_1 = 0.1162, w_{NMP} = 0.4932, $w_{bmim[TF2N]}$ = 0.3906	0.1886	444.7	167.1	0.004	-0.0000003	-0.0007642	1.404	0.0002	-3.123	2378	0.3

Table L-5: Regressed parameters and statistical deviations (AAD) for viscosity (η), density (ρ) and sound velocity (c) of DGA (1) + H_2O (2) /(NMP (2) + bmim[TF_2N] (3)) with different mass compositions (w).

Sample	A_1	A_2	A_3	AAD(η)	B_1	B_2	B_3	AAD(ρ)	D_1	D_2	AAD(c)
$w_1 = 0.4981$, $w_{NMP} = 0.5019$	0.08869	602.2	157.4	0.009	-0.00000033	-0.0006632	1.2670	0.0004	-3.394	2591	0.4
$w_1 = 0.3102$, $w_{NMP} = 0.6898$	0.33150	245.7	202.0	0.005	-0.00000040	-0.000635	1.2630	0.0002	-3.398	2582	0.2
$w_1 = 0.2923$, $w_{H2O} = 0.7077$	0.02469	705.9	145.4	0.003	-0.00000401	0.001990	0.7885	0.0002	-0.7816	1908	1.7
$w_1 = 0.2981$, $w_{2,NMP} = 0.3096$, $w_4 = 0.3923$	0.10490	630.2	160.7	0.008	-0.00000002	-0.00088040	1.4300	0.0000	-2.965	2336	0.3
$w_1 = 0.3035$, $w_{NMP} = 0.4462$, $w_4 = 0.2503$	0.14150	511.2	166.8	0.006	-0.00000013	-0.00080730	1.3680	0.0002	-3.198	2449	0.4
$w_1 = 0.2840$, $w_{NMP} = 0.6166$, $w_4 = 0.0994$	0.21980	362.6	179.6	0.003	-0.00000022	-0.00074250	1.3080	0.0001	-3.448	2565	0.3
$w_1 = 0.5132$, $w_{H2O} = 0.4868$	0.06539	565.3	177.6	0.013	-0.00000124	0.000075	1.1360	0.0003	-2.450	2503	0.7

APPENDIX M. DATA MODELLING RESULTS

To assess further the validity of the method developed in Chapter 6, the solubility of CO_2 and H_2S in MEA, DEA, DIPA, MDEA and AMP were modelled using this method and results are discussed in this section. It should be mentioned that some of the results obtained for the MEA + H_2O + CO_2 system were presented in Chapter 7.

M.1 MEA + H_2O + CO_2 system

Figures M-1 and M-2 show the modelled results compared with experimental data for the MEA + H_2O + CO_2 system with two different concentrations of MEA viz. w = (0.15 and 0.30). Figure M-1 displays the literature data obtained using the Deshmukh-Mather model [136, 148]. Although the Deshmukh-Mather activity coefficient model is used in the present method, there are some noticeable differences between the results of the present method and the results of Deshmukh-Mather model. As shown in Figure M-1, the results of Deshmukh-Mather model [148] are more compatible with experimental data of Lee et. al (1976-1977) [214, 253], while there is good agreement between results of this work with experimental data of Jones et. al (1959) [208]. The figure clearly shows that the present model does not predict the solubility of CO_2 at very low pressures depending on the concentration of amine and temperature, but this problem can be solved with determining the new interaction parameters especially for very low pressures and considering the effect of pressure on the interaction parameters. Figure M-2 shows the results predicted with the present model and the original Kent-Eisenberg model which the apparent equilibrium constants reported by Kent and Eisenberg (1976) [135] were used in. The figure shows that the Kent-Eisenberg model is not able to predict accurately the solubility data beyond the regressed range of the apparent equilibrium constants (the parameters of apparent equilibrium constants were regressed for the MEA + CO_2 system by forcing a fit between the experimental results measured over the 15.3 wt.% MEA aqueous solution). Furthermore, the present model predicts the measured data more accurately, although the Kent-Eisenberg model is more computationally simpler and converge more easily.
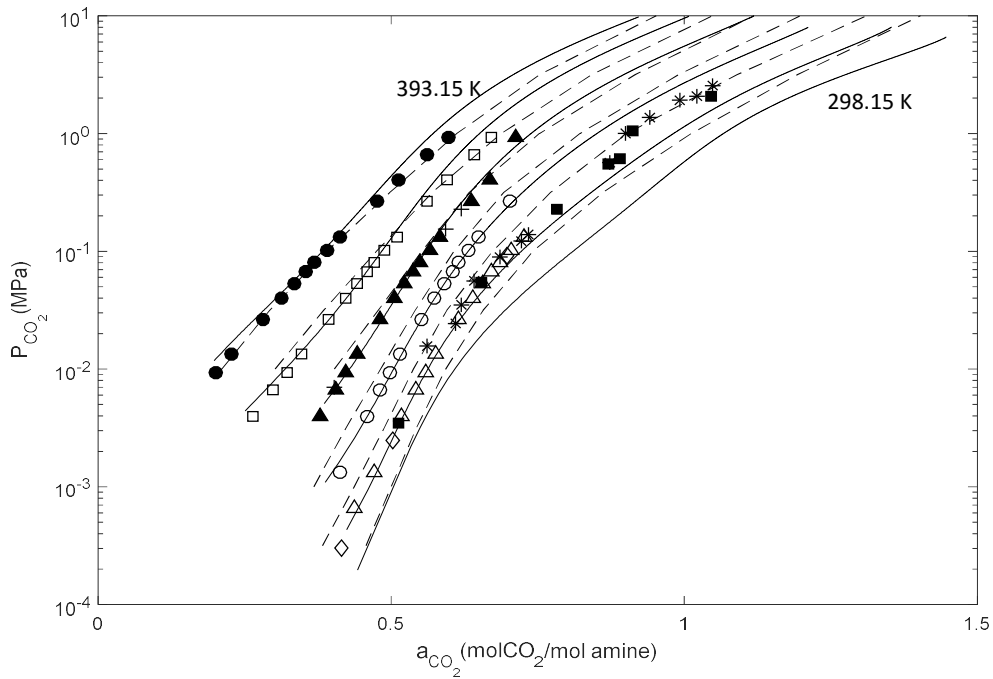
(a)
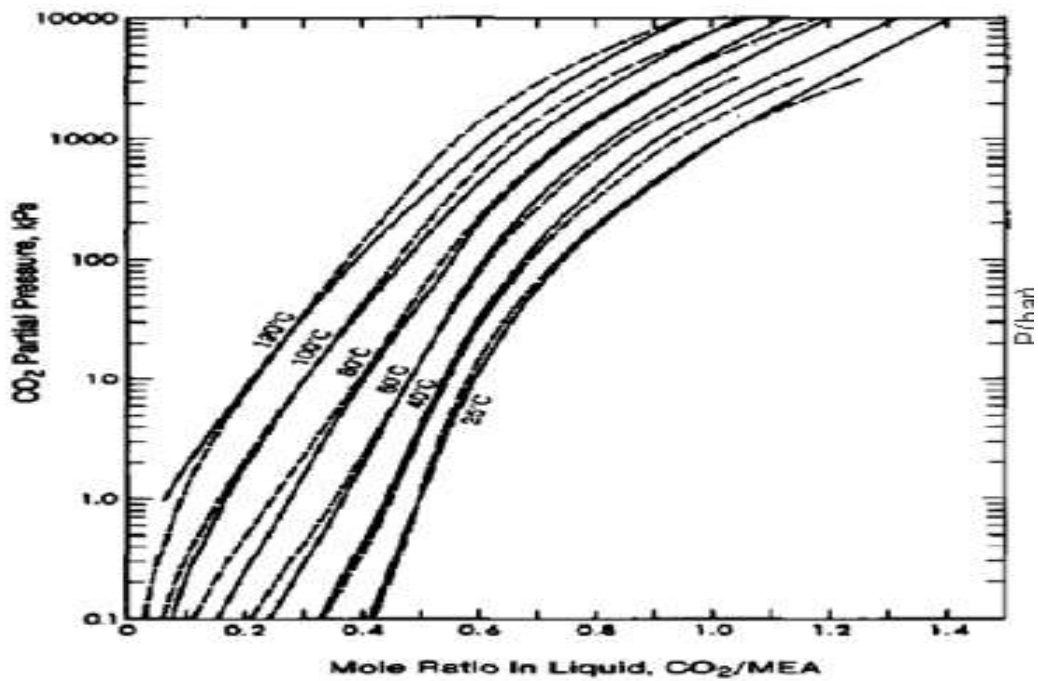
(b)

Figure M-1: Comparison between experimental data [153, 208-210, 214, 253] and: **(a):** modelled results from this work; and **(b):** modelled results by Deshmukh-Mather (1980) [148] for the solubility of CO_2 in the aqueous 15.3% MEA solution. Exp (literature): Shen and Li at 313.15 K (✻) [209]; Park et al. at 313.15 K (■) [210]; Austgen and Rochelle at 313.15 K (◇) and 353.15 K (＋) [153]; Jones et al. at 313.15 K (△), 333.15 K (○), 353.15 K (▲), 373.15 K (□), and 393.15 K (●) [208]. The dashed lines and solid lines in (a) and (b) depict the experimental results from Lee et al. (1974 & 1976) [214, 253] and modelled data at 298.15 to 393.15 K (from the right to left), respectively.
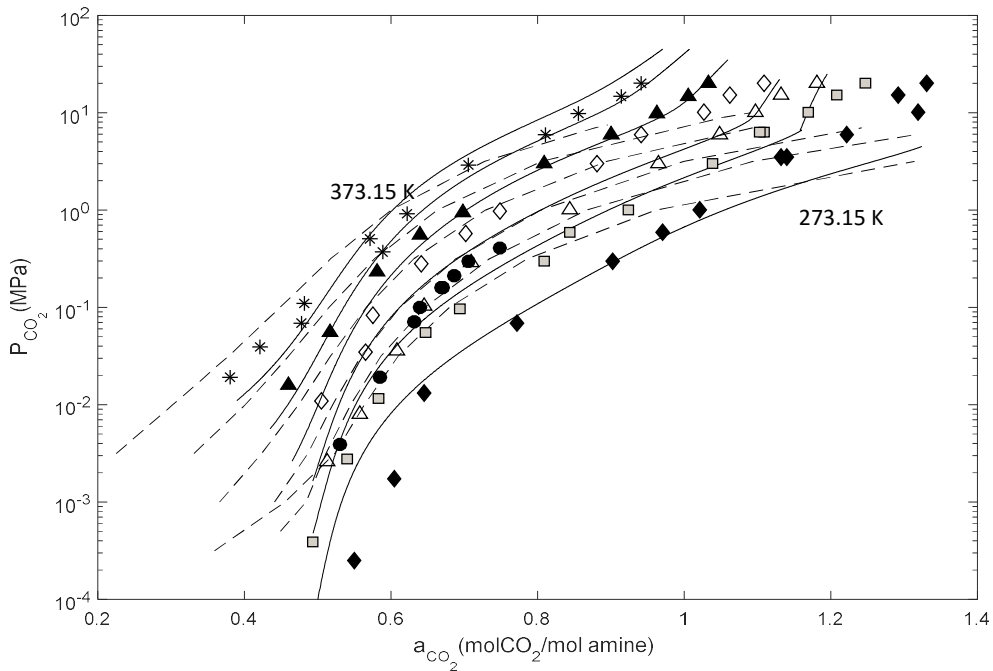
Figure M-2: Comparison between experimental data [119, 136, 212] and modelled results for the solubility of CO_2 in the aqueous 30% MEA solution. Exp (literature): Jou et al. at 273.15 K (◆), 298.15 K (▣), 313.15 K (△), 333.15 K (◇), 353.15 K (▲), and 373.15 K (✳) [119]; Tong et al. at 313.15 K (●) [136]. The dashed lines and solid lines depict the Kent-Eisenberg model results and the modelled data (this work) at 273.15 to 373.15 K (from the right to left), respectively.

M.2 MDEA + H₂O + CO₂ system

Figures M-3 to M-6 show the modelled results compared with the literature experimental data for the MDEA + H₂O + CO₂ system with different initial amine loading concentrations viz. $w = $ (.236, 0.35, 0.5, 0.488 and 0.234). The modelled predictions agree well with the experimental results except for some high pressures. Figures M-4 and M-5 display clearly the predictions at high pressures. Figures show that the accuracy of the model at high pressures increases with an increase in temperature, but the present model has undeniable uncertainty with increasing pressure at low temperatures. Additionally, Figure M-6 compares the experimental data with the results originating from the modified Kent-Eisenberg model [144] and the results of the present model to validate further the present method. It seems that the experimental data are more compatible with the results of the present model, especially at high temperatures.
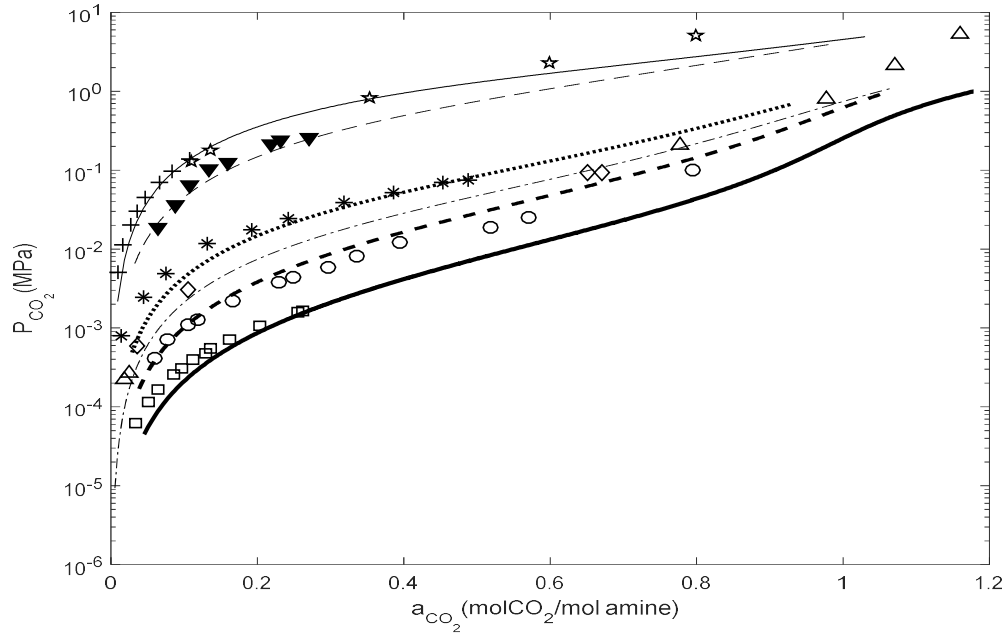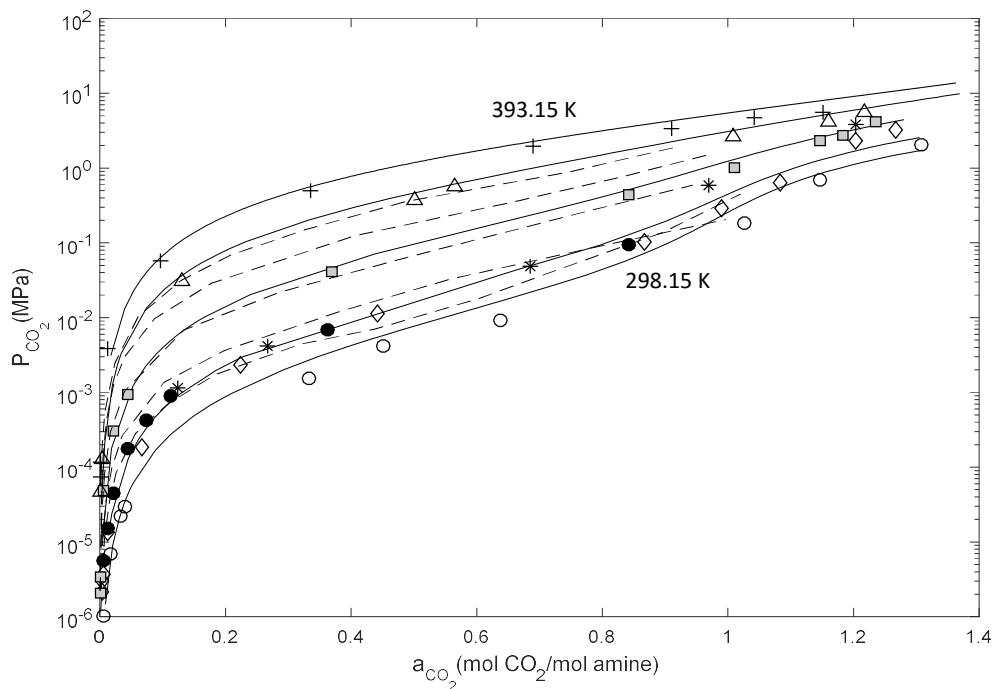
Figure M-3: Comparison between experimental data [119, 153, 168, 254-257] and modelled results for the solubility of CO_2 in MDEA solutions. Exp (literature): Lemoine et al., the 23.63% MDEA solution at 297.7 K (□) [168]; Fang-Yuan Jou, the 35% MDEA solution at 313.15 K (○), and 373.15 K (▼) [256]; Austgen and Rochelle, the 50% MDEA solution at 313.15 K (◇) [153]; Huang and Ng, the 50% MDEA solution at 313.15 K (△), and 373.15 K (✳) [254]; Park and Sandall, the 50% MDEA solution at 323.15 K (✳) [257]; Rho et al., the 50% MDEA solution at 373.15 K (+) [255]. Modelled data (this work): the 23.63% MDEA solution at 297.7 K (bold solid line); the 35% MDEA solution at 313.15 K (bold dashed line), and 373.15 K (dashed line); and the 50% MDEA solution at 313.15 K (dash-dot line), 323.15 K (bold dotted line) and 373.15 K (solid line).
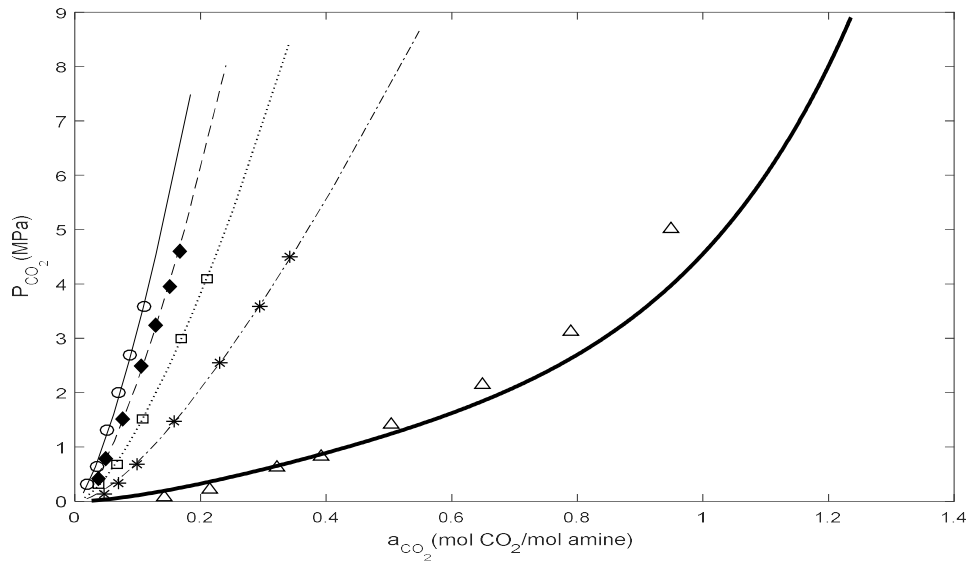
Figure M-4: Comparison between experimental data [142] and modelled results for the solubility of CO_2 in the 48.80% MDEA solution. Exp (literature): Chakma and Meisen at 473.15 K (○), 453.15 K (◆), 433.15 K (□), 413.15 K (✳), and 373.15 K (△) [142]. Modelled data (this work): at 473.15 K (solid line), 453.15 K (dashed line), 433.15 K (dotted line), 413.15 K (dash-dot line) and 373.15 K (bold-solid line).
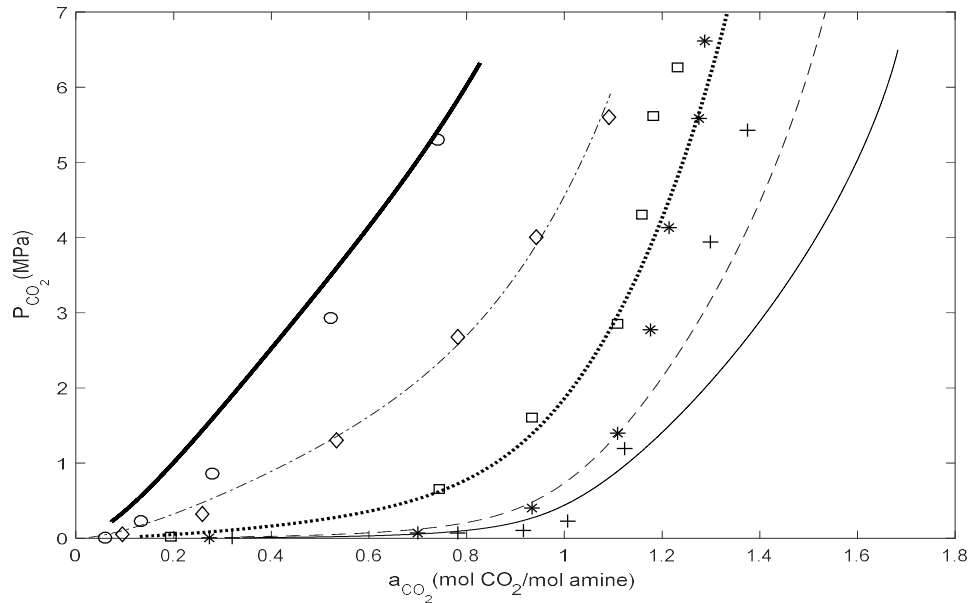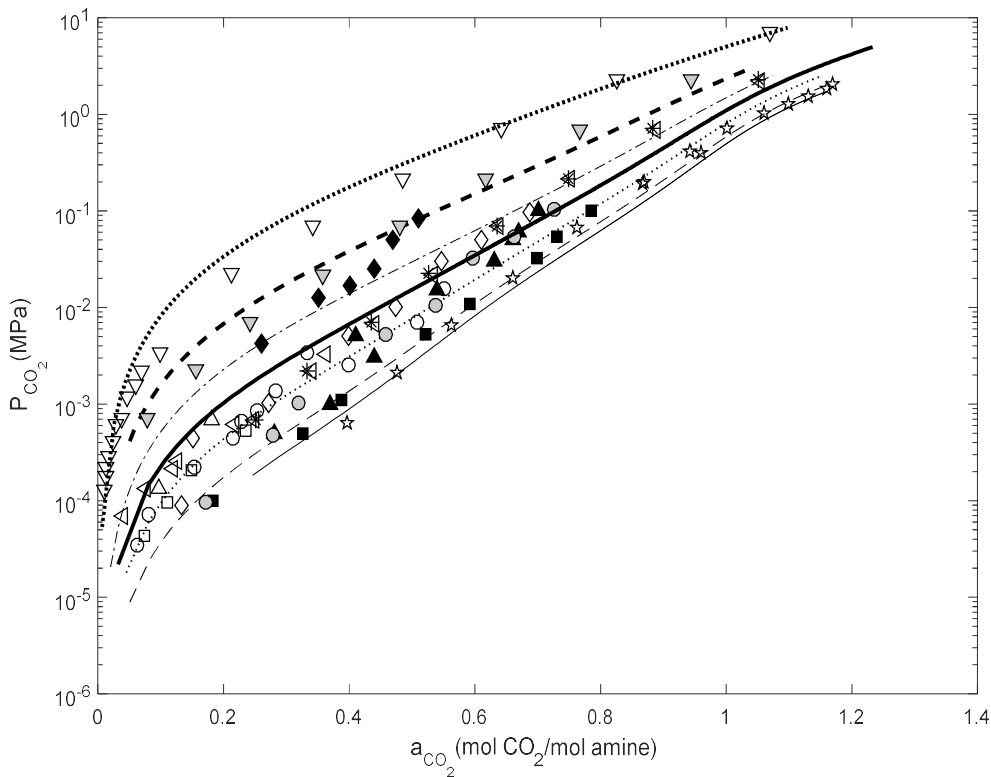
Figure M-5: Comparison between experimental data [143] and modelled results for the solubility of CO_2 in the 48.80% MDEA solution. Exp (literature): Jou et al. at 393 K (○), 373 K (◇), 343 K (□), 313 K (✳), and 298 K (+) [143]. Modelled data (this work): at 393 K (bold-solid line), 373 K (dash-dot line), 343 K (bold dotted line), 313 K (dashed line), and 298 K (solid line).
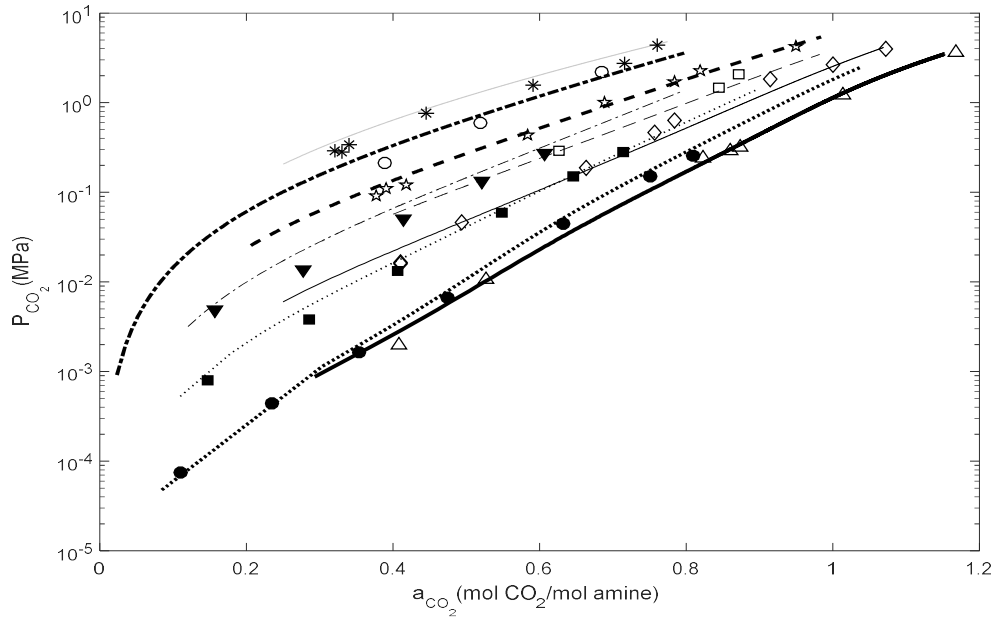

Figure M-6: Comparison between experimental data [143, 153, 175] and modelled results for the solubility of CO_2 in the 23.4% MDEA solution. Exp (literature): Jou et al. at 298.15 (○), 313.15 K (◇), 343.15 K (▨), 373.15 K (△), and 393.15 K (+) [143] ; Macgregor et al. at 313.15 K (✳) [175]; Austgen et al. at 313.15 K (●) [153]. The dashed lines and solid lines depict the modified Kent-Eisenberg model results by Haji-Sulaiman et al. [144] and the modelled data (this work) at 298.15 to 393.15 K (from the right to left), respectively.

M.3 DEA + H₂O + CO₂ system

Figures M-7 to M-9 show the predicted results compared with the experimental data of the CO_2 capture in the DEA aqueous solution with different initial concentrations viz. w = (0.206, 0.30 and 0.25). Although the experimental data reported in various references undeniably scatter (especially data shown in Figure M-7) indicating a high degree of uncertainty, the present method can give good predictions of the CO_2 capture. Furthermore, Figure M-9 compares the experimental data with the results modelled using the modified Kent-Eisenberg model [144] and the results of the present model. Totally, the experimental data are more compatible with the results modelled in this work.

Figure M-7: Comparison between experimental data [50, 144, 173, 258-260] and modelled results for the solubility of CO_2 in the 20.6% DEA solution. Exp (literature): Vallee' et al. at 298.15 K (✳), 323.15 K (✳), 348.15 K (▽), and 373.15 K (▽) [258]; Haji-Sulaiman et al. at 303.15 K (■), 303.15 K (▲), 313.15 K (◯), 323.15 K (◇), and 333.15 K (◆) [144, 173]; Huttenhuis et al. at 323.15 K (◯) [259]; Lee et al. at 323.15 K (◁) [260]; and Bullin et al. at 323.15 K (□), and 323.15 K (△) [50]. Modelled data (this work): at 298.15 K (solid line), 303.15 K (dashed line), 313.15 K (dotted line), 323.15 K (bold solid line), 333.15 K (dash-dot line), 348.15 K (bold dashed line), and 373.15 K (bold dotted line).

Figure M-8: Comparison between experimental data [211, 261] and modelled results for the solubility of CO_2 in DEA solutions. Exp (literature): Park et al., the 30% DEA solution at 313.15 K (●), 333.15 K (■), and 353.15 K (▼) [261]; and Lawson and Gars, the 25% DEA solution at 310.93 K (△), 338.71 K (◇), 352.59 K (□), 366.48 K (✳), 380.37 K (○), 394.26 K (✳) [211]. Modelled data (this work): the 30% DEA solution at 313.15 K (bold dotted line), 333.15 K (dotted line), and 353.15 K (dash-dot line); the 25% DEA solution at 310.93 K (bold solid line), 338.71 K (solid line), 352.59 K (dashed line), 366.48 (bold-dashed line), 380.37 K (bold dash-dot line), and 394.26 K (grey line).
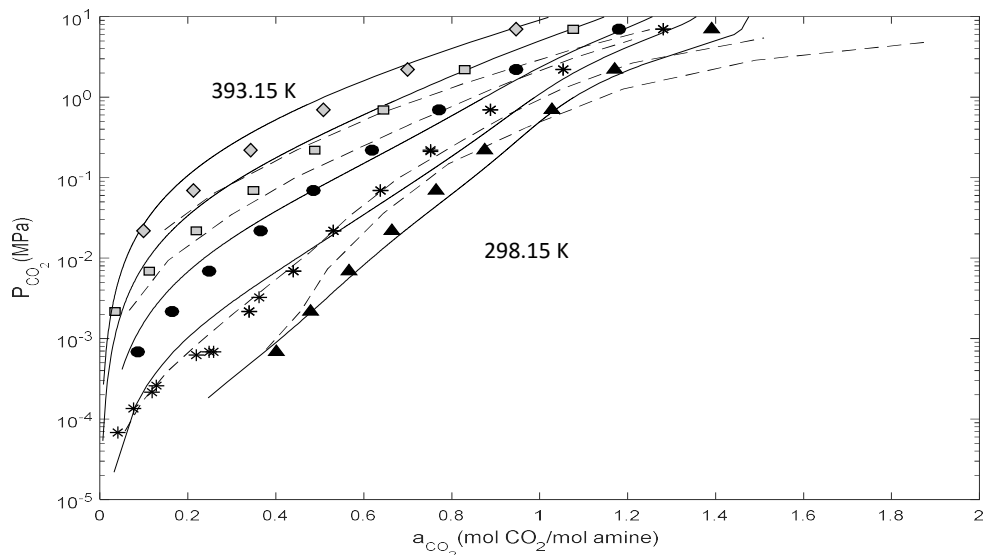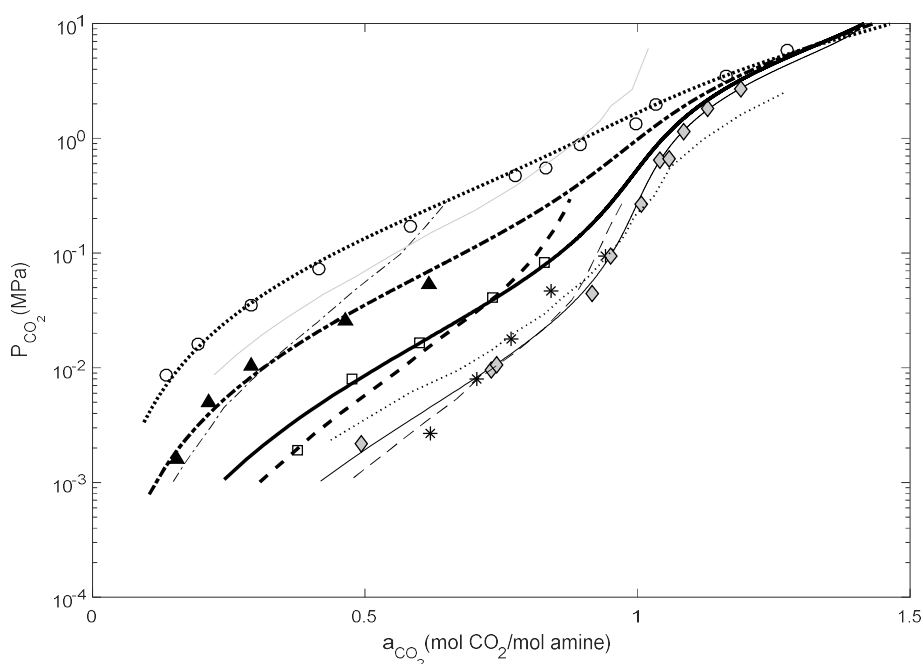

Figure M-9: Comparison between experimental data [260, 262] and modelled results for the solubility of CO_2 in the aqueous 20.6% DEA solution. Exp (literature): Lee at al. at 298.15 K (▲), 323.15 K (✳), 348.15 K (●), 373.15 K (□), and 393.15 K (◈) [260, 262]. The dashed lines and solid lines depict the modified Kent-Eisenberg model results by Haji-Sulaiman et al. [144] and the modelled data (this work) at 298.15 to 393.15 K (from the right to left), respectively.

M.4 AMP/DIPA + H₂O + CO₂ system

Figures M-10 and M-11 compare the predicted results with the experimental data of the CO_2 solubility in the AMP aqueous solution with different initial concentrations viz. w = (0.1792, 0.2692 and 0.3078). The modelled data shows a good agreement to the experimental data. In addition, the figures illustrate the data modelled using the modified Kent-Eisenberg model [138, 145]. It is clear from the figures that results of the present model are more compatible with the experimental data, in comparison to the results of the Kent-Eisenberg model. At 313.15 K, these figures show two groups of data predicted using two different modified Kent-Eisenberg models but they do not have the same trend and accuracy. It means that the precision of the modified Kent-Eisenberg model is highly dependent on the accuracy of the apparent equilibrium constants since the non-idealities of the system are lumped into these parameters.

Figure M-12 displays a reasonable agreement between the experimental data and the modelled results for the DIPA + water + CO₂ system. Experimental data involving the solubility of CO_2 in the DIPA aqueous solution are rare, thus, specific interaction parameters determined for this system may not be reliable enough for a wide range of temperature, pressures and initial concentrations.

Figure M-10: Comparison between experimental data [138, 263] and modelled results for the solubility of CO_2 in the aqueous 17.92% AMP solution. Exp (literature): Tontiwachwuthikul et al. at 313.15 K (✳), 333.15 K (□), and 353.15 K (▲) [138]. Roberts and Mather at 313.15 K (◇), and 373.15 K (○) [263]. The modified Kent-Eisenberg model data by Hu and Chakma at 313.15 K (dotted line), and 373.15 K (grey line) [145]; and Tontlwachwuthlkul et al. at 313.15 K (dashed line), 333.15 K (bold dashed line), and 353.15 K (dash-dot line) [138]. Modelled data (this work): at 313.15 K (solid line), 333.15 K (bold solid line), 353.15 K (bold dash-dot line), and 373.15 K (bold dotted line).
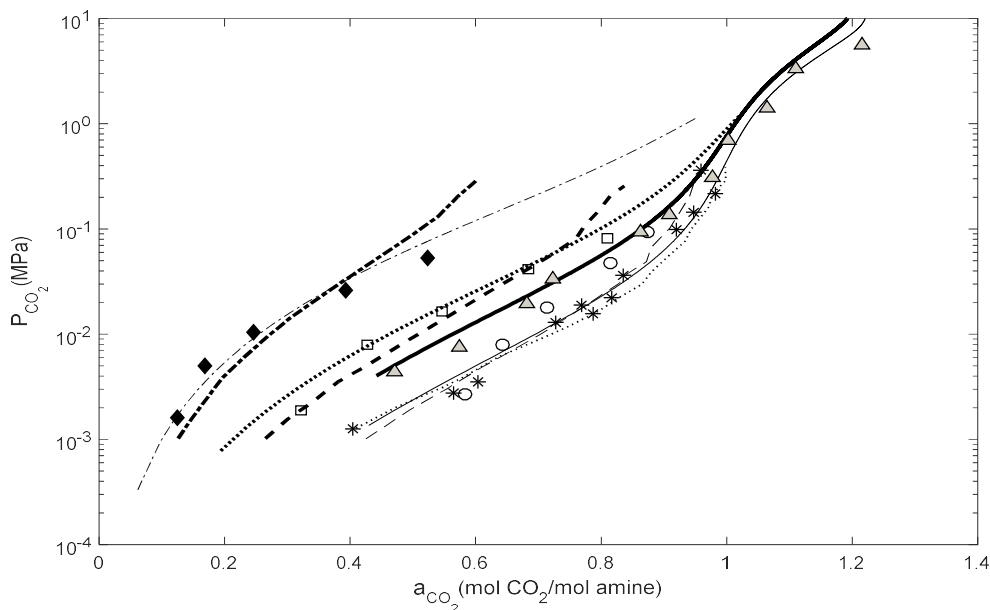
Figure M-11: Comparison between experimental data [138, 263, 264] and modelled results for the solubility of CO_2 in AMP solutions. Exp (literature): Tontiwachwuthikul et al., the 26.92% AMP solution at 313.15 K (○), 333.15 K (□), and 353.15 K (◆) [138]; Roberts and Mather at 313.15 K (✳) [263]; and Teng and Mather, the 30.78% AMP solution at 323.15 K (▲) [264]. the modified Kent-Eisenberg model data for the 30.78% AMP solution by Hu and Chakma at 313.15 K (dotted line) [145]; and Tontlwachwuthlkul et al. at 313.15 K (dashed line), 333.15 K (bold dashed line), and 353.15 K (bold dash-dot line) [138]. Modelled data (this work): the 26.92% AMP solution at 313.15 K (solid line), 333.15 K (bold dotted line), and 353.15 K (dash-dot line); and the 30.78% AMP solution at 323.15 K (bold solid line).
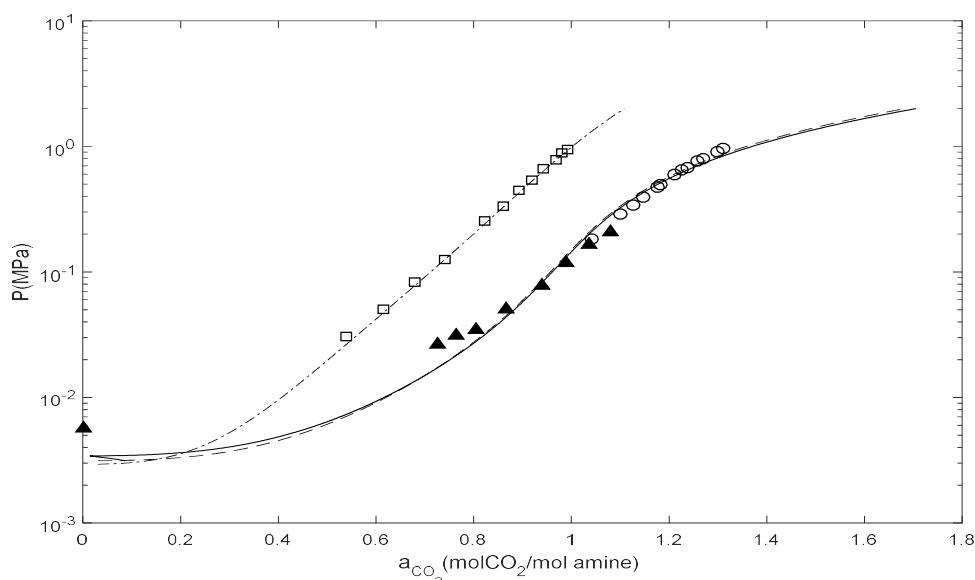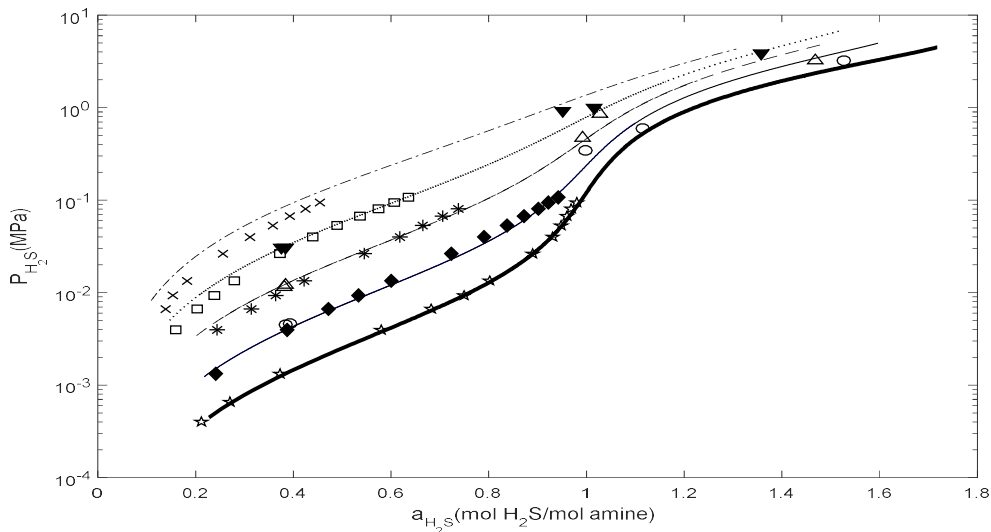

Figure M-12: Comparison between experimental data [265] and modelled results for the solubility of CO_2 in DIPA solutions. Exp (literature): Dell'Era et al., the 33.9% DIPA solution at 298.29 K (□), the 11% DIPA solution at 298.22 K (○), and the 10.1% DIPA solution at 299.72 K (▲) [265]. Modelled data (this work): the 33.9% DIPA solution at 298.29 K (dash-dot line), the 11% DIPA solution at 298.22 K (dashed line), and the 10.1% DIPA solution at 299.72 K (solid line).

## M.5 MEA/ MDEA/DEA/AMP + H_2O + H_2S system

Figures M-13 and M-14 present the modelled results and the experimental data for the solubility of H_2S in the MEA aqueous solution. Additionally, Figure M-14 shows the results predicted with the original Kent-Eisenberg model in which the apparent equilibrium constants reported by Kent and Eisenberg (1976) [135] were used. There is a good agreement between the experimental data and the results of the present model except for high temperatures at low pressures. The Kent-Eisenberg model predicts the measured data at these conditions more accurately than the present model.

Figure M-15 to M-17 show the modelled results compared with experimental data for the MDEA + H_2O + H_2S system with different initial amine loading concentrations viz. $w = (0.1868, 0.1999, 0.322, 0.35, 0.4678, 0.488, 0.5,$ and $0.4990)$. Figures M-18 to M-20 display the predicted results and the experimental data of the H_2S capture in the aqueous DEA solution with different initial concentrations viz. $w = (0.052, 0.206$ and $0.354)$. Totally, the consistency between the two groups of data confirms the validity of the developed method. Figure M-21compares the experimental data with the results of the present model and the results originating from the modified Kent-Eisenberg model by Hu and Chakma (1990) [145]. It shows that both models are able to give a relatively good prediction for the H_2S capture in the AMP solutions.
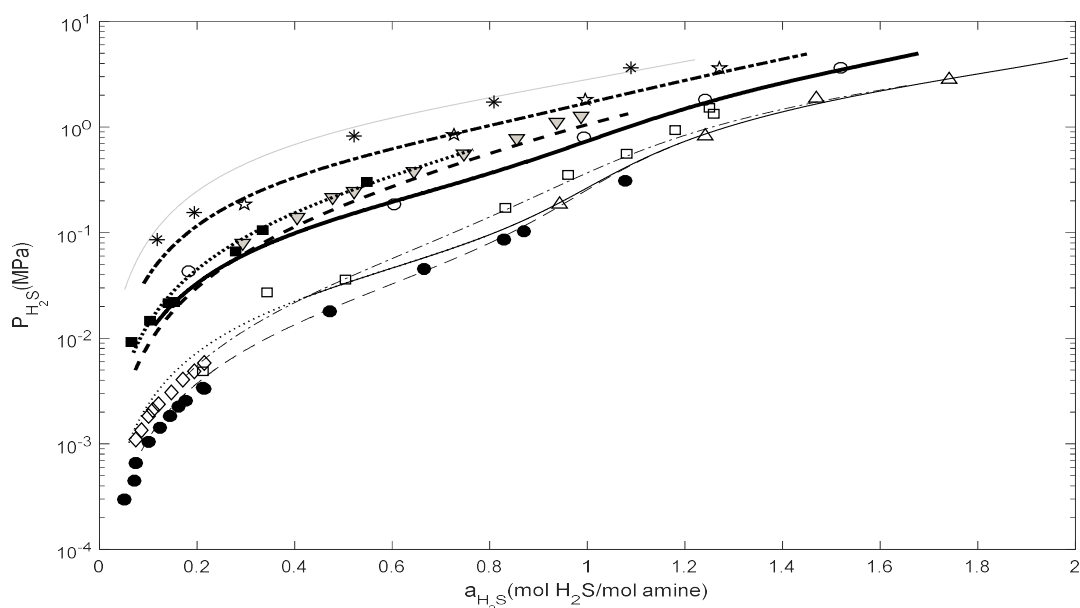

Figure M-13: Comparison between experimental data [208, 211] and modelled results for the solubility of H_2S in MEA solutions. Exp (literature): Jones et al., the 15.3% MEA solution at 313.15 K (✳), 333.15 K (◆), 353.15 K (✳), 373.15 K (□), and 393.15 K (✕) [208]; and Lawson and Garst, the 15.2% MEA solution at 333.15 K (○), 353.15 K (△), and 373.15 K (▼) [211]. Modelled data (this work): the 15.3% MEA solution at 313.15 K (bold solid line), 333.15 K (solid line), 353.15 K (dashed line), 373.15 K (dotted line), and 393.15 K (dash-dot line); the 15.2% MEA solution at 333.15 K (solid line), 353.15 K (dashed line), and 373.15 K (dotted line).
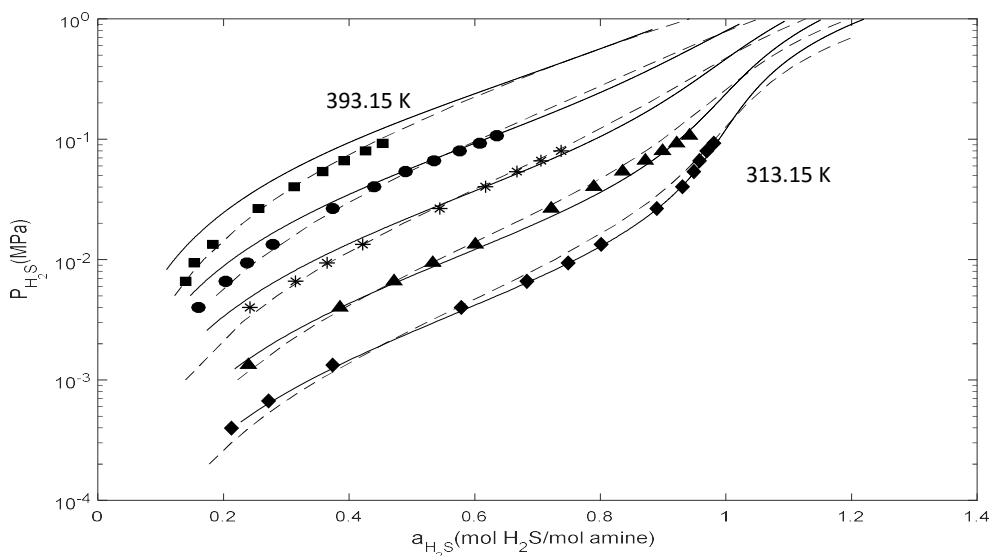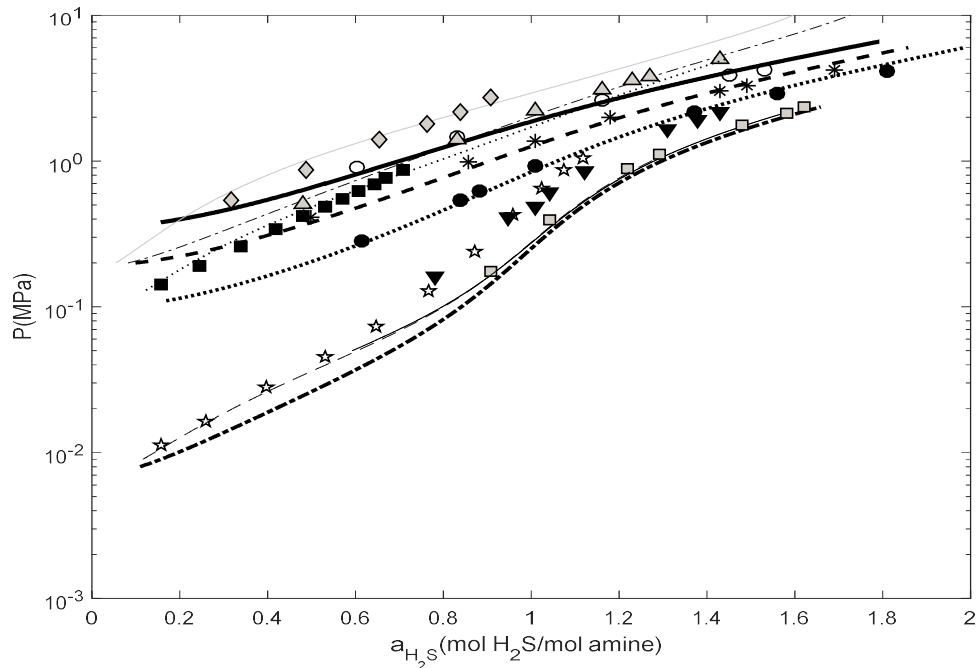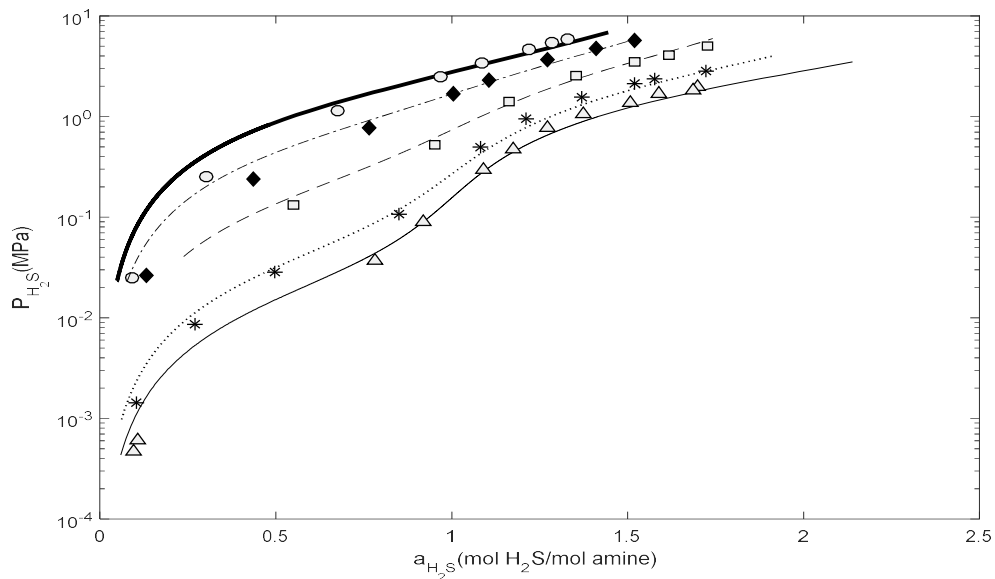
Figure M-14: Comparison between experimental data [208] and modelled results for the solubility of H₂S in the 15.3% MEA solutions. Exp (literature): Jones et al. at 313.15 K (◆), 333.15 K (▲), 353.15 K (✳), 373.15 K (●), and 393.15 K (■) [208]. The dashed lines and solid lines depict the Kent-Eisenberg model results and the modelled data (this work) at 313.15 to 393.15 K (from the right to left), respectively.

Figure M-15: Comparison between experimental data [254, 266] and modelled results for the solubility of H₂S in MDEA solution. Exp (literature): Maddox et al., the 19.99% MDEA solution at 388.65 K (▽), and 338.65 (□) [254]; Huang et al., the 49.9% MDEA solution at 393.15 K (✳), 373.15 K (✳), 343.15 K (○), and 313.15 K (△) [254]; and Jou et al., the 50% MDEA solution at 313.15 K (◇), the 35% MDEA solution at 313.15 K (●), and 373.15 K (■) [266]. Modelled data (this work): the 19.99% MDEA solution at 388.65 K (bold dashed line), and 338.65 K (dash-dote line); the 49.9% MDEA solution at 393.15 K (grey line), 373.15 K (bold dash-dot line), 343.15 K (bold solid line), and 313.15 K (solid line); the 50% MDEA solution at 313.15 K (dotted line); the 35% MDEA solution at 313.15 K (dashed line), and 373.15 K (bold dotted line).
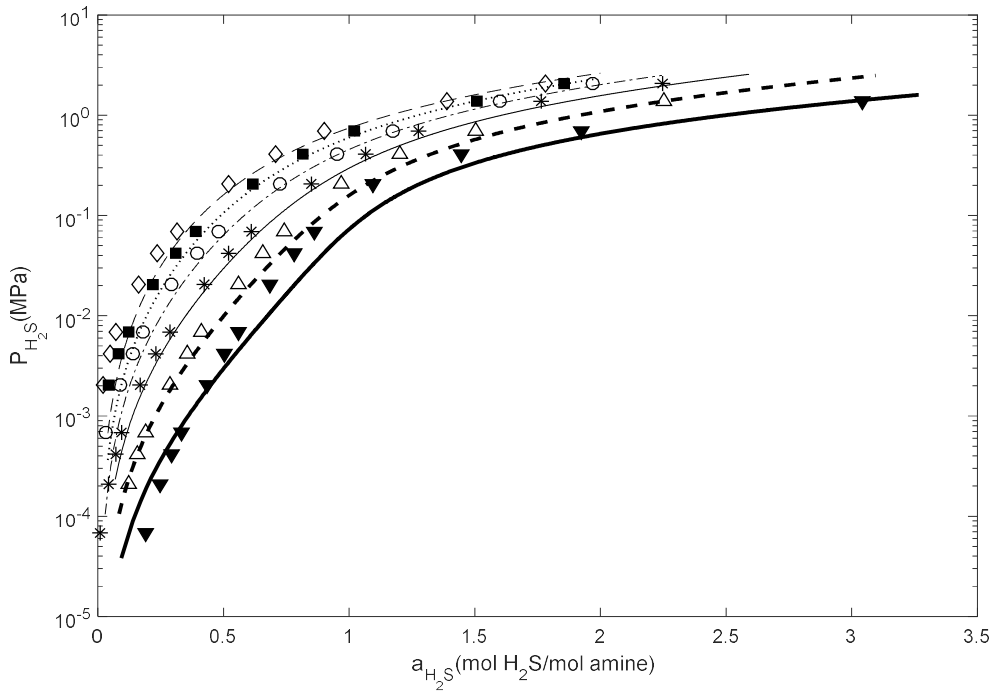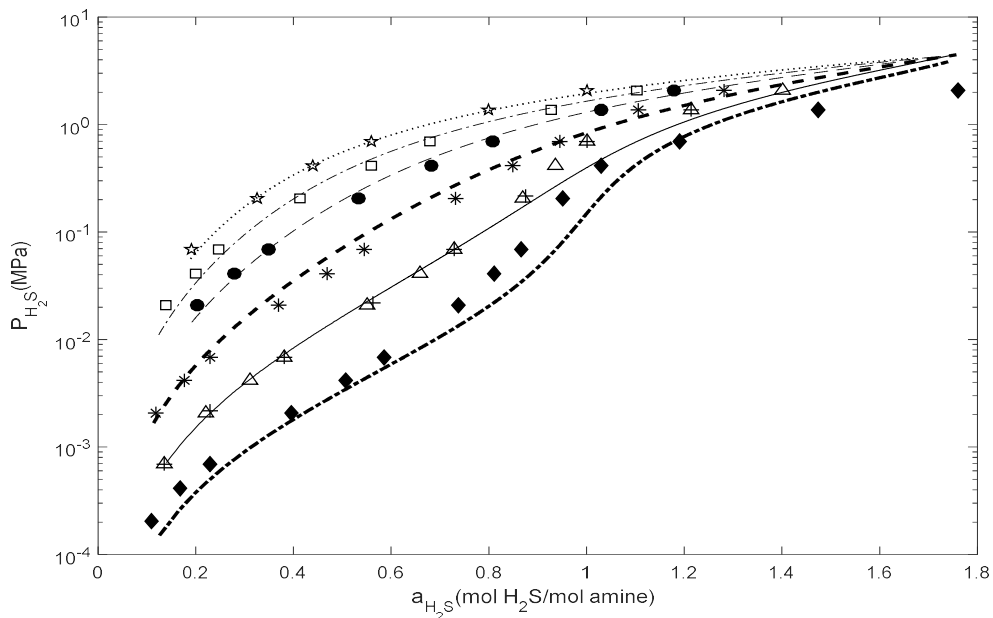
Figure M-16: Comparison between experimental data [163, 164, 212, 267] and modelled results for the solubility of H_2S in MDEA solution. Exp (literature): Kuranov et al., the 18.68% MDEA mol solution at 413.15 K (○), 393.15 K (✳), and 373.15 K (●); Kamps et al., the 48.8% MDEA solution at 393.15 K (◇), and 313.15 K (▼); Kuranov et al., the 32.2% MDEA solution at 393.15 K (△), and 313.15 K (▢); Sidi et al., the 46.78% MDEA solution at 373.01 K (■), and 313.15 K (✳). Modelled data (this work): the 18.68% MDEA mol solution at 413.15 K (solid line), 393.15 K (bold dashed line), and 373.15 K (bold dotted line); the 48.8% MDEA solution at 393.15 K (grey line), and 313.15 K (solid line); the 32.2% MDEA solution at 393.15 K (dash-dot line), 313.15 K (bold dash-dot line); the 46.78% MDEA solution at 373.01 K (dotted line), and 313.15 K (dashed line).
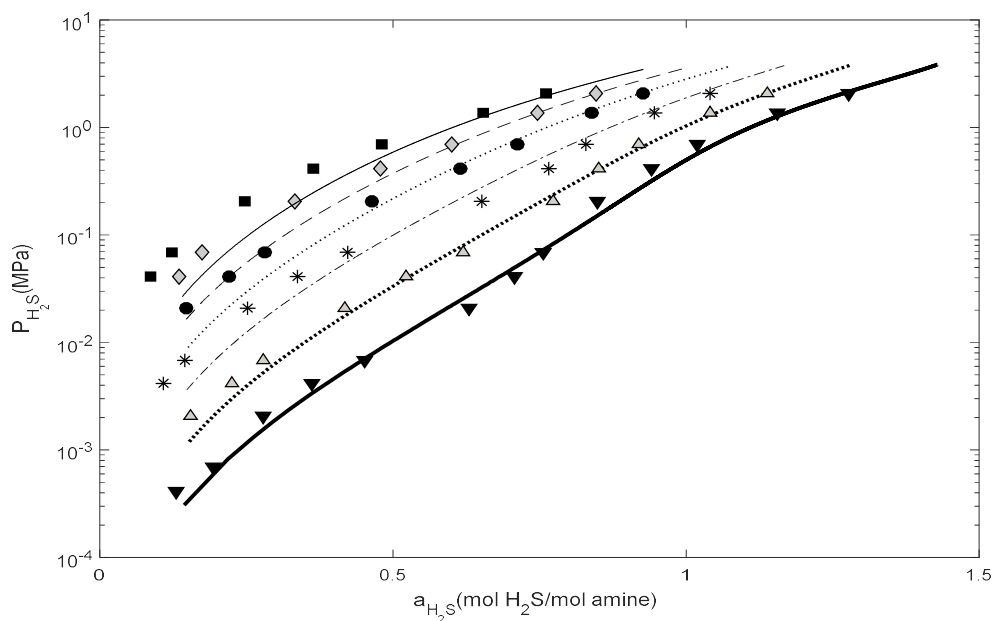

Figure M-17: Comparison between experimental data [143] and modelled results for the solubility of H_2S in the 48.8% MDEA solution. Exp (literature): Jou et al. at 393.15 (○), 373.15 (◆), 343.15 (▢), 313.15 (✳), and 298.15 (△) [143]. Modelled data (this work): at 393.15 (bold solid line), 373.15 (dash-dot line), 343.15 (dashed line), 313.15 (dotted line), and 298.15 (solid line).

Figure M-18: Comparison between experimental data [268] and modelled results for the solubility of H_2S in the 5.2% DEA solution. Exp (literature): Lee et al. at 298.15 K (▼), 323.15 K (△), 348.15 K (✳), 373.15 K (○), 393.15 K (■), and 413.15 K (◇) [268]. Modelled data (this work): at 298.15 K (bold solid line), 323.15 K (bold dashed line), 348.15 K (solid line), 373.15 K (dash-dot line), 393.15 K (dotted line), and 413.15 K (dashed line).

Figure M-19: Comparison between experimental data [260, 268] and modelled results for the solubility of H_2S in the 20.6% DEA solution. Exp (literature): Lee et al. at 298.15 K (◆), 323.15 K (△,+), 348.15 K (✳), 373.15 K (●), 393.15 K (□), and 413.15 K (✳) [260, 268]. Modelled data (this work): at 298.15 K (bold dash-dot line), 323.15 K (solid line), 348.15 K (bold dashed line), 373.15 K (dashed line), 393.15 K (dash-dot line), and 413.15 K (dotted line).

Figure M-20: Comparison between experimental data [268] and modelled results for the solubility of H_2S in the 35.4% DEA solution. Exp (literature): Lee et al. at 298.15 K (▼), 323.15 K (△), 348.15 K (✳), 373.15 K (●), 393.15 K (◇), and 413.15 K (■). Modelled data (this work): at 298.15 K (bold solid line), 323.15 K (bold dotted line), 348.15 K (dash-dot line), 373.15 K (dotted line), 393.15 K (dashed line), and 413.15 K (solid line).
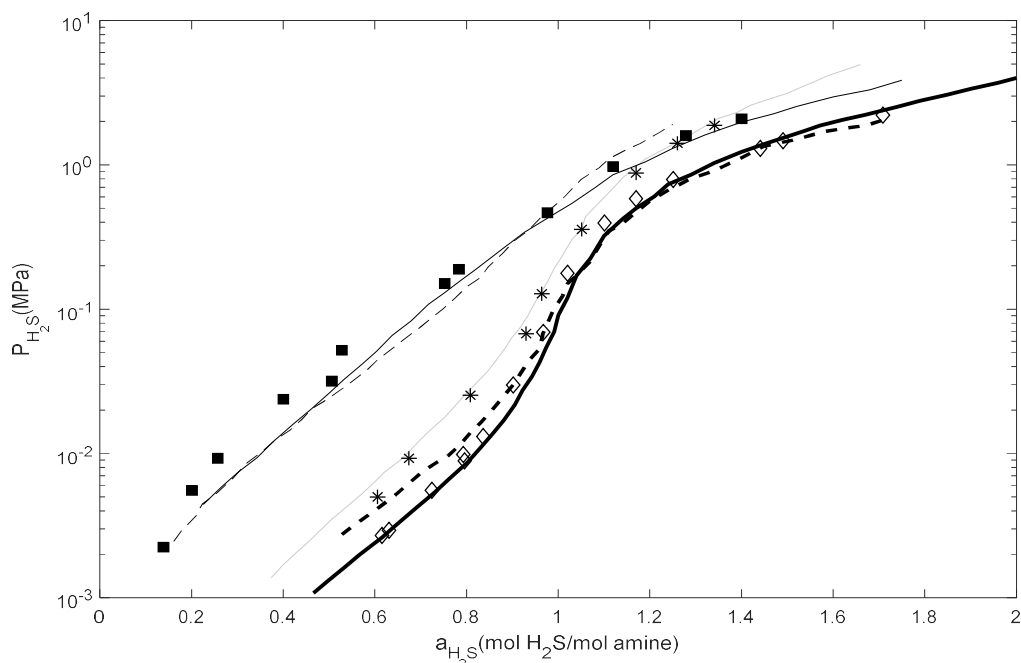

Figure M-21: Comparison between experimental data [263, 264] and modelled results for the solubility of H_2S in the AMP solutions. Exp (literature): Teng and Mather, the 30.78% AMP solution at 323.15 K (✳) [264]; Roberts and Mather, the 17.92% AMP solution at 313.15 K (◇), and 373.15 K (■) [263]. The modified Kent-Eisenberg model data for the 30.78% AMP solution by Hu and Chakma at 313.15 K (bold dashed line), and 373.15 K (dashed line) [145]. Modelled data (this work): the 30.78% AMP solution at 323.15 K (grey line), the 17.92% AMP solution at 313.15 K (bold solid line), and 373.15 K (solid line).

In order to assess further the validity of the developed method, the solubility of H₂S in pure water was anticipated. The results shown in Figure M-22, perfectly match with the experimental data reported in the literature.

Figure M-33 illustrates the parity diagram of the predicted values by the method developed in this study. As clear from the figure, the model can satisfactorily predict the experimental loadings data. At high loadings, there is more deviation where model mostly underestimates the gas solubility at high pressures and low temperatures.
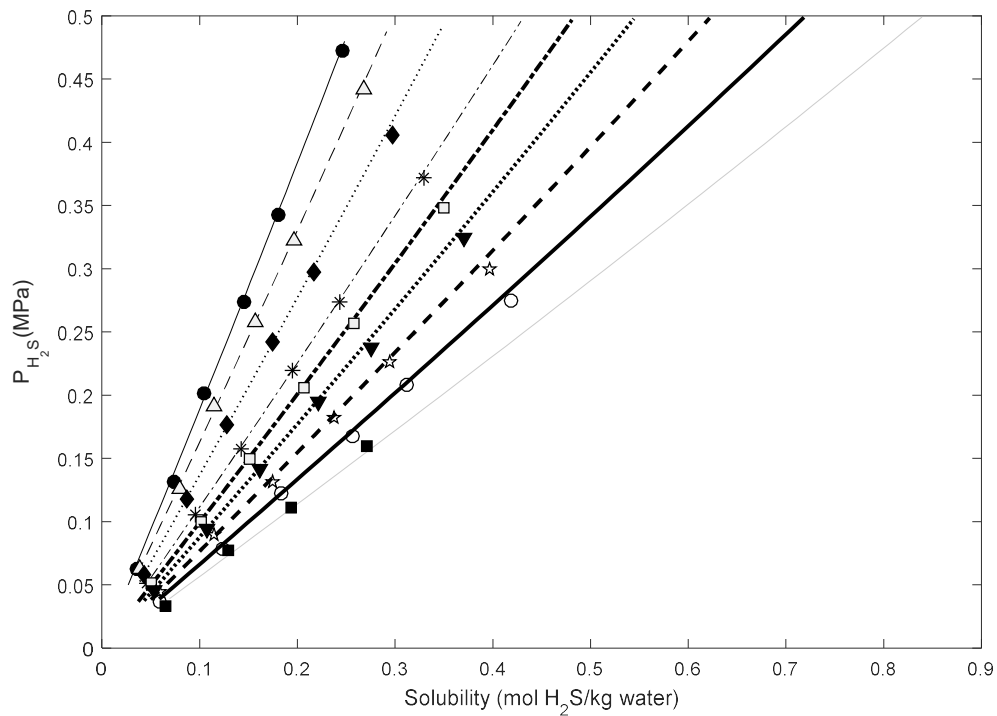
Figure M-22: Comparison between experimental data [269] and modelled results for the solubility of H₂S in water. Exp (literature): Wright and Maass at 333.15 K (●), 323.15 K (△), 313.15 K (◆), 303.15 K (✳), 298.15 K (□), 293.15 K (▼), 288.15 K (✳), 283.15 K (○), and 278.15 K (■) [269]. Modelled data (this work): at 333.15 K (solid line), 323.15 K (dashed line), 313.15 K (dotted line), 303.15 K (dash-dot line), 298.15 K (bold dash-dot line), 293.15 K (bold dotted line), 288.15 K (bold dashed line), 283.15 K (bold solid line), 278.15 K (grey line).
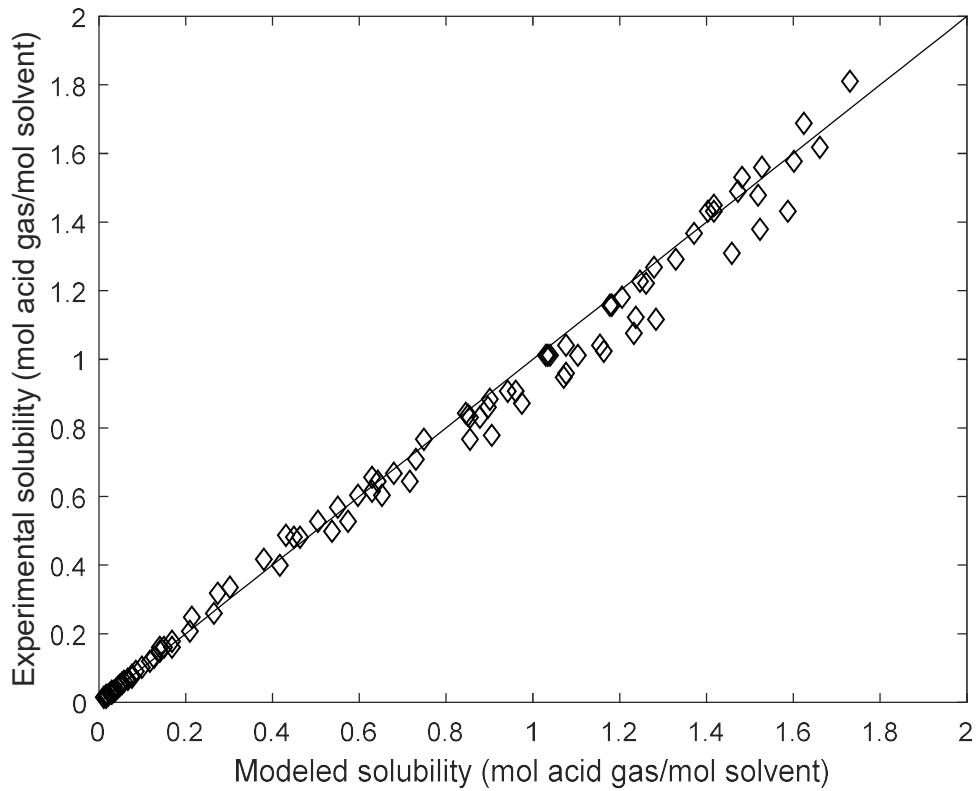
Figure M-23: Parity plot of CO_2 or H_2S solubility in aqueous MDEA.

Equation 6-53 developed in this study is a comprehensive combination of all equations controlling the liquid phase of the CO_2 + MEA + water system at equilibrium state. In other words, its parameters, A_1 to A_6, obtained in the last iteration of the proposed algorithm are specific functions of pressure, temperature and initial concentration of amine that all are the inputs required in the algorithm. For instance, the function of A_1 is as follow:

$$A_1 = d_1.\exp(d_2.P) + d_3.\exp(d_4.P) + d_5 \tag{M-1}$$

Where d_1 to d_5 are degree-five polynomials depending on temperature:

$$d_1 = e_1 T^5 + e_2 T^4 + e_3 T^3 + e_4 T^2 + e_5 T + e_6 \tag{M-2}$$

And finally, e_1 to e_6 are second-degree polynomials depending on the initial concentration of amine. These equations were derived from the regression of the data calculated using the proposed algorithm to predict the solubility of CO_2 in the aqueous MEA. Therefore, similarly, if in the Kent-Eisenberg model, the apparent equilibrium constants are regressed as a function of temperature, pressure and initial concentration of amine, the accuracy of model predictions increases.

References

1.   IEA, *World Energy Outlook (WEO) 2013 (New Policies scenario).* 2013.

2.   Yang, H., et al., *Progress in carbon dioxide separation and capture: A review.* Journal of Environmental Sciences, 2008. 20(1): p. 14-27.

3.   Global CCS Institute 2014*, The Global Status of CCS: 2014,* Melbourne, Australia.

4.   IEA, *World Energy Outlook (WEO) 2007.* 2007.

5.   IEA, *World Energy Outlook (WEO) 2017 (New Policies scenario).* 2017.

6.   Faramawy, S., T. Zaki, and A.A.E. Sakr, *Natural gas origin, composition, and processing: A review.* Journal of Natural Gas Science and Engineering, 2016. 34: p. 34-54.

7.   Karadas, F., M. Atilhan, and S. Aparicio, *Review on the Use of Ionic Liquids (ILs) as Alternative Fluids for CO_2 Capture and Natural Gas Sweetening.* Energy & Fuels, 2010. 24(11): p. 5817-5828.

8.   Demirbas, A., *Methane Gas Hydrate.* 2010: Springer. 186.

9.   Shimekit , B. and H. Mukhtar *Natural Gas Purification Technologies - Major Advances for CO_2 Separation and Future Directions*, in *Advances in Natural Gas Technology*, H.A. Al-Megren, Editor. 2012, InTech.

10.   Mushtaq, A., et al., *A Review: Fabrication of Enhanced Polymeric Blend Membrane with Amines for Removal of CO_2 from Natural Gas.* International Journal of Emerging Technology and Advanced Engineering, 2013. 3(6).

11.   Haghtalab, A. and A. Izadi, *Simultaneous measurement solubility of carbon dioxide + hydrogen sulfide into aqueous blends of alkanolamines at high pressure.* Fluid Phase Equilibria, 2014. 375: p. 181-190.

12.   Haghtalab, A. and A. Izadi, *Solubility and thermodynamic modeling of hydrogen sulfide in aqueous (diisopropanolamine + 2-amino-2-methyl-1-propanol + piperazine) solution at high pressure.* The Journal of Chemical Thermodynamics, 2015. 90: p. 106-115.

13.   Bhide, B.D., A. Voskericyan, and S.A. Stern, *Hybrid processes for the removal of acid gases from natural gas.* Journal of Membrane Science, 1998. 140(1): p. 27-49.

14.   *global climate change (2018),*Online available from: https://climate.nasa.gov/resources/global-warming/.

15.   *Carbon Dioxide.* online available from: https://climate.nasa.gov/vital-signs/carbon-dioxide/.

16.   *Overview of natural gas (2013).* Online available from: http://naturalgas.org/overview/.

17.   Kidnay;, A.J., W.R. Parrish;, and D.G. McCartney, *Fundamentals of Natural Gas Processing.* second ed. 2011: Taylor & Francis Group. 574.

18. Torralba-Calleja, E., et al., *CO₂ Capture in Ionic Liquids: A Review of Solubilities and Experimental Methods.* Journal of Chemistry, 2013. 2013: p. 16.

19. Guo, B., et al., *Absorption and Oxidation of H2S in Caprolactam Tetrabutyl Ammonium Bromide Ionic Liquid.* Energy & Fuels, 2011. 25(1): p. 159-161.

20. Jalili, A.H., et al., *Solubility of H₂S in Ionic Liquids [bmim][PF₆], [bmim][BF₄], and [bmim][Tf₂N].* Journal of Chemical & Engineering Data, 2009. 54(6): p. 1844-1849.

21. Baj, S., et al., *Monoethanolamine and ionic liquid aqueous solutions as effective systems for CO₂ capture.* Society of Chemical Industry, 2013. 88: p. 1220-1227.

22. Lu, B.-H., et al., *Absorption of carbon dioxide into aqueous blend of monoethanolamine and 1-butyl-3-methylimidazolium tetrafluoroborate.* International Journal of Greenhouse Gas Control, 2012. 11: p. 152-157.

23. Huang, K., Y.-T. Wu, and X.-B. Hu, *Effect of alkalinity on absorption capacity and selectivity of SO₂ and H₂S over CO₂: Substituted benzoate-based ionic liquids as the study platform.* Chemical Engineering Journal, 2016. 297(Supplement C): p. 265-276.

24. Yokozeki, A., et al., *Physical and Chemical Absorptions of Carbon Dioxide in Room-Temperature Ionic Liquids.* The Journal of Physical Chemistry B, 2008. 112(51): p. 16654-16663.

25. Pomelli, C.S., et al., *Influence of the Interaction between Hydrogen Sulfide and Ionic Liquids on Solubility: Experimental and Theoretical Investigation.* The Journal of Physical Chemistry B, 2007. 111(45): p. 13014-13019.

26. Poole, C.F., *Chromatographic and spectroscopic methods for the determination of solvent properties of room temperature ionic liquids.* Journal of Chromatography A, 2004. 1037(1): p. 49-82.

27. Rao, A.B. and E.S. Rubin, *A Technical, Economic, and Environmental Assessment of Amine-Based CO₂ Capture Technology for Power Plant Greenhouse Gas Control.* Environmental Science & Technology, 2002. 36(20): p. 4467-4475.

28. Mahin Rameshni, P.E., *Selection Criteria for Claus Tail Gas Treating Processes.* WorleyParsons, Resources & Energy.

29. Mahin Rameshni, P.E., *gas processing - state of the art - design guide line.* Rameshni & Associates Technology & Engineering LLc.

30. Jalili, A.H., et al., *Solubility of CO₂ and H₂S in the ionic liquid 1-ethyl-3-methylimidazolium tris(pentafluoroethyl)trifluorophosphate.* The Journal of Chemical Thermodynamics, 2013. 67: p. 55-62.

31. PRODEM, *"Oil and gas processing plant design and operation training course" "gas sweetening processes".* 2002.

32. PRODEM, E.f., *Oil and gas processing plant design and operation training course, gas sweetening processes.* 2002. p. 1-43.

33. Althuluth, M.A.M., *Natural Gas Sweetening Using Ionic Liquids.* 2014, Eindhoven University of Technology.

34. Galán Sánchez, L.M., G.W. Meindersma, and A.B. de Haan, *Solvent Properties of Functionalized Ionic Liquids for CO₂ Absorption.* Chemical Engineering Research and Design, 2007. 85(1): p. 31-39.

35. Olivier-Bourbigou, H., L. Magna, and D. Morvan, *Ionic liquids and catalysis: Recent progress from knowledge to applications.* Applied Catalysis A: General, 2010. 373(1): p. 1-56.

36. Available from: https://www.sciencedirect.com/topics/engineering/rectisol-process.

37. Heintz, Y.J., et al., *Hydrogen Sulfide and Carbon Dioxide Removal from Dry Fuel Gas Streams Using an Ionic Liquid as a Physical Solvent.* Energy & Fuels, 2009. 23(10): p. 4822-4830.

38. Kumar, S., J.H. Cho, and I. Moon, *Ionic liquid-amine blends and CO2BOLs: Prospective solvents for natural gas sweetening and CO2 capture technology—A review.* International Journal of Greenhouse Gas Control, 2014. 20: p. 87-116.

39. Kohl, A., and R. Nielsen, *Gas purification*. 5 ed. 1997: Gulf Publishing Company.

40. Haynes, W.M., *Handbook of Chemistry and Physics* 95th ed. 2014: CRC Press Taylor & Francis Group.

41. Nasirzadeh, K., R. Neueder, and W. Kunz, *Vapor Pressures of Propylene Carbonate and N,N-Dimethylacetamide.* Journal of Chemical & Engineering Data, 2005. 50(1): p. 26-28.

42. Muhuri, P.K. and D.K. Hazra, *Density and Viscosity of Propylene Carbonate + 2-Methoxyethanol at 298.15, 308.15, and 318.15 K.* Journal of Chemical & Engineering Data, 1995. 40(3): p. 582-585.

43. Burr, B. and L. Lyddon, *A Comparison of Physical Solvents for Acid Gas Removal.* Bryan Research & Engineering, Inc. Bryan, Texas, U.S.A.

44. Available from: https://www.engineeringtoolbox.com/methanol-methyl-alcohol-properties-CH3OH-d_2031.html.

45. Mohd Salleh, R., *Volumetric properties and absorption of carbon dioxide in aqueous solutions of piperazine and activated diethanolamine / Ruzitah binti Mohd Salleh.* 2005, University of Malaya.

46. Ying Wu, J.J.C., Weiyao Zhu, *Acid Gas Extraction for Disposal and Related Topics.* 2016, United States of America: Scrivener.

47. Wang, T., *Thermodynamic aspects of the capture of acid gas from natural gas*, in *Chemical engineering.* 2017, PSL Research University.

48. Wikipedia contributors, *Amine.* Wikipedia, The Free Encyclopedia, 2018, May 6.

49. *Gate; H₂S Scavenging: Amine Systems;* available from: https://www.gateinc.com/gatekeeper/gat2004-gkp-2014-06. 2014.

50. Polasek, J. and J.A. Bullin, *Selecting Amines for Sweetening Units.* Proceedings GPA Regional Meeting. "Process Considerations in Selecting Amine" Tulsa, September, Gas Processors Association, OK, 1994.

51.   *Newpoint Gas; Amine Treating Plants;* available from: https://www.newpointgas.com/services/amine-treating-plants/. 2017.

52.   Zare Aliabad, H. and S. Mirzaei, *Removal of CO_2 and H_2S Using Aqueous Alkanolamine Solutions.* International Journal of Chemical and Molecular Engineering, 2009. **3**: p. 50-59.

53.   Panah, H.S., A.H. Mohammadi, and D. Ramjugernath, *Development of a novel approach for modeling acid gas solubility in alkanolamine aqueous solution.* Journal of Natural Gas Science and Engineering, 2016. 34: p. 112-123.

54.   *Technical Data Sheet;* avaiable from:

        http://msdssearch.dow.com/PublishedLiteratureDOWCOM/dh_005c/0901b8038005c44 f.pdf?filepath=amines/pdfs/noreg/111-01411.pdf&fromPage=GetDoc.

55.   *Technical Data Sheet;* available from:

        https://www.huntsman.com/performance_products/Media%20Library/a_MC348531CF A3EA9A2E040EBCD2B6B7B06/Products_MC348531D0B9FA9A2E040EBCD2B6B 7B06/Amines_MC348531D0BECA9A2E040EBCD2B6B7B06/Alkylalkanolamines_M C348531D0C39A9A2E040EBCD2B6B7B06/files/mdea.pdf.

56.   Belabbaci, A., et al., *Isothermal Vapor−Liquid Equilibria of (Monoethanolamine + Water) and (4-Methylmorpholine + Water) Binary Systems at Several Temperatures.* Journal of Chemical & Engineering Data, 2009. 54(8): p. 2312-2316.

57.   Verevkin, S.P., et al., *Vapor Pressures and Enthalpies of Vaporization of a Series of Low-Volatile Alkanolamines.* Journal of Chemical & Engineering Data, 2011. 56(12): p. 4400-4406.

58.   Kurnia, K.A., C.D. Wilfred, and T. Murugesan, *Thermophysical properties of hydroxyl ammonium ionic liquids.* The Journal of Chemical Thermodynamics, 2009. 41(4): p. 517-521.

59.   Xiao, M., et al., *CO_2 capture with hybrid absorbents of low viscosity imidazolium-based ionic liquids and amine.* Applied Energy, 2019. 235: p. 311-319.

60.   Hagiwara, R. and Y. Ito, *Room temperature ionic liquids of alkylimidazolium cations and fluoroanions.* Journal of Fluorine Chemistry, 2000. 105(2): p. 221-227.

61.   Maginn, E.J., *Design and Evaluation of Ionic Liquids as Novel CO_2 Absorbents.* 2007: University of Notre Dame.

62.   Jalili, A.H., et al., *Solubility and diffusion of CO_2 and H_2S in the ionic liquid 1-ethyl-3-methylimidazolium ethylsulfate.* The Journal of Chemical Thermodynamics, 2010. 42(10): p. 1298-1303.

63.   Chang, R., *Chemistry (8th Edition).* 8th ed. 2004.

64.   Xue, H., R. Verma, and J.n.M. Shreeve, *Review of ionic liquids with fluorine-containing anions.* Journal of Fluorine Chemistry, 2006. 127(2): p. 159-176.

65. Wang, T., et al., *Description of the pVT behavior of ionic liquids and the solubility of gases in ionic liquids using an equation of state.* Fluid Phase Equilibria, 2006. 250(1): p. 150-157.

66. Wang, G., et al., *Low-Viscosity Triethylbutylammonium Acetate as a Task-Specific Ionic Liquid for Reversible CO_2 Absorption.* Journal of Chemical & Engineering Data, 2011. 56(4): p. 1125-1133.

67. Huang, K., et al., *Thermodynamic Validation of 1-Alkyl-3-methylimidazolium Carboxylates as Task-Specific Ionic Liquids for H_2S Absorption.* AIChE Journal, 2012. 59: p. 2227–2235.

68. Soriano, A.N., B.T. Doma, and M.-H. Li, *Solubility of Carbon Dioxide in 1-Ethyl-3-methylimidazolium Tetrafluoroborate.* Journal of Chemical & Engineering Data, 2008. 53(11): p. 2550-2555.

69. Anderson, J.L., et al., *Measurement of SO2 Solubility in Ionic Liquids.* The Journal of Physical Chemistry B, 2006. 110(31): p. 15059-15062.

70. Kurnia, K.A., et al., *Thermodynamic properties of CO2 absorption in hydroxyl ammonium ionic liquids at pressures of (100–1600)kPa.* The Journal of Chemical Thermodynamics, 2009. 41(10): p. 1069-1073.

71. Anderson, J.L., J.K. Dixon, and J.F. Brennecke, *Solubility of CO_2, CH_4, C_2H_6, C_2H_4, O_2, and N_2 in 1-Hexyl-3-methylpyridinium Bis(trifluoromethylsulfonyl)imide: Comparison to Other Ionic Liquids.* Accounts of Chemical Research, 2007. 40(11): p. 1208-1216.

72. Camper, D., et al., *Gas Solubilities in Room-Temperature Ionic Liquids.* Industrial & Engineering Chemistry Research, 2004. 43(12): p. 3049-3054.

73. Liu, W., et al., *The Physical Properties of Aqueous Solutions of the Ionic Liquid [BMIM][BF_4].* Journal of Solution Chemistry, 2006. 35(10): p. 1337-1346.

74. Liu, H., J. Huang, and P. Pendleton, *Experimental and modelling study of CO_2 absorption in ionic liquids containing Zn (II) ions.* Energy Procedia, 2011. 4: p. 59-66.

75. Nie, Y., et al., *Extractive Desulfurization of Gasoline Using Imidazolium-Based Phosphoric Ionic Liquids.* Energy & Fuels, 2006. 20(5): p. 2083-2087.

76. Kroon, M.C., et al., *High-Pressure Phase Behavior of Systems with Ionic Liquids: Part V. The Binary System Carbon Dioxide + 1-Butyl-3-methylimidazolium Tetrafluoroborate.* Journal of Chemical & Engineering Data, 2005. 50(1): p. 173-176.

77. Shin, E.-K. and B.-C. Lee, *High-Pressure Phase Behavior of Carbon Dioxide with Ionic Liquids: 1-Alkyl-3-methylimidazolium Trifluoromethanesulfonate.* Journal of Chemical & Engineering Data, 2008. 53(12): p. 2728-2734.

78. Carvalho, P.J., et al., *Specific Solvation Interactions of CO_2 on Acetate and Trifluoroacetate Imidazolium Based Ionic Liquids at High Pressures.* The Journal of Physical Chemistry B, 2009. 113(19): p. 6803-6812.

79. Shariati, A. and C.J. Peters, *High-pressure phase behavior of systems with ionic liquids: II. The binary system carbon dioxide+1-ethyl-3-methylimidazolium hexafluorophosphate.* The Journal of Supercritical Fluids, 2004. 29(1): p. 43-48.

80. Blanchard, L.A., Z. Gu, and J.F. Brennecke, *High-Pressure Phase Behavior of Ionic Liquid/CO$_2$ Systems.* The Journal of Physical Chemistry B, 2001. 105(12): p. 2437-2444.

81. Kim, Y.S., et al., *Solubility measurement and prediction of carbon dioxide in ionic liquids.* Fluid Phase Equilibria, 2005. 228-229: p. 439-445.

82. Zhimin, L., et al., *Study on the Phase Behaviors, Viscosities, and Thermodynamic Properties of CO$_2$/[C$_4$mim][PF$_6$]/Methanol System at Elevated Pressures.* Chemistry: A European Journal, 2003. 9(16).

83. Shiflett, M.B. and A. Yokozeki, *Solubilities and Diffusivities of Carbon Dioxide in Ionic Liquids: [bmim][PF$_6$] and [bmim][BF$_4$].* Industrial & Engineering Chemistry Research, 2005. 44(12): p. 4453-4464.

84. Alireza Shariati, A., K. Gutkowski, and C.J. Peters, *Comparison of the phase behavior of some selected binary systems with ionic liquids.* AIChE Journal, 2005. 51(5).

85. Scovazzo, P., et al., *Regular Solution Theory and CO$_2$ Gas Solubility in Room-Temperature Ionic Liquids.* Industrial & Engineering Chemistry Research, 2004. 43(21): p. 6855-6860.

86. Pérez-Salado Kamps, Á., et al., *Solubility of CO$_2$ in the Ionic Liquid [bmim][PF$_6$].* Journal of Chemical & Engineering Data, 2003. 48(3): p. 746-749.

87. Shariati, A. and C.J. Peters, *High-pressure phase behavior of systems with ionic liquids: Part III. The binary system carbon dioxide + 1-hexyl-3-methylimidazolium hexafluorophosphate.* The Journal of Supercritical Fluids, 2004. 30(2): p. 139-144.

88. Revelli, A.-L., F. Mutelet, and J.-N. Jaubert, *High Carbon Dioxide Solubilities in Imidazolium-Based Ionic Liquids and in Poly(ethylene glycol) Dimethyl Ether.* The Journal of Physical Chemistry B, 2010. 114(40): p. 12908-12913.

89. Aki, S.N.V.K., et al., *High-Pressure Phase Behavior of Carbon Dioxide with Imidazolium-Based Ionic Liquids.* The Journal of Physical Chemistry B, 2004. 108(52): p. 20355-20365.

90. Husson-Borg, P., V. Majer, and M.F. Costa Gomes, *Solubilities of Oxygen and Carbon Dioxide in Butyl Methyl Imidazolium Tetrafluoroborate as a Function of Temperature and at Pressures Close to Atmospheric Pressure.* Journal of Chemical & Engineering Data, 2003. 48(3): p. 480-485.

91. Costantini, M., et al., *High-Pressure Phase Behavior of Systems with Ionic Liquids: Part IV. Binary System Carbon Dioxide + 1-Hexyl-3-methylimidazolium Tetrafluoroborate.* Journal of Chemical & Engineering Data, 2005. 50(1): p. 52-55.

92. Shiflett, M.B. and A. Yokozeki, *Phase Behavior of Carbon Dioxide in Ionic Liquids: [emim][Acetate], [emim][Trifluoroacetate], and [emim][Acetate] + [emim][Trifluoroacetate] Mixtures.* Journal of Chemical & Engineering Data, 2009. 54(1): p. 108-114.

93. Oh, D. and B. Lee, *High-pressure phase behavior of carbon dioxide in ionic liquid 1-butyl-3-methylimidazolium bis(trifluoromethylsulfonyl)imide.* Korean Journal of Chemical Engineering, 2006. 23(5).

94.   Ren, W. and A. Scurto, *High-pressure phase equilibria with compressed gases.* Rev. Sci. Instrum., 125104 (2007). 78.

95.   Xiaochun, Z., L. Zhiping, and W. Wenchuan, *Screening of Ionic Liquids to Capture CO2 by COSMO-RS and Experiments.* AIChE Journal, 2008. 54(10): p. 2717-2728.

96.   Yuan, X., et al., *Solubilities of CO2 in hydroxyl ammonium ionic liquids at elevated pressures.* Fluid Phase Equilibria, 2007. 257(2): p. 195-200.

97.   Haghtalab, A. and A. Shojaeian, *High pressure measurement and thermodynamic modelling of the solubility of carbon dioxide in N-methyldiethanolamine and 1-butyl-3-methylimidazolium acetate mixture.* The Journal of Chemical Thermodynamics, 2015. 81: p. 237-244.

98.   Shojaeian, A. and A. Haghtalab, *Solubility and density of carbon dioxide in different aqueous alkanolamine solutions blended with 1-butyl-3-methylimidazolium acetate ionic liquid at high pressure.* Journal of Molecular Liquids, 2013. 187: p. 218-225.

99.   Akbar, M.M. and T. Murugesan, *Thermophysical properties for the binary mixtures of 1-hexyl-3-methylimidazolium bis(trifluoromethylsulfonyl)imide [hmim][Tf2N]+N-methyldiethanolamine (MDEA) at temperatures (303.15 to 323.15) K.* Journal of Molecular Liquids, 2012. 169: p. 95-101.

100.   Bernard, F.L., et al., *Anticorrosion Protection by Amine–Ionic Liquid Mixtures: Experiments and Simulations.* Journal of Chemical & Engineering Data, 2016. 61(5): p. 1803-1810.

101.   Ahmady, A., M.A. Hashim, and M.K. Aroua, *Kinetics of Carbon Dioxide absorption into aqueous MDEA+[bmim][BF4] solutions from 303 to 333K.* Chemical Engineering Journal, 2012. 200-202: p. 317-328.

102.   Gao, J., et al., *Ionic liquids tailored amine aqueous solution for pre-combustion CO2 capture: Role of imidazolium-based ionic liquids.* Applied Energy, 2015. 154: p. 771-780.

103.   Yang, J., et al., *CO2 Capture Using Amine Solution Mixed with Ionic Liquid.* Industrial & Engineering Chemistry Research, 2014. 53(7): p. 2790-2799.

104.   Li, Y., et al., *Solubilities of CO2 in, and Densities and Viscosities of, the Piperazine + 1-Ethyl-3-methyl-imidazolium Acetate + H2O System.* Journal of Chemical & Engineering Data, 2014. 59(3): p. 618-625.

105.   McCrellis, C., et al., *Effect of the Presence of MEA on the CO2 Capture Ability of Superbase Ionic Liquids.* Journal of Chemical & Engineering Data, 2016. 61(3): p. 1092-1100.

106.   Ahmady, A., M.A. Hashim, and M.K. Aroua, *Absorption of carbon dioxide in the aqueous mixtures of methyldiethanolamine with three types of imidazolium-based ionic liquids.* Fluid Phase Equilibria, 2011. 309(1): p. 76-82.

107.   Aziz, N., R. Yusoff, and M.K. Aroua, *Absorption of CO2 in aqueous mixtures of N-methyldiethanolamine and guanidinium tris(pentafluoroethyl)trifluorophosphate ionic liquid at high-pressure.* Fluid Phase Equilibria, 2012. 322-323: p. 120-125.

108.   Iliuta, I., M. Hasib-ur-Rahman, and F. Larachi, *CO₂ absorption in diethanolamine/ionic liquid emulsions – Chemical kinetics and mass transfer study.* Chemical Engineering Journal, 2014. 240: p. 16-23.

109.   Lei, Z., et al., *Solubility of CO₂ in Methanol, 1-Octyl-3-methylimidazolium Bis(trifluoromethylsulfonyl)imide, and Their Mixtures.* Chinese Journal of Chemical Engineering, 2013. 21(3): p. 310-317.

110.   Shokouhi, M., et al., *Experimental Investigation on the Solubility and Initial Rate of Absorption of CO₂ in Mixture of Amine-Functionalized Ionic Liquids and Physical Solvents.* Iranian Journal of Chemical Engineering(IJChE), 2015. 12(1): p. 68-77.

111.   Tian, S., et al., *Physical Properties of 1-Butyl-3-methylimidazolium Tetrafluoroborate/N-Methyl-2-pyrrolidone Mixtures and the Solubility of CO₂ in the System at Elevated Pressures.* Journal of Chemical & Engineering Data, 2012. 57(3): p. 756-763.

112.   Bogatu, C., R. Vîlcu, and A. DuŃă, *Experimental Methods for Study High-Pressure. Phase Behaviour. Part I. Static Methods.* Annals of the University of Bucharest, 2005. I-II: p. 193-203.

113.   Nelson, W.M., *Separation of Trichlorosilane: Measurement, Modeling And Simulation.* 2012, University of KwaZulu-Natal.

114.   Bengesai, P., *High Pressure Vapour-Liquid Equilibrium Measurements For R116 and Ethane with Perfluorohexane and Perfluorooctane.* 2016, University of KwaZulu-Natal.

115.   Megne Motchelaho, A.M., *Vapour-Liquid Equilibrium Measurements using a Static Total Pressure Apparatus* in *of Chemical Engineering,.* 2006, University of KwaZulu-Natal.

116.   Tong, D., *Development of Advanced Amine Systems with Accurate Vapour-liquid Equilibrium Measurement.* 2012, University of London.

117.   Zhang, F., et al., *An improved static–analytic apparatus for vapor–liquid equilibrium (PTxy) measurement using modified in-situ samplers.* Fluid Phase Equilibria, 2016. 409: p. 425-433.

118.   Eduard Hâla, et al., *Vapour-Liquid Equilibrium.* 2nd English Edition ed. 1967, Institute of Chemical Process Fundamentals, Czechoslovak Academy of Science and Department of Physical Chemistry, Institute of Chemical Technology, Prague, Czechoslovakia.

119.   Jou, F.-Y., A.E. Mather, and F.D. Otto, *The solubility of CO₂ in a 30 mass percent monoethanolamine solution.* The Canadian Journal of Chemical Engineering, 1995. 73(1): p. 140-147.

120.   Jou, F. and A.E. Mather, *Solubility of Hydrogen Sulfide in [bmim][PF₆].* Int J Thermophys, 2007. 28(2).

121.   Shiflett, M.B., A.M.S. Niehaus, and A. Yokozeki, *Separation of CO₂ and H₂S Using Room-Temperature Ionic Liquid [bmim][MeSO₄].* Journal of Chemical & Engineering Data, 2010. 55(11): p. 4785-4793.

122.   Huang, K., et al., *Thermodynamic validation of 1-alkyl-3-methylimidazolium carboxylates as task-specific ionic liquids for H₂S absorption.* AIChE Journal, 2012. 59(6): p. 2227-2235.

123. Pennline, H.W., et al., *Progress in carbon dioxide capture and separation research for gasification-based power generation point sources.* Fuel Processing Technology, 2008. 89(9): p. 897-907.

124. Heintz, Y.J., et al., *Novel Physical Solvents for Selective CO_2 Capture from Fuel Gas Streams at Elevated Pressures and Temperatures.* Energy & Fuels, 2008. 22(6): p. 3824-3837.

125. Nelson, W.M. and D. Ramjugernath, *Experimental Solubility Data for Binary Mixtures of Ethane and 2,2,4-Trimethylpentane at Pressures up to 6 MPa Using a New Variable-Volume Sapphire Cell.* Journal of Chemical & Engineering Data, 2017. 62(11): p. 3915-3920.

126. Nelson, W.M., et al., *High-pressure phase equilibria data for mixtures involving ethene and perfluoro-n-octane from 293 to 353K.* Fluid Phase Equilibria, 2016. 408: p. 33-37.

127. Linde Gas Division, L.G.G., *Safety Advice. 12 – Working with Carbon dioxide* CO_2.available from: https://www.linde-gas.pt/en/images/Safety_Advice_12_tcm303-25938.pdf.

128. Lazzaroni, M.J., et al., *High-Pressure Vapor−Liquid Equilbria of Some Carbon Dioxide + Organic Binary Systems.* Journal of Chemical & Engineering Data, 2005. 50(1): p. 60-65.

.

129. B.N. Taylor and C.E. Kuyatt, *NIST Technical Note 1297: Guidelines for Evaluating and Expressing the Uncertainty of NIST Measurement Results.* 1994, National Institute of Standards and Technology, Gaithersburg.

130. Danesh, A., *PVT and Phase Behaviour of Petroleum Reservoir Fluids.* 1th ed. Vol. 47. 1998: Elsevier Science.

131. Ahmed, T., *Equations of State and PVT Analysis.* 2007, Houston, Texas: Gulf Publishing Company.

132. John M. Prausnitz, Rudiger N. Lichtenthaler, and E.G.d. Azevedo, *Molecular Thermodynamics of Fluid-Phase Equilibria.* third ed. 1998. 864.

133. Fouad, W.A. and A.S. Berrouk, *Prediction of H_2S and CO_2 Solubilities in Aqueous Triethanolamine Solutions Using a Simple Model of Kent–Eisenberg Type.* Industrial & Engineering Chemistry Research, 2012. 51(18): p. 6591-6597.

134. Patil, P., Z. Malik, and M. Jobson, *Prediction of CO_2 and H_2S solubility in aqueous MDEA solutions using an extended Kent and Eisenberg model.* Institution of Chemical Engineers Symposium Series, 2006. 152: p. 498-510.

135. Kent, R.L. and B. Eisenberg, *Better data for amine treating.* Hydrocarbon Process, 1976. 55(2).

136. Tong, D., et al., *Solubility of carbon dioxide in aqueous solution of monoethanolamine or 2-amino-2-methyl-1-propanol: Experimental measurements and modelling.* International Journal of Greenhouse Gas Control, 2012. 6: p. 37-47.

137. Mondal, T.K., *Phase Equilibrium Modeling in Gas Purification System*, in *Chemical Engineering* 2009, National Institute of Technology.

138. Tontiwachwuthikul, P., A. Meisen, and C.J. Lim, *Solubility of carbon dioxide in 2-amino-2-methyl-1-propanol solutions.* Journal of Chemical & Engineering Data, 1991. 36(1): p. 130-133.

139. Li, M-H. and K-P. Shen, *Calculation of equilibrium solubility of carbon dioxide in aqueous mixtures of monoethanolamine with methyldiethanolamine.* Fluid Phase Equilibria, 1993. 85: p. 129-140.

140. Li, M-H.and B-C. Chang, *Solubilities of Carbon Dioxide in Water + Monoethanolamine + 2 -Amino -2-me t h yl- 1 -propanol.* Journal of Chemical & Engineering Data, 1994. 39: p. 448-452.

141. Dong, L., J. Chen, and G. Gao, *Solubility of Carbon Dioxide in Aqueous Solutions of 3-Amino-1-propanol.* Journal of Chemical & Engineering Data, 2010. 55(2): p. 1030-1034.

142. Chakma, A. and A. Meisen, *Solubility of carbon dioxide in aqueous methyldiethanolamine and N,N-bis(hydroxyethyl)piperazine solutions.* Industrial & Engineering Chemistry Research, 1987. 26(12): p. 2461-2466.

143. Jou, F.Y., A.E. Mather, and F.D. Otto, *Solubility of hydrogen sulfide and carbon dioxide in aqueous methyldiethanolamine solutions.* Industrial & Engineering Chemistry Process Design and Development, 1982. 21(4): p. 539-544.

144. Haji-Sulaiman, M.Z., M.K. Aroua, and A. Benamor, *Analysis of Equilibrium Data of CO2 in Aqueous Solutions of Diethanolamine (DEA), Methyldiethanolamine (MDEA) and Their Mixtures Using the Modified Kent Eisenberg Model.* Chemical Engineering Research and Design, 1998. 76(8): p. 961-968.

145. Hu, W. and A. Chakma, *Modelling of Equilibrium Solubility of CO_2 And H_2S In Aqueous Amino Methyl Propanol (AMP) Solutions.* Chemical Engineering Communications, 1990. 94(1): p. 53-61.

146. Kritpiphat, W. and P. Tontiwachwuthikul, *New modified kent-eisenberg model for predicting carbon dioxide solubility in aqueous 2-amino-2-methyl-1-propanol (AMP) solutions.* Chemical Engineering Communications, 1996. 144(1): p. 73-83.

147. Mondal, B.K., S.S. Bandyopadhyay, and A.N. Samanta, *Experimental measurement and Kent-Eisenberg modelling of CO_2 solubility in aqueous mixture of 2-amino-2-methyl-1-propanol and hexamethylenediamine.* Fluid Phase Equilibria, 2017. 437: p. 118-126.

148. Deshmukh, R.D. and A.E. Mather, *A Mathematical Model for Equilibrium Solubility of Hydrogen Sulfide and Carbon Dioxide in Aqueous Alkanolamine Solutions.* Chemical engineering science, 1981. 36: p. 355-362.

149. Pitzer, K.S., *Thermodynamics of electrolytes. I. Theoretical basis and general equations.* The Journal of Physical Chemistry, 1973. 77(2): p. 268-277.

150. Chen, C-C., et al., *Local composition model for excess Gibbs energy of electrolyte systems. Part I: Single solvent, single completely dissociated electrolyte systems.* AIChE Journal, 1982. 28(4): p. 588-596.

151. Sander, B., P. Rasmussen, and A. Fredenslund, *Calculation of solid-liquid equilibria in aqueous solutions of nitrate salts using an extended UNIQUAC equation.* Chemical Engineering Science, 1986. 41(5): p. 1197-1202.

152. Wong, M.K., A.M. Shariff, and M.A. Bustam, *Raman spectroscopic study on the equilibrium of carbon dioxide in aqueous monoethanolamine.* RSC Advances, 2016. 6(13): p. 10816-10823.

153. Austgen , D.M. and G.T. Rochelle, *Model of vapor-liquid equilibria for aqueous acid gas-alkanolamine systems. 2. Representation of hydrogen sulfide and carbon dioxide solubility in aqueous MDEA and carbon dioxide solubility in aqueous mixtures of MDEA with MEA or DEA.* Industrial & Engineering Chemistry Research, 1991. 30: p. 543-555.

154. Chang, H.T., M. Posey, and G.T. Rochelle, *Thermodynamics of alkanolamine-water solutions from freezing point measurements.* Industrial & Engineering Chemistry Research, 1993. 32(10): p. 2324-2335.

155. Liu, Y., L. Zhang, and S. Watanasiri, *Representing Vapor−Liquid Equilibrium for an Aqueous MEA−CO₂ System Using the Electrolyte Nonrandom-Two-Liquid Model.* Industrial & Engineering Chemistry Research, 1999. 38(5): p. 2080-2090.

156. Aroua, M.K., M.Z. Haji-Sulaiman, and K. Ramasamy, *Modelling of carbon dioxide absorption in aqueous solutions of AMP and MDEA and their blends using Aspenplus.* Separation and Purification Technology, 2002. 29(2): p. 153-162.

157. Zhang, Y., H. Que, and C.-C. Chen, *Thermodynamic modeling for CO₂ absorption in aqueous MEA solution with electrolyte NRTL model.* Fluid Phase Equilibria, 2011. 311: p. 67-75.

158. Dash, S.K., et al., *Vapour liquid equilibria of carbon dioxide in dilute and concentrated aqueous solutions of piperazine at low to high pressure.* Fluid Phase Equilibria, 2011. 300(1–2): p. 145-154.

159. Barreau, A., et al., *Absorption of H₂S and CO₂ in Alkanolamine Aqueous Solution: Experimental Data and Modelling with the Electrolyte-NRTL Model.* Oil & Gas Science and Technology 2006. 61: p. 345-361.

160. Edwards, T.J., et al., *Vapor-liquid equilibria in multicomponent aqueous solutions of volatile weak electrolytes.* AIChE Journal, 1978. 24(6): p. 966-976.

161. Pitzer, K.S. and J.M. Simonson, *Thermodynamics of multicomponent, miscible, ionic systems: theory and equations.* The Journal of Physical Chemistry, 1986. 90(13): p. 3005-3009.

162. Li, Y.-G. and A.E. Mather, *Correlation and Prediction of the Solubility of Carbon Dioxide in a Mixed Alkanolamine Solution.* Industrial & Engineering Chemistry Research, 1994. 33(8): p. 2006-2015.

163. Kuranov, G., et al., *Solubility of Single Gases Carbon Dioxide and Hydrogen Sulfide in Aqueous Solutions of N-Methyldiethanolamine in the Temperature Range 313−413 K at Pressures up to 5 MPa.* Industrial & Engineering Chemistry Research, 1996. 35(6): p. 1959-1966.

164. Kamps, Á.P.-S., et al., *Solubility of Single Gases Carbon Dioxide and Hydrogen Sulfide in Aqueous Solutions of N-Methyldiethanolamine at Temperatures from 313 to 393 K and Pressures up to 7.6 MPa: New Experimental Data and Model Extension.* Industrial & Engineering Chemistry Research, 2001. 40(2): p. 696-706.

165. Arcis, H., et al., *Enthalpy of solution of CO₂ in aqueous solutions of methyldiethanolamine at T = 372.9 K and pressures up to 5 MPa.* The Journal of Chemical Thermodynamics, 2009. 41(7): p. 836-841.

166. Böttinger, W., M. Maiwald, and H. Hasse, *Online NMR spectroscopic study of species distribution in MEA–H₂O–CO₂ and DEA–H₂O–CO₂.* Fluid Phase Equilibria, 2008. 263(2): p. 131-143.

167. Rumpf, B. and G. Maurer, *An Experimental and Theoretical Investigation on the Solubility of Carbon Dioxide in Aqueous Solutions of Strong Electrolytes.* Berichte der Bunsengesellschaft für physikalische Chemie, 1993. 97(1): p. 85-97.

168. Lemoine, B., et al., *Partial vapor pressure of CO₂ and H₂S over aqueous methyldiethanolamine solutions.* Fluid Phase Equilibria, 2000. 172(2): p. 261-277.

169. Thomsen, K. and P. Rasmussen, *Modeling of vapor–liquid–solid equilibrium in gas–aqueous electrolyte systems.* Chemical Engineering Science, 1999. 54(12): p. 1787-1802.

170. Addicks, J., et al., *Solubility of Carbon Dioxide and Methane in Aqueous Methyldiethanolamine Solutions.* Journal of Chemical & Engineering Data, 2002. 47(4): p. 855-860.

171. Faramarzi, L., et al., *Extended UNIQUAC model for thermodynamic modeling of CO₂ absorption in aqueous alkanolamine solutions.* Fluid Phase Equilibria, 2009. 282(2): p. 121-132.

172. Sadegh, N., E.H. Stenby, and K. Thomsen, *Thermodynamic modeling of CO₂ absorption in aqueous N-Methyldiethanolamine using Extended UNIQUAC model.* Fuel, 2015. 144: p. 295-306.

173. Haji-Sulaiman, M.Z. and M.K. Aroua, *Equilibrium of CO₂ in aqueous diethanolamine(DEA) and amino methyl propanol (AMP) solutions.* Chemical Engineering Communications, 1995. 140(1): p. 157-171.

174. Jane, I.S. and M.-H. Li, *Solubilities of Mixtures of Carbon Dioxide and Hydrogen Sulfide in Water + Diethanolamine + 2-Amino-2-methyl-1-propanol.* Journal of Chemical & Engineering Data, 1997. 42(1): p. 98-105.

175. Macgregor, R.J. and A.E. Mather, *Equilibrium solubility of H2S and CO₂ and their mixtures in a mixed solvent.* The Canadian Journal of Chemical Engineering, 1991. 69(6): p. 1357-1366.

176. Hartono, A., et al., *Solubility of carbon dioxide in aqueous 2.5 M of diethylenetriamine (DETA) solution.* Energy Procedia, 2011. 4: p. 179-186.

177. Benamor, A. and M.K. Aroua, *Modeling of CO₂ solubility and carbamate concentration in DEA, MDEA and their mixtures using the Deshmukh–Mather model.* Fluid Phase Equilibria, 2005. 231(2): p. 150-162.

178. Pahlavanzadeh, H., S. Nourani, and M. Saber, *Experimental analysis and modeling of CO₂ solubility in AMP (2-amino-2-methyl-1-propanol) at low CO₂ partial pressure using the models of Deshmukh–Mather and the artificial neural network.* The Journal of Chemical Thermodynamics, 2011. 43(12): p. 1775-1783.

179. Zhou, Q., L.-S. Wang, and H.-P. Chen, *Densities and Viscosities of 1-Butyl-3-methylimidazolium Tetrafluoroborate + H_2O Binary Mixtures from (303.15 to 353.15) K.* Journal of Chemical & Engineering Data, 2006. 51(3): p. 905-908.

180. Nelson, W.M., et al., *Experimental Phase Equilibrium for the Binary System of n-Pentane +2-Propanol Using a New Equilibrium Cell and the Static Total Pressure Method.* Journal of Chemical & Engineering Data, 2018. 63(3): p. 732-740.

181. Khan, S.N., et al., *Thermophysical properties of aqueous N-methyldiethanolamine (MDEA) and ionic liquids 1-butyl-3-methylimidazolium trifluoromethanesulfonate [bmim][OTf], 1-butyl-3-methylimidazolium acetate [bmim][Ac] hybrid solvents for CO_2 capture.* Chemical Engineering Research and Design, 2017. 121: p. 69-80.

182. García, S., et al., *Liquid−Liquid Extraction of Toluene from Heptane Using 1-Alkyl-3-methylimidazolium Bis(trifluoromethylsulfonyl)imide Ionic Liquids.* Journal of Chemical & Engineering Data, 2011. 56(1): p. 113-118.

183. Lee, M.-J. and T.-K. Lin, *Density and Viscosity for Monoethanolamine + Water, + Ethanol, and + 2-Propanol.* Journal of Chemical & Engineering Data, 1995. 40(1): p. 336-339.

184. Henni, A., et al., *Volumetric Properties and Viscosities for Aqueous Diglycolamine Solutions from 25 °C to 70 °C.* Journal of Chemical & Engineering Data, 2001. 46(1): p. 56-62.

185. García-Abuín, A., et al., *Density, Speed of Sound, Viscosity, Refractive Index, and Excess Volume of N-Methyl-2-pyrrolidone + Ethanol (or Water or Ethanolamine) from T = (293.15 to 323.15) K.* Journal of Chemical & Engineering Data, 2011. 56(3): p. 646-651.

186. Mascato, E., et al., *Thermodynamic properties of mixing for (1-alkanol + an-alkane+ a cyclic alkane) atT= 298.15 K. I. (n-Hexane + cyclohexane + 1-butanol).* The Journal of Chemical Thermodynamics, 2001. 33(3): p. 269-285.

187. Masilo, K., *Influence of Temperature, Concentration, Anion and Alkyl Chain Length in the Imidazolium Cation on the Thermophysical Properties of Imidazolium Based Ionic Liquids with Acetophenone.* 2016, Science and Technology North-West University.

188. Tseng, Y.-M. and A.R. Thompson, *Densities and Refractive Indices of Aqueous Monoethanolamine, Diethanolamine, Triethanolamine.* Journal of Chemical & Engineering Data, 1964. 9(2): p. 264-267.

189. Li, Y.-H., K.H. Dillard, and R.L. Robinson, *Vapor-liquid phase equilibrium for carbon dioxide-n-hexane at 40, 80, and 120 .degree.C.* Journal of Chemical & Engineering Data, 1981. 26(1): p. 53-55.

190. Wagner, Z. and I. Wichterle, *High-pressure vapour—liquid equilibrium in systems containing carbon dioxide, 1-hexene, and n-hexane.* Fluid Phase Equilibria, 1987. 33(1): p. 109-123.

191. Murrieta-Guevara, F. and A. Trejo Rodriguez, *Solubility of carbon dioxide, hydrogen sulfide, and methane in pure and mixed solvents.* Journal of Chemical & Engineering Data, 1984. 29(4): p. 456-460.

192. Sweeney, C.W., *Solubilities and partial molar enthalpies of solution for polar gas-liquid systems determined by gas chromatography.* Chromatographia, 1984. 18(12).

193. Zubchenko, Y.P., Shakhova, S.F. and Ladygina, O.P., *Solubility of carbon dioxide in N-methyl pyrrolidone under Pressure.* 1985. 9.

194. Murrieta-Guevara, F., A. Romero-Martinez, and A. Trejo, *Solubilities of carbon dioxide and hydrogen sulfide in propylene carbonate, N-methylpyrrolidone and sulfolane.* Fluid Phase Equilibria, 1988. 44(1): p. 105-115.

195. Bohloul, M.R., A. Vatani, and S.M. Peyghambarzadeh, *Experimental and theoretical study of CO2 solubility in N-methyl-2-pyrrolidone (NMP).* Fluid Phase Equilibria, 2014. 365(Supplement C): p. 106-111.

196. Taylor, B.N. and C.E. Kuyatt, *Guidelines for Evaluating and Expressing the Uncertainty of NIST Measurement Results.* NIST Technical Note 1297, 1994.

197. Shariati, A., et al., *Critical properties and acentric factors of ionic liquids.* Korean Journal of Chemical Engineering, 2013. 30: p. 187-193.

198. Frenkel, M., et al., *NIST ThermoData Engine 6.0. National Institute of Standards and Technology.* Thermodynamics Research Center (TRC), NIST Applied Chemicals and Materials Division, 2005.

199. Vural, U., M. V, and V. Sedat, *Excess molar volumes, and refractive index of binary mixtures of glycerol + methanol and glycerol + water at 298.15 K and 303.15 K.* Bulletin of the Chemical Society of Ethiopia, 2011. 25.

200. Derdar;, M.M.Z. and M.M. Amer, *Excess Molar Volume, Excess Viscosity and Excess Activation Energy for Binary Systems of Toluene with n-Alkanes at Different Temperatures.* AL-OSTATH, 2015(8).

201. Nain, A.K., P. Droliya, and J. Gupta, *Deviations in viscosity and thermodynamics of viscous flow for binary mixtures of methyl acrylate with 1-alkanols at different temperatures.* Indian Journal of chemistry, 2018. 57A: p. 761-769.

202. Dikio, E., et al., *Density, Dynamic Viscosity and Derived Properties of Binary Mixtures of Methanol, Ethanol, n-Propanol, and n-Butanol with Pyridine at T = (293.15, 303.15, 313.15 and 323.15) K.* International Journal of Electrochemical Science, 2012. 7: p. 11101-11122.

203. Ciocirlan, O., O. Croitoru, and O. Iulian, *Densities and Viscosities for Binary Mixtures of 1-Butyl-3-Methylimidazolium Tetrafluoroborate Ionic Liquid with Molecular Solvents.* Journal of Chemical & Engineering Data, 2011. 56(4): p. 1526-1534.

204. Maurice Stewart, K.A., *Gas Sweetening and Processing Field Manual.* 2011: Gulf Professional Publishing-Elsevier.

205. Osman, K.W. and M. Vasagam, *Gas Sweetening Process - Problems And Remedial Measures*, in *Abu Dhabi International Petroleum Exhibition and Conference.* 2002, Society of Petroleum Engineers: Abu Dhabi, United Arab Emirates. p. 7.

206. Fürhacker, M., A. Pressl, and R. Allabashi, *Aerobic biodegradability of methyldiethanolamine (MDEA) used in natural gas sweetening plants in batch tests and continuous flow experiments.* Chemosphere, 2003. 52(10): p. 1743-1748.

207. Aschenbrenner, O., et al., *Measurement of vapour pressures of ionic liquids and other low vapour pressure solvents.* Green Chemistry, 2009. 11(8): p. 1217-1221.

208. Jones, J.H., H.R. Froning, and E.E. Claytor, *Solubility of Acidic Gases in Aqueous Monoethanolamine.* Journal of Chemical & Engineering Data, 1959. 4(1): p. 85-92.

209. Shen, K.P. and M.H. Li, *Solubility of carbon dioxide in aqueous mixtures of monoethanolamine with methyldiethanolamine.* Journal of Chemical & Engineering Data, 1992. 37(1): p. 96-100.

210. Park, S.-B., et al., *Solubilities of carbon dioxide in the aqueous potassium carbonate and potassium carbonate poly(ethylene glycol) solutions.* Fluid Phase Equilibria, 1997. 134(1): p. 141-149.

211. Lawson, J.D. and A.W. Garst, *Gas sweetening data: equilibrium solubility of hydrogen sulfide and carbon dioxide in aqueous monoethanolamine and aqueous diethanolamine solutions.* Journal of Chemical & Engineering Data, 1976. 21(1): p. 20-30.

212. Ma'mun, S., et al., *Solubility of Carbon Dioxide in 30 mass % Monoethanolamine and 50 mass % Methyldiethanolamine Solutions.* Journal of Chemical & Engineering Data, 2005. 50(2): p. 630-634.

213. Xu, F., et al., *Solubility of CO_2 in aqueous mixtures of monoethanolamine and dicyanamide-based ionic liquids.* Fluid Phase Equilibria, 2014. 365: p. 80-87.

214. Lee, J.I., F.D. Otto, and A.E. Mather, *Equilibrium between carbon dioxide and aqueous monoethanolamine solutions.* Journal of Applied Chemistry and Biotechnology, 1976. 26(1): p. 541-549.

215. Mortazavi-Manesh, S., M.A. Satyro, and R.A. Marriott, *Screening Ionic Liquids as Candidates for Separation of Acid Gases: Solubility of Hydrogen Sulfide, Methane, and Ethane.* AIChE Journal, 2013. 59(8): p. 2993-3005.

216. Lu, B., et al., *Kinetics of Carbon Dioxide Absorption into Mixed Aqueous Solutions of MEA + [Bmim]BF_4 Using a Double Stirred Cell.* Energy & Fuels, 2013. 27(10): p. 6002-6009.

217. Ahmady, A., M.A. Hashim, and M.K. Aroua, *Experimental Investigation on the Solubility and Initial Rate of Absorption of CO_2 in Aqueous Mixtures of Methyldiethanolamine with the Ionic Liquid 1-Butyl-3-methylimidazolium Tetrafluoroborate.* Journal of Chemical & Engineering Data, 2010. 55(12): p. 5733-5738.

218. Sairi, N.A., et al., *Solubilities of CO_2 in aqueous N-methyldiethanolamine and guanidinium trifluoromethanesulfonate ionic liquid systems at elevated pressures.* Fluid Phase Equilibria, 2011. 300(1): p. 89-94.

219. Feng, Z., et al., *Absorption of CO_2 in the aqueous solutions of functionalized ionic liquids and MDEA.* Chemical Engineering Journal, 2010. 160(2): p. 691-697.

220. Feng, Z., et al., *Study on the absorption of carbon dioxide in high concentrated MDEA and ILs solutions.* Chemical Engineering Journal, 2012. 181-182: p. 222-228.

221. Hasib-ur-Rahman, M. and F. Larachi, *Kinetic behavior of carbon dioxide absorption in diethanolamine/ionic-liquid emulsions.* Separation and Purification Technology, 2013. 118: p. 757-761.

222. Feng, Z., et al., *Regeneration performance of amino acid ionic liquid (AAIL) activated MDEA solutions for CO₂ capture.* Chemical Engineering Journal, 2013. 223: p. 371-378.

223. Gao, Y., et al., *Absorption of CO₂ in amino acid ionic liquid (AAIL) activated MDEA solutions.* International Journal of Greenhouse Gas Control, 2013. 19: p. 379-386.

224. Ghani, N.A., et al., *Density, Surface Tension, and Viscosity of Ionic Liquids (1-Ethyl-3-methylimidazolium diethylphosphate and 1,3-Dimethylimidazolium dimethylphosphate) Aqueous Ternary Mixtures with MDEA.* Journal of Chemical & Engineering Data, 2014. 59(6): p. 1737-1746.

225. Aparicio, S. and M. Atilhan, *Water effect on CO₂ absorption for hydroxylammonium based ionic liquids: A molecular dynamics study.* Chemical Physics, 2012. 400: p. 118-125.

226. Yang, J., et al., *CO₂ capture with the absorbent of a mixed ionic liquid and amine solution considering the effects of SO₂ and O₂.* Applied Energy, 2017. 194: p. 9-18.

227. Chang, Y.-T., R. B. Leron, and M.-H. Li, *Carbon dioxide solubility in aqueous potassium salt solutions of L-proline and DL-α-aminobutyric acid at high pressures.* Journal of Chemical Thermodynamics, 2015. 83: p. 110-116.

228. Vahidi, M., et al., *Equilibrium Solubility of Carbon Dioxide in an Aqueous Mixture of N-Methyldiethanolamine and Diisopropanolamine: An Experimental and Modeling Study.* Journal of Chemical & Engineering Data, 2013. 58(7): p. 1963-1968.

229. Wang, J., et al., *A volumetric and viscosity study for the mixtures of 1-n-butyl-3-methylimidazolium tetrafluoroborate ionic liquid with acetonitrile, dichloromethane, 2-butanone and N, N – dimethylformamide.* Green Chemistry, 2003. 5(5): p. 618-622.

230. Zhao, Y., et al., *Density, Viscosity, and Performances of Carbon Dioxide Capture in 16 Absorbents of Amine + Ionic Liquid + H₂O, Ionic Liquid + H₂O, and Amine + H₂O Systems.* Journal of Chemical & Engineering Data, 2010. 55(9): p. 3513-3519.

231. Henni, A., et al., *Volumetric Properties and Viscosities for Aqueous N-Methyl-2-pyrrolidone Solutions from 25 °C to 70 °C.* Journal of Chemical & Engineering Data, 2004. 49(2): p. 231-234.

232. Pal, A. and R.K. Bhardwaj, *Excess Molar Volumes and Viscosities for Binary Mixtures of 2-Propoxyethanol and of 2-Isopropoxyethanol with Propylamine and Dipropylamine at (298.15, 308.15, and 318.15) K.* Journal of Chemical & Engineering Data, 2001. 46(4): p. 933-938.

233. Yang, C., et al., *Thermodynamic properties of binary mixtures of N-methyl-2-pyrrolidinone with cyclohexane, benzene, toluene at (303.15 to 353.15)K and atmospheric pressure.* The Journal of Chemical Thermodynamics, 2007. 39(1): p. 28-38.

234. Amundsen, T.G., L.E. Øi, and D.A. Eimer, *Density and Viscosity of Monoethanolamine + Water + Carbon Dioxide from (25 to 80) °C.* Journal of Chemical & Engineering Data, 2009. 54(11): p. 3096-3100.

235. Udara S. P. R. Arachchige, et al., *Viscosities of Pure and Aqueous Solutions of Monoethanolamine (MEA), Diethanolamine (DEA) and N-Methyldiethanolamine (MDEA).* Annual Transactions of the Nordic Rheology Society, 2013. 21.

236. Harris, K.R., M. Kanakubo, and L.A. Woolf, *Temperature and Pressure Dependence of the Viscosity of the Ionic Liquids 1-Hexyl-3-methylimidazolium Hexafluorophosphate and 1-Butyl-3-methylimidazolium Bis(trifluoromethylsulfonyl)imide.* Journal of Chemical & Engineering Data, 2007. 52(3): p. 1080-1085.

237. Mokhtarani, B., et al., *Density and viscosity of pyridinium-based ionic liquids and their binary mixtures with water at several temperatures.* The Journal of Chemical Thermodynamics, 2009. 41(3): p. 323-329.

238. Ebrahiminejadhasanabadi, M., et al., *Experimental measurement of carbon dioxide solubility in 1-methylpyrrolidin-2-one (NMP) + 1-butyl-3-methyl-1H-imidazol-3-ium tetrafluoroborate ([bmim][BF$_4$]) mixtures using a new static-synthetic cell.* Fluid Phase Equilibria, 2018.

239. Fattahi, M. and H. Iloukhani, *Excess molar volume, viscosity, and refractive index study for the ternary mixture {2-methyl-2-butanol (1)+tetrahydrofuran (2)+propylamine (3)} at different temperatures. Application of the ERAS-model and Peng–Robinson–Stryjek–Vera equation of state.* The Journal of Chemical Thermodynamics, 2010. 42(11): p. 1335-1345.

240. Rezaei-Sameti, M., H. Iloukhani, and M. Rakhshi, *Excess thermodynamic parameters of binary mixtures of methanol, ethanol, 1-propanol, and 2-butanol + chloroform at (288.15–323.15 K) and comparison with the Flory theory.* Russian Journal of Physical Chemistry, 2010. 84: p. 2023-2032.

241. Stec, M., et al., *Densities, Excess Molar Volumes, and Thermal Expansion Coefficients of Aqueous Aminoethylethanolamine Solutions at Temperatures from 283.15 to 343.15 K.* Journal of solution chemistry, 2014. 43: p. 959-971.

242. Rezaei-Sameti, M. and M. Rakhshi, *Excess parameters of binary and ternary mixtures of {1-Butanol + hexylamine + n-heptane} at different temperatures and comparison with the Flory theory.* African Journal of Pure and Applied Chemistry, 2011. 5: p. 158-167.

243. Domańska, U. and M. Królikowska, *Density and Viscosity of Binary Mixtures of Thiocyanate Ionic Liquids + Water as a Function of Temperature.* Journal of Solution Chemistry, 2012. 41.

244. Kumar, D.B.K., et al., *Measurements of some physical properties of binary liquid mixtures (N-methyl-2-pyrrolidone+an aliphatic ester) at several temperatures and data processing of viscosity and ultrasonic speed.* Journal of Molecular Liquids, 2013. 183: p. 31-44.

245. Grgurić, I.R., et al., *Volumetric properties of the ternary system ethanol + 2-butanone + benzene by the van der Waals and Twu–Coon–Bluck–Tilton mixing rules: experimental data, correlation and prediction.* Thermochimica Acta, 2004. 412(1): p. 25-31.

246. Aktar, Sh., et al., *Excess molar volumes and deviations in viscosity of the binary mixtures of 1-pentanol + aromatic hydrocarbons at t = 298.15 k.* European Scientific Journal, 2015. 11(15).

247. Dzyuba, S. and R. A Bartsch, *Influence of Structural Variations in 1-Alkyl(aralkyl)-3-Methylimidazolium Hexafluorophosphates and Bis(trifluoromethylsulfonyl)imides on Physical Properties of the Ionic Liquids.* Chemphyschem, 2002. 3: p. 161-6.

248. Katsuta, S., et al., *Stability of Ion Pairs of Bis(trifluoromethanesulfonyl)amide-Based Ionic Liquids in Dichloromethane.* Journal of Chemical & Engineering Data, 2010. 55(4): p. 1588-1593.

249. Hamidova, R., et al., *Thermophysical properties of 1-butyl-3-methylimidazolium bis(trifluoromethylsulfonyl)imide at high temperatures and pressures.* Brazilian Journal of Chemical Engineering, 2015. 32: p. 303-316.

250. Troncoso, J., et al., *Thermodynamic Properties of Imidazolium-Based Ionic Liquids: Densities, Heat Capacities, and Enthalpies of Fusion of [bmim][PF$_6$] and [bmim][NTf$_2$].* Journal of Chemical & Engineering Data, 2006. 51(5): p. 1856-1859.

251. Vranes, M., et al., *Physicochemical Characterization of 1-Butyl-3-methylimidazolium and 1-Butyl-1-methylpyrrolidinium Bis(trifluoromethylsulfonyl)imide.* Journal of Chemical & Engineering Data, 2012. 57(4): p. 1072-1077.

252. Wandschneider, A., J.K. Lehmann, and A. Heintz, *Surface Tension and Density of Pure Ionic Liquids and Some Binary Mixtures with 1-Propanol and 1-Butanol.* Journal of Chemical & Engineering Data, 2008. 53(2): p. 596-599.

253. Lee, J.I., F.D. Otto, and A.E. Mather, *The solubility of H2S and CO$_2$ in aqueous monoethanolamine solutions.* The Canadian Journal of Chemical Engineering, 1974. 52(6): p. 803-805.

254. Sadegh, N., *Acid Gas Removal from Natural Gas with Alkanolamines: A Modeling and Experimental Study.* 2013, Technical University of Denmark.

255. Rho, S.-W., et al., *Solubility of CO$_2$ in Aqueous Methyldiethanolamine Solutions.* Journal of Chemical & Engineering Data, 1997. 42(6): p. 1161-1164.

256. Jou, F.Y., et al., *Solubility of mixtures of hydrogen sulfide and carbon dioxide in aqueous N-methyldiethanolamine solutions.* Journal of Chemical & Engineering Data, 1993. 38(1): p. 75-77.

257. Park, M.K. and O.C. Sandall, *Solubility of Carbon Dioxide and Nitrous Oxide in 50 mass Methyldiethanolamine.* Journal of Chemical & Engineering Data, 2001. 46(1): p. 166-168.

258. Vallée, G., et al., *Representation of CO$_2$ and H$_2$S Absorption by Aqueous Solutions of Diethanolamine Using an Electrolyte Equation of State.* Industrial & Engineering Chemistry Research, 1999. 38(9): p. 3473-3480.

259. Huttenhuis, P.J.G., et al., *Gas solubility of H2S and CO$_2$ in aqueous solutions of N-methyldiethanolamine.* Journal of Petroleum Science and Engineering, 2007. 55(1–2): p. 122-134.

260. Lee, J.I., F.D. Otto, and A.E. Mather, *The solubility of mixtures of carbon dioxide and hydrogen sulphide in aqueous diethanolamine solutions.* The Canadian Journal of Chemical Engineering, 1974. 52(1): p. 125-127.

261. Park, S.H., et al., *Correlation and Prediction of the Solubility of Carbon Dioxide in Aqueous Alkanolamine and Mixed Alkanolamine Solutions.* Industrial & Engineering Chemistry Research, 2002. 41(6): p. 1658-1665.

262. Lee, J.I., F.D. Otto, and A.E. Mather, *Solubility of carbon dioxide in aqueous diethanolamine solutions at high pressures.* Journal of Chemical & Engineering Data, 1972. 17(4): p. 465-468.

263. Roberts, B.E. and A.E. Mather, *Solubility of CO_2 and H_2S in a hindered amine solution.* Chemical Engineering Communications, 1988. 64(1): p. 105-111.

264. Teng, T.T. and A.E. Mather, *Solubility of H_2S, CO_2 and their mixtures in an AMP solution.* The Canadian Journal of Chemical Engineering, 1989. 67(5): p. 846-850.

265. Dell'Era, C., et al., *Solubility of carbon dioxide in aqueous solutions of diisopropanolamine and methyldiethanolamine.* Fluid Phase Equilibria, 2010. 293(1): p. 101-109.

266. Jou, F.Y., et al., *The solubility of carbon dioxide and hydrogen sulfide in a 35 wt% aqueous solution of methyldiethanolamine.* The Canadian Journal of Chemical Engineering, 1993. 71(2): p. 264-268.

267. Sidi-Boumedine, R., et al., *Experimental determination of hydrogen sulfide solubility data in aqueous alkanolamine solutions.* Fluid Phase Equilibria, 2004. 218(1): p. 149-155.

268. Lee, J.I., F.D. Otto, and A.E. Mather, *Partial pressures of hydrogen sulfide over diethanolamine solutions.* Journal of Chemical & Engineering Data, 1973. 18(4): p. 420-420.

269. Wright, R.H. and O. Maass, *The Solubility of Hydrogen Sulphide in Water from the Vapor Pressures of the Solutions.* Canadian Journal of Research, 1932. 6(1): p. 94-101.